The Molecular & Cellular Interactions of Wound-Induced Hydrogen Peroxide in the Regenerating Larval Zebrafish Tail

Gareth McCathie

Submitted for the degree of Doctor of Philosophy

August 2017

The Bateson Centre

Department of Biomedical Science

The University of Sheffield

Contents

Figures

Tables

Acknowledgements

I would like to take this opportunity to extend my thanks to a number of people for their help over the course of my PhD:

Firstly, my supervisor Henry Roehl for direction, oversight, technical aid and help as needed but freedom to direct my own project.

To the entire Roehl Lab, past and present, for practical help, training in the lab techniques and general advice.

To the Whitfield Lab for an alternative source of advice and emergency aliquots of just about every chemical I've used over my projects.

To my PhD student colleagues in BMS and MBB for scientific discussions and general advice but mainly empathy, understanding and a de-stress session over a pint or two.

To Felix Ellett, Nik Ogryzko, Cat Loynes, Steve Renshaw and Caz Butcher for getting me up and running with the nitroreductase ablation system.

To Aga Skowronek for training in & troubleshooting with qPCR work.

To my advisors Freek Van Eeden & David Strutt, for the stimulating and always very useful discussions of my work.

To the aquarium staff who have done a fantastic job of maintaining all our zebrafish lines and helping with any husbandry issues and all things fishy.

Finally, to all my friends and family who have had to endure my mood swings and rants. I promise I will be better now!

Abstract

The ability of humans to heal from wounding is fairly limited; whilst certain organs such as the blood and skin have an in-built capacity for homeostatic regeneration to maintain physiological function, we are generally poor at reparative regeneration following injury. Zebrafish, however, have a much greater capacity for healing and are able to restore both form and function in multiple organs when damaged. This trait is shared between multiple species and relies on the reactivation of conserved developmental pathways.

The precise interactions that determine whether a wound regenerates or not are currently not clear, and more work must be done to understand the molecular and cellular interactions which mediate the regenerative response. This could identify the limiting steps in our own wound-healing processes that we are able to manipulate in order to induce regeneration and improve clinical outcomes and quality of life for millions of patients including amputees, paralysed trauma victims, and sufferers of stroke or heart failure.

Here, I present evidence that wound-induced hydrogen peroxide (H_2O_2) is required for the initiation of regeneration in the larval zebrafish tail via the activation of the Hedgehog (Hh), and subsequently the Wnt and FGF pathways. H_2O_2 induces activation of SFKs in the epithelial cells at the wound margin which trigger the extrusion of the severed notochord following tail amputation. This physical extrusion is necessary to induce upregulation of the Hh ligands Shh and Ihh in the notochord cells which stimulates Hh pathway activation in the surrounding tissue in a paracrine fashion, acting as a redox-sensitive central organiser. This pro-regenerative effect of H_2O_2 appears to be independent of its role as a pro-inflammatory signal, and shows that H_2O_2 exerts control over multiple parallel wound responses. Continued work will be required to characterise the full extent of regulatory control that this promiscuous wound signal possesses.

List of abbreviations

AEBSF: 4-(2-Aminomethyl)benzenesulfonyl fluoride
AER: Apical ectodermal ridge
AP: Alkaline Phosphatase
Bim-1: Bisindolylmaleimide-1
csf1ra: Colony stimulating factor 1 receptor a
Ctrl: Control
CyHex: Cycloheximide
DAMP: Damage associated molecular pattern
DIG: Digoxigenin
dpf: Days post fertilisation
DPI: Diphenyleneiodonium
Duox: Dual oxidase
ECM: Extracellular matrix
EtOH: Ethanol
H_2O_2: Hydrogen peroxide
Hh: Hedgehog
hpa: Hours post amputation
hpf: Hours post fertilisation
IGF: Insulin-like growth factor
IHC: Immunohistochemistry
lcp1: Lymphocyte cytosolic protein 1 / L-plastin
MCI-186: 3-Methyl-1-phenyl-2-pyrazolin-5-one
MeOH: Methanol
mpa: Minutes post amputation
mpeg1: Macrophage expressed gene 1
mpx: Myeloperoxidase
Mtz: Metronidazole
NBCS: New born calf serum
NEB: New England Biolabs
Noc: Nocodazole
Nox: NADPH oxidase
Ntr: Nitroreductase
PBS: Phosphate buffered saline
PBST: Phosphate buffered saline / tween
PFA: Paraformaldehyde
PFBSF: Pentafluorobenzenesulfonyl fluorescein
PKC: Protein kinase C
PMA: Phorbol 12-myristate 13-acetate
RA: Retinoic acid
ROI: Region of interest
ROS: Reactive oxygen species
RT: Room temperature
SCI: Spinal cord injury
SFK: Src family kinase
SOD: Superoxide dismutase
UAS: Upstream activation sequence
UNM: UAS-nitroreductase-mCherry
WISH: Whole-mount *in situ* hybridisation
ZPA: Zone of polarising activity

Chapter 1. Introduction

1.1 Introduction

Regenerative biology has been fascinating scientists for centuries, but we have only recently developed the tools required to investigate the molecular and cellular basis of regeneration making it a relatively new field. Regenerative healing is an incredible feat that many organisms from a surprising number of branches of the tree of life can accomplish. The ability to repair their body completely after wounding to restore form and function confers obvious survival advantages. The extent of regeneration can vary form limited cell & tissue restoration to the regrowth of large body segments or even, in extreme circumstances, an entire organism from a single cell[1]. Unfortunately for us, the regenerative capacity of humans is very limited in both the range of tissue types that we are capable of regenerating and the extent of damage that we regenerate from. More often than not, human wounds have to resort to depositing scar tissue in order to heal, but scar tissue is a poor substitute for biologically active cells, and is essentially the body's 'pollyfiller' – a quick fix that allows rapid closure of the wound and re-establishment of homeostasis, but at the expense of both form and function. Replacing lost cells with scar tissue results in reduced functional capacity at the wound site, which can severely impact the quality of life subsequently experienced by an individual.

Our understanding of the process of regeneration is still fairly limited, although progress is being made by the combined efforts of studying multiple highly regenerative model organisms. Currently, we are at the stage where we know many of the players in the game but we do not know the relative importance of each interaction or the hierarchy between regeneration regulation mechanisms. We have evidence that many developmental signalling pathways are essential for regeneration, an unsurprising finding given that both processes rely on the coordinated proliferation, differentiation and migration of cells, but additional cellular processes are also essential for regeneration to proceed. Reactive oxygen species (ROS), apoptosis, bioelectricity, miRNA regulation, epigenetics, hypoxia, innervation, autophagy and inflammation have all been shown to regulate regeneration and the appropriate activation of each is essential for successful regeneration. With such a complex web of signals to be integrated, there is no consensus on the key regulators of regeneration and as the field progresses bioinformatic systems biology approaches may be required to shed light on such questions.

The continued characterisation of the molecular and cellular interactions employed in regeneration is essential to understand how tissue regrowth is stimulated and why some organisms regenerate extensively whilst others regenerate very poorly. Given that many of the molecular mediators of regeneration are highly conserved even in non-regenerating organisms, it is thought that they still possess the machinery required to regenerate but that the differences in the regulation of these mediators is responsible for the loss of this ability. Therefore, sufficient understanding of the regenerative mechanism may lead to the identification of the negative regulators of regeneration in humans with the goal of manipulating these to allow us to repair and regrow lost tissue much more fully. Translation of this research to the clinic would have clear medical benefits to a variety of patients worldwide – from paralysed trauma victims and amputees, to those suffering from stroke or heart failure. For example, regional estimates of the current prevalence of spinal cord injury (SCI) ranged from 906 per million to 250 per million and therefore millions of people worldwide are living with some form of SCI[2]. In addition, the majority of SCI patients are younger than 30, creating a significant and lasting economic burden[3]. A recent meta-study calculated a global estimate of the number of stroke survivors (potentially with permanent brain damage) to be around 33 million[4], and another suggested that the number suffering from heart failure was at least 26 million[5]. These startlingly large numbers of people living with damaged organs that have healed incompletely highlight the potential impact the regenerative medicine field could have, and whilst clinical applications are still many decades away, this basic research is setting us on a path to reach that goal.

1.2 Aims

The aim of this project is to push forward our current understanding of the basic molecular and cellular interactions required for the initiation of regeneration. I have chosen to investigate the initiation of regeneration because it represents the most upstream position in the regulatory cascade and therefore will have the most significant and wide-reaching effect on the whole regenerative process. In order to achieve this I will use larval zebrafish tail regeneration as a model of complex and coordinated multicellular appendage regrowth as it is rapid, genetically tractable and well suited to pharmacological treatments and genetic analysis. I will specifically focus on the role hydrogen peroxide (H_2O_2) plays in the initiation of regeneration to try and understand how this early and transient wound response can act as an essential regenerative signal by identifying molecular & cellular targets of H_2O_2. Once

identified, these targets could be studied in the human wound response to identify key differences in regulation which could be pharmacologically manipulated to improve healing in humans.

In order to accomplish these aims I will focus on the following questions:

1) Does wound-induced H_2O_2 stimulate regeneration directly via the regulation of developmental signalling pathways?
2) Does wound-induced H_2O_2 stimulate regeneration indirectly via the initiation of inflammation?
3) What are the pro-regenerative molecular effectors of wound-induced H_2O_2?
4) Does H_2O_2 play a similar role in tail development as it does in tail regeneration?

My accompanying hypotheses are:

1) Wound-induced H_2O_2 triggers one or more developmental pathways which are essential for regeneration to proceed.
2) Wound-induced H_2O_2 dependent inflammation is required for regeneration to proceed.
3) Redox sensitive cellular regulators transduce the wound-induced H_2O_2 signal to biochemical signalling pathways essential for regeneration.
4) Wound-induced H_2O_2 has been co-opted as a regulator of regeneration by recapitulating a growth-promoting role also present in tail development.

Each of these questions and their corresponding hypotheses will be addressed in a separate results chapter and conclusions drawn from the data presented. Figure 1.1 below shows an outline of the wound responses triggered by H_2O_2 and highlights the areas where investigating these questions will deepen our understanding of the zebrafish regeneration process.

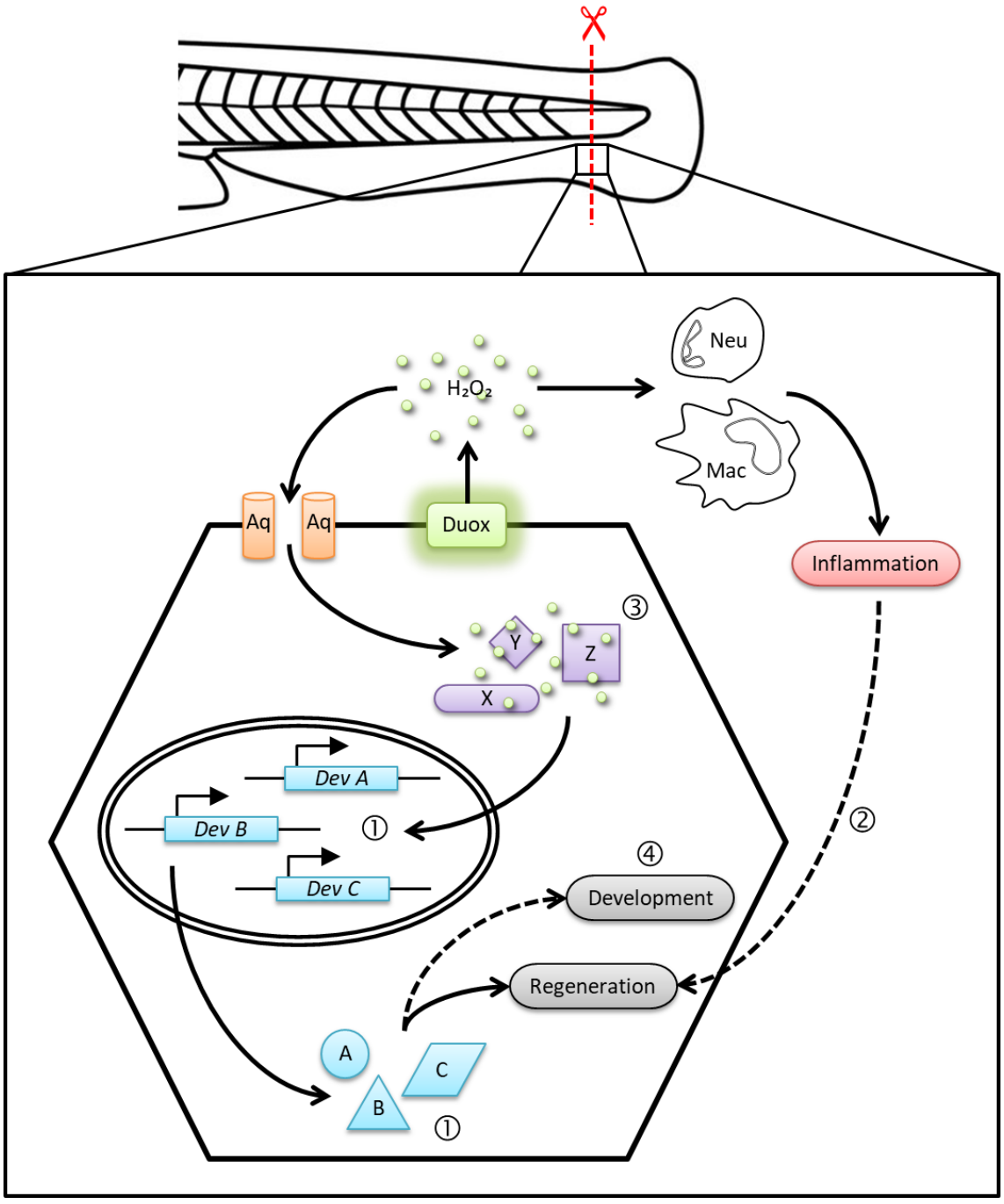

Figure 1.1 – Wound-induced H_2O_2 activation of cellular & molecular responses.
Outline of the cellular & molecular responses to wounding in the larval zebrafish tail. Following tail amputation, Duox enzymes are activated in keratinocytes at the wound (inset), producing H_2O_2 which acts extracellularly as well as diffusing into the cells via aquaporins (Aq) to trigger regeneration via molecular and cellular reactions. I aim to study 4 main parts of the process, 1) Are developmental genes & their subsequent signalling pathways required for H_2O_2 driven regeneration? 2) Does the pro-inflammatory role of H_2O_2 mediate regeneration indirectly via the recruitment and activation of neutrophils (Neu) and macrophages (Mac)? 3) What are the intra-cellular molecular effectors of the H_2O_2 signal required to initiate regeneration? And 4) Does regulation of tail development utilise the same redox-sensitive pathways and interactions?

1.3 Introduction to regeneration

Regeneration is the physiological process used to replace lost or damaged cells to completely re-establish form and function of the damaged area, and can be sub-divided into two general types – homeostatic or reparative regeneration. Homeostatic regeneration is classed as the mechanism by which tissues and organs maintain their function as cells are damaged or lost through their normal physiological function, whereas reparative regeneration is the mechanism by which tissues and organs can restore their form and function after injury. As such, homeostatic regeneration functions continuously to ensure the replacement of small numbers of cells at a time, via compensatory proliferation of progenitor cells e.g. for intestinal epithelia, skin and blood[6]; in comparison, reparative regeneration responds to rapid and severe damage following sudden injury which can often involve the loss of large volumes of tissue containing multiple cell lineages & organs. It should be noted that in this project I am studying reparative regeneration rather than homeostatic regeneration and throughout this thesis when I mention 'regeneration' I am referring to the reparative process.

1.3.1 Human Regeneration

As mentioned above, there are multiple example of homeostatic regeneration in humans in tissues with high cellular turnover such as epithelia and blood, but the extent of reparative regeneration is very limited. Whilst it is becoming clear that many organs are in fact capable of minor reparative regeneration from resident adult stem cells[7–13], the extent of damage which we can sucessfully heal from is very limited. If we suffer a severe wound, our bodies resort to scarring to close the wound rapidly and protect us from potentially lethal infection and blood loss at the apparent expense of maintaining a pro-regenerative environment.

In contrast, the human liver is know for its ability to regenerate to normal size following surgical resection (e.g. tumour removal) and exploited in live-patient liver transplants for decades[14]. Human surgeries often involve removal of one lobe of the liver (~50% of the toal volume) with function recovery within weeks and full cell mass recovery in 3-6 months[15].

Experiments in rodents as a mammalian model of liver regeneration have ellucidated the molecular driver of regeneration following liver damage or resection. This regeneration involves the proliferation of multiple mature cell types (hepatocytes, biliary epithelial cells, endothelial cells, Kupffer cells and hepatic stellate cells) which are activated in response to

wounding via the upregulation and interaction of multiple cytokines, mitogens, extracellular matrix (ECM) components and ECM remodelling enzymes[16]. Perhaps unsurprisingly, the mitogenic activity of growth factors appears to mimic that of the developing liver with a strong requirement for hepatocyte growth factor, EGF and β-catenin pathway activation[17–21]. One significant difference between this form of regeneration and that employed by more regenerative organisms (as described below) is that it restores cell mass by compensatory hyperplasia (and no blastema-like structure is formed, as described below) in the remaining lobes which restores liver function but does not fully restore organ form.

There is also mounting evidence that resident adult stem cell populations also contribute to liver regeneration in humans[22,23], further differentiating it from classical examples of reparative regeneration. Despite the differences and limitations of this form of regeneration it is encouraging to see that the human body is, indeed capable of such advanced healing without our intervention and knowledge of this process may aid in our attempts to improve healing of other organs.

1.3.2 Regeneration in highly regenerative organisms

Highly regenerative organisms carry out reparative regeneration by two general mechanisms – epimorphic and morphallactic regeneration (Figure 1.2). These processes differ in how the new tissue is formed following injury with epimorphic regeneration characterised by the formation of a proliferative mass of cells (the blastema) which divide to give rise to the cells of the newly formed tissue compared to morphallactic regeneration which primarily relies on the redistribution and remodelling of the remaining cells of the organism to reform a complete organism.

Most highly regenerative organisms make use of epimorphic regeneration but one notable exception is the cnidarian polyp *Hydra* which is capable of rapidly regenerating from small body pieces and achieves this by morphallactic regeneration[24]. This process can be incredibly powerful as, in addition to regenerating lost tissue, individuals can even reform from single-cell dissociates[25,26] but one limitation of this process is that in the absence of significant proliferation the size of the regenerated organism is the same as the size of the original tissue segment, therefore considerable cellular remodelling is required. *Hydra* are relatively simple animals with less than ten mature cell types which maintain a higher level of plasticity than normal mature cells, two characteristics which lend themselves to this type of remodelling[24,27].

Furthermore, adult *Hydra* continually grow by division of stem cells and reproduce by budding excess cells to form another organism, therefore the natural life-cycle of *Hydra* provides a ready-made mechanism to restore body size after morphallactic regeneration, without the need for significant proliferation in the regenerative process itself. These considerations may explain why higher animals use epimorphic regeneration instead, as it is a more simple and efficient way to regrow lost tissue in more complex body plans containing more committed mature cell types and in the absence of high levels of constitutive adult stem-cell division.

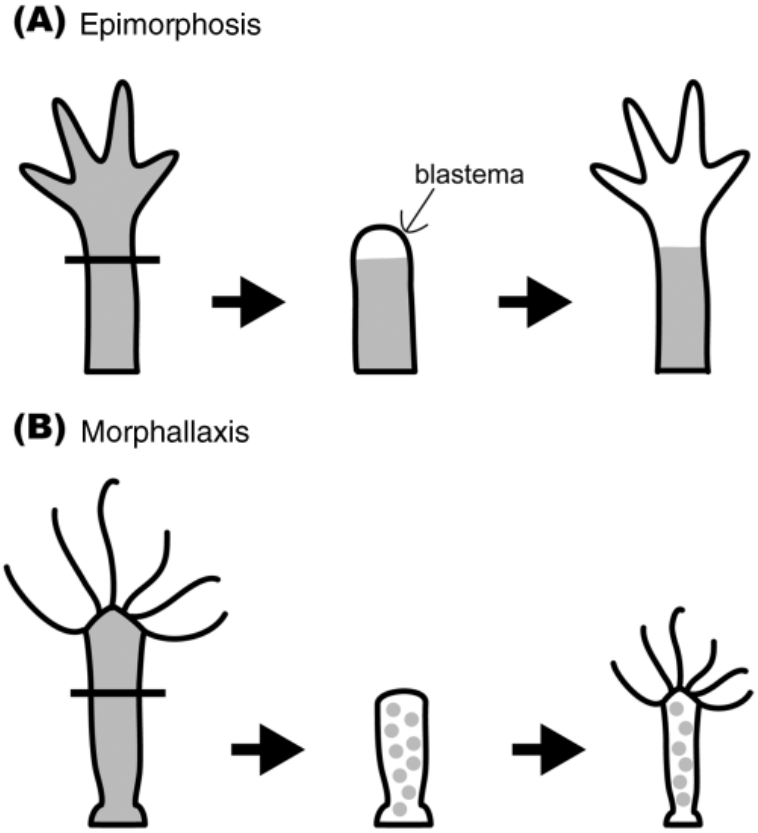

Figure 1.2 – Classical examples of epimorphic and morphallactic regeneration (reproduced from Agata *et al.*, 2007[28]).
A) Amphibian limb regeneration is a classical example of epimorphic regeneration which requireds the formation of a proliferative blastema to divide and replace the lost tissue. **B)** Tissue regeneration in *Hydra* is a classical example of morphallactic regeneration where a discrete blastema is not formed and the lost tissue is replaced by an active re-arrangement of pre-existing cells with little proliferative growth.

Although epimorphic regeneration is normally responsible for the regeneration of tissues on a more organ-level specificity (e.g. limb, tail, heart), the flatworm planaria makes extensive use of epimorphic regeneration and can restore its whole body by this mechanism. Planaria are

often considered to be the pinnacle of regeneration and are capable of regenerating entire organisms from as little as 1/279th of its original body[29] or even from a single cell in a permissive environment[1]. Planarian regeneration has been classed as epimorphic because of the formation of the blastema at the wound, but some studies have provided evidence that the blastema itself does not contain proliferating progenitors of all cell types and acts as a local signalling centre to impart positional information to the reforming tissue[30,31]. This has cast doubt on the suitability of the definitions epimorphic and morphallactic regeneration and some have suggested that these terms, inherited from classical regeneration studies from over a century ago, are inappropriate for the classification of regeneration. They have suggested that these arbitrary classifications of regeneration sub-types are counterproductive and that all forms of reparative regeneration require two universal processes – determination of positional identity and then proliferation of the appropriate tissue using this spatial information[28]. They present evidence from multiple regeneration models that the first step in regeneration is the distalisation of tissues at the wound site, followed by intercalary proliferation. How well this model would convert to non-linear organ level regeneration where there is no single distal point is questionable, but this process still maintains the same requirements of determining positional identity and appropriate proliferation to restore organ form and so similar mechanisms are likely to be employed. Although the authors concede that different organisms (and even different organs within one organism) can achieve these ends via different processes, they argue that identifying universal principles instead of classifying them as separate forms of regeneration can better inform our understanding of the regeneration process as a whole and highlight commonalities between regenerative programs previously thought to be incompatible.

1.4 Evolution of regeneration

Another debate within the regenerative field is based on the origins of regenerative capacity. With such widespread regenerative capabilities within metazoans and significant conservation between the regulatory components and the mitogenic cell signalling pathways required for regeneration, it was generally thought that regeneration is a survival trait inherited from a common ancestor which has been subsequently de-activated in non-regenerating organisms rather than a trait which spontaneously evolved to make use of common processes[32–35]. However, whilst this sounds the most likely explanation for widely conserved regenerative mechanisms, there is certainly evidence of spontaneously evolved regenerative traits that are

species-specific[36–40]. It is probably most likely that the prevalence of regeneration is a combination of both of these factors, but the knowledge that poorly-regenerating organisms such as humans may potentially still harbour ancient and conserved regenerative mechanisms in a latent state is encouraging and fuels the idea that reactivation of these processes may be all that is required to induce regeneration again.

1.5 Zebrafish as a model of regeneration

There are now multiple established model organisms in which to study regeneration, but I have chosen to use the zebrafish for a number of reasons: Firstly, and most importantly, zebrafish are highly regenerative and are capable of regrowing multiple tissues including heart, CNS & peripheral nerves, bone, muscle, fins, kidney and liver[41–46].

Secondly, as vertebrates they possess a high degree of biological similarity to humans, especially on the cellular and organ levels. Their genome encodes orthologues for over 80% of all known disease-linked human genes and shows ~70% homology to the human genome overall[47], and vertebrates possess highly conserved cellular signalling therefore studies in zebrafish have been used extensively to inform human cell biology, development, disease and toxicology[47–53].

Thirdly, transcriptional analysis is quick, easy and reliable using RNA *in situ* hybridisation techniques. The historical use of the zebrafish as a developmental biology model organism means that there is a plethora of validated RNA *in situ* hybridisation probes with well documented spatiotemporal expression patterns[54]; the small size and transparency of zebrafish larvae allows whole-mount techniques to allow high-resolution visualisation of the distribution of gene expression over entire animals, a technique I make abundant use of in this thesis.

Fourthly, they are highly genetically tractable with a number of well validated genetic engineering tools & techniques make the zebrafish a useful tool for creating transgenic lines for both knockouts and transgene delivery[55]. Large clutch numbers and short generation times aid in the rapid establishment of stable transgenic lines. Zebrafish are also amenable to gene silencing via RNAi and morpholino methods either systemically by injection into the embryo at the 1-cell stage or locally by targeted injection at later developmental stages[56].

Fifthly, the larval zebrafish is almost completely transparent, which, in combination with the insertion of fluorescent reporter transgenes can allow spatio-temporal visualisation of distinct cell populations or even individual cells. Labelled cells can be monitored in live embryos in real time in order to study complex tissue-scale responses to wounding such as cell migration and inflammation[57–59], feats which are either difficult or impossible in other model regenerative organisms. As an extension of this, pigmentation mutant lines have been selectively bred to create fish which maintain transparency into adulthood, allowing these techniques to be applied in fully developed fish[60].

Finally, on top of all these reasons, there are several practical concerns which make the zebrafish a suitable choice. For instance, zebrafish lay hundreds of eggs in a single clutch, they are very small and easily handled allowing for the simple collection of large numbers of genetically similar siblings. Larval zebrafish are also unprotected by ASPA until five days post fertilisation circumventing any ethical concerns whilst still generating *in vivo* data from a higher vertebrate model organism. Additionally, drug & small molecule treatments can easily be administered via direct addition to the water in which the larvae are being raised, which can also allow tight temporal control of treatments. Most importantly, they regenerate their tails rapidly and completely allowing multiple experiments to be conducted in a relatively short timeframe for *in vivo* work. For example, larval tail regeneration is largely complete within 72hrs of injury whereas other popular regeneration models such as the newt takes months to regrow amputated limbs[61].

1.5.1 Mechanisms of zebrafish fin regeneration

To date, most work performed on zebrafish to dissect the roles of developmental signalling networks in regeneration have been carried out on the fins of adult fish due to their ease of access for amputation and observations of regrowth. This has yielded great insights into the molecular & cellular interactions regulating the regenerative process and although we do not fully understand the integration of all of these signals, we have extensive evidence that multiple processes can positively regulate regeneration. These range from molecular & genetic level interactions of intracellular signalling pathways, epigenetics and miRNA regulation, to cellular processes such as inflammation, apoptosis, autophagy and innervation, to supracellular wound environment conditions such as ROS levels, hypoxia, bioelectrical currents and vascularisation[37,62–71]. Although there are differences in the regulation of regeneration

between different model organisms in which it is studied, there appear to be more and more interactions identified in one species which are at least partially conserved in others, suggesting that there may be a core set of conserved interactions required to stimulate regeneration. Some of the most well conserved and most well studied mechanisms of regeneration are the reactivation of essential mitogenic and morphogenic developmental signalling pathways. Here, I will present a brief overview of the regenerative application of these developmental signals as we currently understand them, focusing on adult zebrafish fin but drawing parallels to other organ systems and regenerative organisms as appropriate to highlight the conserved nature of these interactions.

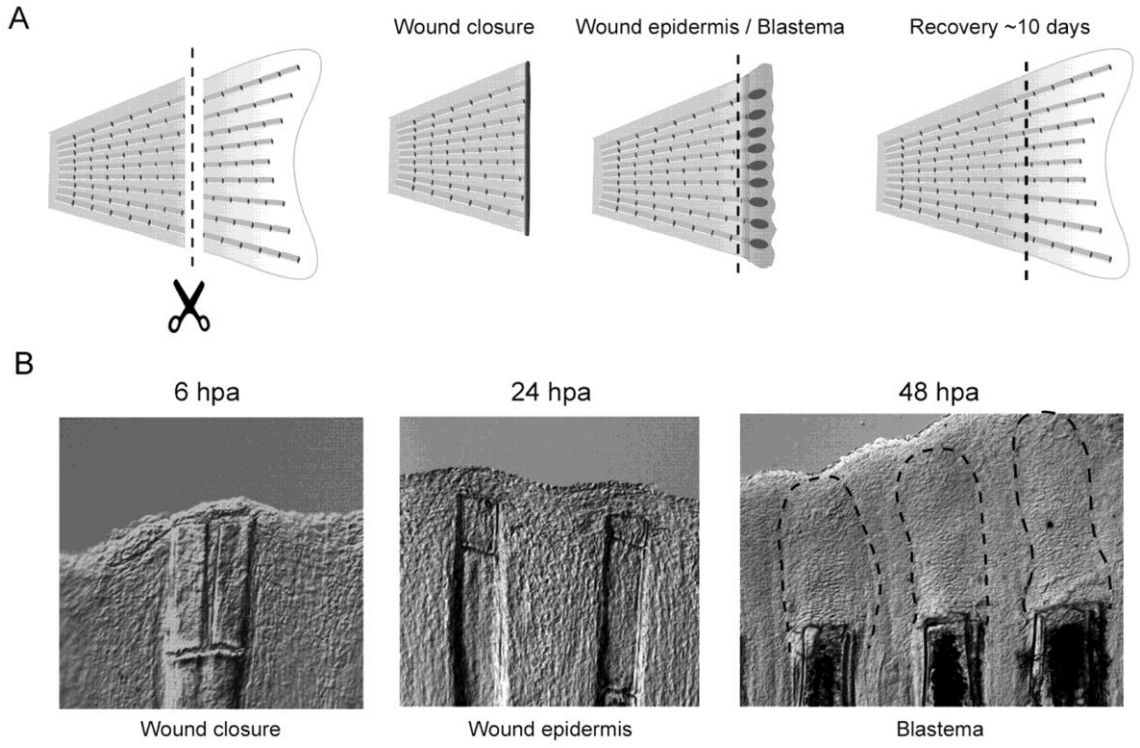

Figure 1.3 – Processes of adult fin regeneration (reproduced from Yoshinari & Kawakami, 2011[42]).
A) Schematic of the main steps in adult zebrafish caudal fin regeneration. **B)** Brightfield images of the regenerating fin tissues at key regeneration steps. The blastemal regions are outlined by the dashed lines.

Amputation of the adult zebrafish caudal fin results in wound healing and regenerative regrowth to restore a fully functional fin within 2-3 weeks of injury[42]. This is an example of epimorphic regeneration and is characterised by a number of steps – wound closure, wound epithelium & blastemal formation, proliferative outgrowth and termination of growth (Figure

1.3). Studies in the zebrafish have given us insights into the molecular and cellular regulation of these processes but much is still unknown, the current understanding is as follows.

1.5.1.1 Formation of the wound epithelium & blastema

The first priority after wounding is the restoration of epithelial barrier function in order to prevent further influx of pathogens and to begin the process of restoring tissue homeostasis. The breached epithelium is therefore rapidly restored by the migration of epithelial cells to close the wound. This process appears to have no contribution from cell division, likely due to the immediate availability of mature epithelial cells allowing more rapid wound closure than a proliferation-dependent process[72–74]. After closing the wound the epithelium thickens and forms an essential regenerative structure called the wound epithelium (also known as the wound epidermis). The wound epithelium is essential for regeneration in zebrafish, and its cells have a distinctive expression profile, including the upregulation of a number of homeobox transcription factors[75,76] and stimulate the formation and subsequent proliferation of the blastema at its proximal boundary via the release of trophic factors[77]. The wound epithelium is also essential for the initiation of regeneration in axolotl where preventing its formation or removing it daily both result in a failure to regenerate[78–81]. After wounding, the wound epithelial cells upregulate the expression of *fgf24*, and the mesenchymal cells proximal to the wound epithelia express the FGF surface receptor FGFr1 and are therefore capable of responding to FGF signalling. Chemical or morpholino-based inhibition of FGF signalling reduced the expression of blastemal-specific genes and blocked the overall blastema formation[82,83]. Additionally, the *devoid of blastema* mutant line carries a missense mutation in the *fgf20a* gene and forms an abnormal wound epithelium after amputation that cannot successfully initiate blastema formation[84]. Taken together, these studies show a strong role for FGF signalling from the wound epithelium to stimulate blastemal formation in zebrafish fins, a characteristic which is shared with zebrafish heart regeneration which requires FGF signalling from the myocardium to stimulate proliferation of new muscle[85].

The wound epithelium also upregulates both Wnt ligands and Wnt target genes, suggesting an autocrine signal that is important in wound epithelium maintainance[86–88], and additional studies have shown a requirement for Wnt signalling in the formation and proliferation of the blastema[88]. Further inter-species comparisons suggest that Wnt signalling may be a common feature of vertebrate epimorphic regeneration as it is absolutely required in zebrafish, *Xenopus* and axolotl[87,89]. In adult zebrafish, this Wnt signalling acts upstream of FGF signalling and

shows no reciprocal regulation[87,88,90], a relationship that appears to be conserved in larval regeneration as demonstrated by work from our own lab[91]. In contrast, however, adult fish express *shh* in a Wnt-dependent fashion[41,77,90], and Hedgehog (Hh) is unable to regulate Wnt signalling[90], suggesting that Hh is a downstream effector of Wnt signalling that drives blastemal proliferation[92] but in larval fish we identified Hh as the upstream regulator of Wnt, is devoid of any reciprocal regulation by Wnt, and induces proliferation via Wnt-dependent FGF activation[91].

Although the wound epithelium forms before the blastema, and defects in its signalling clearly retard formation of the blastema, there is mounting evidence that the blastema can also regulate the wound epithelium[93]. This suggests that, once formed, these regions interact in a co-regulatory manner to maintain their reciprocal activity. For instance, the formation of the blastema is dependent on retinoic acid (RA)-induced apoptosis of a sub-set of wound epithelium cells[94,95], however during regeneration, the expression of *aldh1a2* (encoding the enzyme catalysing the rate-limiting step in RA synthesis) is specifically upregulated in the mesenchymal cells proximal to the wound epithelium that will become the blastema, and therefore these cells are likely the source of that RA[96,97]. In addition, insulin-like growth factor (IGF) signalling appears to regulate cross-talk between the wound epithelium and the blastema. During regeneration, *igf2b* is upregulated in the blastema which acts in a paracrine manner to activate signalling in the wound epithelium[98]. Chemical or morpholino-based inhibition of IGF signalling resulted in impaired blastemal proliferation and regrowth concomitant with a decrease in Wnt signalling and increased apoptosis in the wound epithelium. As such it appears that IGF signalling acts in a positive feedback loop to maintain the cells of the wound epithelium and thus maintain their reciprocal pro-blastemal Wnt signalling.

In addition to the pathways described above, a number of other developmental regulators have been implicated as mitogenic & morphogenic regulators of regeneration including Notch, activin, PDGF, JNK, VEGF and mTOR[42,99,100] demonstrating further complexity in the control systems employed during regeneration that is supported by transcriptional analysis of regeneration-induced changes in gene expression patterns[76].

1.5.1.2 Proliferative outgrowth

It was initially assumed that the blastema was a homogenous collection of de-differentiated mesenchymal cells which proliferated to form all multiple tissue types in the regenerate[101], but elegant lineage tracing experiments using the Cre/Lox system to induce a permanent and heritable reporter within mature cells have shown that in zebrafish the blastema actually consists of a number of lineage-restricted progenitors. These progenitors are mature cells which have de-differentiated to a more plastic state where they are capable of proliferating to form new cells of the same lineage i.e. new osteoblasts were formed from mature osteoblasts and new fibroblasts were derived from mature fibroblasts[57,58,102,103]. There does, however, appear to be a mechanism for the re-establishment of a cell lineage through either transdifferentiation or division of a stem or progenitor cell population as seen by the emergence of *de novo* osteoblasts in osteoblast depleted fish[102]. It may be the case that such redundant mechanisms are maintained for extreme circumstances but lineage-restricted proliferation is the predominant mechanism for regeneration during normal conditions.

Patterning of the newly formed tissue is essential in order to ensure the correct cells are positioned in the correct positions to restore both form and function to the fin. Little is known about the molecular cues used to determine positional identity of the regenerate but some hypothesise that these processes may be linked to the position-sensing growth-rate control mechanisms described below. Studies of the Hh and BMP pathways have, however, shed some light onto the patterning of the growing bony fin rays.

Overexpression of *shh* led to the ectopic deposition of bone with abnormal patterning of the rays, and inhibition of Hh signalling by chemical treatment resulted in a loss of actinotrichia and decreased blastemal proliferation and subsequent outgrowth of the fin[77,90,92,104]. Ectopic expression of *bmp2b* phenocopied that of ectopic *shh*, and simultaneous expression of a BMP inhibitor was able to rescue *shh* overexpression suggesting that Hh controls ray patterning and regrowth via activation of BMP. BMP inhibition was independently shown to hinder regenerative regrowth and patterning but could not regulate *shh*, supporting this relationship[105,106]. Whether this represents a universal patterning mechanism or an osteoblast-specific mechanism is unclear and whether individual cell types will respond to their own population-specific patterning cues is an interesting question that will need much more work before it can be adequately addressed.

1.5.1.3 Termination of outgrowth

Termination of regenerative growth is an oft overlooked aspect of regeneration, yet it is essential to the survival of the organism. An overly-large fin would impair locomotor function, plus unrestrained cellular proliferation would be an energy drain and could be considered a cancer, therefore the full restoration of form and function requires an in-built size-sensing mechanism to terminate growth once the fin has reached the appropriate dimensions. Studies to characterise the molecular interactions of this process have only recently been fruitful and have separately identified 3 seemingly interdependent mechanisms that could potentially function together as a overall control system: Chemical inactivation of the protein phosphatase calcineurin resulted in an increase in the outgrowth of regenerating fins as well as an increase in homeostatic growth of uninjured fins suggesting that calcineurin could regulate both growth processes[107]. During regeneration, calcineurin activity was inversely proportional to the rate of fin regrowth and inhibition of calcineurin increased blastemal proliferation therefore it appears to function as a negative regulator of proliferative outgrowth required to terminate regeneration at the appropriate point. The authors suggest that calcineurin establishes a proximal-distal axis of growth and inhibition of the enzyme impairs the positional memory of the blastema and switches the fin to a more rapid, proximal growth rate. Interestingly, this is associated with an increase in RA signalling which has been shown to induce a more proximal patterning in regenerating fins in zebrafish[108,109] as well as in *Xenopus* and urodele amphibian limbs[110], and therefore may be the mechanism by which the positional identity is induced. Finally, a third study used a heat-shock inducible dominant negative FGF receptor to modulate FGF signalling levels and saw a tight correlation between the level of FGF pathway activation and blastemal proliferation and outgrowth rate, suggesting that FGF signalling levels modulated regeneration rate[111]. This appeared to be an indirect effect as extended obstruction of FGF signalling following wounding did not irreversibly change positional memory, and upon restoration of FGF signalling, fish were capable of regenerating normal patterned fins. The authors were unable to identify the upstream regulator of FGF activity but suggested RA as a likely candidate. Therefore although more work needs to be done to empirically test this hypothesis, I suggest that positional identity of the regenerating fin may be determined by the RA-dependent modulation of calcineurin and FGF signalling.

1.5.1.4 Larval zebrafish as a regeneration model

Although the majority of this work has been carried out using the adult zebrafish, more recently a number of labs have validated the larval zebrafish as regeneration model (Figure 1.4) due to a number of advantages, including a more rapid regenerative response which can be completed within 4 days[75], the ability to use antisense morpholinos for quick and easy genetic knockdown[112], and the ability to perform high-throughput screening to identify chemical regulators of the regenerative response[113]. Although the larval caudal fin is a transient structure of different cellular origin and composition to the adult caudal fin[114,115], it is thought that they employ largely comparable regenerative programs with similar spatio-temporal induction of regeneration genes[42,76,96,116] and a number of regenerative regulators validated in both adult and larval regeneration[75,82,113,117,118].

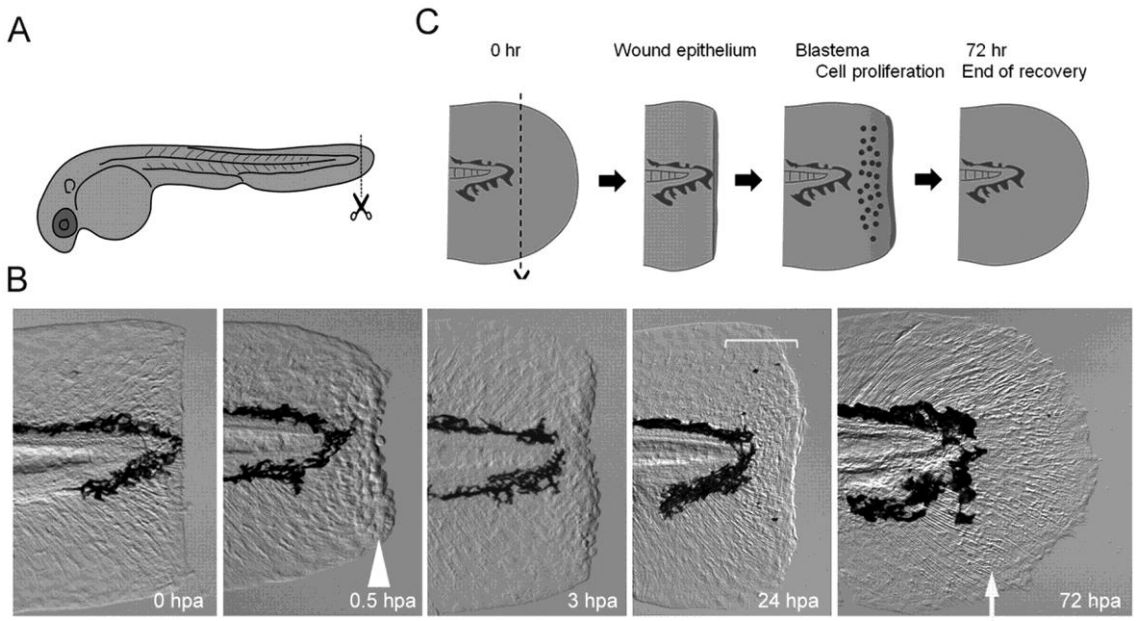

Figure 1.4 – Larval fin-fold regeneration (reproduced from Yoshinari & Kawakami, 2011[42]).
A) Diagram of a zebrafish larvae at 2dpf, showing where a fin-fold amputation would be performed. **B)** Brightfield images of the regenerating fin-fold over time. Within minutes of amputation, wound resident epithelial cells contract to seal the wound (arrowhead). Tissue contraction is terminated by 3 hours post amputation (hpa). From 3-48hpa, partially de-differentiated cells accumulate just proximal to the amputation plane and form a blastemal region (bracket) and divide to produce cells required to regenerate the lost tissue (arrow). **C)** Schematic of the main steps in larval (2dpf) zebrafish caudal fin-fold regeneration.

This larval model of appendage regeneration is what I will use in this thesis to investigate regenerative signalling. I will amputate the tail from the caudal edge of the pigment-gap with a

scalpel blade which will result in the loss of multiple cell types including muscle, notochord, neural tube, sensory axons and epithelia and allow me to study the coordinated regrowth of these varied cell populations. Although there are clear similarities, the regenerative processes employed by larval and mature fish are not identical; for example the wound-induced ROS signal is sustained for much longer in adult fin amputations than in larvae[119,120] and Wnt has been suggested as the most upstream regulator of adult regenerative signalling[90] whereas our lab has found evidence that this role is fulfilled by Hh signalling in larval regeneration[91]. These differences highlights the importance of studying both systems as complementary regeneration models to gain the greatest understanding of regenerative paradigms that we may be able to translate into therapeutic interventions to modulate human wounding.

1.6 Initiation of regeneration by ROS

Recent evidence has shown that H_2O_2 is essential for regeneration and that genetic or pharmacological inhibition of wound-induced H_2O_2 impairs regeneration in multiple species[43,120–129]. This wound-induced production of H_2O_2 has been attributed to the NADPH oxidase (Nox) family enzyme Dual oxidase (Duox) and appears to be a highly conserved wound response in planaria, *Drosophila*, fish, *Xenopus*, mice and humans[119,123,128,130,131]. As such, it represents one of the earliest possible divergence points between regenerating and non-regenerating organisms, therefore a comprehensive understanding of its regulatory effects and molecular and cellular interactions are necessary to compare and contrast the two responses. As one of the most upstream regulators it has the potential to control multiple downstream regenerative processes and therefore mediate wide reaching effects on regeneration. By analysing H_2O_2 effectors in human wounds and identifying any differences in regulation we may be able to identify a druggable target that could mediate similarly wide reaching effects on induced regeneration and improve therapeutic outcomes.

Currently, it is not clear how H_2O_2 mediates its pro-regenerative effects, and this is the central question to my thesis. Historically, the main role of H_2O_2 at the wound has been accepted as an antimicrobial agent via its interaction with invading pathogens. H_2O_2 itself is only mildly antimicrobial, but peroxidase enzymes convert it to much more potent hypothiocyanite, hypochlorous acid & hypoiodous acid which are responsible for the majority of its antimicrobial effects[132,133]. Whilst Duox-derived ROS are clearly important in reducing bacterial load *in vivo*[134], it is unlikely that this is the mechanism by which H_2O_2 stimulates regeneration,

and it is now becoming clear that this wound-induced signal plays multiple roles following injury. To begin with, the H_2O_2 signal is produced at the wound prior to the recruitment of the innate immune cells and their arrival actually causes a downregulation of the local H_2O_2 concentration as it is metabolised by neutrophil myeloperoxidase[135]. It has also been shown that leukocytes can directly sense ROS in multiple species and therefore H_2O_2 actually acts as an initiator of inflammation instead of just a product of the inflammatory response as originally described.

In addition to acting as a chemoattractant for leukocytes, H_2O_2 has been shown to stimulate a number of different pro-regenerative processes in the zebrafish following wounding including mitogenic signalling pathways, apoptosis and innervation[43,120,122,124] (A much more detailed description of the role of ROS in the regulation of regeneration is presented in Chapter 3). Furthermore, work carried out during my MSc project on the role of H_2O_2 in regeneration demonstrated that pharmacological inhibition of H_2O_2 prevents the wound-induced activation of Hh, Wnt and FGF signalling, which are all required for regeneration to proceed[136]. This was the first time that the wound-induced H_2O_2 signal had been shown to regulate developmental pathways required for regeneration but no molecular link was identified to mediate this interaction.

Taken together, there is abundant evidence that ROS can regulate regeneration via a variety of mechanisms, but there appears to be little convergence between studies. This suggests that H_2O_2 may induce multiple parallel pro-regenerative mechanisms. Understanding the relative importance of each of these interactions will be essential to direct our attempts to translate these findings into a human wound context.

1.7 Induced regeneration – proof of concept

One of the greatest challenges in the regenerative research field is the integration of the myriad of positive and negative regulators of regeneration that we are progressively identifying. The field is mainly focused on the reactivation of developmental pathways, but it is becoming clear that regulatory control is shared by a number of additional processes, including epigenetic modifications, miRNA regulation and bioelectricity[67,69,137,138]. Additionally, attempting to identify conserved regenerative mechanisms across species which may then prove amenable targets for clinical manipulation is another challenge, but we have progressed

to the stage where we understand enough to successfully induce *de novo* regeneration by intervention. Below, I discuss some of these successes and speculate about future directions.

Xenopus has been used as a model for the induction of *de novo* regeneration in the vertebrate due to the tadpole's refractory period – a developmental stage where the larvae temporarily loses its regenerative capabilities. This transient loss of regenerative regrowth allows analysis of the biological processes which cause the larvae to convert from regenerative to non-regenerative as well as providing a tractable environment which can be experimentally altered to rescue this regenerative defect. Using this model, gene expression profiles were compared between refractory and non-refractory injuries which highlighted a number of upregulated immune-related genes, suggesting stage-specific inflammatory responses[139]. Immune-regulation was confirmed using immunosuppressants or by preventing immune cell development with morpholino-mediated knockdown of *pu.1*, which both showed a modest improvement in regenerative outgrowth. Although a strong immune response was shown to impair regeneration, no evidence was given as to the mechanism of action or the molecular effectors of this regulation.

In addition to identifying immune inhibition during the refractory period, other *Xenopus* studies have shown differences in the bioelectrical signalling during this developmental period leading to another method for induction of regeneration. Voltage-gated sodium channels were required for regeneration, predicative of regenerative outcome and either misexpression of human voltage-gated sodium channels or chemical induction of a transient Na^+ current was capable of inducing regeneration from during the refractory period[69,140]. A separate study also showed that exogenous H_2O_2 was necessary and sufficient to induce regeneration from refractory tails via the expression of Na^+ channels, suggesting that H_2O_2 is the master regulator of this bioelectric signal[141]. Follow-up studies in the (usually non-regenerative) hindlimbs of stage 57 tadpoles showed that chemical induction of a transient Na^+ current induced hindlimb regeneration with largely normal (though not perfect) patterning suggesting that this process is not specific to tail regeneration or to a particular stage of development, raising the possibility of translating this into adult frogs[69].

As for mammalian examples of induced regeneration, work with cell lines has provided evidence that tumour suppressor genes may be preventing the induction of regenerative programs in mammals. In mice, simultaneous inactivation of the tumour suppressor genes *ARF* and *Rb* caused mature, post-mitotic myotubes to de-differentiate and re-enter the cell cycle. Single cells were capable of growing myofiber colonies and even capable of re-differentiating

into mature cells which fully integrate into existing muscle upon transplantation[142]. An independent study of *ARF* validated its regeneration supressing effects by ectopically expressing it in zebrafish. Introduction of the human *ARF* gene into zebrafish resulted in strong ARF expression in the blastema of regenerating fins and an inhibition of regeneration[143]. The impairment of fin regeneration is mediated via the combined induction of apoptosis and cell-cycle arrest via p53 dependent mechanisms. If vertebrates have lost their regenerative capability as an evolutionary trade-off to prevent cancer progression, this would raise severe complications for translational approaches, however the potential carcinogenic risks of a treatment could be minimised using localised and transient inactivation. Whether these translate to the organ and tissue level this will be interesting.

There have, however, been successful examples of induced regeneration in adult mammals without the need for direct manipulation of tumour suppressor genes. A series of experiments showed the potential power of growth factor regulation following wounding as mouse digit tip regrowth was induced by the simple implantation of a BMP-soaked bead to act as a mitogenic organising centre[144–146]. Despite improper patterning (no joint was formed between the phalangeal elements), the results were quite remarkable considering the crudeness of the treatment raising the possibility of recapitulating multiple mitogenic signalling centres in order to more accurately replicate regeneration conditions and improve patterning of the regrowth.

Another important limiting factor of regeneration appears to be the appropriate remodelling of the ECM. This may be of particular importance to mammalian regeneration given their propensity to deposit fibrous scar tissue at wound sites. For example, the MRL strain of laboratory mouse was discovered to not scar after being ear punched (a standard marking method for mouse experiments) and that the wound closes within four weeks and regenerates new skin with a completely normal macro- and cellular- structure[147]. By extensive outcrossing, this response was shown to be a heritable multigenic trait linked to at least seven loci[148–150]. Since this serendipitous discovery, the MRL house has been shown to be capable of enhanced regrowth following digit amputation and a full functional recovery of heart myocardium following cryoinjury[150,151]. This enhanced regenerative capacity over similar mice strains has been, at least in part, attributed to more active tissue remodelling with the increased MMPs and decreased TIMP activity at the wound allowing the remodelling of both deposited collagen fibres but also basement membranes[150–152]. Similarly, the FOXN1-deficient nude mouse, has been reported to regenerate small ear punches via the formation of a blastema structures[153,154]. The loss of functional FOXN1 precludes the formation of a thymus and subsequently, T-lymphocyte development in the mice and this has, at least in part, been

associated with their increased regenerative capacity. The altered immune response results in a more rapid deposition of collagen following injury but also, importantly, a secondary late-stage upregulation of MMP-9 and MMP-13 not seen in control mice[154]. The authors speculate that this additional spike in MMP activity is responsible for the remodelling and scar-resolution phenotype observed in the nude mice. This ability to remodel the extracellular matrix has also been identified as a pro-regenerative characteristic in other regenerating species including axolotl, newt and *Xenopus*, and even in zebrafish in the absence of scar tissue suggesting that ECM remodelling is required for regeneration in addition to its roles in resolving scarring[116,155–159].

A third mouse model of regeneration that is emmerging as perhaps the best example of extensive mammalian epimorphic regeneration is the African spiny mouse (*Acomys*). In addition to regenerating digit-tip amputations as other mice do[160], and ear punch wounds even larger than those regenerated in nude and MRL mice[161,162], two species of *Acomys* were shown to be able to regenerate up to 60% of their dorsal skin[163]. This appears to be a survival mechanism to avoid predation by autotomy of large patches of skin and is permitted by structural differences in the skin making it more prone to tearing. The mice have a lower overall proportion of connective tissue in the dermis and the collagen that is present is less densely packed and more porous than that seen in *Mus* skin. Together, this reduces the skin's elasticity and tensile strength. The signalling pathways activated during dermal regeneration in *Acomys* (Wnt and BMP) are very similar to those required for skin development, suggesting a recapitulation of developmental regulation not seen in the scarring *Mus* wounds. This has been independently verified in a third specied of Acomys showing complete functional recovery of large ear punch wounds[161]. The reasons for this increased regenerative capacity are still being investigated, but again they appear to be at least partly mediated by differences in inflammation and ECM deposition[164,165] and remodelling and will be discussed further in Chapter 4.

Scar deposition may be equally as important as scar resolution as a number of recent studies have shown that reduced contractile forces at the wound lead to less, or more ordered, deposition of transient scar tissue which is easier to remodel and therefore generates improved regenerative outcomes[166,167]. In addition to this, there is evidence of a conserved requirement of ECM remodelling in human wound healing too as studies of human airway epithelial repair have shown upregulation of MMPs[159,168] suggesting that regeneration may require appropriate control of ECM remodelling in humans. This may seem unsurprising given the extent of tissue remodelling inherent in regeneration but highlights the multifaceted

nature of the wound-response that we will have to deal with during potential therapeutic interventions.

It may be useful to establish a human model of induced regeneration in which translational experiments can be performed. To date, human work has been limited to standard cell culture or to histological analysis of very limited clinical samples. Whilst cell culture is rapidly setup and easy to manipulate experimentally, standard 2D cellular culture methods are not an accurate recreation of *in vivo* conditions, and do not allow analysis of the complex cellular heterogeneity, cell-cell interactions, migration & remodelling present in regenerating organ systems and therefore these methods are of limited use. The development of 3D culture techniques allowing generation of multicellular organoids[169] and 3D tissue printing technologies[170,171] which can replicate organs on biocompatible scaffolds. Analysis of organoid regeneration following wounding in these systems may provide invaluable insights in the transition to the clinic.

In summary, there have been multiple steps made towards *de novo* induced regeneration using a variety of manipulations of the wound response. The successful translation of these findings to a therapeutic intervention will require much more work to determine which of these processes are applicable and effective in human wounds. Indeed, it may be that simultaneous manipulation of multiple aspects of our wound response is required to induce robust regeneration. Successfully integrating these strategies will bring its own challenges but for now we can take them as validation of the principle of induced regeneration and continue to pursue our work characterising the regenerative wound responses with the assurance that this ambitious goal is not quite the moonshot that it first sounds.

Chapter 2. Materials and methods

2.1 Zebrafish husbandry

Zebrafish work was performed within the Bateson Centre at The University of Sheffield under the guidance of the Zebrafish Facility. Work conformed to UK Home Office regulations regarding the Animals (Scientific Procedures) Act 1986. Work was covered by Project Licence numbers 40/3459 and 70/8755 issued to Dr Henry Roehl, 70/8178 issued to Dr Stephen Renshaw, 70/8588 issued to Dr Tim Chico and my Personal Licence (No. 160CD305E).

Adult fish were kept by the Zebrafish Facility staff under a 14hr/10hr light/dark cycle at 28°C and fed twice daily with live Artemia or flaked food.

All "wild type" fish used were AB strain for consistency.

Zebrafish embryos were kept in E3 medium (5.0 mM NaCl, 0.17mM KCl, 0.33mM $CaCl_2$, 0.33mM $MgSO_4$) 40 larvae per petri dish and incubated at 28.5°C. The E3 medium was supplemented with 0.00001% methylene blue from fertilisation until 2 days post fertilisation (dpf) to prevent fungal infection.

For anaesthesia, tricaine (4mg/mL in water, pH 7) was added (at 4.2% total volume) to the medium at a final concentration of 170mg/L.

2.2 Drug-dosing larvae

A number of different chemicals were used to alter the embryos' response to wounding. The duration and concentration of each drug dose were determined empirically either in my Master's degree or the early part of my PhD based on starting ranges described previously where available[113,119,120,122,123,172,173]. Hydrophilic compounds were dissolved directly into E3 to obtain the desired concentration and hydrophobic compounds were prepared as stock solutions in a vehicle solvent (DMSO), then supplemented directly into E3 medium to obtain the final chemical concentration. The concentration of vehicle in the medium was limited to a maximum of 1%. Chemicals solubilised directly in E3: ascorbic acid (Sigma #A4403). Chemicals solubilised in DMSO: DPI (Sigma #D2926), MCI-186 (Merck Millipore #443300), BAPTA-AM (Merck Millipore #196419), PMA (Sigma #P8139), Bim-1 (Santa Cruz Biotechnology #sc-24003),

cycloheximide (Cayman Chemical #14126), PP2 (Cayman Chemical #13198), U0126 (Sigma #U120), beclomethasone (Sigma #B0385), ruxolitinib (Cayman Chemical #11609), SB203580 (Sigma #S8307) and nocodazole (Sigma #M1404). Table 2.1 below lists the timings and concentrations of the standard dosing for each chemical which was used unless otherwise stated in the text.

Chemical	Final Concentration	Duration
DPI	150µM	-1 to 1hpa
MCI-186	2mM	0 to 3hpa
Ascorbic acid	500µM	0 to 3hpa
BAPTA-AM	100µM, 1mM	0 to 30mpa
PMA	10nM, 50nM, 200nM, 400nM	0 to 24hpa
Bim-1	10µM, 100µM	-1 to 3hpa
Cycloheximide	50µg/mL	-1 to 6hpa
PP2	20µM	-1 to 6hpa
U0126	100µM	-1 to 6hpa
Beclomethasone	1µM, 10µM	-1 to 6hpa
Ruxolitinib	10µM	-1 to 6hpa
SB203580	26µM	-1 to 6hpa
Nocodazole	10µg/mL	0 to 6hpa

Table 2.1 – Pharmacological inhibitors.used
Details of the concentrations and duration of doses for the various chemicals used throughout my project.

Stock solutions were aliquoted and stored at -20°C with minimal freeze/thaw cycles to minimise chemical decomposition. Highly reactive compounds (MCI-186, ascorbic acid and cycloheximide) were prepared fresh for each experiment to avoid breakdown and ensure accurate concentrations.

2.3 Tail regeneration assay

The tail regeneration assay was based on previously described larval fin-fold amputations[75], but was performed at two different locations along the anterior-posterior axis of the larvae to examine the effect of different severities of wounding on regenerative signalling. The two amputation positions are detailed below.

2.3.1 Pigment-gap level amputations

2 or 3dpf embryos were anaesthetised with tricaine before amputations were performed with scalpel blades (Swann-Morton No. 15 blades). Transverse resections were made at the caudal edge of the pigment-gap to sever the end of the tail. As I was investigating very early wound responses, all chemical inhibitors were administered 1hr prior to wounding to allow absorption and distribution to the target cells to ensure effective inhibition from the time of wounding.

Embryos were returned to fresh E3 medium (plus drug of interest / vehicle control, as required) until fixation in 4% (wt/vol) paraformaldehyde (PFA) in phosphate buffered saline (PBS) overnight at 4°C. Embryos were dehydrated and rehydrated in methanol (MeOH), before removing endogenous pigmentation with a bleaching solution (0.5X SSC with 10% H_2O_2 and 5% formamide) and transferring into glycerol.

Embryos were mounted under cover-slips, examined with DIC illumination using a Leica MS5 stereomicroscope and photographed using a Jenoptik ProgRes C4 camera with ProgRes Capture software.

Regeneration was quantified using the open-source image analysis software Fiji[174] by measuring either 1) the linear distance from the caudal tip of the notochord to the caudal edge of the caudal fin, or 2) the total area of tissue beyond the caudal tip of the notochord as shown in Figure 2.1 below.

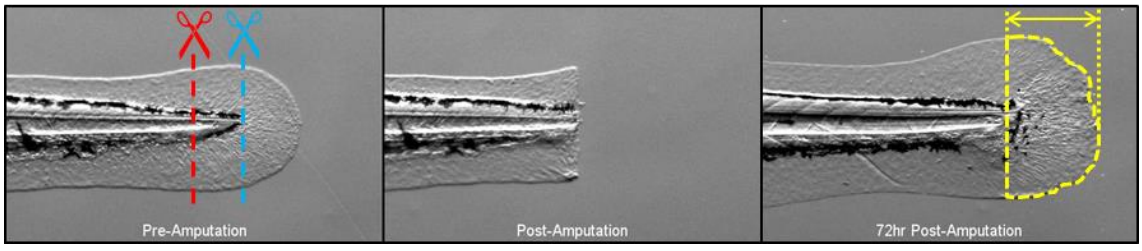

Figure 2.1 – Example larval tail regeneration assay.
The basic tail regeneration assay consists of an amputation of the tail, usually at the caudal tip of the fin-fold for the standard tail regeneration assay (red dashed line) or at the caudal tip of the body to study fin-fold regeneration only (blue dashed line). The extent of regeneration was measured either by linear distance from the caudal tip of the notochord to the caudal edge of the fin-fold (yellow dotted lines) or by the total area of tissue beyond the caudal tip of the notochord (yellow dashed region).

To quantify the extent of notochord extrusion, Fiji[174] was used to measure the area of the tissue protruding from the wound as show in Figure 2.2.

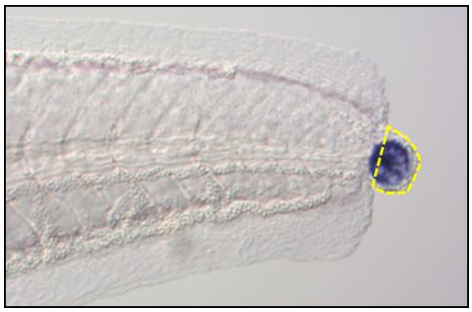

Figure 2.2 – Example notochord extrusion assay.
The notochord extrusion assay quantifies the area of tissue extruded past the end of the amputation plane (yellow dashed region).

In order to avoid any bias in the analysis, these, and all subsequent images, were analysed blindly after using a self-written Fiji macro to randomly rename the images (see Appendix A, Section 8.1). Briefly, the macro copies the selected images to a new folder and assigns a randomly generated number as the new image name; a list of original & blinded file names is also generated to reverse the process. The blinded images were then analysed by the methods above before those measurements were matched to the corresponding original images.

2.3.2 Fin-fold only amputation

In order to determine the cell-specificity of the wound-induced *ihhb* response, additional tail cuts were performed at the tip of the body where only the caudal fin-fold epithelium was removed, leaving the notochord intact (Figure 2.1 above, blue dotted line). 3dpf embryos were pre-dosed for 1hr with DPI or vehicle control, anaesthetised and the caudal fin-fold was resected with a scalpel. Embryos were fixed at 24 hours post amputation (hpa) or 48hpa to determine regenerate morphology or 6hpa for *ihhb in situ*

2.4 Wound-induced H_2O_2 assay

The H_2O_2 assay was based on the previously described method of detecting H_2O_2 in wounded zebrafish larvae[43]. 3dpf embryos were anaesthetised with tricaine before amputations were performed with scalpel blades (Swann-Morton No. 15 blades). Transverse resections were made at the caudal edge of the pigment-gap to sever the end of the tail. All chemical inhibitors were administered 1hr prior to wounding, for the same reasons as outlined above.

Embryos were returned to fresh E3 medium supplemented with 10µM of pentafluorobenzenesulfonyl fluorescein (PFBSF; a H_2O_2-specific fluorescent sensor; Santa Cruz Biotechnology #sc-205429) plus drug of interest / vehicle control, as required. At 30 minutes post amputation (mpa) embryos were imaged under a Zeiss Axio Zoom.V16 stereomicroscope with an AxioCam MRm camera and Zen 2 (Blue Edition) software. 2-channel, brightfield & fluorescent (YFP filter: 489-505/516/524-546) images were taken.

The H_2O_2 signal was quantified in Fiji using a self-written macro (see Appendix A, Section 8.2) in order to maximise reproducibility whilst minimising human error and subjectivity. Briefly, the macro automatically detects the embryo outline, measures the mean fluorescent intensity within 50µm of the wound edge and the median fluorescent intensity from an area of trunk distal to the wound. The median fluorescent intensity of the trunk is then subtracted from the mean fluorescent intensity of the wound to control for the basal oxidative state within each embryo. An example is shown below, with the fish, wound area and trunk regions outlined in white, yellow and red, respectively.

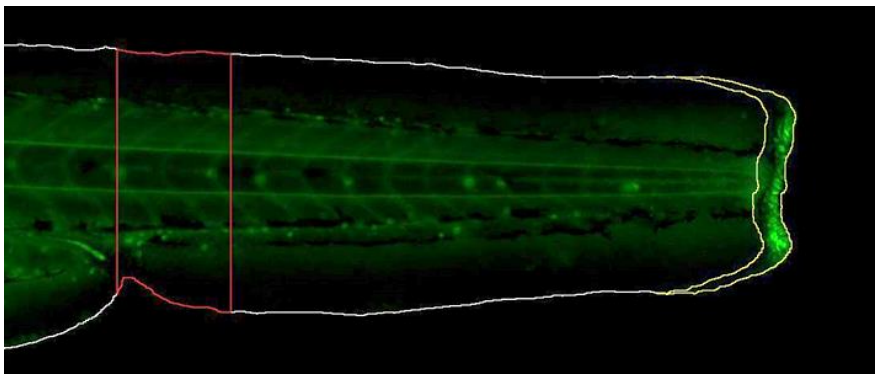

Figure 2.3 – Example amputation-induced H_2O_2 assay.
The extent of H_2O_2 production following wounding was quantified using a fluorescent H_2O_2 reporter dye (PFBSF) shown here in green. The body of the fish is outlined in white, the wound area to be quantified in yellow and a distal trunk region for normalisation of the data in red.

2.5 Whole-mount *in situ* hybridisation (WISH)

2.5.1 Probe synthesis

Antisense RNA probes were synthesised from template DNA as follows:

2.5.1.1 Template DNA synthesis

For probes contained in plasmid vectors, vector-specific primers were used to PCR-amplify the target probe sequence; for probes synthesised directly from cDNA, probe-specific primers were used for nested / semi-nested PCR reactions to specifically amplify the target probe sequence. Taq DNA polymerase (New England Biolabs (NEB) #M0273) was used for all reactions in the PCR reaction mix outlined in Table 2.2.

Reagent	Amount Added	Final Concentration
10X Taq reaction buffer	10µL	1X
dNTPs (25mM)	1µL	200µM
Forward primer (100µM)	1µL	200nM
Reverse primer (100µM)	1µL	200nM
Template DNA	20ng	200pg/µL
Taq DNA polymerase (5U/µL)	2µL	100mU/µL
MilliQ water	Up to 100µL	-

Table 2.2 – PCR reaction mix.
Details of the standard PCR reaction mix for the amplification of DNA.

PCR reactions were carried out with the following incubation program: 95°C for 60s, 35 cycles of {95°C for 30s, T_{Anneal} for 45s, 68°C for 1min/kb}, 68°C 5min. PCR reactions were purified with Amicon Ultra 50K centrifugal filters (Millipore #UFC505024) before running on a 1% agarose gel to check amplification specificity. Concentration was determined using a NanoDrop ND-1000 spectrometer (Thermo Fisher).

2.5.1.2 Probe transcription

Digoxigenin (DIG)-labelled RNA probes were transcribed for 2hrs in 30µL reactions as outlined in Table 2.3.

Reagent	Amount Added	Final Concentration
Template DNA	1µg	33.3ng/µL
10X transcription buffer	3µL	1X
10X DIG DNA labelling mix (Roche #11277065910)	3µL	1X
RNase Inhibitor (NEB #M0314)	1.5µL	2U/µL
T3(NEB #M0378) or T7 (NEB #M0251) RNA polymerase	1.5µL	2.5U/µL
Nuclease-free water	Up to 30µL	-

Table 2.3 – DIG-labelled RNA probe synthesis.
Details of the transcription reaction mix for the synthesis of DIG-labelled antisense RNA probes for WISH.

After synthesis, the reaction mix was purified via RNAse free DNAse (NEB #M0303) treatment and SigmaSpin columns (Sigma #S5059). Probes were eluted into 14µL RNAlater (Sigma # R0901), run on a fresh 1% agarose gel to check transcription specificity & yield, and stored at -20°C until use.

2.5.1.3 List of WISH probes used

Table 2.4 below describes the RNA *in situ* probes used throughout my project:

Probe	Plasmid Backbone	Forward Primer	Reverse Primer	Probe Sequence	Pol	Conc^{n} for WISH
ihhb	pUC18	M13F	M13R	5'-GAATTCGAGCTCGGTACCCGGGGATCCGGGGGGTCTNAAATTNGGGGGGTCTNAAATTATCGCTAAATATAGCGACAAAGTCACTAAGT TGGCAACNCNGTTCAACTGACATCAAATTAATTTCAATTTTTGACATTTTTAATGTGTTTTTGATGTCGTTTGACATCAAGGTGACCTTTTACAT CACAAACCCTGAGCTTGTGATCATCTCTTTTGACAACTCTCTCCACCAATCCCTGCGTTTCATTTCAATCCATCATCTCTCAGTTGCCTCTAAGGC CAAAGGGTGGAAGAGTTCTGAGTCTAGCAGTAGTTTTCCCAAACCTATCAGGACCTGAGAGTACCAGTGTAAGCCATTCTTAAGGACCTGAT CTGGTCCGGTCCAGCTATACAGCAAGCGTAGAGGTGCAAAAGCCCAATGAGCAAGTCTTTGCCTGTTCACCGCAGCATAACAAGAGGTGAG CACATCGTTCACCACTACAGTCCCATGAGCAGTAAGTGGAGGGTATAACCCCTGGTCCTCCCGAACCCCAACATGAGTGATCTGTGAAAAAC GCTTCCTGAGTTTACCCAGCAGCAAACACTGACCCACTTGAGCATCGCTGGCAAATATCGTCCGGACTGCTCCTGGTTTGGGTTCCCCCCTGTT GGAGCAGTTTCCAACCCTCATAAACAGTAAATGAGCCGCTGTTAAAGACACGCTGGCCCCATCCTCAGTGCGGATCACATAGAAGTGCTTCT GGGTAATGGGGCGACGGTCCAAAAAGGTGAGGACTTCACTATAGATGAGGTCTCCTGTCCCGTCGCTTCCCTCAGAGGCCAGAACCAAGTC TCCTGCCTGCAAATCACGGATTTGTCGATGGGAACCATCCTTCATGGTCACCAGAGCCCTTCCAGGAAAACAGCCTCCTGTTTTTGCTGCTACT GAATGCTCTGATTTGACACTGCAGTGTACGTGGCCTTTGGATTCGTAATAGACCCAGTCGAAGCCTGCTTCCACCGCAAGACGAGCCAGCAT GCGGTACTTGTTGCGATCGCGGTCCGAGGTAGTAATGTCCACCGCTCTGCCCTCATAATGCAGAGATTCTTCAGAGTGTAGTCCGTCCTCATC CCAGCCCTCCGTCACACGCAGACGCACACCGGGCCACAGGTTCATCACCGAGATGGCCAGAGAGTTCAGCTTATCCTTGCAGCGCTGCGTCA TCATGCGGTCCGCACCTGTGTTCTCCTCATCCTTGAAGATGATGTCCGGGTTGTAGTTTGGGGTCAGCTCTTTAAAGCGCTCGGAGCTGGGG GTGACCTTCCCCTCATATCTCCCGCTCGCCCCCAGCGTTTTCTCGGCTACGTTCGGACTGAACTGCTTATAGGCGAGAGGCGTGAGTTTCCGC GGAGTCCGTCTCTTGCCGTAACCTCTGCCCGGTCCACAGCCGTCGTACGCCGGCGAGAAAGCCAAGATGAAGCCGGTGAGGAGCGCCGCCG CCGTGGAGAGTCTCATTCTAGAGTCGACCTGCAGGCATGCAAGCTTATTCCCTTTAGTGAGGGTTAATTTATATAGCTTGGCACTGGCCGTCG TTTTAC-3'	T7	2%
shha	cDNA	5'-CCTCTGA CCGAGACA AGAGC-3'	5'-(GGATC CAATTAAC CCTCACTA AAGGGAA) GCCACGTT CCCATTTG ATAC-3'	5'-GCCACGTTCCCATTTGATACAGGAGCCTGGAGTACCAGTGGACCCCCTCCTGTTGTAAAGTCGCATTGGACCGACTGCTGGAGTTTTGGG GGAACAGGAATGATGACACGTAATAATAGAGCCTGGCGGGCGCGAAGGCCAAATGCGCAAGCCCCTGGTCCTCTATTACGGCGTAACAGG ACGCCAGTATTCTGTCGACCACAATGGTCCCATGTGCAGTCACTGGTGCGAACGAGCCCCGCTGCTCCTCCGTGTATATCCGCTGCACGATGA CAGATTTAAGCTGACCGCTATCATCAACAACCATCACCTTTTGTCCGGCTCTGACACTGCTGGCATACGCGGCGGTCATGGTGTGGAGATCTT CCGTTGAGTTGTCGAGGACAAAAAGGAGGTGAGCGGCGGTGAGGGTGATCTTTTCAACGGGTTCTTGCGTTTCTATGACGTAAAACACACG TCGCGTCGTGGAGTCTCGGTCTGTGAACATGATGAAGTCGCTGAACACCAGGTTTCCCGCGCTGTCTGCCGCCAGCACCTTGTCTCCGGGGT TCAGGTCCTTCACGGCCTTCTGTCCTCCGTCCTGGAGCGAGACCAGAGCCGAACCTGGGAAACAGCCCCCAGATTTCGCAGCAACCGAATTTT CTGCTTTGACAGAGCAATGAATGTGGGCTTTGGACTCGTAATAGACCCAGTCAAATCCAGCCTCCACAGCTAGGCGAGACAGTGTCCCGTAT TTGCTCTTGTCTCGGTCAGAGG-3'	T3	4%
ptch1	pBSK	M13F	M13R	full length cDNA clone	T3	4%
dlx5a	cDNA	5'-ATCTCCA ACCCTACCG GAGT-3'	5'-(GGATC CATTAACC CTCACTAA AGGGAA)G GAGACT GCGGTGA GTTAC-3'	5'-GGGAGACTGCGGTGAGTTACACGCCATTGGGTCGCTGGAGCTGGGGCTGTGTTCTGGGGGCAGTTCGCCGTTTTTCATAATCTTCTTTAG TTTTGATCTTTTGTTCTGGAACCAGATTTTCACCTGTGTCTGTGTGAGTCCCAGCGATGCGGCGAGCTCGGCTCTTTCTGGAAGCGCGAGGTA TTGCGTGTTCTGAAACCTTCTCTGTAAAGCTGCGAGCTGGAAACTGGAGTAAATGGTTCGGGGCTTCCGGACTTTTTTGGGTTTTCCGTTGAC CATCCTTACTTCGGGCTCGGCTGTTTCTTTTTCTTGCGGGCTCGGTTGTGATTGCACTCTGTTATATGTTCCTGCGTATTGGTGATACGCTGTG GAGTATGAGCCGTAATCAGGGTAGGATTTTGCAGAGTAATTTCCAGAAGATCCATTGACTCCGTGGTATTGGTACTGATAGGCATTAAGAGG TTTCCCATAGGTGCCCGAGTTCGGTGAACAATAGCCATGATGAACTCCTCCGGCAGGGCTGTAATAGCCAGAATCCGTGGCTGTGGACTCCG GTAGGGTTGGAGAT-3'	T3	2%

Probe	Plasmid Backbone	Forward Primer	Reverse Primer	Probe Sequence	Pol	Conc^{n} for WISH
msxc	cDNA	5'-CAGAACAAGCTCACGGACTTT-3'	5'-(GGATCCATTAACCCTCACTAAAGGGAA)ACGCAGGTAATAACGGCTTG-3'	5'-CATTTTGAATCCTCCGAAAGGACACTGGCAGGACAGGGCGTTATAACAGTTAATCCAGACGGTGCCGGCCTGCACTGCTGCAGAGATGGTCATGGCCTTGCTGATATCTCTGGTGAAGACGGCCGCTGCCAGACCGTATTCTGTGTTGTTGGCTCTCTCAATCACTTCTTCAATTGTTTTGAACTTCATGATTTGCTGCACTGGCCCAAATATCTCCTCCTTGGCGATGCGCATGTGGTCCTTCACATTAGAGAAAACTGTGGGCTCCACGAAGAAGCCTTTAGTAGGAGGAGCTTTGCCTCCACACTCCAGTTTGGCTCCTTCAGTGATGCCACTCTGGATGAGCTCCAGCACACGTCTCTGCTGCTCCTCGCTCACCTGAGGTCCGTGTTCAGTGGTTGGGTCAAAGGGATTTCCCACTTTCCTCCTCTGTGCTCTCTCAACACTTCTTCTCACAAACTCATCATAAATGGGCTCCTCAACAAAGATACGGGAACCAGCAGTGCAGCATTGACCGTTATTGAAGAAAACCCCCTGATGGGCCTGTTCTAATGCCAGCTCAAAATCAGCATCTGCAAAAATGATGTTGGGACTCTTTCCCCCGAGCTCCAGCGTGACTCTCTTCAGATTGCTCTTTCCTGCTGCTTCTTGGATCAGCTTGCCTACCTCAGTCGATCCTGTGAACGCCACTTTGTCTATGCCCATGTGCGAAGAGATCGCGGCTCCTGCGGTTGGCCCATAGCCTGGCAAAATATTGACGACTCCCGGTGGAAACCCAGCCTCTTTGATCAGAGCGCCGAGGTAGAGGCAGGTGAGAGGGGTTTGCTCAGCAGGTTTCAGGACAACCGTGTTCCCGCAGCTCAGCGCCGGCCCCAATTTCCATGCTGTCATCACCAGGGGGAAGTTCCAAGGAATGAT-3'	T3	3%
aldh1a2	cDNA	5'-ATCATTCCTTGGAACTTCCC-3'	5'-(TAATACGACTCACTATAGG)CATTTTGAATCCTCCGAAAGG-3'	5'-CATTTTGAATCCTCCGAAAGGACACTGGCAGGACAGGGCGTTATAACAGTTAATCCAGACGGTGCCGGCCTGCACTGCTGCAGAGATGGTCATGGCCTTGCTGATATCTCTGGTGAAGACGGCCGCTGCCAGACCGTATTCTGTGTTGTTGGCTCTCTCAATCACTTCTTCAATTGTTTTGAACTTCATGATTTGCTGCACTGGCCCAAATATCTCCTCCTTGGCGATGCGCATGTGGTCCTTCACATTAGAGAAAACTGTGGGCTCCACGAAGAAGCCTTTAGTAGGAGGAGCTTTGCCTCCACACTCCAGTTTGGCTCCTTCAGTGATGCCACTCTGGATGAGCTCCAGCACACGTCTCTGCTGCTCCTCGCTCACCTGAGGTCCGTGTTCAGTGGTTGGGTCAAAGGGATTTCCCACTTTCCTCCTCTGTGCTCTCTCAACACTTCTTCTCACAAACTCATCATAAATGGGCTCCTCAACAAAGATACGGGAACCAGCAGTGCAGCATTGACCGTTATTGAAGAAAACCCCCTGATGGGCCTGTTCTAATGCCAGCTCAAAATCAGCATCTGCAAAAATGATGTTGGGACTCTTTCCCCCGAGCTCCAGCGTGACTCTCTTCAGATTGCTCTTTCCTGCTGCTTCTTGGATCAGCTTGCCTACCTCAGTCGATCCTGTGAACGCCACTTTGTCTATGCCCATGTGCGAAGAGATCGCGGCTCCTGCGGTTGGCCCATAGCCTGGCAAAATATTGACGACTCCCGGTGGAAACCCAGCCTCTTTGATCAGAGCGCCGAGGTAGAGGCAGGTGAGAGGGGTTTGCTCAGCAGGTTTCAGGACAACCGTGTTCCCGCAGCTCAGCGCCGGCCCCAATTTCCATGCTGTCATCACCAGGGGGAAGTTCCAAGGAATGAT-3'	T7	1.5%
axin2	cDNA	5'-GGAAGAGGGTGAGACGACAT-3'	5'-(GGATCCATTAACCCTCACTAAAGGGAA)ATCCGCACACCAGCTTTAGA-3'	5'-ATCCGCACACCAGCTTTAGACCTCCTAGACCATTGGGATTCACATGACTGGGGTTCTCGCACCCAGTTCTGACATACTCGAGGTATATGTCCGAGGTCAAAAACATCTGATAGGCATTCTCCTCCATAGCCGTCTGGATCTCCATTTGAGCCTGATCAAACATTGCAGAGTCAATCTGCTGACGCTTAATATTATCCCTAATAAAGGTCTTAGTGGCAGGTTTAAGCTGCTTGGCCACAATGCTGTTGTTCTCAATATACCGCTTGTAAATGGCTTTGGCAACTCTGTGCGTTTTGGTATCCTTGAGGTCCATTTGTCTGAAACCATTGCAGGCAAACCAAAAATCTAAAGTGTCCACACATTTCTCGCGTTCAAGGTATGCCCGGAAAAGTTGAGCACCATCCTGGTCCCCGAGAAGAAAATGCAAAGATTTGGTCCACCGGGCAAGAGGGGAGTCCGGGGGATGCGCTGCCCTCAGGTTCCCCAAGTCCATCCTCATCCCTCCTGGCCGTGGAACAACGAAGATCAGCCATAATGGTCTTGACAGGATCCTTCGGTCTCATCATGGCCAGTTTGCTGGGATGGTGGCATGTCGTCTCACCCTCTTCC-3'	T3	2%
pea2	pBSK	M13F	M13R	full length cDNA clone	T7	2%
col11a1a	cDNA	5'-TTCCCTCGTCCTGGTTCTGC-3'	5'-(GGATCCATTAACCCTCACTAAAGGGAA)GTCGTAAGCTGCTTTAGGGTCAG-3'	5'-AGTCGTAAGCTGCTTTAGGGTCAGCCACAATCAGCAGTTGTTGTATATCACCCTCAAAAGATTCCTCATCCAGGATCCTGGTGCCAAAAACGGTGATACCCTTGGTGTCGATACTGGCATGGTCACTCCTGCCCAATGGCTTGGTCAGCTTCTTCTTACAGTCGACAACAATAGTCACTGTCTTCTTCTCAACGCTGATGCCTACGCGATGCCACTTTCCGTCGGCCAGATTGAGAGCGCGGAACAGAGGGTAATCCTCCGGGGCAGGTTTGCCCTCCTGATCCTCGTACAGGAAGACAGGTGAACGGCCCACCTCCACGCCCAGCTGCTGGACGCCTTTCTCATTGTAGATGGACAGGAGGAAGGACTGGATCCCTGCTTTGGGCTTGATCGTGGTTAGGATGGAGAAGTCTTCAGGGAAAACGCCATCTGGGAAAAGCTGCTTGGTCGGGGCACTGAGCTGGGCATTCTTGCTGATTTTGTAGGCCGCGTCTGGCTGTGATGCTCTTCGGTTTGTGCAGAATCCTGACGTTTTCTCTACTCCTTCTGGGACAGTGGGAAATTCTAATACTTTTAAGACATCCACGGGTTCTGCTCTGACATGTGGAGCCTGCAGAACCAGGACGAGGGAA-3'	T3	2%

Probe	Plasmid Backbone	Forward Primer	Reverse Primer	Probe Sequence	Pol	Conc^{n} for WISH
tcf7	PCR2	5'-TCATCACTGGTCAGCGAGAC-3'	5'-(TAATACGACTCACTATAGG)ACCAGTCCGTCTGTTGGTTC-3'	5'-ACCAGTCCGTCTGTTGGTTCAGGCCGAAGCGAGCGCGGCATTTCTTTGGAGAGCCAGGCCCTGTACTGGAGTCCTGCTGCTTGTCCCGTTTCCTCCGCTTCTTTTTGCCCAAAGCACTCACGTAGTTGTCACGGGCCGACCAGCTGGGGTAGAGCTGCACGTGCAGCTGCCGCTCCTTACGGGCCAGCTCATAGTACTTGGCCTGTTCCTCACGGGTCAGAGCGTGCCACCGGCGGCCCAGGATCTGGTTGATGGCGGCGCTCTCCTTCAGTGTGCACTCTGCGATCACTTTAGCGCGCATCTCCTTCATGTACAGCATGAACGCATTCAGAGGCTTCTTGATCACCGGCTTCTTGGGCTCCTTCTCCCGCTTGGCCTCCGCATGAGACTTGTTATAAATGCTCCTGTCGAACTGATCGTGCTCCTGCTTTCCTGAAGGGGGCACTATAGCGGGGTGAGGGATTCCTGTGGGGTGCATACCGGACTGCAGCATCAGAGAGTGAGAGAACCAGTTCATGGAGGGCGTGATCTGACCCTGAGGCAGCGAGTAGAAACCCGAAATCTCCTGCGTCTGATGTCTGTGAACACCTGGTTTCTGTCCTCCGTCTGTGGGCATGTGTGTGGGACTGGGGTTGAAGTGTTCATACGGCAGCAGCGGCGTCAGCGGATGCATCCCCTGCTGGACCACCGACACCTTGTTGGAAGGTGGAGAGACGGGTCCGTTGGGCAGATACGGCTCCGGCAGCATCAGGAACGGGTATCCGGAGTACGGCGCTTTATACATCCCTCCATCGTGATGTTTGGGCACGTCGTCCAGATGTTCTCGTTTATCGCTGTAGATCCTCTGCTCGTCCTGCTGTCCTCTTCTGATCACGGCTGGGCTCTGGCTGATCTCGGTCTCGCTGACCAGTGATGA-3'	T7	2%
mpx	cDNA	5'-CCCTAACACCTGTCTCCCTG-3'	5'-(GGATCCATTAACCCTCACTAAAGGGAA)AGGGCTGGATAGTCAAGTGG-3'	5'-AGGGCTGGATAGTCAAGTGGGCAAAACGGAAAGCAGCAGTGGCAAAGACGTTCGCAATGGTAGGGTCCACATTCTCATTGTAACCTGGATATGGTCCAAGGTGTCTATTGTAAGCATCAGGGCCTACAATTAGTGGCAAGTATTCCTTGATCACCAAGATCTGATTGAATGCACCAACAATTTTTCTTGCTTCTTGATAAAGAGTTTCACTACTCCATGTAGGGTTGAGCACATGAAGGGCACGAGCCAATCTATTGTGCTCCCTTACAAAAAGTGTGTGTAAGGAGTTCAGAGCAGGATTCTCATCGACACGAGCATCACCCGCAATGAAGCAAGGAACCTCTGTCAGAGTGCTGTCGTTGAGGATTTTCTGACGAGTGGCGCACAAGTTGGTGTTAACACTAGTAAAGGGCAGGAGCTCTCGTCCATTGTCTTTAAAACGATTATTGACACGTAAAAGACCACCATCATTAGTAAGGTCCCGCAGTTCCTTTGCTAGTCCATCCTCTGAACCGTAAACTTGTCCAGCATCTAGGTAAGCTGTTAGAGTATTGATCTGTTCCCGAACATTTGGGACTTCACCAAACATGTAGGCAGTGTGCCCAGAACCACAAGTCGGTGCTGACCGGAAGACAGGGAGACAGGTGTTAGGG-3'	T3	2%

Table 2.4 – Primers for RNA probe synthesis.
Details of the primers used and probes synthesised for WISH.

2.5.2 WISH protocol

The protocol was adapted from the 2010 update[175] to the Thisse & Thisse whole-mount *in situ* hybridisation protocol[176]. The standard methods were used with the following modifications:

- Embryo preparation
    - Embryos were fixed in 4% PFA overnight at 4°C, washed in PBS + 0.1% Tween (PBST), then gradually dehydrated in a series of MeOH washes (1 X 30% / 1 X 60% / 3 X 100%) before being stored overnight in 100% MeOH at -20°C.
    - Rehydration steps were carried out with the reversed series of MeOH dilutions, back into PBST.
- Permeabilisation with proteinase K (Sigma #P6556)
    - 18hpf: 5min
    - 2-4dpf tail staining: 10min
- Pre-antibody block was performed for 4hrs.
- Alkaline Phosphatase (AP) conjugated anti-DIG Fab fragments (Roche #11903274910) were used at 1:10,000 dilution (in block)
- Probes were diluted in Hyb^+ buffer to 1-4%, (exact concentrations for each probe are listed in Table 2.4 above)
- NBT/BCIP staining was carried out at room temperature (RT) for 1-3hrs, depending on the probe, and was stopped when a strong signal had developed.
- At the end of the labelling reaction – i.e. after inactivating the AP with EDTA:
    - Embryos were post-fixed in PFA for 30min at RT, before being incubated in 100% MeOH overnight to remove background staining.
    - Embryos were gradually transferred back into PBST in a series of washes of decreasing MeOH concentration.
    - For any embryos that had developed natural pigmentation (all 2dpf and 3dpf larvae tested here), bleaching is required to lighten the markings enough to allow clear differentiation between pigment and positive staining. Embryos were incubated in bleaching solution (0.5X SSC with 10% H_2O_2 and 5% formamide) for 10-20min and the reaction was stopped by multiple PBST rinses.
    - Embryos were mounted in 100% glycerol for imaging and long-term storage.
    - Embryos were mounted under cover-slips, examined with DIC illumination using a Leica MS5 stereomicroscope and photographed using a Jenoptik ProgRes C4 camera with ProgRes Capture software or a Zeiss Axioskop2 stereomicroscope and photographed using a Zeiss AxioCam ERc 5s camera with AxioVision 4.8 software.

2.5.3 Quantification of WISH images

After imaging, the extent of expression of the target gene was quantified using FIJI using self-written macros (see Appendix A, Section 8.3) in order to maximise reproducibility whilst

minimising human error and subjectivity. Two macros were written, one to set the limits for the quantification, and a second to quantify the area of staining.

The RGB images obtained from my WISH experiments can be converted into three 8-bit greyscale images representing the red, green and blue channels and each pixel has a value between 0 and 255 based on its intensity in that channel. RGB colour thresholds simply set a maximum and minimum intensity for each of the red, green and blue channels, and then select all pixels which fall within the set ranges for all three channels. This allows pixels of a specific colour to be automatically selected based on their RGB intensity values.

For this analysis, strong and weak stainings were manually analysed to determine appropriate RGB colour threshold values which defined the area of the blue dye (oxidised BCIP) deposited during the WISH procedure. These RGB thresholds were manually set for each experiment due to the inherent variations in the enzymatic WISH staining procedure, combined with differences in probe staining patterns, but remained constant during quantification to allow comparative analysis. In practice, the RGB thresholds varied little due to similar staining and imaging protocols. Once manually determined by a trail-and-error procedure and visual confirmation, these values for each of the RGB channels are input to the first macro which saves them to a temporary file. The second macro imports these RGB threshold values from the temporary files and quantifies the number of pixels within the wound area which fall within this RGB threshold. This macro also records the mean RGB value of the staining area, intended to give some information on the average colour (and therefore intensity) of the stain (weak staining is lighter than strong staining), but this was not used in any subsequent analysis.

2.6 Quantitative PCR

2.6.1 RNA extraction & cDNA synthesis

For developmental gene expression, 30 x 18 hours post fertilisation (hpf) larvae were pooled, and for wound-specific gene expression, 100 wounds from 3dpf larvae (~0.16mm² tissue) were pooled. Samples were transferred immediately into 1mL TRI Reagent (Sigma #T9424) and homogenised.

RNA was extracted from homogenate by addition of 200µL chloroform and vigorous mixing by hand for 60s. Samples were incubated at RT for 5min and centrifuged at 12,000g for 15min at 4°C. 500µL of the aqueous fraction was transferred to a fresh tube with 500µL isopropanol,

mixed and incubated for 10min at RT before being centrifuged at 12,000g for 10min at 4°C. Supernatant was removed, the RNA pellet washed by gentle inversion in 1mL 70% ethanol (EtOH) and samples re-centrifuged at 7,500g for 5min at 4°C. This EtOH wash was repeated twice more. After the final wash, EtOH was removed and the RNA pellets were left to air-dry before being re-suspended in 25µL RNAse-free water. RNA quality was assessed with a NanoDrop ND-1000 spectrometer via 260/230 and 260/280 ratios[177].

cDNA synthesis was performed using a SuperScript II reverse transcriptase kit (Thermo Fisher #18064014) as follows: A 20µL reaction was performed with 500-700ng and 1µg RNA for wound-specific qPCRs or whole embryo qPCRs respectively. Input RNA was diluted in 8µL MilliQ water and 1µL oligo dT (500µg/mL) and 1µL dNTP (10mM) were added. Samples were incubated at 65°C for 5min, and chilled on ice for 10min. 2µL 5X FS buffer, 4µL $MgCl_2$ (25mM), 2µL DTT (0.1mM) and 1µL RNase OUT (Invitrogen #10777019) were added to each tube, and incubated at 42°C for 5min. Finally, 1µL SuperScript II (for test samples) or 1µL MilliQ water (for -RT controls) was added and samples were incubated at 42°C for 1hr, terminated at 70°C for 15min and treated with RNAse H (Affymetrix #70054Y) to remove template RNA.

2.6.2 qPCR primer design & optimisation

For all qPCR reactions, the Takyon SYBR (blue dTTP) qPCR kit (Eurogentec #UF-NSMT-B0701) was used with a Bio-Rad CFX96 Touch™ Real-Time PCR Detection System.

qPCR primers were selected from the Roche Universal ProbeLibrary or designed manually using the Primer3 Web Tool to produce intron-spanning amplicons of 50-150 nucleotides in length. Multiple primer sets for each target were tested over a range of annealing temperatures to identify the optimum conditions for specific target amplification with minimal primer-dimer formation. Effective primer sets were then analysed for qPCR suitability by testing linear amplification over a range of starting RNA concentrations plus efficiency over a range of cDNA dilutions. Efficiencies of 90-110% were considered acceptable and used for subsequent quantification of samples. Final primer pairs used are described in Table 2.5 below.

The final, optimised qPCR protocol used for all sample analysis was: 95°C 3min, 40 cycles of {95°C 10s, 63.3°C 20s, 72°C 20s}. The PCR reaction was followed by melt curve analysis to check specificity of amplification. This consisted of 60 cycles of 5s incubations increasing at 0.5°C per cycle, starting at 65°C and finishing at 95°C.

Target	Gene Symbol	Accession Number	Forward Primer	Reverse Primer	Amplicon
beta-2-microglobulin	*b2m / β2m*	NM_001159768.1	5'-ACATCACTGTACAGGGGAAAGTC-3'	5'-TCCGTTCTTCAGCAGTTCAA-3'	5'-ACATCACTGTACAGGGGAAAGTCTCCACTCCGAAAGTTCATGTGTACAGTCATTTTCCAGGAGAGTATGGAAAACCAAACACCCTGATCTGCTATGTGAGCAGCTTCCATCCTCCAGATATCTCCATTGAACTGCTGAAGAACGGA-3'
collagen, type XI, alpha 1a	*col11a1a*	NM_001083844.1	5'-GAGAAAGGACACAGGGGTGA-3'	5'-TCCATCCTCTCCAGTTGGTC-3'	5'-GAGAAAGGACACAGGGGTGAGACCGGCCCTGCTGGACCCCCGGGACCAACTGGAGAGGATGGA-3'
indian hedgehog homolog b	*ihhb*	NM_131088.1	5'-AAGGATGAGGAGAACACAGGT-3'	5'-TTCAGAGTGTAGTCCGTCCT-3'	5'-AAGGATGAGGAGAACACAGGTGCGGACCGCATGATGACGCAGCGCTGCAAGGATAAGCTGAACTCTCTGGCCATCTCGGTGATGAACCTGTGGCCCGGTGTGCGTCTGCGTGTGACGGAGGGCTGGGATGAGGACGGACTACACTCTGAA-3'

Table 2.5 – qPCR primers.
Details of the primers used for qPCR quantification of expression levels.

2.6.3 qPCR analysis

Each experiment included two negative controls – a reaction containing no cDNA (no template control – NTC) to check for non-specific amplification and a reaction containing the RNA sample processed without reverse transcriptase enzyme (-RT control) to check for amplification of genomic DNA. In all experiments, neither controls showed significant detection of PCR product with Cts of >35 in all cases.

Each sample was assayed in triplicate wells to act as technical replicates, and RNA extraction from pooled biological samples was repeated on three separate occasions to act as biological replicates. The final data presented is the average fold change of these three biological replicates as described here[178].

2.7 Transgenic zebrafish lines

A number of pre-validated transgenic zebrafish lines were used in this project for various experiments. Table 2.6 below describes these lines and where they were sourced from.

Transgenic Line	Construct #ZFIN ID	Lab of Origin	Effect of Transgene
mpeg1:GAL4	Tg2(*mpeg1*:*GAL4-VP16*) #ZDB-ALT-131203-1	Professor Stephen Renshaw (The University of Sheffield)[179]	The *UAS* trans-activator GAL4 (fused to VP16 for increased activity[180]) is expressed under the macrophage-specific macrophage expressed gene 1 (*mpeg1*) promoter. This transgene does not produce a phenotype without a corresponding *UAS* element.
mpx:GAL4	*TgBAC(mpx:GAL4-VP16)* #ZDB-ALT-160322-6	Professor Stephen Renshaw (The University of Sheffield)[181]	As above, but GAL4 is driven by the neutrophil-specific myeloperoxidase (*mpx*) promoter.
csf1ra:GAL4	*TgBAC(csf1ra:GAL4-VP16)* #ZDB-ALT-110707-2	Dr Timothy Chico (The University of Sheffield)[182]	As above, but GAL4 is driven by the macrophage & xanthophore specific colony stimulating factor 1 receptor α (*csf1ra*) promoter.
UNM	*Tg(UAS-E1b:NTR-mCherry)* #ZDB-ALT-110707-1	Dr Timothy Chico (The University of Sheffield)[183]	Upstream activation sequence (*UAS*) enhancer elements upstream of an adenovirus-derived E1b minimal promoter result in a GAL4-responsive regulatory sequence. Expression of a nitroreductase-mCherry fusion protein is thus driven in cells simultaneously expressing GAL4. This transgene does not produce a phenotype without a corresponding GAL4 element. This transgene acts an inducible cell ablation system via the nitroreductase-catalysed conversion of a non-toxic pro-drug (Metronidazole (Mtz; Sigma #M3761)) into a cytotoxic form. The mCherry fusion simply allows visualisation of the transgenic cells.
hs:dkk1-GFP	*Tg(hsp70l:dkk1b-GFP)* #ZDB-ALT-070403-1	Professor Randall Moon (the University of Washington)[88], via Dr Gilbert Weidinger (Ulm University)	Expression of a Dkk1-GFP fusion protein can be induced via the heat-shock promoter *hsp70* after exposing fish to increased temperature.

Table 2.6 – Transgenic zebrafish lines.
Details of the transgenic zebrafish lines used in this project.

2.8 Leukocyte ablation using the *GAL4*/*UNM* system

The UAS-nitroreductase-mCherry (UNM) genetic ablation system has been previously validated in zebrafish[184] and the transgenic lines described above were crossed to produce embryos with the desired genotype to allow specific ablation of macrophages & xanthophores (*csf1ra:GAL4*/*UNM*), macrophages (*mpeg1:GAL4*/*UNM*), neutrophils (*mpx:GAL4*/*UNM*), or macrophages & neutrophils (*mpeg1:GAL4*/*mpx:GAL4*/*UNM*).

Embryos were screened to identify strongly-expressing transgenic individuals. *csf1ra*-driven transgenic embryos were screened at 1dpf after the onset of xanthophore development and *mpeg1* and *mpx* driven transgenic embryos were screened at 2dpf after the onset of leukocyte development. Embryos were pre-treated with Mtz (final concentration of 5 or 10mM with 0.1% DMSO) for 18hrs before wounding and kept in Mtz-dosed medium continuously after wounding; embryos were transferred into new medium every 24hrs to maintain the level of Mtz.

2 & 3dpf embryos were subjected to the standard tail regeneration assay (Section 2.3). Additionally, 3dpf embryos were injured by transverse resections made at the caudal tip of the tail to remove only the caudal fin-fold.

At 6hpa, transgenic embryos were imaged under a Zeiss Axio Zoom.V16 stereomicroscope with an AxioCam MRm camera and Zen 2 (Blue Edition) software. 2-channel, brightfield & fluorescent (RFP filter: 557-587/594/600-680) images were taken.

The extent of macrophage recruitment to the wound was quantified in Fiji using a self-written macro (see Appendix A, Section 8.4) in order to maximise reproducibility whilst minimising human error and subjectivity. Briefly, the macro allows the user to draw a line along the edge of the wound from the brightfield image, and then creates a region of interest (ROI) extending 200µm into the tail to which all subsequent analysis is limited. The macro is designed to measure the area of pixels within this ROI which exceed a set fluorescent intensity – this was set manually for each experiment but varied little between experiments and remained fixed within a single experiment to allow comparative analysis between all samples. In addition to this, the macro counts the number of fluorescent maxima within this area, but these data was not used for subsequent analysis.

In order to determine the extent of regeneration, embryos were fixed at 5dpf (48hpa or 72hpa), bleached, transferred into glycerol and imaged as per the standard tail regeneration assay (Section 2.3).

2.9 Neutrophil quantification by sudan black staining

2.9.1 Basic sudan black staining

Sudan black staining was used to visualise neutrophils[185] recruited to the wound in larvae. For this staining, larvae were fixed in 4% PFA overnight, rinsed 3 x 5min in PBS and submerged in sudan black staining solution (Sigma #380B) for 20min. To remove background staining, larvae were rinsed in 70% EtOH 3 times, and then 3 x 20min washes with 70% EtOH. Larvae were rehydrated into PBST via a series of EtOH/PBST dilutions, and then transferred to glycerol for imaging. This method was provided from the Renshaw lab at Sheffield University[186].

2.9.2 Combined WISH and sudan black staining

When combined with WISH staining, the basic sudan black staining was performed first (as above), and the WISH staining was performed second. Larvae were treated as above until rehydration into PBST after which they were transferred to the WISH protocol at the MeOH dehydration step in day 1 of the protocol.

2.10 Combined fluorescent-WISH and IHC staining

To further quantify leukocyte recruitment and analyse the relationship between leukocytes and wound-induced *ihhb* expression, a fluorescent-WISH was combined with fluorescent immunohistochemistry (IHC) staining for the leukocyte marker L-plastin[187,188]. This allowed simultaneous quantification of wound-induced *ihhb* expression and leukocyte recruitment within individual fish.

2.10.1 Fluorescent WISH

The Fluorescent-WISH protocol was adapted from the standard WISH protocol outlined in Section 2.5 using a TSA Plus Cyanine 3 Amplification System (Perkin Elmer #NEL744001KT). The standard WISH methods were followed up until the blocking step, and then the following amendments were made:

- Sample blocking was performed for 2hrs with maleic blocking buffer (Roche blocking reagent (Roche #11096176001) diluted in maleic buffer (maleic acid (Merck Millipore #800380))).
- Embryos were incubated overnight at 4°C in anti-DIG-POD Fab fragments (Roche #11207733910) diluted in maleic blocking buffer at 1:500.
- Addition of the Cy3-tyramide substrate visualised RNA probes via localised, POD-catalysed, conjugation of Cy3. Samples were incubated (30min at RT) in 100µL of Cy3-tyramide reagent (diluted 1:50 in Amplification Buffer PLUS). Un-bound Cy3 was removed with multiple PBST washes (6 x 20min).

2.10.2 IHC staining

Lymphocyte cytosolic protein 1 / L-plastin (lcp1) detection was performed immediately after the fluorescent WISH protocol:

- Embryos were blocked with maleic blocking buffer for 2hrs and incubated at 4°C overnight with Rabbit anti-*lcp1* (sourced from Dr Paul Martin[189], via Prof Stephen Renshaw) (1:400 in maleic blocking buffer).
- Embryos were washed and blocked with maleic blocking buffer for 2hrs and incubated at 4°C overnight with Alexa Fluor 488-conjugated, goat anti-rabbit antibody (Invitrogen #A-11008) (1:200 in maleic blocking buffer).
- Embryos were washed thoroughly, post-fixed in PFA and transferred into Vectashield anti-fade mounting medium with DAPI (Vector labs #H-1200).

2.10.3 Visualisation of samples

Embryos were mounted in Vectashield under coverslips and imaged using an Olympus Fluoview FV1000 BX61 confocal microscope and the Fluoview V4.2 capture software. 3-channel images, covering the full depth of the tail with 3µm Z-stack separation were taken using the 405, 488 and 534nm lasers to excite DAPI, Alexa Fluor 488 and Cy3 respectively.

The extent of macrophage recruitment to the wound as well as *ihhb* expression was quantified in Fiji using a self-written macro (see Appendix A, Section 8.5) in order to maximise reproducibility whilst minimising human error and subjectivity. Briefly, the macro automatically detects the embryo outline from a maximum intensity projection of the DAPI channel and creates a ROI extending 200µm away from the wound (after adjusting for tissue shrinkage caused by mounting in Vectashield*) to which all subsequent analysis is limited. A maximum intensity projection of the *ihhb in situ* channel is produced and the area of fluorescence over a certain threshold is measured. This threshold is set manually but remains fixed within each experiment to allow comparative analysis between samples. The 3D Objects Counter plugin[190] was used to determine the number and volume of objects in the *lcp1* channel. The macro results in the 4 wound-area metrics: *ihhb* positive area, *lcp1* positive cell count and average *lcp1* positive cell volume which are used to calculate the final metric – total *lcp1* positive cell volume.

*Vectashield caused significant tissue shrinkage in the embryos and therefore the extension of the ROI was scaled appropriately in order to reflect a distance of 200µm under physiological conditions. Scaling was estimated by comparing the average tail width of 20 unpaired samples before and after immersion in Vectashield. The extension of the ROI is set to 107µm which corresponds to a normal physiological width of 200µm – the same distance used previously to determine leukocyte wound recruitment.

2.11 Inhibition of protein synthesis with cycloheximide

In order to determine if *ihhb* was regulated as a wound-induced immediate early gene, it's expression was determined by WISH following treatment with the translation blocking compound cycloheximide (Cayman Chemical #14126)[191].

2.11.1 Optimisation of cycloheximide treatment

Cycloheximide treatment was optimised using the *hs:dkk1-GFP* line in order to validate the inhibition of *de novo* Dkk1-GFP translation after heat shock induction. Preliminary experiments identified 50µg/mL as the highest tolerated dose with no visible effects on embryo health.

Embryos were pre-treated with 50µg/mL cycloheximide for 1hr and heat shocked at 38.8°C for 2hrs, then returned to 28°C for 4hrs. Whole-body GFP expression was quantified using a Zeiss Axio Zoom.V16 stereomicroscope with an AxioCam MRm camera and Zen 2 (Blue Edition) software.

2.11.2 Wound-induced *ihhb* quantification

3dpf embryos were treated with 50µg/mL cycloheximide from 1hr prior to amputation until fixation. Tail amputations were performed as for the standard tail regeneration assay above. At 6hpa, larvae were fixed and analysed by WISH for *ihhb* as previously described (Section 2.5).

2.12 Fluorescent-IHC staining for pSFK & keratan sulfate

Fluorescent IHC staining was used to visualise wound-induced Src family kinase (SFK) activation with an anti-phospho-SFK (Tyr416) antibody (Cell Signaling Technology #6943). This antibody binds specifically to SFKs which have been activated by tyrosine phosphorylation in the activation loop of the kinase domain (Tyr416) and therefore acts as a reporter of SFK activation[122].

2.12.1 Single antibody staining protocol

Embryos were processed as for the standard WISH protocol (Section 2.5) up until the blocking step. At this point, blocking was performed with 10% new born calf serum (NBCS) in PBST for 2hrs at RT. Embryos were incubated overnight at 4°C in blocking buffer supplemented with primary antibody at the dilutions listed in Table 2.7 below. Embryos were washed, blocked and incubated in secondary antibody at the dilutions listed in Table 2.7 below.

2.12.2 Double antibody staining protocol

For double staining experiments, an anti-keratan sulfate antibody (Developmental Studies Hybridoma Bank #3H1) was used to simultaneously label the perinotochordal basement membrane, therefore outlining the notochord cells[192]. This allowed comparative localisation of

the activated SFKs in relation to the notochord. Double antibody staining was performed sequentially with the first antibody staining carried out as above, then post-fixed with PFA to, before repeating the staining protocol with the second antibody pair. Primary and secondary antibody concentrations are listed in Table 2.7 below.

Primary Antibodies	Dilution
Rabbit anti-pSFK	1:300
Mouse anti-keratan sulfate	1:100
Secondary Antibodies	**Dilution**
Goat anti-rabbit (Alexa Fluor 488 conjugated)	1:200
Goat anti-mouse (Alexa Fluor 647 conjugated)	1:200

Table 2.7 – Immunhistochemistry antibodies.
Details of the antibodies used in my project for immunofluorescence.

2.12.3 Visualisation & quantification

Embryos stained with just the anti-pSFK antibody were mounted under coverslips and imaged under a Zeiss Axio Zoom.V16 stereomicroscope with an AxioCam MRm camera and Zen 2 (Blue Edition) software. 2-channel fluorescent (DAPI filter: 352-402/409/417-477; YFP filter: 489-505/516/524-546) images were taken. Images were analysed using FIJI to quantify the average fluorescent intensity of the pSFK antibody within 200µm of the wound.

Dual-stained embryos were mounted under coverslips and imaged using a Perkin Elmer UltraView Vox Spinning Disk IX81 confocal microscope and the Velocity V6.3 capture software. 3-channel images, covering the full depth of the tail with 3µm Z-stack separation were taken using the 405, 488 and 640nm lasers to excite DAPI, Alexa Fluor 488 and Alexa Fluor 647 respectively. Images were analysed using FIJI to observe co-localisation using the orthogonal views function.

2.13 Tail development morphology and WISH

In order to analyse early embryonic gene expression & tail development, embryos were dechorionated, staged to 14hpf and dosed with chemicals / vehicle for 4hrs. At 18hpf, embryos were either fixed for WISH analysis of tail bud gene expression or transferred to fresh E3 to continue developing before fixation and morphological analysis of tail development at 24hpf.

2.14 Statistical analysis

Unless otherwise stated, grouped data was analysed in Graphpad Prism 6 using the following statistical methods: Groups were assessed for normal distribution by the D'Agostino & Pearson omnibus normality test and the Shapiro-Wilk normality test. If all groups passed at least one of the tests they were considered to conform to a normal Gaussian distribution and therefore analysed by parametric tests: for data with only two groups, an unpaired, two-tailed T-Test was used; and for data with three groups or more an unpaired One-Way ANOVA (with Dunnett's multiple comparisons test to assess the significance of differences between groups) was used. If one or more groups failed to pass both normality tests, non-parametric analysis was performed: for data with only two groups, an unpaired, two-tailed Mann-Whitney U test was used; and for data with three or more groups an unpaired Kruskal-Wallis test (with Dunn's multiple comparisons test to assess the significance of differences between groups) was used. For all tests, a p-value of <0.05 was considered significant. Additionally, if sample numbers were too small for normality tests, then non-parametric tests were performed in order to reduce the change of false positives when determining significance.

Unless otherwise stated, the following parameters were used for data analysis and presentation: three biological replicates of ~10 embryos were analysed; each individual embryo is plotted as a separate point on each graph to show total numbers of embryos used; lines indicate sample mean with the 95% confidence intervals as error bars; statistical comparisons on graphs are labelled as follows: $p>0.05$ (ns), $p\leq 0.05$ (*), $p\leq 0.01$ (**), $p\leq 0.001$ (***), $p\leq 0.0001$ (****).

Chapter 3. H_2O_2 is required for regeneration and stimulates developmental signalling pathways

3.1 Introduction

3.1.1 Aims

The aim of the work covered in this chapter was to examine the effects of H_2O_2 in the wound-induced regenerative response. Little is known about the effectors or the mechanisms of transduction by which the wound-induced H_2O_2 signal leads to a successful regenerative outcome, so I began from a very rudimentary position. Work presented here examined the effects of H_2O_2 depletion on the morphology of the regenerating tissue, the anatomy of the regenerative structures and the regulation of developmental signalling pathways known to be essential initiators of the regenerative response. Given the early onset of the H_2O_2 signal and its short-lived & transient nature, it was hypothesised that H_2O_2 depletion would prevent the activation of some or all of these early regeneration mechanisms in order to impair late-stage regenerative outgrowth at a time when the H_2O_2 signal has long been resolved.

3.1.2 Background

When an organism is wounded, a collection of responses are rapidly set into motion that aim to restore barrier function at the site of injury, clear any invading pathogens, remove cell debris and restore tissue homeostasis. In humans and most other mammals, this is the end of the wound response and often involves the deposition of scar tissue which restores barrier function at the sight of injury but at the expense of biological function. In zebrafish and other regenerating organisms however, the healing response is extended to incorporate regrowth of the lost or damaged cells to restore both form and function. We do not currently know the reasons for the differences between these two mechanisms of healing and how organisms trigger a regenerative wound response in the first place. Work presented in this thesis hopes to address this derth of information.

3.1.2.1 Wound-induced ROS

ROS are one of the first chemical signals that are actively synthesised after injury and they are generally considered early wound signals due to their incredibly rapid production and their transient nature that sets them apart from more longer-lived transcriptional responses to injury. ROS production was previously thought not to occur until after recruited leukocytes have triggered the inflammatory respiratory burst, but recent evidence demonstrated that H_2O_2 can be detected within 3 minutes of wounding[119], a timeframe that precedes leukocyte recruitment. It has also been shown to act as a chemoattractant to initiate inflammation[119,173,193], and to be down-regulated on the arrival of the first neutrophils via a myeloperoxidase-dependent conversion[135]. Taken together, these observations point to an injury-induced H_2O_2 signal that should be considered separate from the anti-microbial and pro-inflammatory ROS produced during the respiratory burst.

ROS has long been known to function as a pro-healing signal and is even currently used in some public healthcare applications. Topical application of H_2O_2 had been used primarily as an antimicrobial, but treatments have also exhibited enhanced wound closure in a manner unaccountable for by simple sterilisation effects[194]; a response also seen in mouse models and human cell lines[64,195]. Additionally, hyperbaric oxygen therapy results in both an increase in the amount of ROS generated throughout the body as well as a concomitant improvement in would healing in diabetic ulcers[196]. Furthermore, the historically noted pro-healing effects of honey have been partially attributed to the H_2O_2 produced as a by-product of glucose oxidation by the glucose oxidase enzyme[197]. Although the mechanisms of action by which ROS can improve healing outcomes are not completely characterised, we are aware of some. Many of these effectors are the same as those induced by other injury-induced messengers, allowing for amplification & functional redundancy as well as a level of fine-tuning by appropriately integrating multiple wound-signals.

The function of ROS at the wound is multifactorial, but at high concentrations they mainly act as antimicrobials to sterilise the wound. Due to their radical chemistry, ROS non-selectively react with molecules that they come into contact with, often altering tertiary structures and disrupting protein folding, therefore ROS can damage or kill invading pathogens either directly via oxidative damage[198–200] or following neutrophil-mediated conversion to more potent antimicrobials such as hypochlorous acid[133].

On top of this, ROS are powerful drivers of inflammation, acting at a distance to attract leukocytes to an injury and therefore initiate inflammation[119,201,202]. This appears to be

mediated by direct oxidative activation of the Lyn Src family kinase (SFK) within neutrophils[173] but ROS may also contribute to the eicosanoid-dependent chemotaxis mentioned above[203–206]. Additionally, ROS-mediated stimulation of migration is seen in epithelial cells to aid wound closure[131]. Inflammation can be further amplified by the H_2O_2 induced stimulation of angiogenesis[195,207] via the induction of VEGF[208–210]. Formation of new blood vessels serving the injury site allow more rapid accumulation of leukocytes at the wound but also promote healing by ensuring adequate delivery of nutrients and oxygen.

There are generally two sources of ROS from within cells – mitochondria and Nox family enzymes. Whilst mitochondria-derived ROS has been shown to accelerate wound closure in *C. elegans* via cytoskeletal rearrangements[211], mitochondrial ROS has not been studied extensively in other models of healing and regeneration and the primary source of pro-regenerative ROS appears to be derived from the activation of Nox family enzymes such as Duox. Pharmacological inhibition and morpholino-based knockdown have shown that this H_2O_2 signal is produced by epithelial cells at the site of injury by Duox[43,119]. This production of ROS following injury is triggered by both biophysical and biochemical changes induced by wounding.

3.1.2.2 Biochemical factors stimulating ROS production

Physical damage at the wound causes cell rupture and necrosis leading to the release of intracellular molecules. These transcriptionally-independent signals serve as the first available chemical wound signals for an organism to detect damage. Cell lysis releases a myriad of cellular molecules into the environment, collectively known as damage-associated molecular patterns (DAMPs) which are capable of alerting neighbouring cells of the injury (Figure 3.1). Two of the most well studied DAMPs are ATP and calcium ions (Ca^{2+}).

ATP, which is present at much higher concentrations in the cytoplasm compared to the extracellular compartment resulting in a significant rise upon its passive release by necrotic, ruptured cells. In addition, ATP can be actively secreted by viable cells, in an attempt to prevent additional damage by relieving injury-induced cellular stress before it leads to cell death via apoptotis[212]. This creates a increase in extracellular ATP concentration localised to the wound.

As for Ca^{2+}, cytosolic levels are maintained at low concentrations (10-100nM) with extracellular levels generally four orders of magnitude higher[213]. Ca^{2+} is, however, actively

sequestered in intracellular stores such as the ER and mitochondria[214] which can act as a rapidly available local source of Ca^{2+} for the cell. Ca^{2+} signalling is more complex than ATP and relies on an initial spike in cytosolic levels which, within seconds, propagates away from the wound through the release of Ca^{2+} from internal stores in neighbouring, viable cells to cover distances of up to 300µm[215]. The propagation of this Ca^{2+} wave *in vivo* appears dependent on cell-cell communication mediated via Ca^{2+} permeable gap-junctions and TRPM channels[216], although sometimes this signal can be transmitted across cell-free spaces[217–219]. This amplification mechanism presumably aids the detection of even small wounds and is highly conserved from mammals and fish to simple invertebrates such as *Drosophila* and *C. elegans*[122,216,220,221].

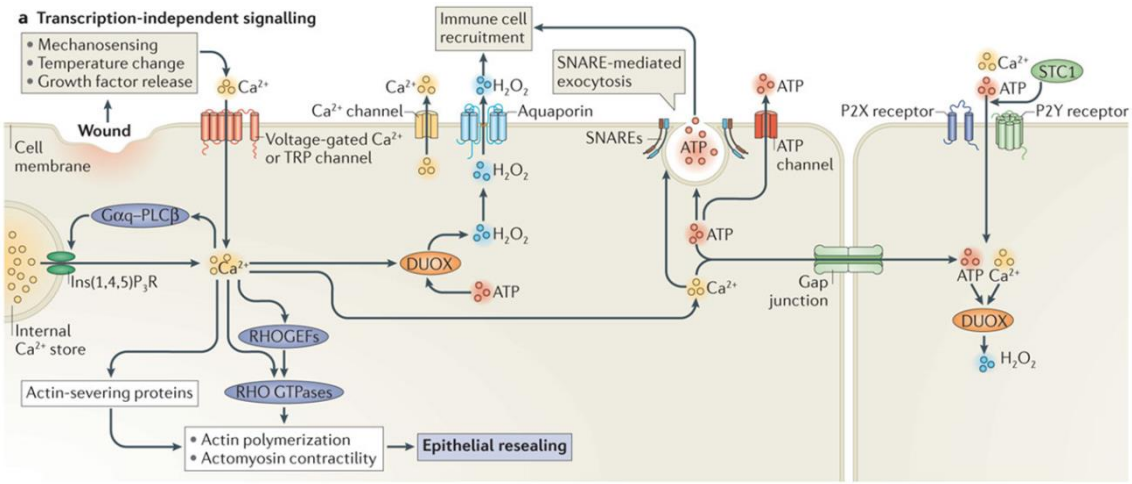

Figure 3.1 – Translation-independent damage signalling pathways (reproduced from Cordeiro & Jacinto, 2013[222]).
Following wounding, DAMPs are released from ruptured, apoptosing and stressed cells at the wound site. Ca^{2+}, ATP and H_2O_2 are the main DAMPs released to initiate the wound response and interact in a complex network, patrially outlined above. The regulation and interaction of these DAMPs is explained more fully in the text.

These ATP and Ca^{2+} signals serve multiple healing roles including aiding wound closure via stimulating epithelial cell migration[223–227], wound contraction[228–231] and stimulating inflammation[226,232–234], but here I will focus on their ability to stimulate the wound-induced H_2O_2 signal. There is evidence that ATP and Ca^{2+} signalling are required for successful late-stage zebrafish fin regrowth[122,235], and this is likely via their direct or indirect stimulation of H_2O_2 after wounding. Indeed, zebrafish models support this theory as the wound-induced H_2O_2 signal is dependent on both ATP and Ca^{2+} signalling[236].

ATP stimulates H_2O_2 indirectly via initiating or amplifying the Ca^{2+} flash by activating purinergic receptors[217–219,225], and the Ca^{2+} flash itself has been shown to be directly capable of activating H_2O_2 production in *Drosophila* by binding to the EF hand domains on Duox[216]. This comprehensive study showed that ROS can be stimulated even in the absence of wounding by triggering an influx of Ca^{2+} through temperature-sensitive TRP channels, and that RNAi knockdown of Duox can be rescued by the expression of exogenous Duox, but not a truncated Duox mutant lacking EF hands. Taken together, these data strongly imply that Ca^{2+} is both necessary and sufficient to stimulate H_2O_2 production by Duox in *Drosophila*, and considering the conservation of the EF hands between *Drosophila* and other species[237], it is highly likely that this regulatory role is also conserved. Whilst this relationship appears to hold true in mammalian cells[238–240], in zebrafish there is evidence both for and against.

Studies using thapsigargin – an inhibitor of ER ATPase, resulting in the depletion of intracellular ER Ca^{2+} stores – initially suggested that wound-induced H_2O_2 was independent of a wound-induced Ca^{2+} wave[122], however, subsequent data has challenged this assertation by quantifying an attenuation of both wound-induced H_2O_2 and the subsequent neutrophil recruitment following thapsigargin treatment[236]. The later study also demonstrated a rescue of H_2O_2 mediated neutrophil recruitment by the injection of a calcium ionophore in a Duox-dependent manner, further supporting a positive role for Ca^{2+} signalling in Duox regulation. Due to the uncertainty of this potential interaction, this is something I investigated during my project and the data is presented later in this chapter.

3.1.2.3 Biophysical factors stimulating ROS production

In addition to the more well studied biochemical perturbations, wounding induces biophysical changes which are of equal importance to proper healing. Damage to epithelia from mechanical injury can rupture cells releasing tension held in tissues by cell-cell contacts and supracellular structures such as basement membranes. Finally, compartmental mixing following a breach of the epithelial barrier results in rapid changes to the extracellular environment which is a useful cue to detect injury. Osmotic shock and bioelectric currents induced respectively from water & ion flows between the environment and cells act as some of the most immediate wound signals given that they do not rely on any active response from the organism to be initiated[232,241]. All these signals are capable of stimulating the production of ROS following injury. Below I outline some of the mechanisms by which these biophysical stimuli can be transduced to pro-ROS signals.

3.1.2.3.1 Mechanical Stress

The very first impact of epithelial breach will be an immediate release in membrane tension normally held by cell-cell and cell-ECM contacts. This disruption to the physical homeostasis can be detected by mechanotransduction mechanisms. Mechanically-gated ion channels appear to be the main method of detecting such forces. Mechanically-induced Ca^{2+} signalling can therefore stimulate H_2O_2 production as outline above.

For example, TRPP2 and TRPC1 (members of the TRP family of cation channels[242]) have been shown to mediate Ca^{2+} influx in blood-brain barrier endothelial cells following stretch-induced injury, directly linking mechanical injury to Ca^{2+} currents[243]. Additionally, TRPM has been shown to mediate wound-induced Ca^{2+} currents in *Drosophila* and *C. elegans*[211,216,230,231]. Whilst it has not been empirically determined what activates these channels, as a member of the TRP family it is likely that mechanical or osmotic stress are prime candidates. In addition, the Piezo proteins are another type of mechanosensitive channels capable of transducing mechanical signals. As non-selective cation channels, the Piezo proteins are capable of modulating bioelectrical currents and have also been specifically demonstrated to allow the flow of calcium ions[244–246]. Although no direct evidence has directly implicated them in mediating wound-induced Ca^{2+} waves, they would certainly be capable of such an interaction. Mechanical forces can also modulate Ca^{2+} signalling by altering cell adhesion, substrate rigidity and cell-cell gap junctions[247], potentially fine-tuning wound responses.

Furthermore, the mechanically-induced release of ATP is prevalent across many cell types[212], often via extracellular-facing hemichannels[225]. This release can be triggered by even gentle stimuli, so the transduction of a large physical wound would likely result in a considerable increase in ATP concentration which, in turn, can propagate long-range Ca^{2+} signalling and therefore H_2O_2 production.

3.1.2.3.2 Osmostic Stress

A physical breach of the epithelial barrier in aquatic organisms or a mucosal epithelium in terrestrial organisms connects the interstitial fluid with a liquid external environment. The hypotonicity of the external environment leads to a rapid influx of water into exposed cells by osmosis, causing cell swelling at the injury site. Transduction of these forces to biochemical signals appear to mainly converge on ATP and Ca^{2+} release.

Osmotically-induced cell swelling can trigger ATP release in multiple different cell types[248] (potentially via the same mechanically-induced ATP release mentioned previously[212], in response to swelling-induced membrane tension), a mechanism that has been observed in zebrafish epithelial wounds[226]. Similarly, Ca^{2+} signalling has been observed in multiple cell types (mostly of epithelial origin) following cell swelling[248]. This effect has been suggested to rely on extracellular calcium influx through osmosensitive TRP channels[242]. Therefore Osmotic stress, like mechanical stress can stimulate H_2O_2 production indirectly via Ca^{2+} signalling.

3.1.2.3.3 Bioelectricity

Even non-excitable cells maintain a resting membrane potential induced by the difference in relative concentrations of anions and cations within the cell compared to the interstitial fluid and are therefore primed to induce currents upon active or passive ion flow. Here, I use the term bioelectricity to refer to these membrane potentials and the currents produced during the flow of ions into or out of the cells.

Cell lysis, compartmental mixing and mechanical stresses can all contribute to the abnormal release and flow of ions in and around the wound environment. The movement of these particles will induce a current and the resulting concentration differences across cell membranes will create voltage potentials. Cells may be depolarised by the opening of osmosensitive TRP channels[242] leading to wound-induced currents. In addition, the osmotically-induced arachidonic acid can regulate both cation and anion channels, conceivably altering membrane potentials at the wound[249].

Bioelectrical signals appear to have not only pro-healing effects, but strong pro-regenerative effects; they are predictive of regenerative capacity, essential for the initiation of physiological regneration, impart severe patterning defects when altered and can even induce *de novo* regeneration[69,140,141,250]. Taken together, these data show that bioelectricity can function as a master regulator and supports its position upstream of many wound responses. The transduction of these signals is currently incompletely understood, but some downstream molecular & cellular effectors have already been identified. As well as stimulating wound closure & inflammation via galvanotaxis (the stimulation of cell migration based on electrical stimuli[251]), the wound-induced Ca^{2+} wave can be potentiated by voltage-gated Ca^{2+} channels which can be triggered following depolarisation of cells to allow influx of calcium ions[252,253]. These channels have been directly implicated in regenerative patterning in multiple

organisms[107,254–256], highlighting the importance of both bioelectricity and Ca^{2+} signalling in healing, potentially via the initiation of the ROS signal.

Whilst the multiple wound signals discussed above have numerous divergent effectors, there appears to be a strong convergence on ROS as a downstream signal highlighting its importance in the healing and regeneration process.

3.1.2.4 ROS and regeneration

As well as being responsible for mediating pro-healing mechanisms, ROS have been identified as essential regulators of regeneration in multiple species. The pro-regenerative functions of ROS have only recently begun to be characterised, but most major regenerative model organisms have already been shown to have some reliance on ROS for proper regeneration and no data has been published demonstrating that ROS signalling is dispensable for regenerative healing in any organism. Since the initial characterisation of the wound-induced H_2O_2 signal in zebrafish by Niethammer *et al.*[119] and the discovery that this response is required for regeneration to proceed in larval zebrafish fin[122], similar pro-regenerative H_2O_2 signals have been identified in zebrafish adult fin, nerves and heart[43,120,124], *Hydra*[125], planaria[128], *Drosophila*[121,126,130], *Xenopus*[123], newt[127], gecko[129] and even human airway epithelial repair[131,168,257].

In larval zebrafish, the transient production of H_2O_2 after fin-fold amputation was required for complete regrowth. Pharmacological inhibition of Duox with diphenyleneiodonium (DPI) or Duox knockdown via anti-sense morpholino both significantly impaired the amount of tissue regenerated[122]. Interestingly, after transient inactivation of Duox during an initial wound with DPI treatment, re-amputation of the fin after removing the inhibitor from the media resulted in completely normal regeneration. This places H_2O_2 as an early and essential initiator of regeneration, required to set-in motion the regenerative healing response despite returning to pre-wounding levels within a few hours. Further chemical and genetic knockdown experiments show that these effects are mediated by the H_2O_2 dependent activation of the SFK family member Fynb. Unfortunately, SFKs are promiscuous kinases capable of regulating many downstream effectors via post-translational modification and the specific targets of Fynb in this context remain unknown.

ROS are also induced in adult zebrafish after injury but they appear to be sustained for a much longer period of time. They are produced over many hours, gradually accumulating at the tip

of the injured fin until peaking at around 16hpa. This signal is then rapidly cleared, returning to baseline levels by 18hpa. The extended ROS production is required to promote regeneration via an induction of apoptosis at these late timepoints[120]. The authors suggested that ROS-dependent voltage gated potassium channels could mediate this link although they did not test this hypothesis. It is possible, however, that at this time ROS levels simply reach cytotoxic levels via non-specific oxidative damage. One molecular link the study did identify was a ROS-dependent activation of JNK which was subsequently responsible for stimulating epidermal proliferation but JNK inhibition did not affect cell death suggesting that ROS promotes regeneration via apoptosis and JNK activation as two parallel responses. The authors suggest that these separate signalling mechanisms of ROS may a dose-dependent response with high levels causing cell death at the wound edge but lower concentrations at more distal areas triggering signalling without cellular damage.

Another study in adult zebrafish discovered a requirement for wound-induced H_2O_2 in heart regeneration, but as for adult fin regeneration, the H_2O_2 signal was sustained for a much longer time than larval fin regeneration. In wounded heart, no H_2O_2 could be detected within an hour of injury but elevated H_2O_2 could be detected at 3, 7 and 14dpa and returned to basal levels by 30dpa as regeneration was completing[124]. H_2O_2 was shown to be necessary for regeneration by pharmacological inhibition of Nox enzymes and also by scavenging H_2O_2 by the overexpression of catalase. In addition, exogenous H_2O_2 was sufficient to rescue the regenerative defects confirming that this was a H_2O_2 specific effect. The study went on to identify a molecular target of H_2O_2 as Dusp6, a redox-sensitive phosphatase which is inhibited by high concentrations of H_2O_2. This inhibition is likely mediated by a reversible oxidation of the catalytic cysteine of Dusp6, rendering it incapable of dephosphorylating its targets. Furthermore, oxidative inhibition of Dusp6 coincided with a reciprocal increase in Erk1/2 phosphorylation and activation which was required for regeneration. Altogether, this study demonstrates how H_2O_2 can interact with other signalling pathways to regulate regeneration but the delayed onset of the H_2O_2 signal may demonstrate that it is utilised in a different regulatory mechanism in the heart than it is in the fin.

In addition to fin and heart regeneration, H_2O_2 has been shown to positively regulate axon regrowth in zebrafish following injury[43]. A previous study by the group had shown that following precise laser axotomy in zebrafish, sensory axons do not normally regrow into denervated areas after ~36hpf[258], but they later found that a wound microenvironment stimulated axon regrowth rate and permitted reinnervation of denervated tissue following axotomy. Amputation of the larval tail resulted in a local (~50µm) and transient (~6hr)

stimulation of axon regrowth, roughly matching the spatiotemporal characteristics of the H_2O_2 wound signal. This pro-regrowth effect could also be mimicked by laser ablation of keratinocytes, but only when the wound was severe enough to produce a detectable H_2O_2 signal. Further experiments using antisense morpholinos to prevent H_2O_2 production via inhibition of Duox translation, showed that this effect required Duox activity and that exogenous H_2O_2 could rescue this defect. Taken together, this provided strong evidence that H_2O_2 stimulates regrowth following axon injury, and innervation of the regenerating tail may also convey further pro-regenerative signals[259]. Although the molecular effectors of this interaction were not characterised, the authors show that the pro-regenerative effect of H_2O_2 is independent of inflammation and, rather than directly stimulating axon growth, acts indirectly by relieving an inhibition of axon regrowth.

This type of prolonged regenerative ROS signal has also been observed in *Xenopus* tadpole tail regeneration. Within minutes of wounding, *Xenopus* tadpoles induce a strong, localised production of ROS at the wound by Nox family enzymes which is required for successful regeneration[123]. This signal is induced rapidly but is maintained till 4dpa suggesting H_2O_2 may be acting as both an early initiator of regeneration and a late-stage regulator. Inhibition of Nox and scavenging of ROS by antioxidants severely impaired regeneration as well as the induction of Wnt and FGF. Although this study linked ROS to the activation of essential regeneration signalling pathways, no molecular link was identified in this organism.

A subsequent study was, however, able to identify some downstream effectors of H_2O_2 during regeneration. During development, *Xenopus* tadpoles are capable of regenerating their tail following amputation except during a short refractory period[260], but interestingly, addition of exogenous H_2O_2 is sufficient to partially rescue this regenerative defect[261]. The study demonstrated that H_2O_2 induces bioelectrical currents via the activation of voltage-gated Na^+ channels to induce regeneration, although, once again, no direct molecular links of this redox-activation were identified.

Altogether, the current literature points to H_2O_2 as an important downstream effector of multiple wound signals (Figure 3.2), therefore we decided that H_2O_2 would be an exciting and important early wound signal to investigate further, sitting at the interface of signalling where wound-sensing triggers healing responses. The conservation of this wound-induced H_2O_2 signal from simple invertebrates all the way to humans, combined with its powerful regulatory control of many healing responses, highlights its central role in the injury response and justifies further study to fully understand this important mediator.

Despite the discovery of these phenotypic links between ROS and regeneration, little is known about the precise molecular effectors of the H_2O_2 signal and by what means ROS are transduced to regulate regeneration. I therefore aimed to characterise the H_2O_2 wound signal and its downstream interactions in order to understand its regulatory control in a regenerating species. I hope that this work will allow molecular and cellular level comparisons between regenerating and non-regenerating organisms to help the field move towards a potential therapeutic application where we could manipulate our own wound microenvironment to act more like it does in the zebrafish and initiate repair and regeneration instead of scarring.

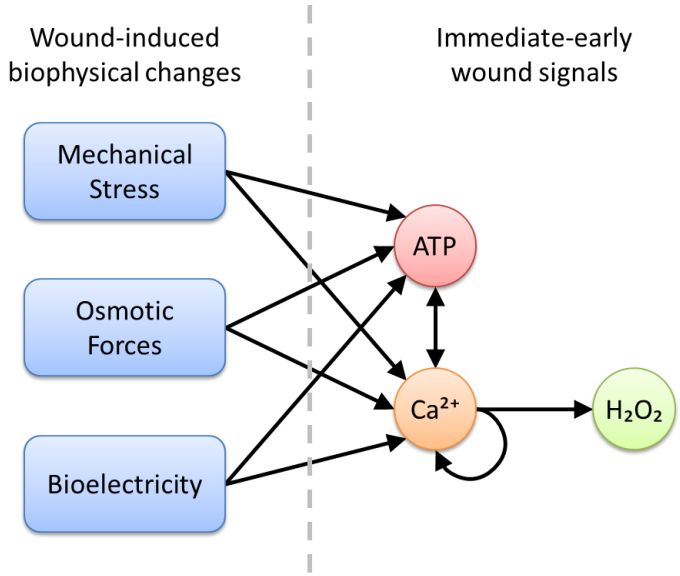

Figure 3.2 – Induction of early wound signals and ROS.
Schematic of the biophysical changes that induce immediate-early, translation-independent wound signals, their interactions and how they culminate in H_2O_2 production.

3.2 Results

Work presented in this chapter aims to study the roles of H_2O_2 in wounding and regeneration in the larval zebrafish by using tail amputation as a model wounding system, both under normal physiological conditions and after perturbation of the ROS levels by various means. Chemicals were used to either inhibit the production of the H_2O_2 wave or to sequester H_2O_2 once produced with anti-oxidant scavengers. Rescue experiments using exogenous H_2O_2 were carried out in order to address the specificity of these findings. I characterise the effect of H_2O_2 on the regenerative anatomy, identify regenerative signalling targets of H_2O_2 as well as

investigate the regulation of H_2O_2 production at the wound. Finally, the effect of perturbating Ca^{2+} signalling on the wound-induced H_2O_2 signal was analysed in order to investigate Ca^{2+} dependent regulation of Duox.

The precise injury used in the following experiments was an amputation of the tail from the caudal edge of the pigment-gap as shown in Figure 2.1. This resulted in the resection of roughly 100,000μm² of tissue including fin-fold epithelia, muscle, notochord, neural tube and blood vessels and represented a reasonably complex and severe injury requiring the regrowth of multiple different cell sub-populations. Tail amputations were performed on 2dpf larvae in order to assess regenerate morphology which had neared completion at 72hpa or on 3dpf larvae in order to assess regeneration signalling at earlier timepoints.

3.2.1 Inhibition of amputation-induced H_2O_2 production

In order to examine the roles of this H_2O_2 signal, I first aimed to compare regenerate morphology, formation of regenerative structures and regenerative signalling pathway activation in the presence and absence of H_2O_2. Wound-induced production of H_2O_2 is mediated by the activation of Duox within epithelial cells at the site of injury and pharmacological inhibition of Nox family enzymes can be achieved using multiple different small molecules[262]. The most widely used enzyme to inhibit Nox family production of H_2O_2 is the flavoenzyme inhibitor DPI. The Nox family enzymes are all flavoenzymes; that is, they require a flavin moiety to be able to be catalytically active. The enzymes bind flavin in the form of FAD at FAD binding domains in the catalytic regions of the proteins[237]. DPI inhibits Nox enzymes by binding irreversibly to the FAD cofactor, rapidly blocking the activity of the holoenzyme[263]. Due to this mechanism of action, DPI is known to target multiple other enzymes within cells[264,265], leading to potentially undesirable off-target effects following DPI treatment; however, DPI has been successfully used *in vivo* to abrogate wound-induced ROS in multiple species including zebrafish and was therefore my first choice for chemical treatments[119,120,122,123,128,173].

3.2.1.1 DPI inhibits wound-induced H_2O_2 & regenerate length

During my MSc project within this lab, I tested different concentrations and lengths of DPI treatments to identify the most effective dose to inhibit wound-induced H_2O_2 production &

regeneration whilst minimising toxicity. Results from this work are summarised in Figure 3.3 and identified a 2hr exposure (from 1hr prior to wounding to 1hpa) in media supplemented with DPI to a final concentration of 150µM. After dosing, larvae were transferred to a new dish containing fresh E3. This was considered the standard treatment for DPI and was used for all subsequent experiments to block Duox activity (unless otherwise stated).

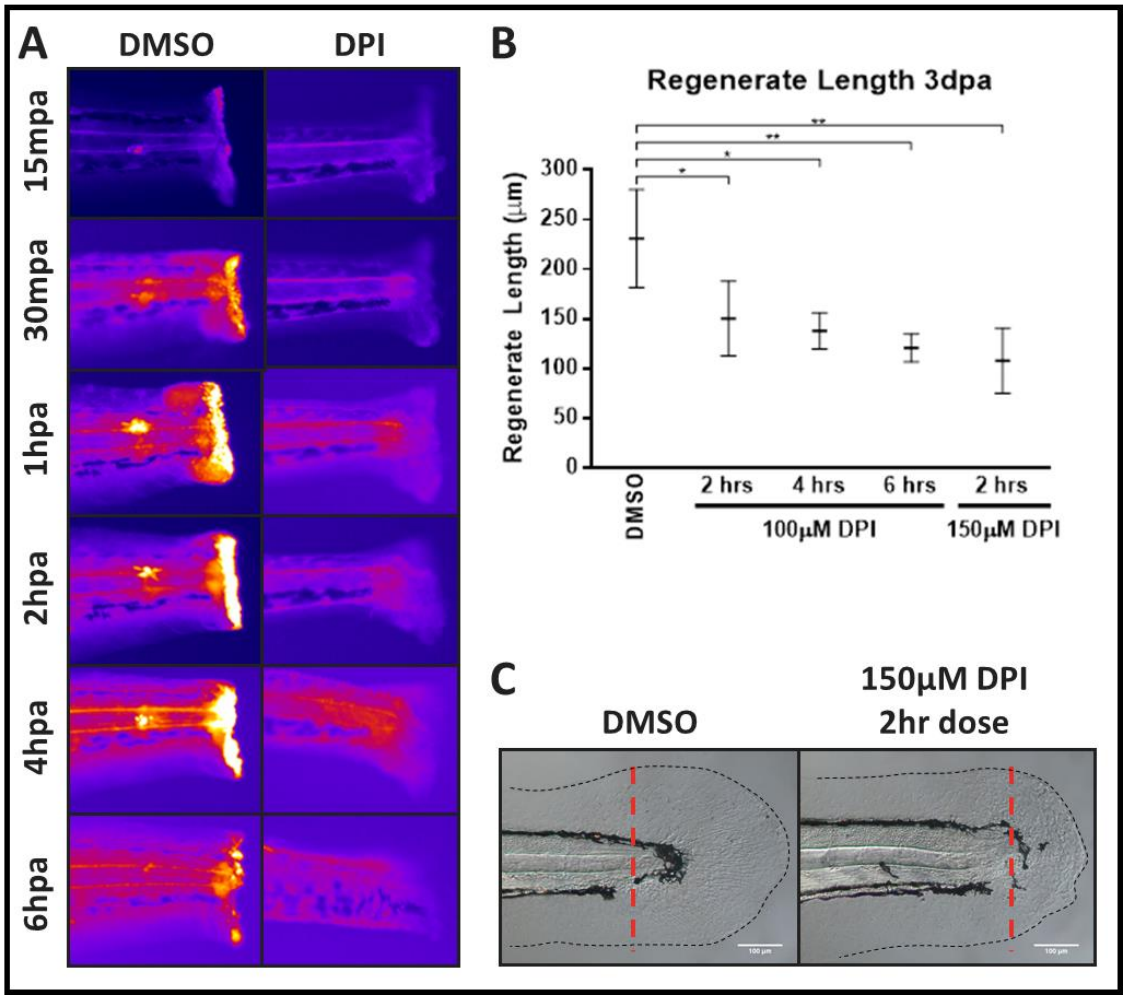

Figure 3.3 – Amputation-induced H_2O_2 is required for regeneration (data obtained during my MSc project[136]).
A) H_2O_2 is detected using PFBSF at the site of injury following amputation of the tail in 3dpf larvae. The amputation-induced H_2O_2 signal is rapidly produced, with signal detected within 15 minutes of injury, peaking at about 2hpa and resolving at around 6hpa (DMSO control, left). This H_2O_2 production is prevented by the addition of DPI (right). **B)** Addition of DPI results in a concomitant inhibition in regenerate length from even short pulse doses at µM concentrations. **C)** Representative images of treatment of larvae with 150µM DPI for 2hrs (1hr pre-amputation till 1hr post). Scale bars: 100µm.

Although the extent of H_2O_2 production was visualised during my MSc[136] (Figure 3.3A), here I have repeated the experiments to accurately quantify the extent of H_2O_2 attenuation following 150µM DPI treatment. H_2O_2 was visualised using pentafluorobenzenesulfonyl fluorescein (PFBSF), a fluorescent reporter specific for H_2O_2 supplemented to the media at the time of wounding[266]. The average fluorescent intensity at the wound site was compared at 30 minutes post amputation (mpa) and DPI treatment resulted in a 78% reduction in H_2O_2 signal intensity, demonstrating a strong inhibition of wound-induced H_2O_2 (Figure 3.4).

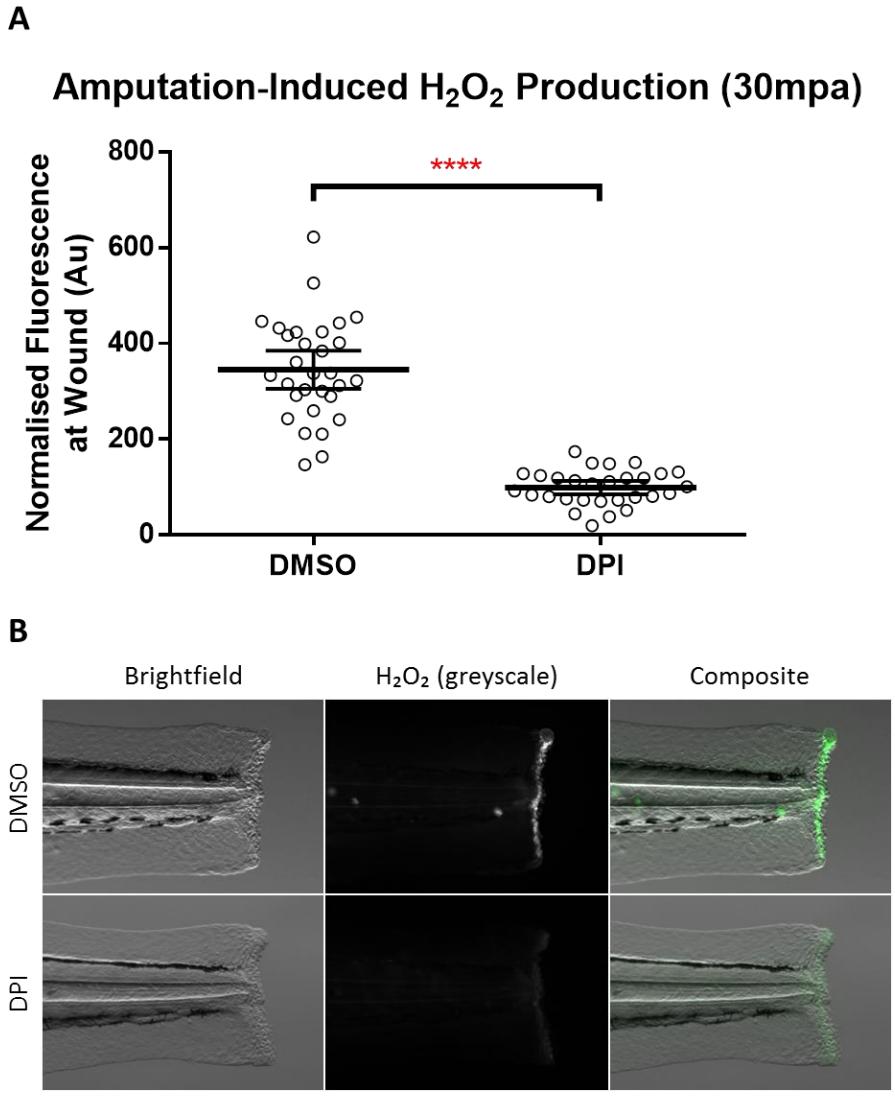

Figure 3.4 – DPI inhibits the production of amputation-induced H_2O_2.
A) Quantification of the mean PFBSF fluorescence at the amputation plane at 30mpa. **B)** Representative images of brightfield, PFBSF fluorescence (H_2O_2) and the composite overlay.

Additionally, experiments were repeated to re-quantify the subsequent decrease in regeneration following H_2O_2 inhibition given that the initial data show here only relied on five data points. Increased numbers of larvae were tested over multiple experimental replicates to increase confidence in the data. Regeneration was assessed as the linear distance between the end of the notochord and the tip of the caudal fin-fold as shown in Figure 2.1. Despite the small numbers of larvae tested initially, estimations for the level of inhibition of regeneration were almost identical. DPI treatment inhibited regeneration by 53% in both data sets (Figure 3.3B 150µM DPI & Figure 3.5) demonstrating a robust and reproducible regeneration defect in the absence of H_2O_2.

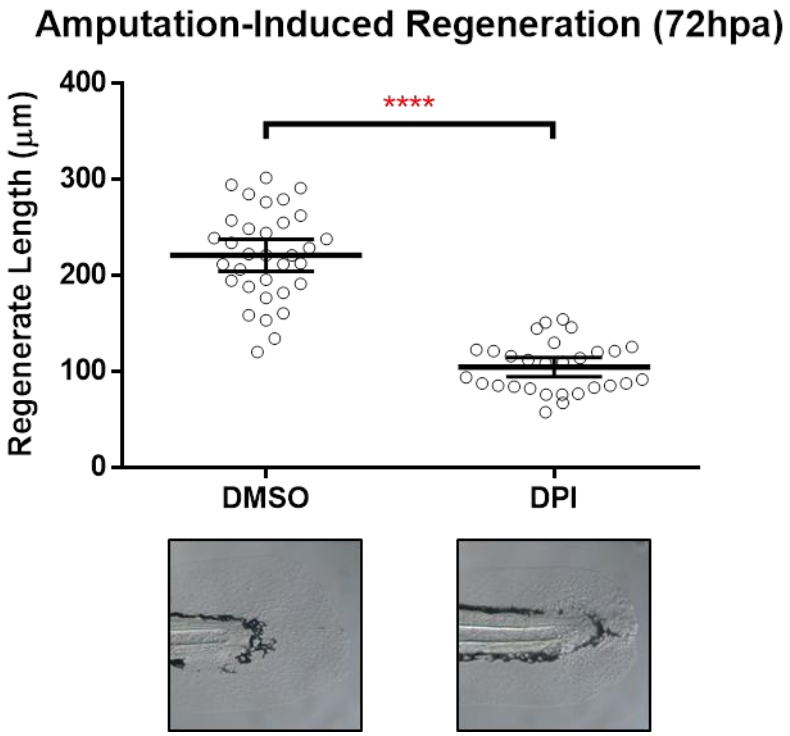

Figure 3.5 – DPI inhibits the regenerative outgrowth of the tail following amputation.
Quantification of the regenerate length at 72hpa with inset representative images.

3.2.1.2 DPI inhibits wound-induced expression of regenerative markers

The DPI-induced regenerative defect in regenerated tissue observed above could result from a failure to properly initiate regeneration, recruit cells to the blastema, induce regenerative proliferation, or a combination of all three. In order to identify which of these regenerative stages requires H_2O_2 to be present, I investigated the effects of depleting H_2O_2 on the

regenerative process at an earlier stage. I carried out whole-mount in situ hybridisation (WISH) for well classified genetic markers to determine the formation of the wound epithelium and blastema at 24hpa.

Expression of the *dlx5a* transcript was chosen as a genetic marker for the wound epithelium as used in previous studies in zebrafish[42,75,113,116,172,267]. This is the zebrafish ortholog of the mammalian *Dlx5* gene which encodes a homeobox transcription factor required for limb development in mammals and it appears to perform a similar function in fin development[268]. A microarray screen of regenerating fins identified a large upregulation of *dlx5a* expression localised to the wound epithelium following wounding[76] suggesting that it may recapitulate its developmental role during regeneration.

The *msxc* gene encodes another homeobox transcription factor upregulated during fin development in a *dlx5a* dependent manner[76,269]. Developmental expression of *msxc* in the caudal fin has terminated by 3dpf and its injury-induced upregulation is restricted to the blastemal cells, making it a good candidate for studying blastemal formation[82,269].

Finally, expression of the *aldh1a2* transcript (which encodes an enzyme responsible for the synthesis of retinoic acid) was used to assess regeneration. Although expression of *aldh1a2* has been shown to be restricted to blastema once it has formed[267,270,271], its expression is initiated before, and indeed required for, the formation of the blastema[66,96,97]. Analysis of *aldh1a2* expression combined with *msxc* expression therefore allows inference of the stage of regeneration – double positive expression will be seen at times after the blastema has successfully formed but *aldh1a2* expression in the absence of *msxc* expression will indicate that signalling to stimulate the formation of the blastema has begun but regenerative cells are yet to migrate to the wound and de-differentiate.

WISH experiments were carried out for all three markers of regeneration at 24hpa in DPI-treated larvae and vehicle-treated controls and their expression levels were compared. The area of staining was quantified for each of the probes using an RGB-threshold as a cut-off to discriminate between “stained” and “unstained”. The expression of *dlx5a* was significantly impaired following DPI treatment with a 60% decrease compared to vehicle-treated controls (Figure 3.6), suggesting that wound-induced H_2O_2 is required to stimulate the formation of the wound epithelium. Secreted mitogenic signals from the wound epithelium stimulate the formation of the blastema; therefore it is unsurprising that the DPI-treatment also resulted in a significant decrease in the expression of both *msxc* and *aldh1a2*. There was a near complete

inhibition of expression of both markers suggesting an inhibition of both pre-blastemal signalling (Figure 3.7A) and blastema formation (Figure 3.7B). The large variation in the control stainings for *msxc* is likely due to assaying expression slightly too early; blastemal formation begins from around 12hpa[75], however this is variable and some larvae had not begun expressing *msxc* even at 24hpa. The absence of expression in any of the DPI-treated larvae still makes a convincing argument that DPI blocks blastema formation, but in hindsight, a later timepoint may have provided more clear evidence by allowing blastemal formation in all control larvae.

Taken together, these data show that inhibition of wound-induced H_2O_2 inhibits regeneration from very early timepoints. Attenuation of the H_2O_2 signal partially inhibits the formation of the wound epithelium and almost completely blocks the formation of the blastema, likely via preventing retinoic acid synthesis. As such, H_2O_2 appears to be responsible for the initiation of regeneration by promoting the formation of the earliest regenerative structures.

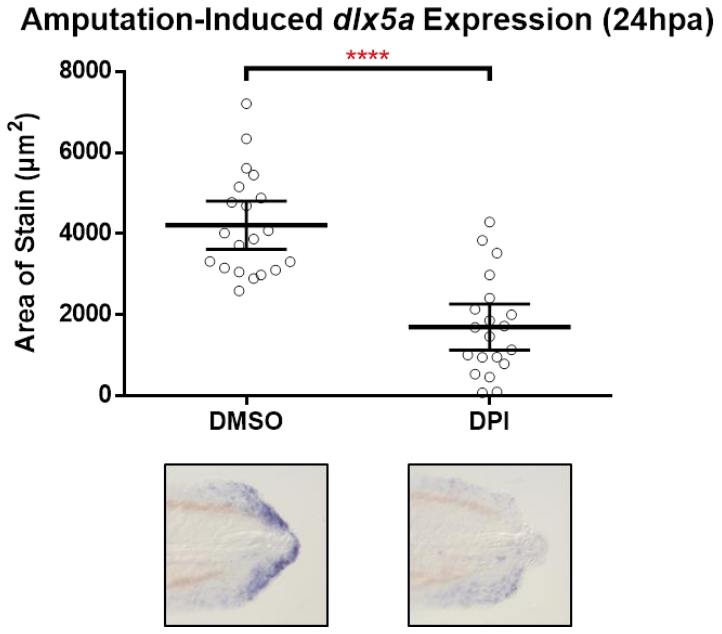

Figure 3.6 – DPI inhibits the amputation-induced expression of the wound epithelium marker *dlx5a*. Quantification of the amputation-induced expression of *dlx5a* at the wound at 24hpa with inset representative images.

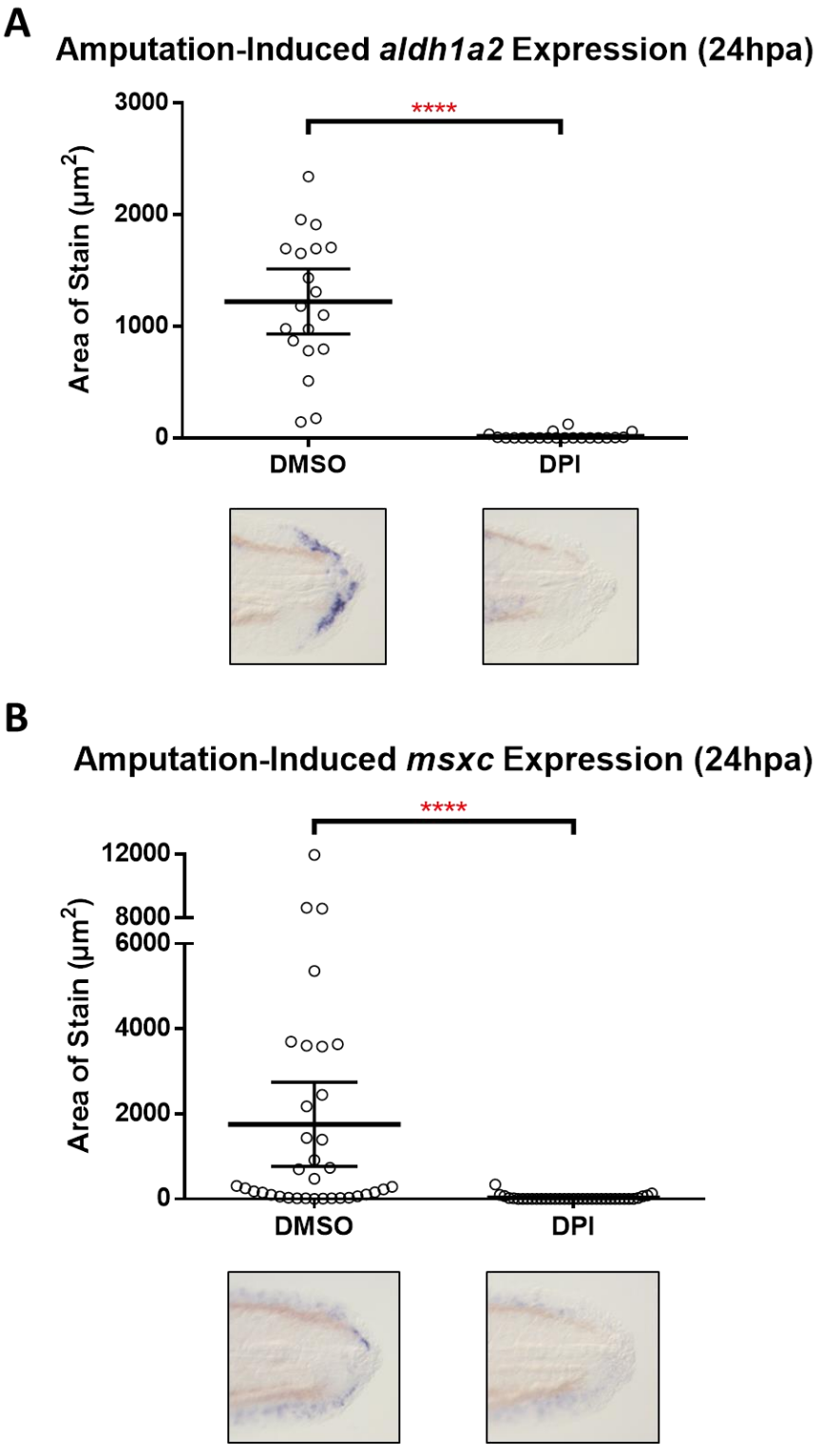

Figure 3.7 – DPI inhibits the amputation-induced expression of blastemal markers *aldh1a2* and *msxc*. Quantification of the amputation-induced expression of *aldh1a2* (**A**) and *msxc* (**B**) at the wound at 24hpa with inset representative images.

3.2.1.3 DPI inhibits regenerative Hh, Wnt & FGF pathway activation

Knowing that H_2O_2 is required for very early events in regeneration, I next attempted to identify potential molecular signalling pathways that may be regulated by H_2O_2 in order to mediate its pro-regenerative effects. Epimorphic regeneration relies on the reactivation of developmental pathways in response to injury to regrow the lost tissue, and multiple developmental pathways have been identified as essential for mediating the regenerative response[66]. This has led people to consider regeneration as akin to re-development and there are often similarities between the two processes.

I decided to investigate the impact of H_2O_2 inhibition on three of these essential regenerative pathways – Hh, Wnt and FGF. Samples were fixed at 24hpa and WISH were carried out for *ptch1*, *tcf7* and *pea3* as markers of Hh, Wnt and FGF pathway activation respectively. Injury-induced H_2O_2 was inhibited with DPI-treatment from 1hr prior to wounding until either 1hpa (pulse dose) or 6hpa (extended dose). Expression of all three transcripts can be seen in vehicle-treated larvae at the wound (Figure 3.8A, B). The cells expressing these markers surround an area of circular tissue which appears to be formed from notochord cells extruding from the end of the extracellular sheath that was severed during wounding. This extruded 'bead' is highly vacuoled and appears to form continuously from the time of wounding, being visible from 1hpa, well-established at 3hpa and reaches its maximum by 6hpa (data not shown). Larvae treated with DPI for either a pulse or extended dose both prevent upregulation of *ptch1*, *tcf7* and *pea3* at the wound (Figure 3.8A, B) but do not appear to affect the normal developmental expression of *ptch1* seen in the trunk or *pea3* seen in the neuromasts (arrowheads in Figure 3.8A, B). Together, these data demonstrate a requirement for H_2O_2 to stimulate a wound-induced activation of Hh, Wnt and FGF signalling, via a regeneration-specific regulatory mechanism not employed for the developmental expression of Hh or FGF signalling.

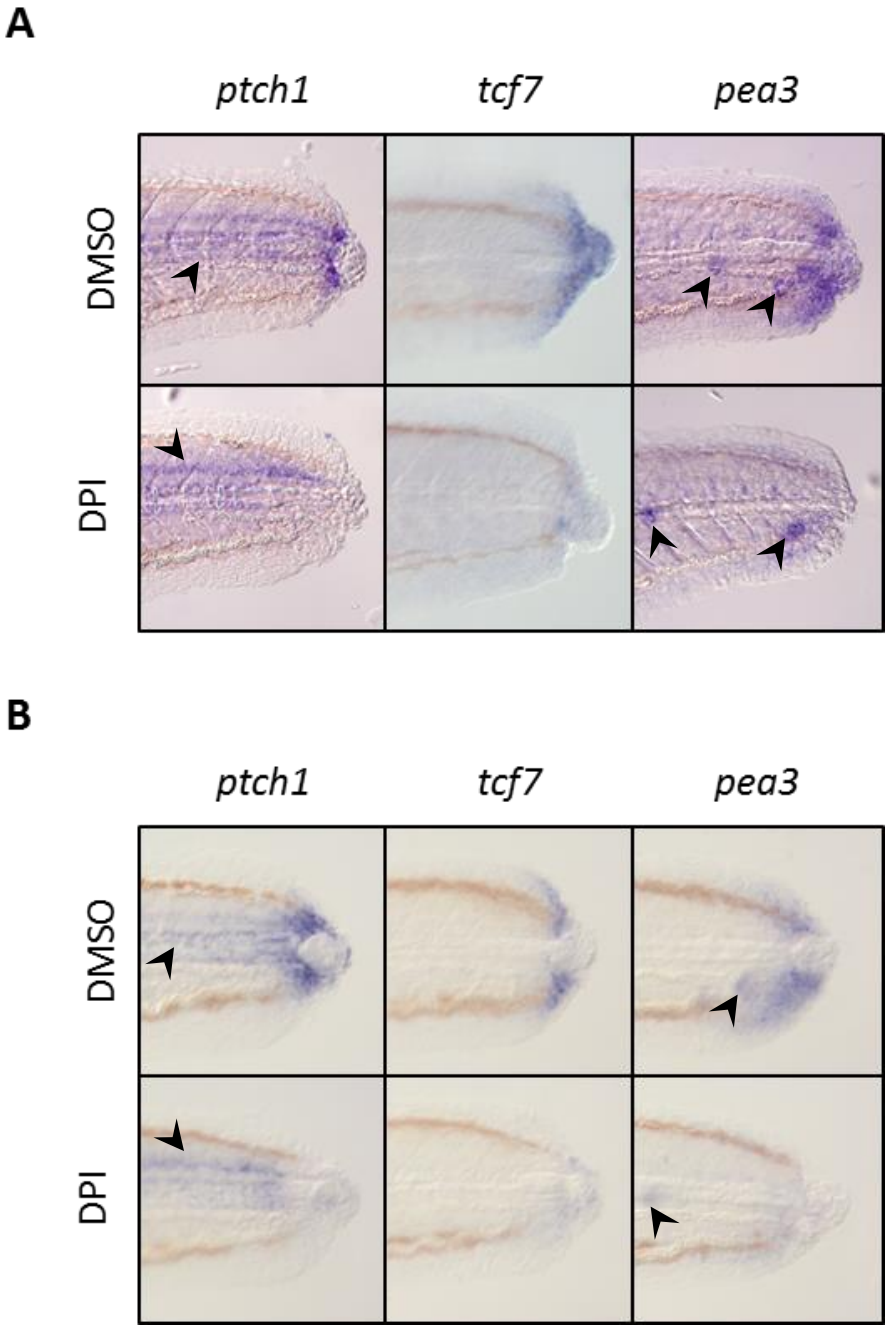

Figure 3.8 – DPI inhibits the amputation-induced expression of the Hh, Wnt and FGF signalling pathways.
Representative images showing the attenuation of amputation-induced expression of *ptch1*, *tcf7* and *pea3*, markers of Hh, Wnt and FGF pathway activation respectively. **A)** Extended dose of DPI from -1hpa to +6hpa, **B)** Pulse dose of DPI from -1hpa to +1hpa. Arrowheads denote developmental expression of the genes; *ptch1* in the notochord and neural tube, and expression of *pea3* in neuromasts.

3.2.1.4 DPI inhibits the wound-induced transcription of Hh ligands in the notochord

At the same time that I was examining the extent of control H_2O_2 exerts over Hh, Wnt and FGF, Maria Garcia Romero of our lab was trying to identify a regulatory hierarchy between these pathways. Based on the timings of pathway activation and chemical epistasis experiments, Hh was identified the upstream regulator of both Wnt and FGF and was responsible for controlling proliferation and regeneration via these two downstream signalling pathways (Summarised in Figure 3.9)[91]. Given this relationship, we hypothesised that Hh was the most upstream target of H_2O_2 signalling and that the downregulation observed in Wnt and FGF in the absence of H_2O_2 is an indirect effect mediated by the attenuation of Hh signalling. Further work in our lab by Phil Jankun, identified specific Hh ligands were rapidly upregulated after amputation[272]; *ihhb* and *shha* were upregulated with identical spatiotemporal profiles whilst *dhh*, *ihha* and *shhb* all remained unexpressed. Wound-induced *ihhb* and *shha* expression increases steadily from the time of wounding, and is detectable at low levels at around 1hpa, robustly expressed at 3hpa, peaks at 6-12hpa and returns to pre-amputation levels by around 30hpa[272]. The rapid onset of *ihhb* and *shha* expression identified these ligands as potential mediators of the H_2O_2 dependent activation of Hh signalling, thus linking the transient wound signal to longer-acting signalling pathways.

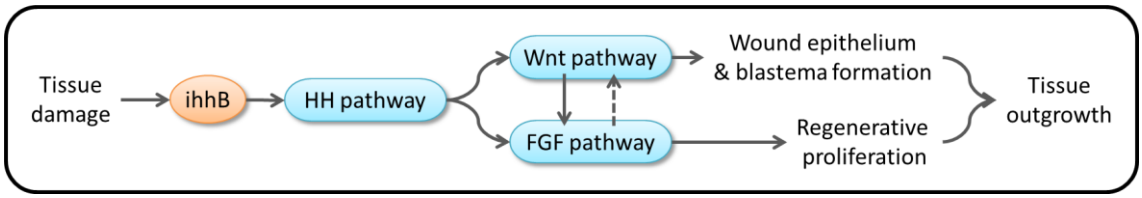

Figure 3.9 – Schematic of the proposed wound-induced signalling hierarchy leading to regeneration.

In order to investigate the relationship between H_2O_2 and wound-induced Hh ligands, WISH was performed in the presence and absence of H_2O_2 and expression levels of both transcripts were compared at 6hpa. Control larvae present a robust, intense and sharply defined expression of *ihhb* and *shha* within the extruded notochord bead at the wound site. Inhibition of H_2O_2 with DPI treatment resulted in an absence of both *ihhb* and *shha* expression in the extruded 'bead' (Figure 3.10) suggesting that both transcripts are regulated by wound-induced H_2O_2, supporting the hypothesis that H_2O_2 directly regulates regenerative Hh signalling. The precise demarcation of the induced expression within the notochord bead further suggests

that this is a cell-specific regulation, a hypothesis which is further supported by the absence of *ihhb* induction in tails where only the caudal fin-fold is resected and the notochord remains uninjured (Figure 3.11).

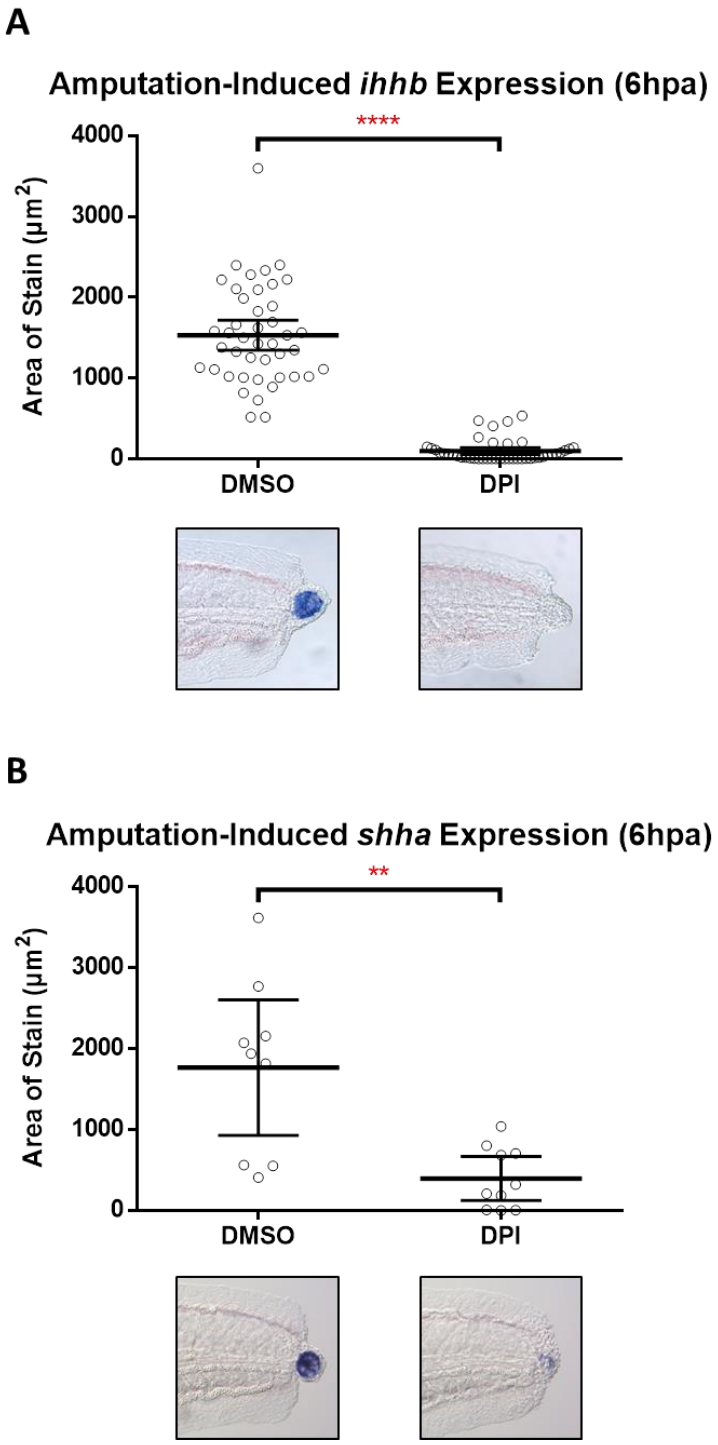

Figure 3.10 – DPI inhibits the amputation-induced expression of the Hh ligands *ihhb* and *shha*. Quantification of the amputation-induced expression of *ihhb* (**A**) and *shha* (**B**) at the wound at 6hpa with inset representative images.

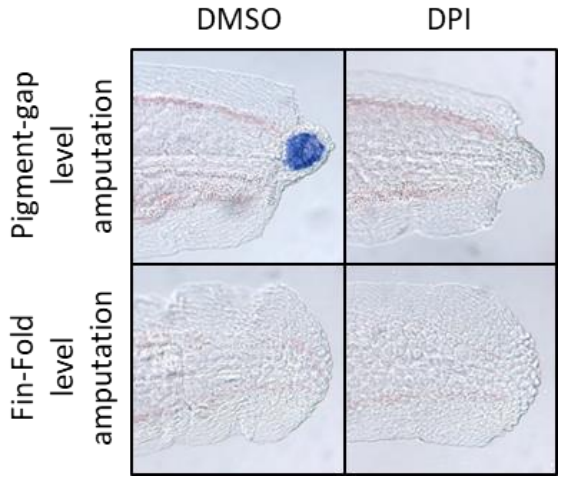

Figure 3.11 – Wound-induced *ihhb* expression required severance of the notochord.
Representative images showing *ihhb* expression in larvae amputated at the pigment-gap (top), resulting in notochord severance and an absence of *ihhb* expression in larvae following fin-fold level amputation which leaves the notochord intact (bottom).

3.2.1.5 Hh ligands are expressed endogenously in the uncut notochord

Although uninjured larval controls do not show expression of Hh ligands, it has been suggested that the strong ECM notochord sheath is hard to permeabilise by standard WISH protocols, and therefore a lack of staining may simply represent a lack of penetration of the anti-sense probe. In order to address this, I repeated the WISH with a genetic marker for notochord cells – *col11a1a*. Col11a1a is a collagen sub-type synthesised in the zebrafish notochord[273], likely to contribute to the extracellular sheath to add rigidity to the organ. This structural protein should be constituently expressed in the notochord cells irrespective of age and therefore WISH with this probe should show a clear staining of the entire organ. In 20hpf larvae, the probe worked well, showing strong and defined staining along the whole length of the notochord (Figure 3.12A). In injured 3dpf larvae however, whilst *col11a1a* expression could be detected in the extruded notochord bead, the probe did not infiltrate further into the notochord suggesting that the intact notochord sheath is preventing detection of transcripts via WISH (Figure 3.12B). The expression pattern of *col11a1a* very closely matched that of *ihhb* and *shha*, raising the possibility that they were actually expressed constituently within the notochord like *col11a1a*, and that it is only upon extrusion of the cells that they can be detected. This would imply a different regulatory mechanism based around release of a pool of

Hh ligand from the ruptured notochord rather than a localised wound-induced upregulation of Hh ligands.

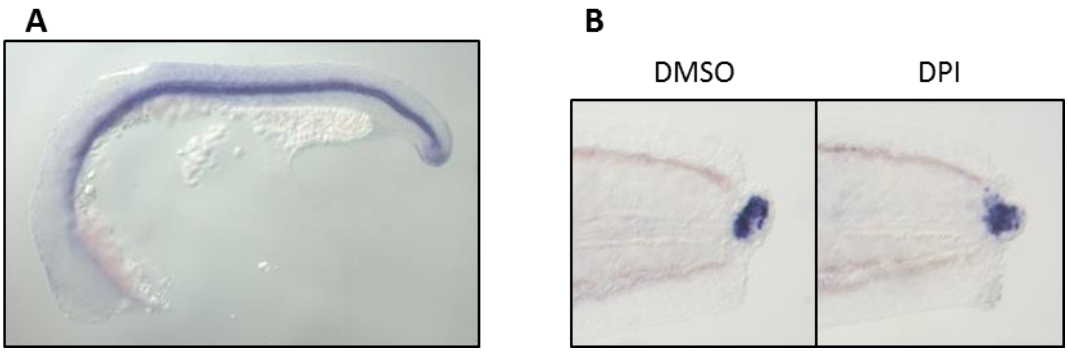

Figure 3.12 – Expression patterns of *col11a1a*.
WISH staining of *col11a1a* in 20hpf larvae (**A**) and 3dpf larvae 6hpa (**B**).

Hh signalling is known to be induced in the developing notochord, but it is unclear exactly when expression of Hh ligands is turned off. In order to address whether developmental Hh ligand expression was still active at the time of wounding, I first attempted to cryo-section larvae along the transverse plane to circumvent poor notochord permeabilisation and allow accurate expression patterns to be observed. Unfortunately, possibly due to the highly vacuoled nature of the notochord cells, I did not obtain any high quality *in situ* stains with this method. As an alternative, unwounded larvae were bisected within the trunk to expose the notochord but only after fixation in order to not induce any biological response. These cut larvae were then subjected to the standard WISH protocol to assess *ihhb* and *shha* expression.

This staining method confirmed that *ihhb* is constituently expressed in the notochord at 3dpf, as strong expression was clearly observed at the in the notochord proximal to the cut (Figure 3.13A). A gradient of expression was detected, with the strongest expression at the bisection site, gradually reducing as it moves caudally. Considering that a proximodistal expression gradient was seen in all larvae, irrespective of the precise position along the trunk where they were bisected, and running both caudally and rostrally from the cut (i.e. in the rostral half of the bisected larvae, a similar pattern was observed with the strongest expression at the bisection site which decreased as it moved rostrally; data not shown), I concluded that this represented a gradient in detection efficiency of the WISH protocol (presumably due to a

penetration issue of the *in situ* probe) rather than a true reflection of a biological expression gradient.

Interestingly however, unlike the *ihhb* expression in the extruded notochord following wounding, *ihhb* expression in endogenous notochord does not appear to be H_2O_2 dependent as treatment with DPI had no effect on expression levels (Figure 3.13A'). Follow-up WISH on 6hpa larvae, bisected in a similar manner post-fixation, confirmed that DPI treatment inhibits *ihhb* expression at the wound, but not in the distal notochord in the trunk (Figure 3.13B, B') therefore supporting the hypothesis that H_2O_2 is required for the wound-induced upregulation of *ihhb* in the extruded notochord cells but not for endogenous *ihhb* expression.

Analysis of *shha* WISH showed that this transcript is also endogenously expressed in the notochord at 3dpf, as well as in the neural tube and the intestine (Figure 3.13C). The notochord-specific expression appeared to be regulated in a similar manner to that of *ihhb*, with DPI treatment inhibiting expression in the extruded notochord at the wound site but having no visible effect on endogenous expression levels in the distal notochord in the trunk (Figure 3.13C').

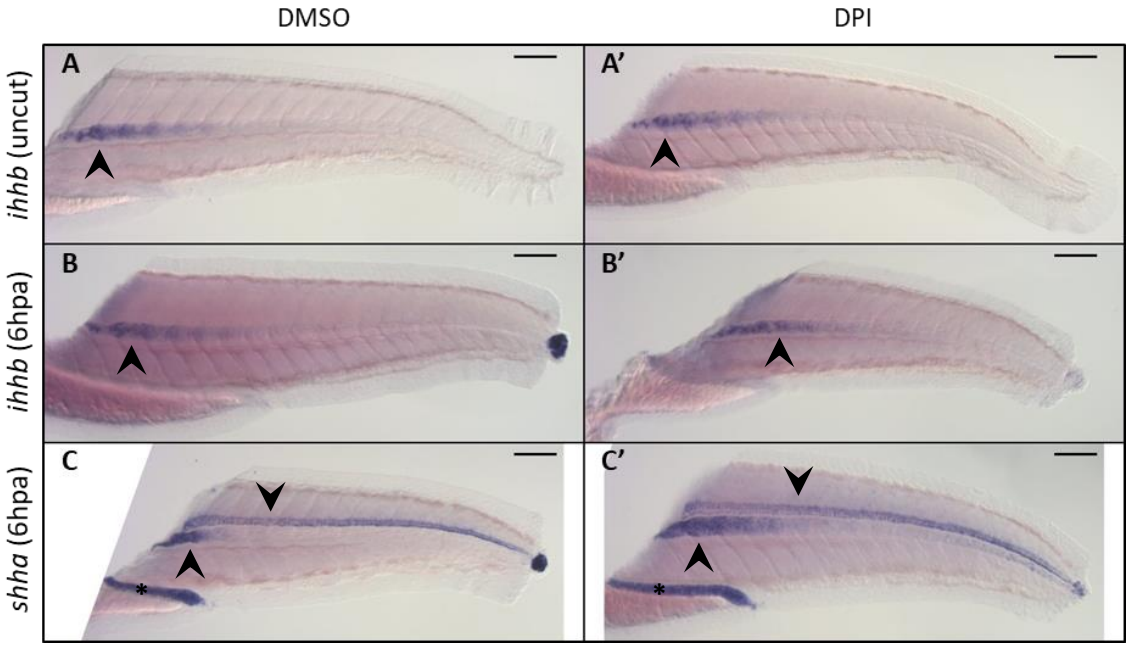

Figure 3.13 – Expression patterns of Hh ligands.
Representative images of WISH analysis of the expression of the Hh ligands *ihhb* and *shha* in the presence (**A**, **B**, **C**) and absence (**A'**, **B'**, **C'**) of DPI. Larvae were bisected post-fixation to expose the notochord without stimulating an injury response. **A)** Endogenous expression of *ihhb* is visible in the notochord (upward arrowhead) and appears unaffected by DPI treatment (**A'**). **B)** Endogenous expression of *ihhb* in the notochord (upward arrowhead) appears unaffected by tail amputation and DPI treatment (**B'**). **C)** Following tail amputation, *shha* is present in the floorplate (downward arrowhead), the notochord (upward arrowhead), the intestine (asterisk) and the extruded notochord. DPI treatment inhibits the expression in the extruded notochord only (**C'**). Scale bars: 200µm.

3.2.1.6 Hh ligands are significantly upregulated following wounding – qPCR quantification

Now knowing that Hh ligands are expressed endogenously in the notochord in 3dpf larvae and that the WISH has limitations in detecting notochord specific expression, the observed wound-induced transcription of *ihhb* could simply be detection of the basal level of expression of these ligands. However, the fact that H_2O_2 is not required for the maintenance of this endogenous expression (Figure 3.13), yet is required for the expression seen following wounding (Figure 3.10A, Figure 3.13B) suggests that there may a H_2O_2 dependent upregulation of basal levels following wounding. In order to investigate this, qPCR was performed in order to more accurately quantify the expression levels of Hh ligand expression. As *ihhb* and *shha* appeared to be jointly regulated during wounding, continued work focused on *ihhb* as the archetype for both Hh ligands.

In order to extract mRNA for quantification, tissue samples were taken from injured and uninjured larvae as shown in Figure 3.14. Due to the localised nature of the *ihhb* upregulation, tissue samples were taken from the wound at 6hpa. Using the height of the larvae as a guide, the distal portion of the tail was resected resulting in a roughly 400µm x 400µm square piece of tissue. This tissue was rapidly transferred into TRI Reagent to fix the sample. For controls, simply taking an equal amount of tissue from the end of the uninjured tail would not be a fair comparison as this would comprise mainly fin-fold epithelial cells instead of the complex mix of epithelial cells, blood vessels, notochord, neural tube and muscle present in the tissue samples taken from the end of the injured larvae's tail. For this reason, immediately before fixation, the standard tail amputation wound was performed to remove the same tissue that was removed from the injured larvae and then a 400µm x 400µm tissue sample was taken to cover the same area of the tail in both injured and uninjured groups. This therefore normalised the difference in relative cellular populations at different positions along the tail and allowed like for like comparison between wounded and unwounded larvae. The removal of the caudal tissue was carried out as quickly as possible to prevent any wound-induced transcriptional changes. Pooled samples for 100 larvae for each group were used to extract sufficient mRNA and to account for biological variance within the pooled samples.

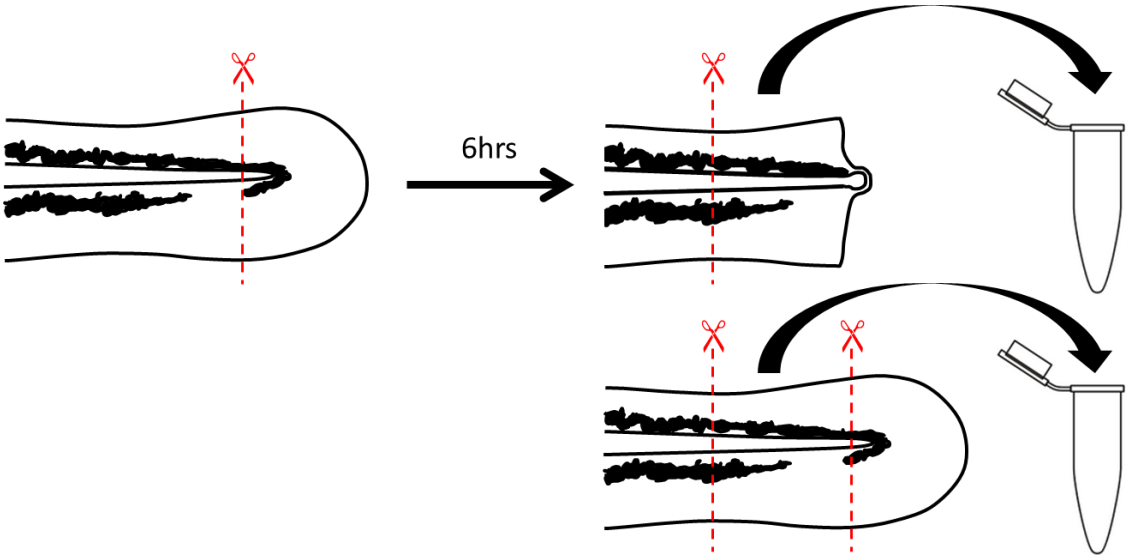

Figure 3.14 – Schematic of tissue samples taken for qPCR expression profiling.
Samples for qPCR analysis of gene expression were pooled from multiple injured larvae at 6hpa (top) or from the equivalent region of tissue removed from uninjured larvae as controls (bottom).

The expression levels of *ihhb* were assessed by qPCR using the ΔCt method. This relative quantification method requires a reference gene in order to normalise samples and return the amount of *ihhb* transcript in relation to the amount of the reference gene transcript. For this quantification, I used two different reference genes in order to gain the most information possible from the experiment and to increase confidence in the data. The first, *β2m*, encodes β(2)-microglobulin which is a sub-unit of the MHC class I molecule and therefore is present on all cells as part of the acquired immune system. It has been empirically shown to be a very stably expressed in zebrafish over different developmental stages and different tissue types[274], making it particularly suited as a reference gene to normalise the cDNA input for variation in total cell number. The second reference gene used was *col11a1a* because, as explained above, this is a specific notochord marker and is therefore be able to normalise for variation in the notochord cell number, potentially allowing comparisons for gene expression in relation to notochord cells specifically.

3.2.1.6.1 qPCR optimisation

Before assessing samples via the qPCR method, careful optimisation was carried out to ensure that the results are quantitative and reliable. Multiple primer sets were tested for specificity and amplification efficiency and primer concentration, annealing temperature and extension time were optimised. The final optimised assay was validated by two methods: 1) testing the dynamic range of reverse transcription to ensure a consistent amplification efficiency over a range of RNA input concentrations, and 2) testing the amplification efficiency over a range of cDNA input concentrations to ensure ΔCt measurements are a valid quantification method.

The dynamic range of the RT reaction can be tested by simply diluting the extracted RNA samples before performing the cDNA synthesis step and then running the qPCR as normal. When plotted against each other, there should be a clear linear relationship between Ct and initial RNA input for each primer pair. This relationship is observed in all three primer pairs used with high correlation coefficients and reasonable efficiencies (Figure 3.15A). When ΔCt values are plotted between the primers at each dilution point, each comparison produces results with minimal fluctuation and flat regression lines (Figure 3.15B). These data demonstrate that fluctuations in the amount of RNA used for cDNA synthesis will not affect the accuracy or quality of the resulting data.

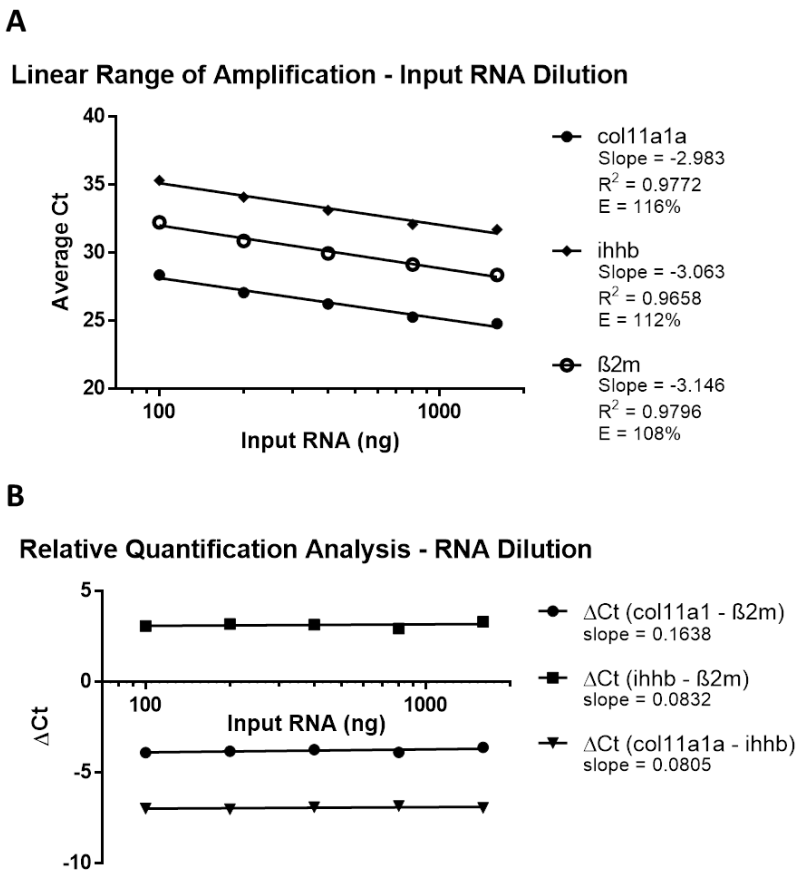

Figure 3.15 – qPCR optimisation: dynamic range of RNA input.
A) Primer sets show linear amplification over a range of initial RNA concentrations. **B)** Comparative analysis of amplification between primer sets shows an acceptably consistent ΔCt over a range of initial RNA concentrations to allow relative quantification to be used.

Next, to establish the amplification efficiency for each primer pair, a similar experiment was performed but this time using a serial dilution of the cDNA added to each well in the qPCR. As for the RNA dilutions, serial cDNA dilutions should produce a clear linear relationship with efficiencies around 100%. When Cts are plotted against cDNA concentration, strong linear relationships can be seen for all primer pairs with high correlation coefficients and efficiencies close to 100% (Figure 3.16A). Plotting ΔCt values for *col11a1a* compared to *β2m* produces a graph with a flat regression line, however when comparing *ihhb* to either *β2m* or *col11a1a*, the regression lines are less flat than is optimal (Figure 3.16B). This will introduce some variation into the data, however, there is no consensus on when this value becomes too high to be used in quantification and I am using qPCR to help validate an already documented upregulation,

not to exactly quantify a novel interaction and therefore I believe that these values are appropriately stringent for the experiments.

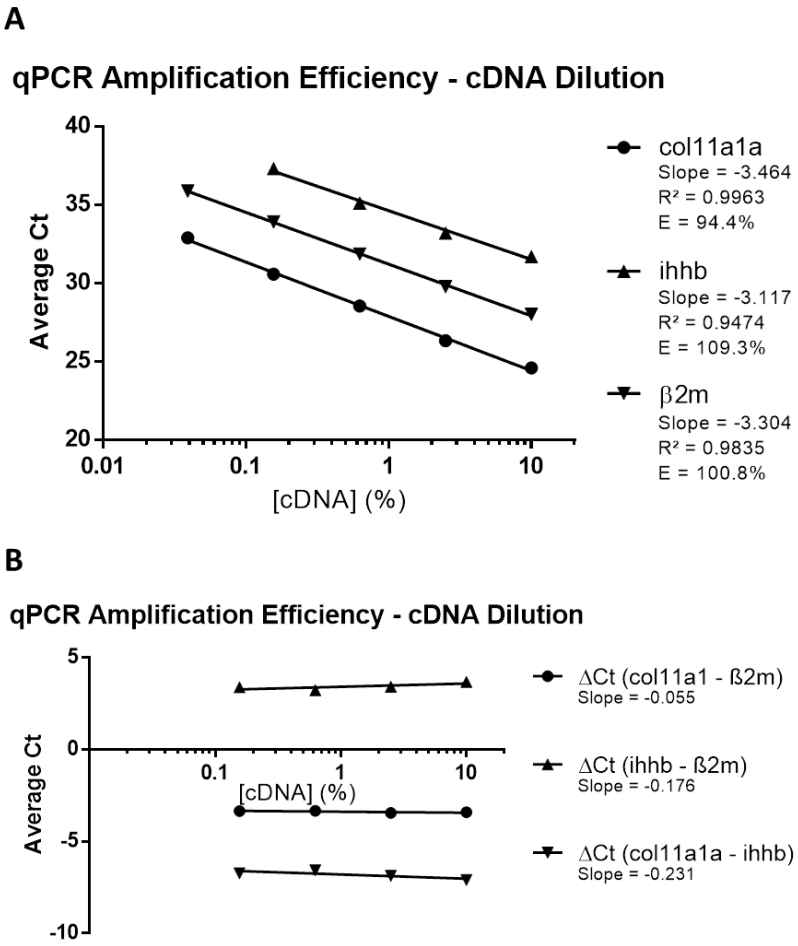

Figure 3.16 – qPCR optimisation: primer efficiency.
A) Primer sets show acceptable efficiency over a range of input cDNA concentrations. **B)** Comparative analysis of primer efficiency between primer sets shows an acceptably consistent ΔCt over a range of input cDNA concentrations to allow relative quantification to be used.

3.2.1.6.2 qPCR quantification

Having optimised and validated the qPCR protocol, it was used to analyse gene expression in test samples of injured and uninjured larvae. The quantification of *ihhb* expression shows a significant increase at 6hpa relative to both *β2m* and *col11a1a* (Figure 3.17A) supporting an upregulation of the gene in response to wounding. The more extreme increase in *ihhb* when compared to *col11a1a* initially appears to support a very high upregulation of *ihhb* within notochord cells specifically, however, closer inspection shows that *col11a1a* is actually

downregulated in response to wounding when compared to *β2m* (Figure 3.17B). After normalising this relative change in *col11a1a*, and re-analysing relative expression of *ihhb*, the result very closely matches that seen by using *β2m* as a reference, increasing confidence in the data set (Figure 3.17C). I hypothesise that *shha* is regulated in a similar fashion, although a repeat of this qPCR would be required to confirm this. Taken together, these data support the hypothesis that *ihhb* (and potentially *shha*) are expressed at low levels in the notochord at 3dpf in a H_2O_2 independent fashion. Upon wounding, the expression of these Hh ligands is rapidly upregulated in a response that requires H_2O_2.

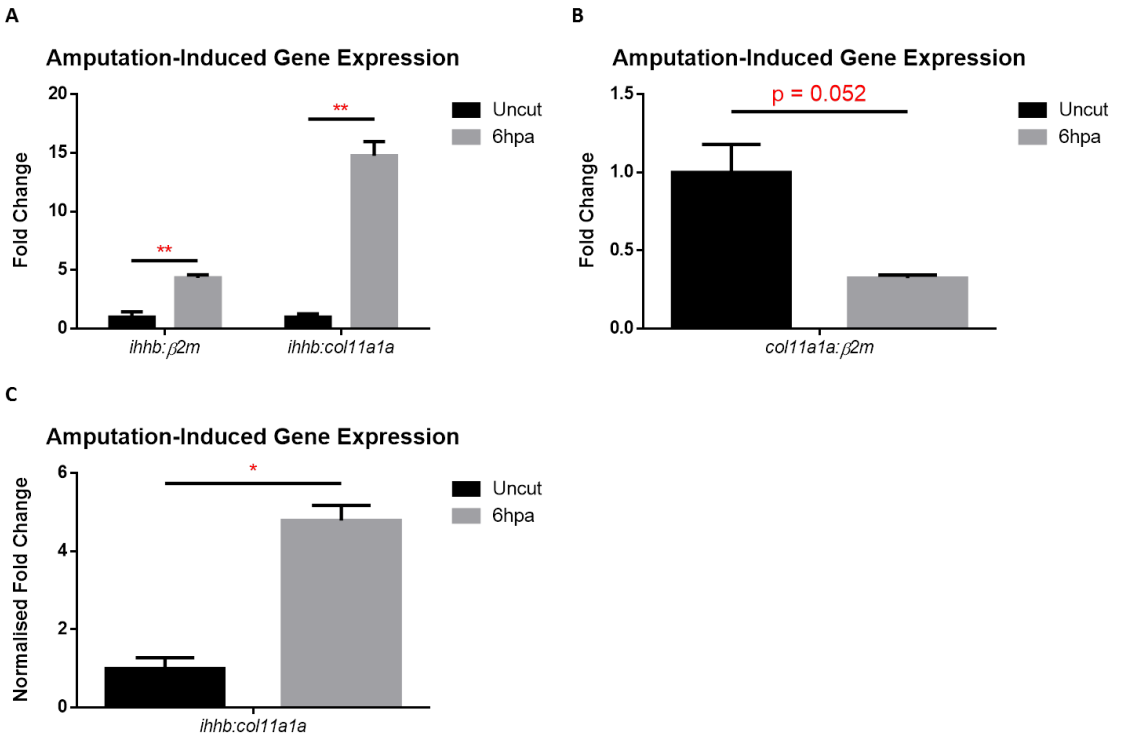

Figure 3.17 – Amputation-induced expression of *ihhb*.
A) Fold-change of *ihhb* expression in uncut and 6hpa larvae relative to *β2m* and *col11a1a*. **B)** Fold-change of *col11a1a* expression in uncut and 6hpa larvae relative to *β2m*. **C)** Fold-change of *ihhb* expression in uncut and 6hpa larvae relative to *col11a1a* after normalising for amputation-induced reduction of *col11a1a* expression.

3.2.2 Scavenging amputation-induced H_2O_2 with antioxidants

DPI is widely used as an inhibitor of Nox family enzymes (often specifically targeting Duox) and has performed robustly and reproducibly in my experiments to prevent the wound-induced synthesis of H_2O_2. One concern with treating larvae with DPI to block Nox enzymes is that as a

flavoenzyme inhibitor it is fairly promiscuous and is known to block the activity of other enzymes *in vivo*[275]. In order to address the possibility that the DPI-induced effects are mediated via interactions unrelated to its ability to prevent H_2O_2 production, I wanted to use additional inhibitors of Duox to reproduce the regenerative defects. Confirming these effects with an unrelated inhibitor would allow me to confidently characterise those responses as H_2O_2 specific.

In my MSc, I tested the anti-inflammatory plant phenol Apocynin and the serine protease inhibitor 4-(2-Aminomethyl)benzenesulfonyl fluoride (AEBSF) as alternatives to DPI. Apocynin has been used successfully as a Nox enzyme inhibitor *in vivo* studies of multiple species, including zebrafish[124,141] although the mechanism of action is incompletely understood. It appears to require activation by myeloperoxidase to function as a Nox inhibitor but even without activation it is capable of attenuating ROS signalling likely by acting as a direct ROS scavenger[276]. AEBSF has been reported to inhibit Nox family enzymes but it has mainly been used in cell culture[275,277,278] due to its low potency[279]. It is also known to have its own unspecific effects including the inhibition of serine proteases[279]. Dosing larvae with these compounds at a variety of concentrations did not result in significant inhibition of regeneration at 48hpa (Figure 3.18), although H_2O_2 production itself was not quantified.

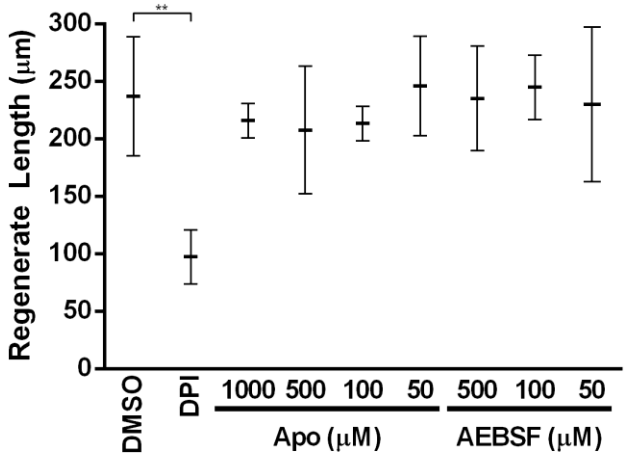

Figure 3.18 – DPI produces significant inhibition of regeneration; apocynin and AEBSF do not (reproduced from my MSc thesis[136]).
2dp larvae were dosed with DMSO (vehicle control), 150μM DPI, apocynin (Apo) or AEBSF 1hr prior to amputation and 1hr post-amputation. Amputation was performed at the caudal tip of the pigment gap of the tail. Length of the regenerated caudal fin was measured at 72hpa. Data represent mean +/- SD. Raw data tables are included in Appendix A. Significance: ** p≤0.01.

In addition to this, in my PhD project I tested VAS2870 – a newly developed and more specific inhibitor of Nox family enzymes, and is often used alongside DPI to test specificity of that interaction[119,120,275,277]. It has been shown to possess no inhibitory effect towards the xanthine oxidase or eNOS, both flavoenzymes targeted by DPI[275]. I found that doses over 1.5µM were rapidly lethal but at 1.5µM or below I could not detect any inhibition of regenerate length (Figure 3.19A). When amputation-induced H_2O_2 production was quantified using PFBSF, VAS appeared much more variable than wild-type with some larvae producing less H_2O_2 and some producing more H_2O_2, but overall there was no significant difference to controls at the highest permissible concentration (Figure 3.19B; VAS (1.5µM)). Lower concentrations also appeared ineffective at inhibiting H_2O_2 and actually appeared to increase H_2O_2 levels (Figure 3.19B; VAS (500nM)). Therefore I was unable to identify an alternative Duox inhibitor capable of a reproducible and robust inhibition of wound-induced H_2O_2 in my model system.

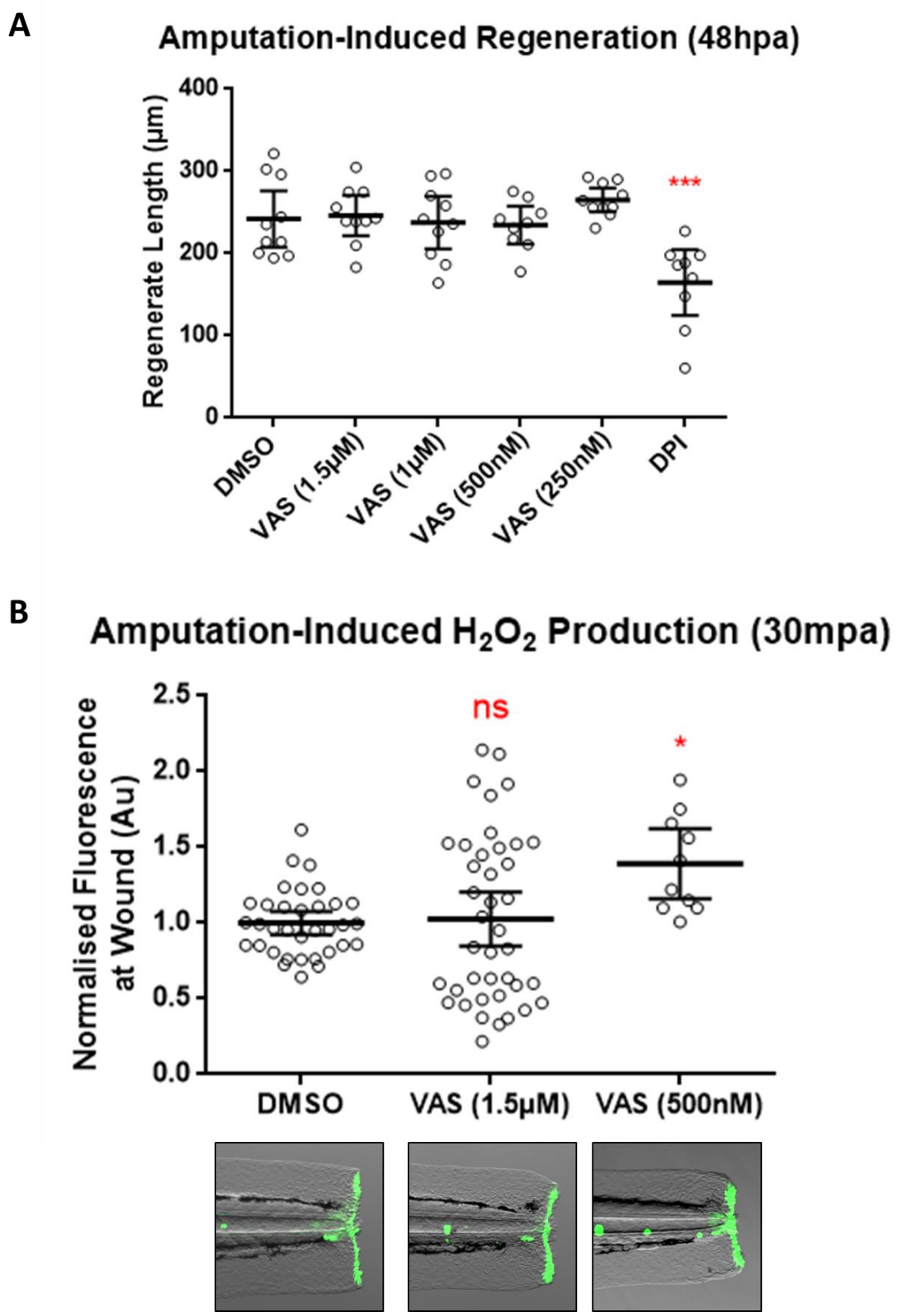

Figure 3.19 – VAS2870 does not impair larval tail regeneration or wound-induced H_2O_2 production. **A)** Quantification of the regenerate length at 48hpa with inset representative images. B) Quantification of the mean PFBSF fluorescence at the amputation plane at 30mpa with inset representative images.

3.2.2.1 MCI-186 inhibits wound-induced H_2O_2, regenerate length and Hh ligand upregulation

As an alternative to inhibiting H_2O_2 production, I then attempted to counteract the induced H_2O_2 signal by sequestering it with antioxidants. 3-Methyl-1-phenyl-2-pyrazolin-5-one (MCI-186) is a free radical scavenger which has previously been used as an anti-oxidant to target ROS *in vivo* in *Xenopus*, and was therefore tested for similar activity in our zebrafish model. Considering the rapid production of H_2O_2 post wounding a high dose of MCI-186 (final concentration of 2mM) was supplemented to the larval media at the time of wounding until 3hpa to scavenge H_2O_2 during the period of its most rapid production. This treatment resulted in a significant decrease in H_2O_2 concentration at the wound to 51% of the vehicle-treated control group (Figure 3.20).

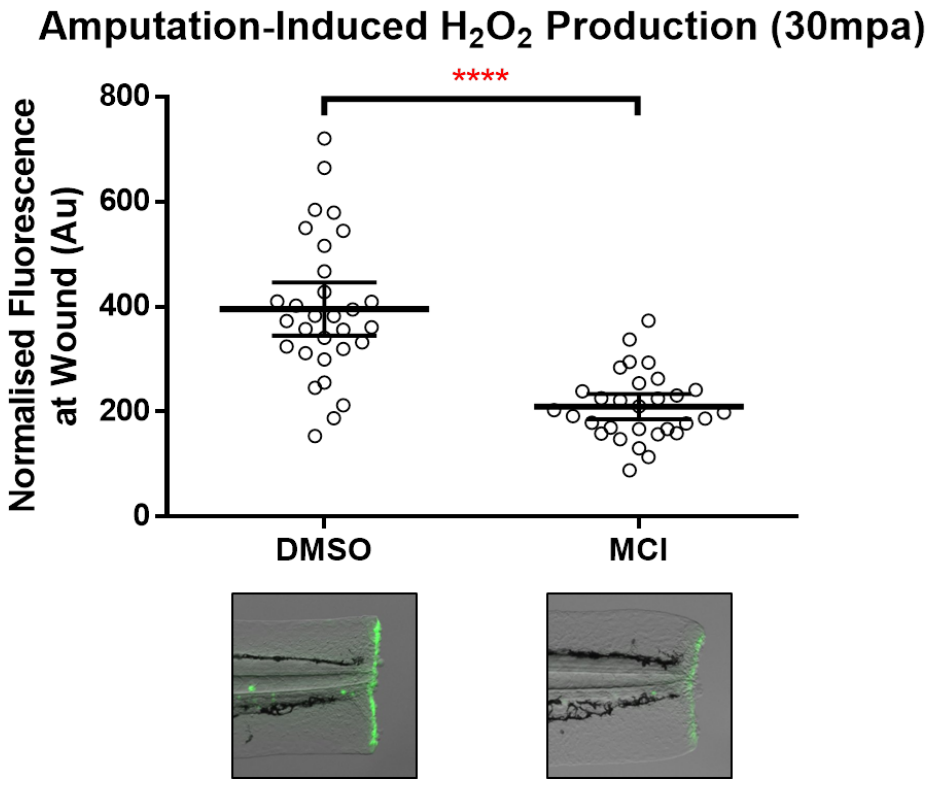

Figure 3.20 – MCI inhibits the production of amputation-induced H_2O_2.
Quantification of the mean PFBSF fluorescence at the amputation plane at 30mpa with inset representative images.

This treatment was, however, more variable than DPI and resulted in a less complete knockdown of H_2O_2 (Figure 3.4) but should be sufficient to corroborate the DPI data. This 3hr pulse dose of MCI-186 was also sufficient to cause a significant decrease in regenerate length at 72hpa (Figure 3.21A), demonstrating that early ROS signals are important for late stage regeneration. The MCI-186 induced regeneration defects were more variable and less severe than for DPI treatments (Figure 3.5), closely matching its effects on the H_2O_2 signal.

Next, this 3hr pulse MCI-186 treatment was also used to assess the wound-induced transcription of *ihhb*. Quantification of WISH stainings showed a significant decrease in *ihhb* expression following MCI-186 treatment (Figure 3.21B), although once again this effect was more moderate than that seen with DPI (Figure 3.10).

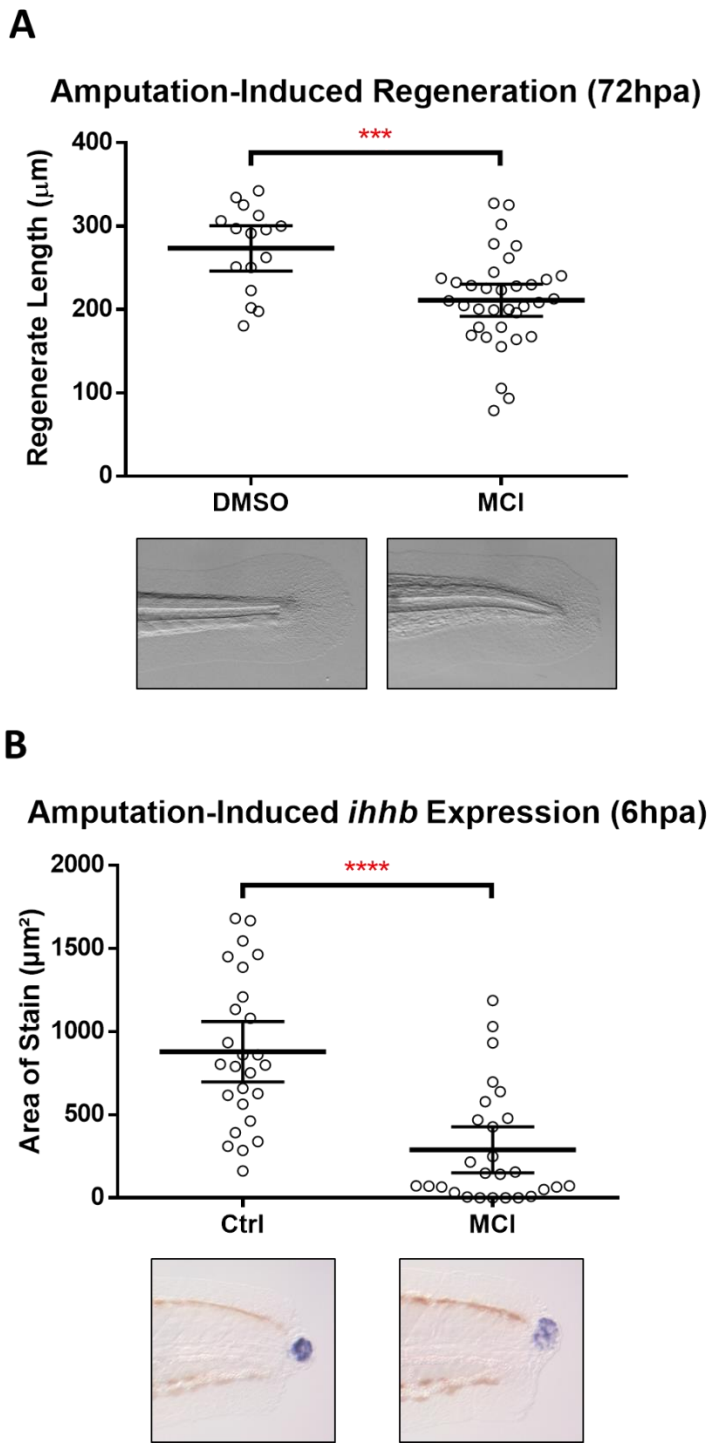

Figure 3.21 – MCI inhibits regenerative signalling and subsequent tail regrowth following amputation. A) Quantification of the regenerate length at 72hpa with inset representative images. **B)** Quantification of the amputation-induced expression of *ihhb* at the wound at 6hpa with inset representative images.

As a final validation of these data, I also tested the effect of a second antioxidant – ascorbic acid (vitamin C) – to see if the effects of MCI-186 could be replicated by an unrelated ROS scavenger. Supplementing the media with 500µM ascorbic acid from 0-3hpa was also able to significantly impair the wound-induced H_2O_2 response (Figure 3.22A) and *ihhb* transcription (Figure 3.22B).

These antioxidant treatments appear to phenocopy the regenerative defects induced by DPI treatments; both early transcriptional regulation (required to initiate regenerative signalling) and late-stage tissue regrowth were inhibited by scavenging ROS and attenuating the injury-induced H_2O_2 signal. Taken altogether, these data provide supporting evidence that the regeneration defects observed in DPI treated larvae are caused by the inhibition of ROS production and that wound-induced H_2O_2 is required to stimulate regeneration via the initiation of Hh signalling.

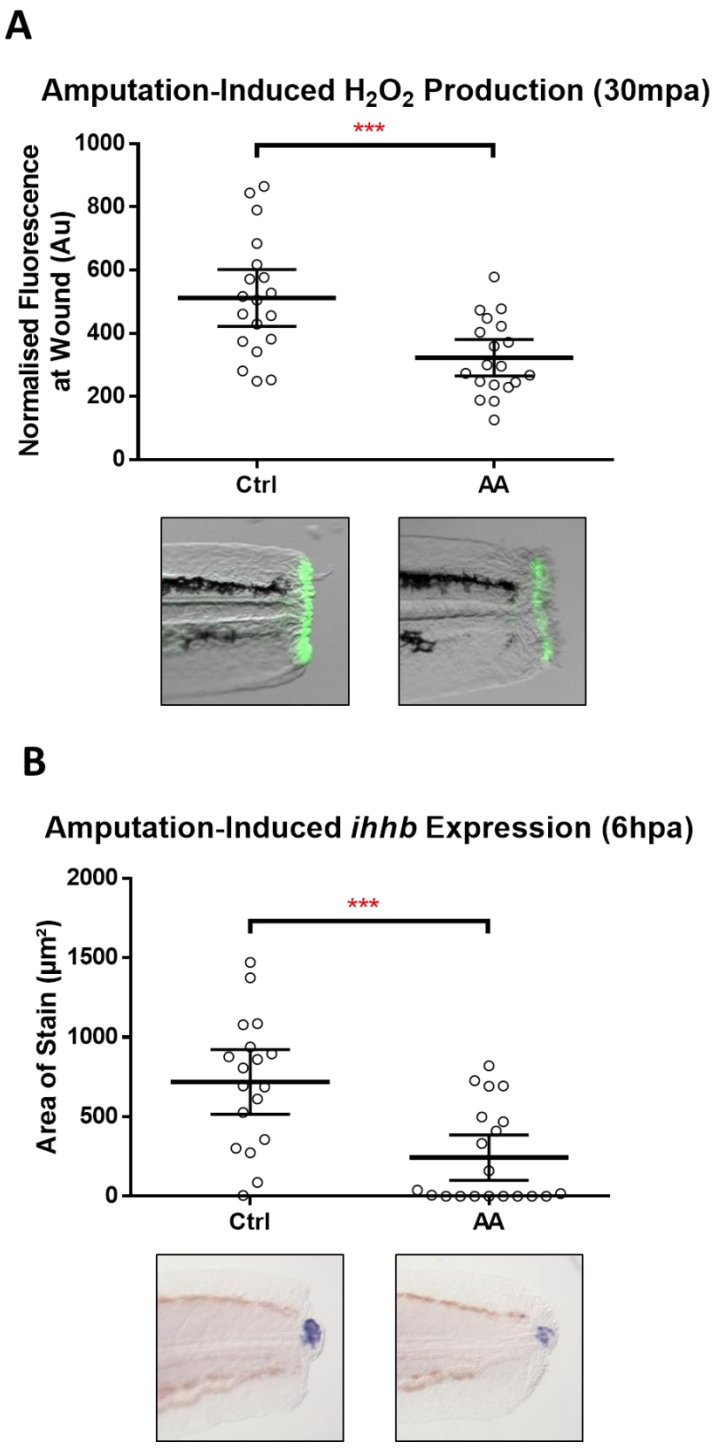

Figure 3.22 – AA inhibits the production of amputation-induced H_2O_2 and subsequent *ihhb* expression. **A)** Quantification of the mean PFBSF fluorescence at the amputation plane at 30mpa with inset representative images. **B)** Quantification of the amputation-induced expression of *ihhb* at the wound at 6hpa with inset representative images.

3.2.3 Exogenous H_2O_2 cannot rescue the regenerative defects caused by inhibition of amputation-induced H_2O_2 production

The data presented demonstrates that H_2O_2 is required to initiate regeneration following injury, but I wanted to examine if H_2O_2 alone is sufficient to induce regenerative responses. During my MSc project I attempted to rescue DPI-induced regenerative defects with the addition of exogenous H_2O_2 to the media following amputation, however I did not examine the effect of H_2O_2 on regenerative signalling. For regenerative morphology, neither pulse treatments nor extended exposure resulted in an increase in the extent of regenerated tissue (reproduced from my MSc dissertation[136] in Figure 3.23). Even when a less severe regenerative defect was induced using a lower concentration of DPI, exogenous H_2O_2 administration was unable to rescue regrowth (reproduced from my MSc dissertation[136] in Figure 3.24).

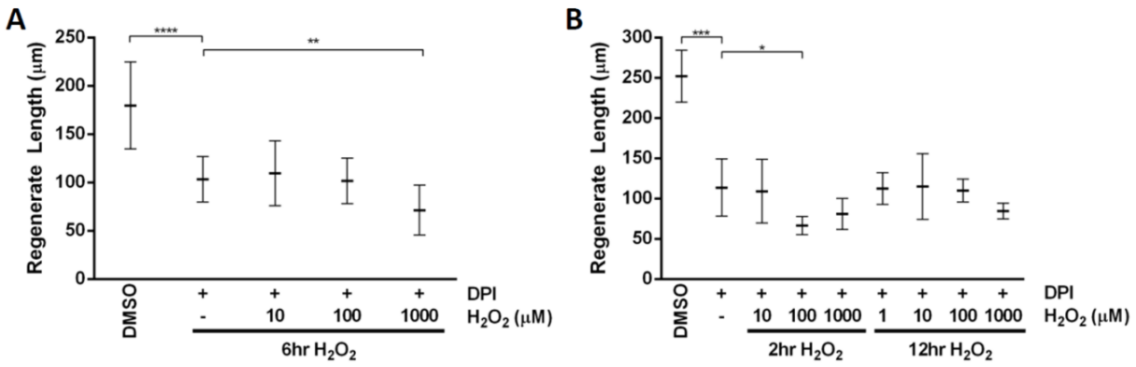

Figure 3.23 – Exogenous H_2O_2 cannot rescue DPI-induced regenerative deficiencies (reproduced from my MSc thesis[136]).
2dp larvae were dosed with DMSO (vehicle control) or 150µM DPI 1hr prior to amputation and 1hr post-amputation. Amputation was performed at the caudal tip of the tail pigment-gap. E3 media was supplemented with H_2O_2 immediately after amputation before larvae were transferred to fresh E3 and left to regenerate until 72hpa. (**A**) 6hr H_2O_2 dose. (**B**) 2 and 12hr H_2O_2 dose. Data represent mean +/- SD. Significance: * p≤0.05, ** p≤0.01, *** p≤0.001, **** p≤0.0001.

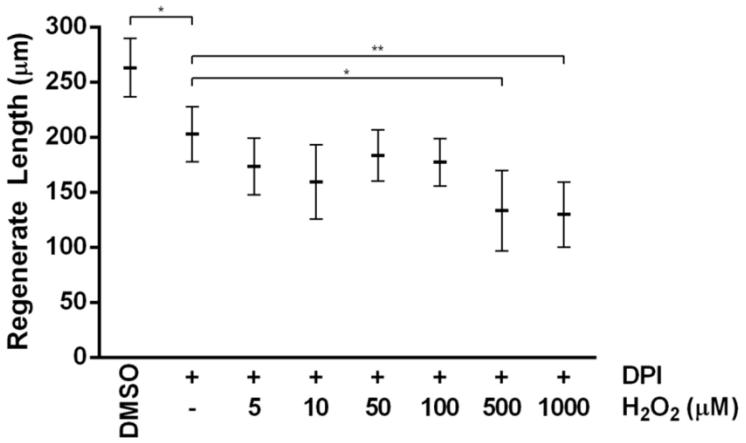

Figure 3.24 – Reproduced from my MSc thesis[136]: Exogenous hydrogen peroxide cannot rescue minimal DPI-induced regenerative deficiencies.
2dp larvae were dosed with DMSO (vehicle control) or 50μM DPI 1hr prior to amputation and 1hr post-amputation. Amputation was performed at the caudal tip of the pigment-gap of the tail. E3 media was supplemented with H_2O_2 immediately after amputation for 6hrs before larvae were transferred to fresh E3 and left to regenerate until 72hpa. Data represent mean +/- SD. Significance: * p≤0.05, ** p≤0.01.

Even though exogenous H_2O_2 cannot rescue regeneration completely, it may still be capable of regulating transcriptional control, possibly only weakly. In order to test this, I analysed pathway activation of Hh, Wnt and FGF in both wounded and unwounded larvae in the presence and absence of exogenous H_2O_2. Two concentrations of H_2O_2 were supplemented to the media of uninjured larvae and left for 6hrs before being transferred to fresh E3 media until fixation at 24hpa. This dosing aimed to induce regenerative signalling in the absence of wounding i.e. to test if H_2O_2 was sufficient for activation of these regenerative pathways. WISH was used to analyse gene expression of the Hh, Wnt and FGF markers *ptch1*, *axin2* and *pea3* respectively. Neither H_2O_2 dose resulted in a significant increase in any of the transcripts (Figure 3.25A, B, C Left). In addition to uninjured larvae, another group of larvae were subjected to the same doses immediately after tail amputations to test if exposure of additional H_2O_2 augmented the injury-induced expression of these markers. As for the uninjured group, supplementing the media with H_2O_2 did not induce a further increase in the wound-induced expression in any of these transcripts (Figure 3.25A, B, C Right). These data suggest that H_2O_2 is insufficient for the activation of these signalling pathways; however, lack of robust activation of these pathways in the 24hpa control group not exposed to exogenous H_2O_2 means that these data should be cautiously interpreted and should be replicated to increase confidence in these conclusions.

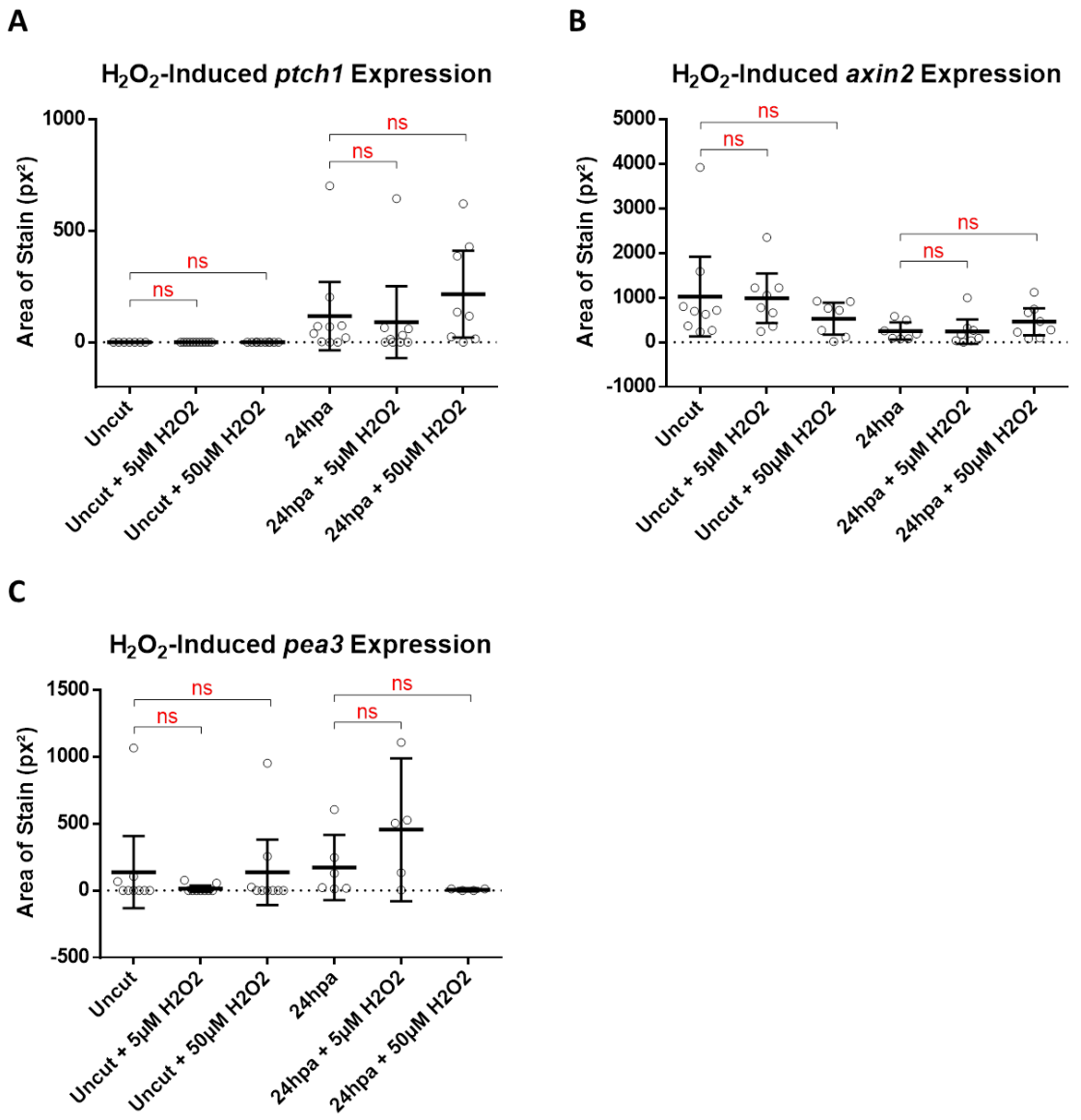

Figure 3.25 – Exogenous H_2O_2 does not stimulate or enhance regenerative signalling pathways.
Application of exogenous H_2O_2 to uninjured larvae does not stimulate the expression of *ptch1* (**A**, left 3 columns), *axin2* (**B**, left 3 columns) or *pea3* (**C**, left 3 columns), markers of Hh, Wnt and FGF pathway activation respectively. Similarly, H_2O_2 does not enhance the amputation-induced expression of these markers (**A**, **B**, **C**, right 3 columns).

Further to trying to induce regenerative signalling via exogenous H_2O_2 administration, I also tested if H_2O_2 administration was capable of rescuing *ihhb* induction following DPI inhibition of Duox. Knowing that Hh is the initiator for these pathways, such induction would support a H_2O_2 specific initiation of regeneration. Multiple concentrations of H_2O_2 were supplemented into the media following tail amputation and larvae were fixed at 6hpa before analysing *ihhb*

expression via WISH. DPI treatment produced a complete inhibition of the wound-induced *ihhb* upregulation and none of the doses of H_2O_2 rescued this expression (Figure 3.26). These data fail to detect an effect of exogenous H_2O_2 administration on *ihhb* expression, suggesting that a one-off addition of H_2O_2 cannot recapitulate the injury induced H_2O_2 signal produced by Duox activation. This is likely due to differences in the position, duration and concentration of the H_2O_2 signal.

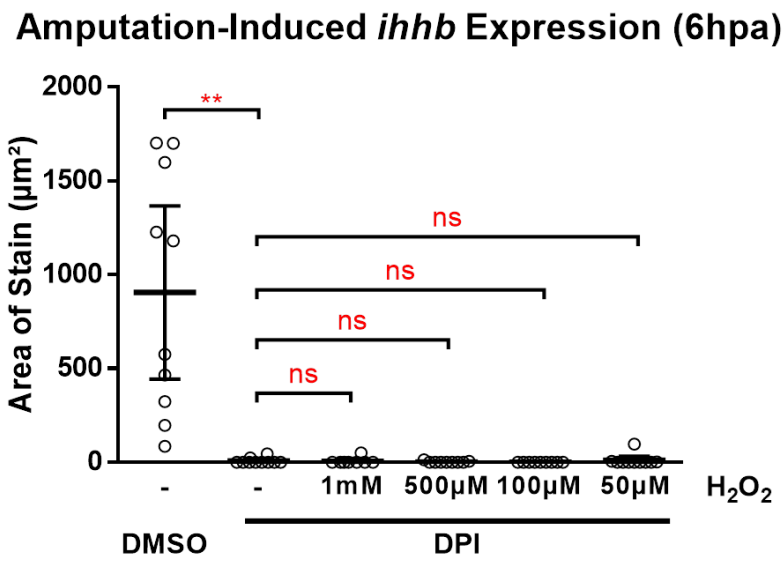

Figure 3.26 – Exogenous H_2O_2 does not rescue DPI-induced attenuation of amputation-induced *ihhb* expression.
Quantification of amputation-induced *ihhb* expression at 6hpa following DPI-treatment (-1 to +1hpa) and addition of exogenous H_2O_2 (0 to 6hpa) at a range of concentrations.

3.2.4 Duox is regulated by calcium signalling

As mentioned previously, wound-induced Duox activation has been shown to be Ca^{2+} dependent in *Drosophila* and mammalian cells[216,238–240], however there is disagreement if Ca^{2+} recapitulates this role in the zebrafish wound response[122,236]; therefore, in addition to examining the role of H_2O_2 in regeneration, work was carried out to characterise how Duox is stimulated in response to injury to produce this regulatory H_2O_2 signal. In order to investigate this relationship Ca^{2+} signalling was perturbed by pharmacological methods and H_2O_2 production and regenerative signalling response was assessed.

3.2.4.1 Duox-derived H_2O_2 is Ca^{2+} dependent

The cell-permeable Ca^{2+} chelator BAPTA-AM was used to sequester intracellular Ca^{2+} and thus prevent the wound-induced Ca^{2+} signalling. Following treatment with both 1mM and 100µM BAPTA-AM, wound-induced H_2O_2 was reduced to 2% and 13% of control levels respectively (Figure 3.27A, B) demonstrating a requirement for Ca^{2+} in H_2O_2 production. This Ca^{2+} dependency likely functions by directly binding the EF hands in Duox as demonstrated clearly in *Drosophila*[216]. There have, however, been reports that Duox can be regulated by the activity of protein kinase C (PKC) which can, in turn, be activated by increases in Ca^{2+} concentration[280], raising a second potential regulatory mechanism. In order to address this possibility, further experiments were performed to study the role of PKC in Duox activation and downstream H_2O_2 signalling.

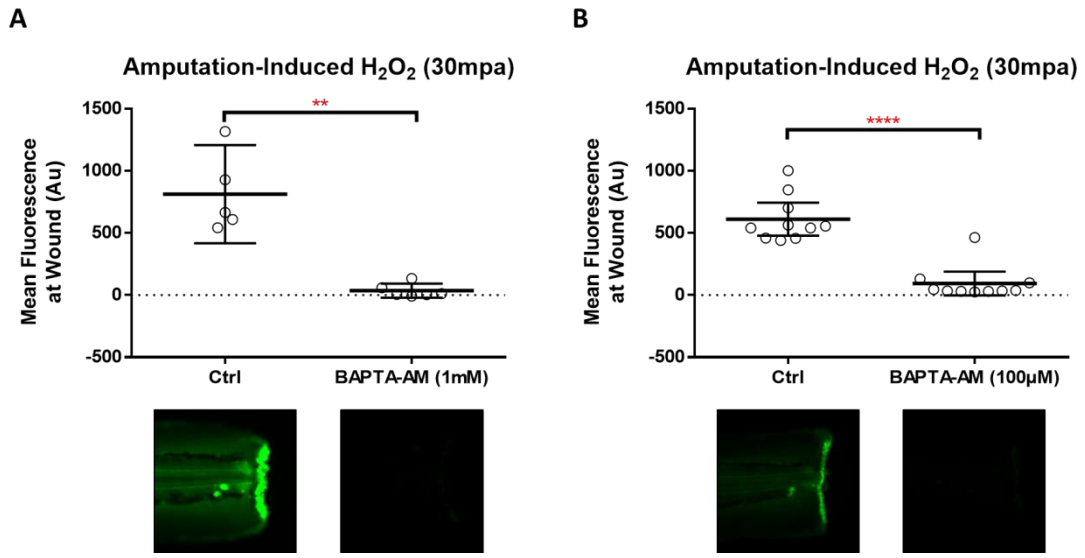

Figure 3.27 – BAPTA-AM inhibits the production of amputation-induced H_2O_2.
Quantification of the mean PFBSF fluorescence at the amputation plane at 30mpa following treatment with the Ca^{2+} chelator BAPTA-AM at 1mM (**A**) and 100µM (**B**) with inset representative images.

3.2.4.2 PKC can stimulate Duox-derived H_2O_2 and downstream Hh signalling

Using the pan-PKC activator phorbol 12-myristate 13-acetate (PMA), it was possible to significantly upregulate wound-induced H_2O_2, an effect that was attenuated in the presence of the pan-PKC inhibitor Bisindolylmaleimide-1 (Bim-1; Figure 3.28), indicating that PKC activity is sufficient to augment wound-induced H_2O_2 production. This adds credence to the hypothesis that Duox can be indirectly regulated by Ca^{2+} via PKC therefore I attempted to rescue the

downregulation of H_2O_2 production seen by sequestering Ca^{2+} with BAPTA-AM by simultaneously activing PKC with PMA. No significant effects could be detected following this rescue treatment even at increased concentrations of PMA (Figure 3.29). These data suggest that Ca^{2+} is required to both directly catalytically activate Duox and to indirectly regulate its activity levels via PKC activation.

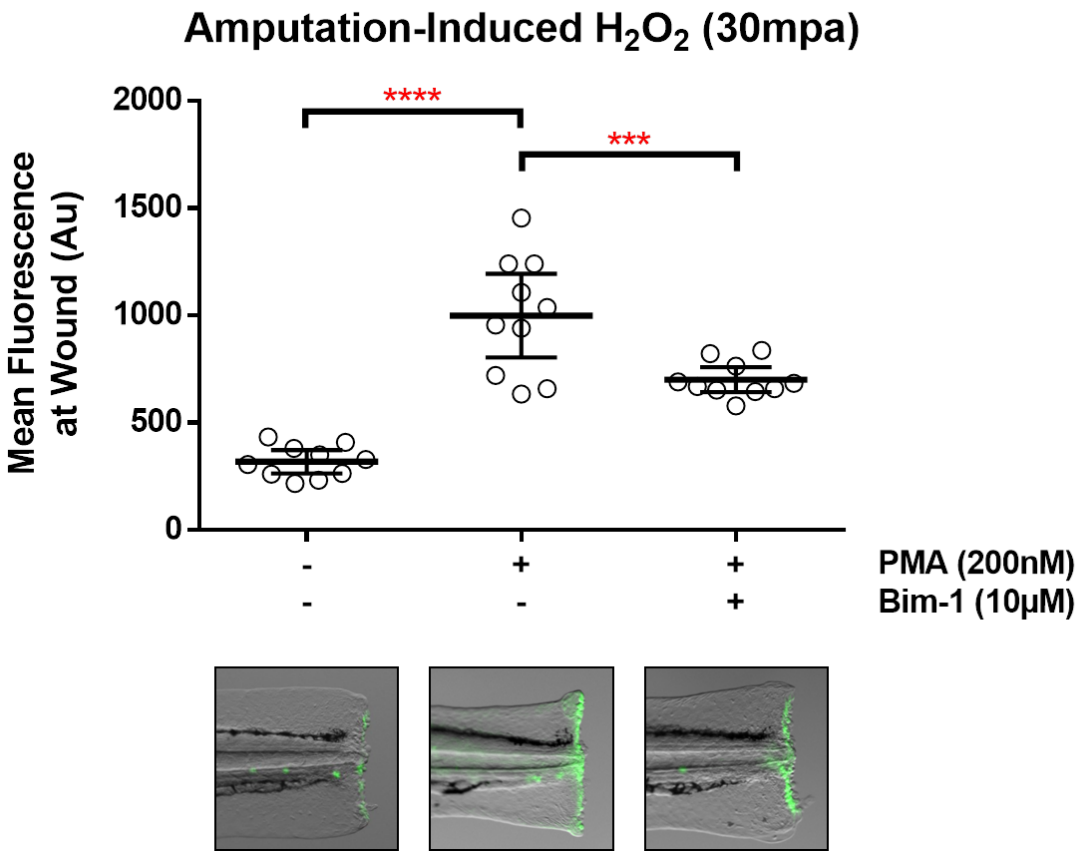

Figure 3.28 – PKC regulation of the production of amputation-induced H_2O_2.
Quantification of the mean PFBSF fluorescence at the amputation plane at 30mpa. Inset: representative composite images of brightfield & PFBSF fluorescence. The effect of PKC on amputation-induced H_2O_2 was studied in the presence of the pan-PKC activator PMA and pan-PKC inhibitor Bim-1.

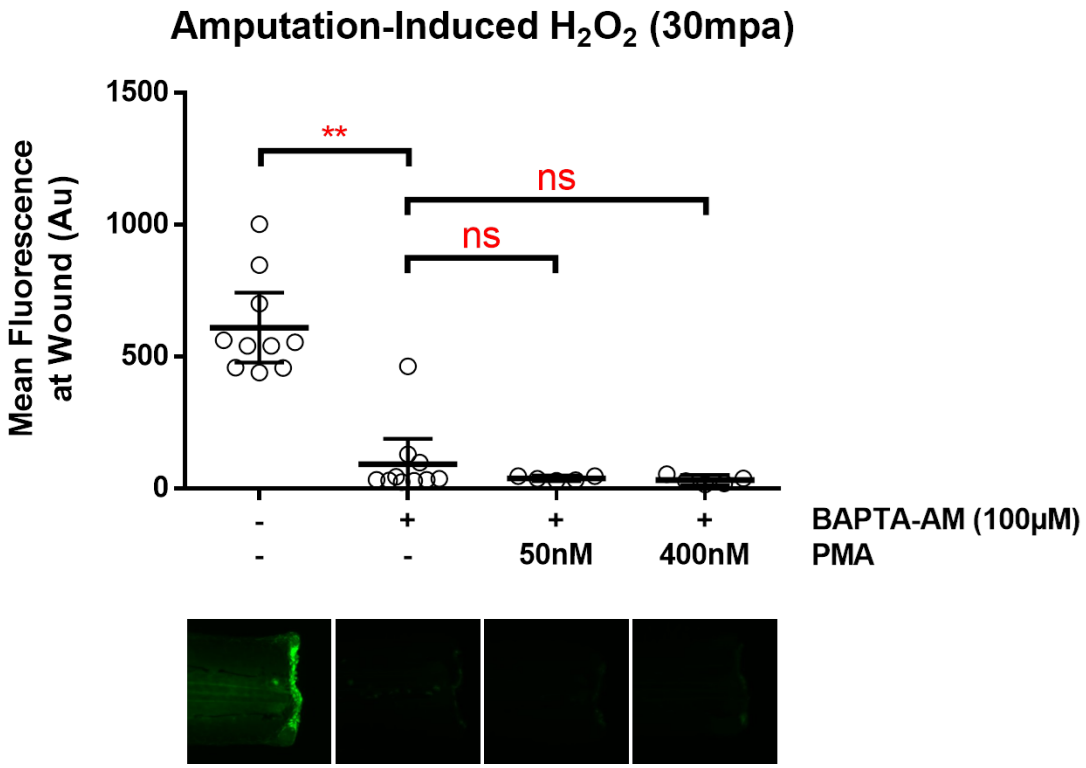

Figure 3.29 – Ca^{2+} and PKC regulation of the production of amputation-induced H_2O_2.
Quantification of the mean PFBSF fluorescence at the amputation plane at 30mpa. Inset: representative images of PFBSF fluorescence. The effect of Ca^{2+} and PKC on amputation-induced H_2O_2 was studied in the presence of the Ca^{2+} chelator BAPTA-AM and the pan-PKC activator PMA.

Knowing that PKC can regulate H_2O_2 production, I wanted to test if PKC stimulation can affect the regenerative signalling downstream of H_2O_2. This was analysed by WISH for both *ihhb* (Hh ligand) & *ptch1* (Hh pathway activation marker) transcripts. No significant increase in the early onset of *ihhb* expression could be detected following continual stimulation of PKC with PMA from 0 till 24hpa (Figure 3.30), suggesting that increased H_2O_2 does not result in more rapid transcription of Hh ligands. Hh pathway activation, however, was significantly increased at 24hpa as seen by the increased expression of *ptch1* (Figure 3.31A). There have, however, been reports that PKC is capable of regulating Hh signalling via upregulation and activation of the GLI transcription factor even in the absence of Hh ligands[281]. Therefore, in my model, PKC could bypass the H_2O_2 driven upregulation of Hh ligands and stimulate Hh signalling directly. In order to address this possibility, I treated larvae simultaneously with PMA and DPI in order to analyse Hh activation in a wound environment with activated PKC but inhibited Duox. The combined treatment abolished the PMA-stimulated augmentation of Hh signalling (Figure

3.31B), and therefore this appears to be a Duox-dependent effect. I therefore concluded that PKC is capable of modulating Hh pathway activation via Duox activation, though it is unclear from these data if it directly modulates *ihhb* transcription.

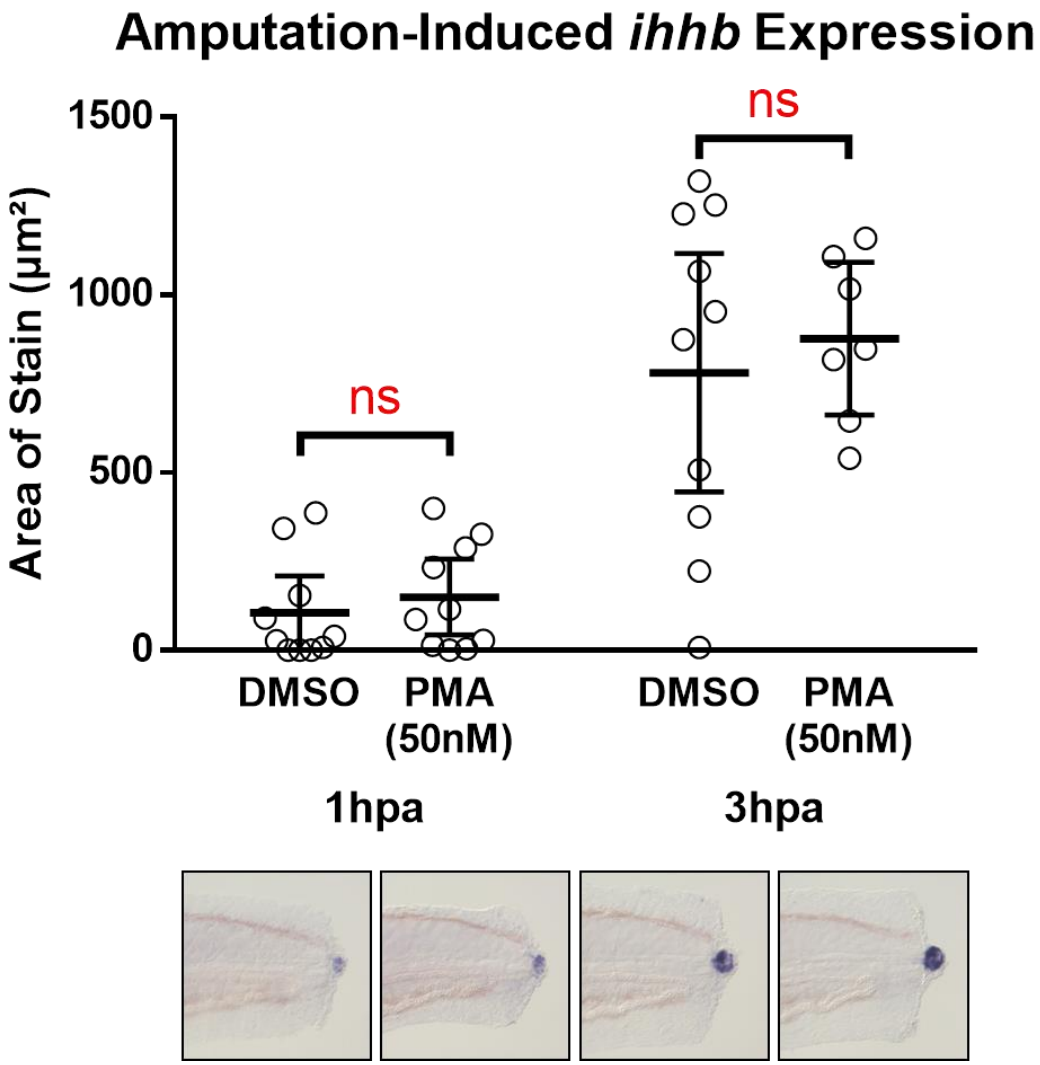

Figure 3.30 – PMA-stimulation of PKC does not affect amputation-induced *ihhb*.
Quantification of amputation-induced *ihhb* in the presence and absence of the pan-PKC activator PMA with inset representative images. Larvae were treated with PMA from the time of amputation and fixed for WISH quantification of *ihhb* at 1hpa (left) or 3hpa (right).

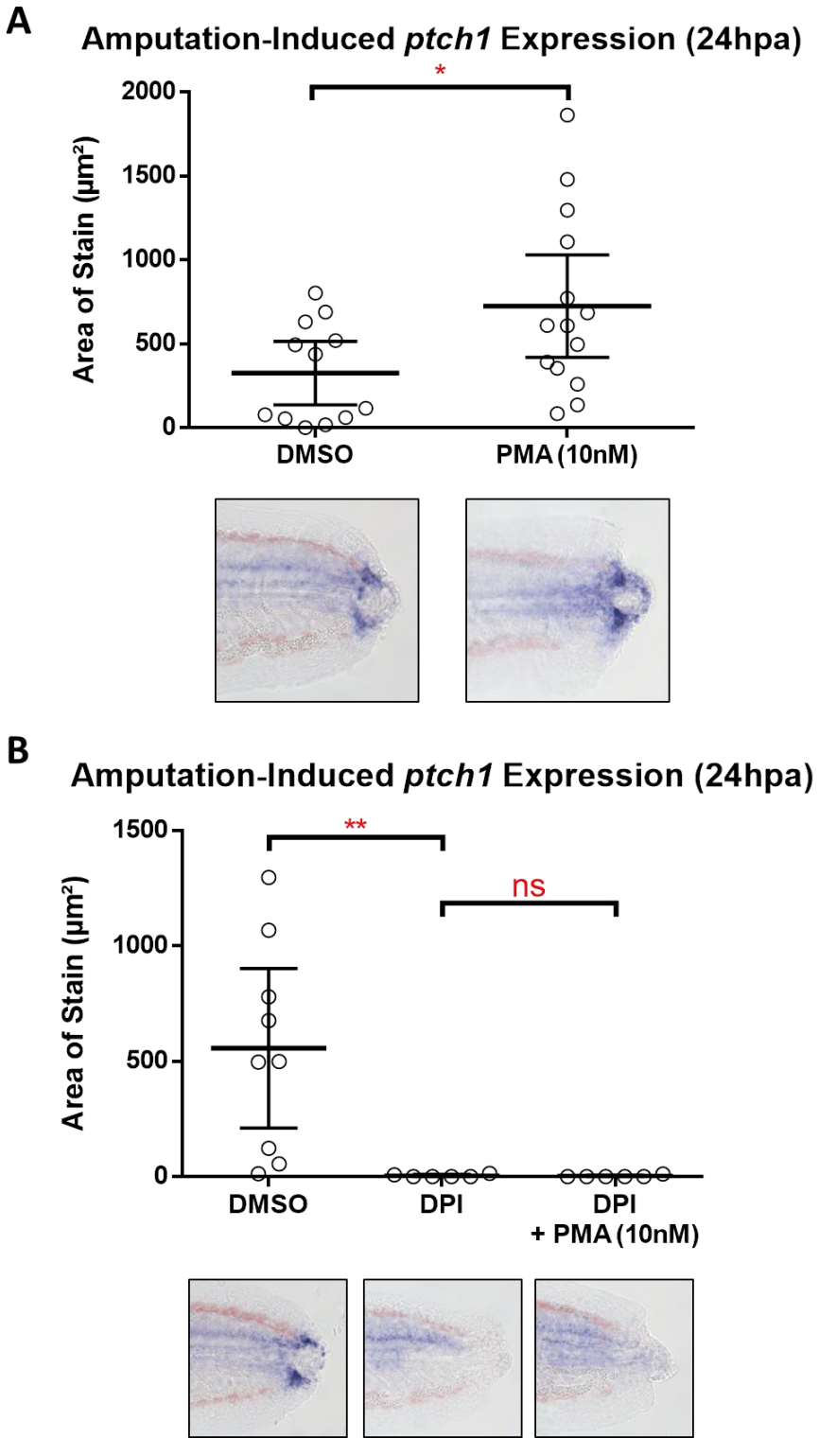

Figure 3.31 – PKC regulation of amputation-induced Hh activation.
Quantification of *ptch1* as a reporter of Hh pathway activation at 24hpa. Larvae were treated with the pan-PKC activator PMA on its own (**A**) and in the presence of DPI (**B**).

3.2.4.3 PKC regulation of Duox may not be implemented in the wound response

Having identified a potential role for PKC in augmenting wound responses, the pan-PKC inhibitor Bim-1 was used in isolation to examine if the absence of PKC activity alone was sufficient to perturb wound-induced H_2O_2 production and *ihhb* upregulation. When used at 10μM (the effective concentration used to inhibit PMA-stimulation of H_2O_2) Bim-1 not only failed to inhibit H_2O_2 production, but significantly increased it; this effect was prevented at a higher concentration (100μM) where treatment with Bim-1 did not significantly alter H_2O_2 production (Figure 3.32A). Given the positive relationship between H_2O_2 and *ihhb* induction, these effects on H_2O_2 production did not match as expected with the induced *ihhb* expression. When H_2O_2 was stimulated by 10μM Bim-1, *ihhb* transcript levels were not significantly altered but when H_2O_2 was unaffected by 100μM, *ihhb* expression was significantly reduced (Figure 3.32B). This apparently conflicting result may be due to the limitations of assaying H_2O_2 at a single timepoint and highlight the importance of the duration and concentration of the H_2O_2 signal. Alternatively, whilst the data above demonstrate a mechanism for Ca^{2+} driven regulation of Duox via PKC, this result is ambiguous as to whether it is actually employed in the physiological response to injury; further work will be needed to investigate this.

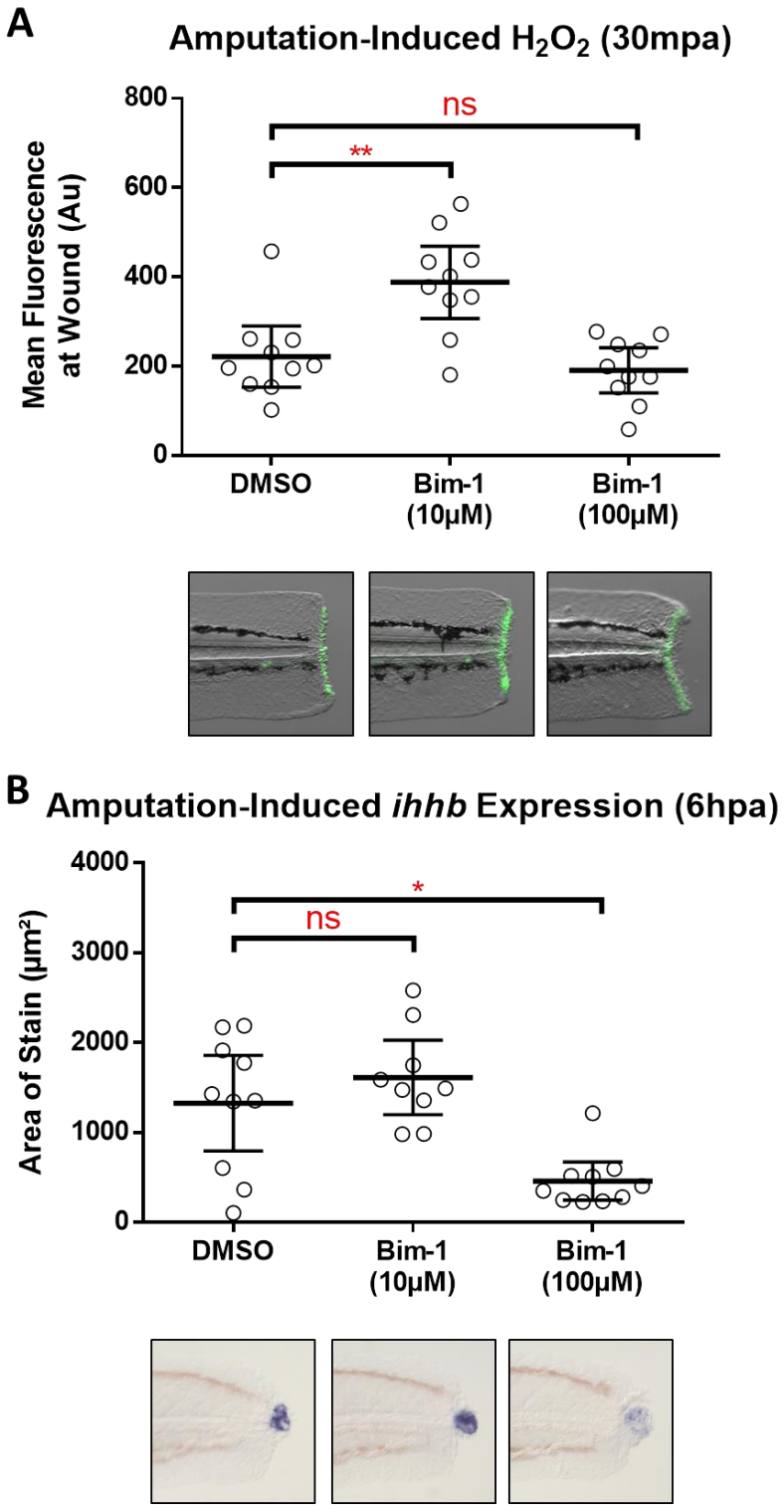

Figure 3.32 – PKC regulation of the production of amputation-induced H_2O_2 and subsequent *ihhb* expression.
3dpf larvae were treated with the pan-PKC inhibitor Bim-1. **A)** Quantification of the mean PFBSF fluorescence at the amputation plane at 30mpa with inset representative images. **B)** Quantification of the amputation-induced expression of *ihhb* at the wound at 6hpa with inset representative images.

Considering these data altogether, they support a role for Ca^{2+} in the regulation of Duox. My current hypothesis is as follows: wound-induced Ca^{2+} is required to bind and catalytically activate Duox directly as well as being required to activate PKC. Activated PKC is then capable of further stimulating Duox to augment H_2O_2 production and this H_2O_2 initiates regenerative signalling through the Hh pathway. The data presented here are, however, inconclusive as to whether this mechanism is actually employed in response to wounding.

3.3 Discussion

Data presented in this chapter aimed to address the effects of wound-induced H_2O_2 at a cellular & molecular level. Whilst recent work has demonstrated that H_2O_2 is essential for regeneration in multiple species, the molecular effectors and mechanism of action required to mediate this effect remain poorly characterised. The conservation of wound-induced ROS even in non-regenerating animals and the role of ROS in driving inflammation and promoting wound closure highlight their importance as a pro-healing factor, but without a complete understanding of the redox interactions following wounding, we are unable to compare and contrast these two models to identify the specific pro-regenerative roles of ROS.

3.3.1 H_2O_2 is required for the formation of regenerative structures and initiation of regenerative signalling

My data adds to the growing body of evidence that H_2O_2 is required for proper regeneration, demonstrating that either preventing H_2O_2 production or scavenging it from the wound environment can significantly inhibit the extent of regrowth (Figure 3.5 & Figure 3.21). My data shows, for the first time, that H_2O_2 stimulates the formation and subsequent signalling of the wound epithelium (Figure 3.6). Synthesis of retinoic acid is required for blastemal formation[90,97] but in the absence of H_2O_2, the wound-induced upregulation of *aldh1a2* is prevented (Figure 3.7A). Lacking the enzyme responsible for the synthesis of retinoic acid, the larvae fail to induce the blastema (Figure 3.7B) and regeneration fails to proceed past this point. This prompt halt to the regeneration process also prevents the activation of Hh, Wnt and FGF signalling (Figure 3.8), all of which are required to be activated to stimulate regeneration[66] and positions H_2O_2 as an early initiator of regeneration, upstream of many of the essential signalling pathways & regenerative processes. Further rescue experiments would

be valuable to identify if Hh is required principally to trigger these signalling pathways or if its other interactions are as important to regeneration. Simultaneously blocking H_2O_2 with DPI and upregulating Hh, for example with the application of purmorphamine (a synthetic smoothened agonist), would address this question. In addition, supporting this pharmacological data with more specific genetic manipulations would be desired to address any concerns of specificity. Whilst I attempted to raise a transgenic line encoding a dominant-negative Duox under the control of a heatshock promoter to allow inducible expression, a stable transgenic line could not be produced.

Simultaneous work from other members of our lab placed Hh upstream of Wnt and FGF as a master regulator of larval regeneration (Figure 3.9), a result which is at odds with the adult regenerative hierarchy which places Wnt at the top of the wound-induced signalling cascade[90]. The adult regeneration study also failed to implicate H_2O_2 in the regulation of Wnt and may suggest that adult and larval regeneration have fundamental differences in their mechanisms of induction. This will be important to investigate the adult response in my own wounding assay to see if I can detect the same larval hierarchy, or confirm separate mechanisms of regeneration.

3.3.2 H_2O_2 regulates regeneration via upregulation of Hh ligands

Wound-induced ROS appear to exert this control over the formation of the regenerate structures and regenerative signalling via transcriptional upregulation of Hh ligands in the notochord (Figure 3.10, Figure 3.21 & Figure 3.22). This regenerative control mimics that seen in *Xenopus* larval tail regeneration where notochord-derived *shh* activates a regenerative program which is impaired in tadpoles treated with cyclopamine to block Hh signalling[282]. A similar requirement for Hh signalling is seen in axolotl regeneration although the source of the Hh ligand is the spinal cord as opposed to the notochord[283]. This suggests a conserved activation mechanism for Hh in tail regeneration across multiple species and it will be interesting to see if this is mirrored in appendage regeneration, which would be more useful for translational approaches. The question as to whether Hh ligands are upregulated in response to injury is interesting as other studies have cited probe penetration issues similar to those experienced in my work[283], and suggested that expression is constituent and not injury-induced, although no evidence was provided to support this claim. In *Xenopus*, Hh ligands appear to be expressed at very low levels pre-amputation and are gradually upregulated over

time[282]. From my qPCR data, larval zebrafish appear to conform to the *Xenopus* model with low-level endogenous Hh ligand expression in the notochord being augmented following injury (Figure 3.13 & Figure 3.17). One characteristic common to all three species is that the source of the Hh ligand appears to be unresponsive to Hh signalling, therefore acting as a paracrine organising centre in the regenerating program.

3.3.3 Exogenous H_2O_2 and rescue of DPI-induced regenerative defects

Although I could not provide evidence that H_2O_2 is sufficient for transcriptional upregulation of Hh ligands (Figure 3.26), regeneration signalling pathways (Figure 3.25) nor regenerate morphology (Figure 3.23) by application of exogenous H_2O_2, other studies have seen some rescue in both zebrafish and *Xenopus* further substantiating the hypothesis that ROS induce strong pro-regenerative effects[43,124,141]. My failure to demonstrate rescue of DPI-induced regenerative defects by exogenous H_2O_2 could indicate additional roles for the *de facto* activity of Duox, independent of H_2O_2 production as has been seen in *Xenopus*[141] where the catalytic activity of Duox requires the transport of electrons across membranes to depolarise cells in a mechanism required for proper regeneration. My failure to detect an effect of exogenous H_2O_2 may also indicate a very narrow physiological window where H_2O_2 can effectively activate its targets without causing non-discriminative oxidative damage and becoming deleterious to wound healing, or a requirement for a gradient of ROS over multi-cellular distances. This would not be surprising given the extensive redox control mechanisms present within cells which could fine-tune such a signal to ensure it carried out its intended physiological function, combined with the fact that the H_2O_2 produced at the wound boundary readily diffuses over a distance of about 200µm thereby establishing a gradient of concentration with the initial high concentration at the wound edge steadily decreasing as it moves away from the wound[119]. It is possible that H_2O_2 plays different roles based on its concentration, something that has been suggested by another group[120]. It should, however, be noted that whilst wound-induced H_2O_2 appears pro-regenerative, both the time and concentration appear vitally important in avoiding toxicity. Long-term accumulation of high levels of ROS appears to induce oxidative DNA damage and reduce regenerating capacity of neonatal mouse hearts[284] and hypoxia induces heart regeneration in adult mice by acting as a ROS protectant[285] possibly via senescence[286,287]. These data indicate that in order to induce pro-regenerative effects, we must be able to precisely control ROS exposure and this will require careful experimental procedures to ensure we do not end up inadvertently inducing damage instead. Therefore,

crude application of a single concentration of H_2O_2 to the media may not be suitable to recapitulate such precise signalling with the required spatiotemporal profile.

3.3.4 Calcium regulation of Duox

In addition to investigating the downstream effectors of Duox-derived H_2O_2, I presented data regarding the activation of Duox by calcium. Currently, the calcium dependency of Duox in zebrafish wounding is unclear, with studies arguing for and against[122,236]. My data show that Ca^{2+} chelation results in a complete abolishment of wound-induced H_2O_2, supporting the hypothesis that Duox requires Ca^{2+} to be catalytically active (Figure 3.27). Whilst this is likely to be due to Ca^{2+} binding of the EF hands within Duox, as it is for *Drosophila*[216], there may also be a secondary influence from PKC. PKC is known to be both stimulated by Ca^{2+} and capable of activating Duox via phosphorylation[280], and therefore would bridge the gap between immediate wound signals and H_2O_2 production. In my experiments, PKC activation is capable of augmenting wound-induced H_2O_2 production (Figure 3.28) and its downstream signalling in a Duox dependent fashion (Figure 3.31), however inhibition of PKC alone produced inconclusive results regarding the normal physiological levels of H_2O_2 and its downstream Hh targets (Figure 3.32). Whilst the data show the potential for such a regulatory circuit, it still remains unclear as to whether this is actually employed in the response to wounding, something which will have to be addressed before this can be conclusively added to our model of regeneration. The multiple subtypes of PKC make further investigation complex, but the joint dependency on Ca^{2+} and phorbol esters suggest that classical PKC subtypes may be employed in this regulation.

3.3.5 Impact

It is interesting to note that Duox is conserved in humans and other non-regenerating mammals, but its expression is much more limited than in regenerating organisms. It is, however, expressed strongly in wet epithelia which are better at healing and regenerating than their dry counterparts[288]. Although thought to be important as part of the innate immune system to produce H_2O_2 as an anti-microbial, Duox may be responsible, either by design or by coincidence, for stimulating a similar reparative mechanism as what we see in the larval zebrafish. Exact parallels are hard to come by as, obviously, *in vivo* experiments are not

possible, and *in vitro* experiments using human and murine airway epithelial cells use scratch wounds which heal mainly via cell migration rather than cell proliferation[131,168,257,289]. Downstream effectors of H_2O_2 have been identified which mediate this migration but Hh activation has not been studied. It would be interesting to see if a more severe wound would result in the activation of Hh and a stimulation of proliferation in these cells, however complex 3D culture models may be required to fully investigate this.

Another potential benefit of this area of research is an increased understanding of the initiation and progression of tumours. Stimulation of cell migration, remodelling of the extracellular matrix, angiogenesis and, of course, cell division are all fundamental processes of wound healing and regeneration but also of cancer progression. The similarities between the two processes have led to cancer being referred to as "wounds that do not heal". Indeed, many wound-induced genes are upregulated in cancers and can even be predictive of invasiveness and patient outcome[290]. Cancerous cells also upregulate their production of ROS above normal physiological levels due to their increased metabolic rate[291]. At the same time, these cells upregulate the anti-oxidative mechanisms to prevent ROS reaching such an elevated state as to induce apoptosis within the cells. These transformations allow the cells to survive and thrive within the hypoxic centre of solid tumours, and this hypoxia can even further increase ROS levels[292]. Research is ongoing aimed at modulating cancerous redox state as a potential therapeutic strategy, but is showing promise[293–296].

These neoplasic effects of ROS can at least in part be attributed to the recruitment of leukocytes to transformed cells which stimulate proliferation by the secretion of prostaglandin E2 [193,297], but it is possible that ROS may also regulate Hh signalling directly as it does in wounding. Perhaps unsurprisingly for an essential developmental signalling pathway, Hh has been linked to cancer progression and transformed cell growth, with a particular role in the maintenance of cancer stem cells[298–300]. This has led to numerous attempts at targeting Hh therapeutically, however until recently this has not proved very sucessful[301]. Some successes has been seen in mice where inhibition of Hh signalling with the naturally occurring ammonium salt berberine resulted in suppression of tumour growth both *in vitro* and *in vivo*[302]. It is tempting to speculate that we could use ROS as an alternative target to modulate Hh in cancers indirectly through careful manipulation of the redox environment. Though no definitive link between ROS and Hh was shown, treatment of pancreatic cancer cells with resveratrol (a plant-derived phenol) resulted in a simultaneous downregulation of hypoxia-driven ROS and Hh signalling thereby inhibiting cancer progression[292]. This finding suggests that in at least some tumour types, ROS and Hh may be closely linked and therefore important

insights in the understanding and potential treatment of cancer may be gained by studying these regenerating models.

3.3.6 Summary

The data presented in this chapter aimed to address the importance of the H_2O_2 signal in regeneration and elucidate its interactions and mechanisms of action. Through the use of small molecules to perturb the wound environment my current model is summarised below in Figure 3.33.

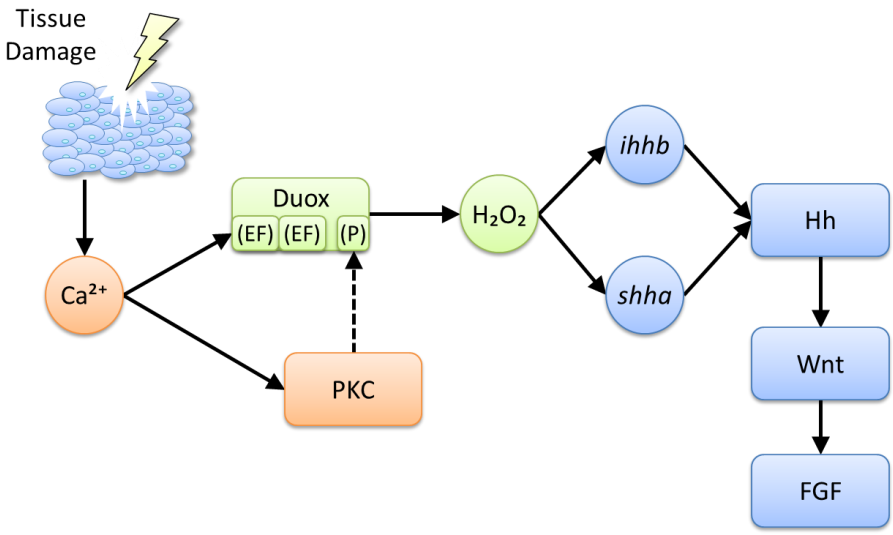

Figure 3.33 – Proposed model for early wound-signal activation of regenerative signalling pathways. Wound-induced Ca^{2+} activates Duox directly and potentially via PKC; Duox produces H_2O_2 at the wound which stimulates the upregulation of Hh ligands *ihhb* and *shha*; these ligands activate Hh signalling which, in turn, activates Wnt and FGF leading to the formation of the wound epithelium and the blastema to allow full regenerative outgrowth of the tail.

The effectiveness of a short pulse inhibition of H_2O_2 shows the importance of this transient wound signal to set in motion a myriad of responses leading to complete and coordinated regeneration and highlights early wound signals as potential targets for modulating regeneration in humans. Whilst the promiscuous nature of H_2O_2 may result in multiple pro-regenerative targets, the activation of these signalling pathways represent an essential and wide-reaching mechanism of action of H_2O_2 which may be sufficient to induce regeneration.

My data support my original hypothesis that "Wound-induced H_2O_2 triggers one or more developmental pathways which are essential for regeneration to proceed", but I can now expand and update this working hypothesis to "Wound-induced H_2O_2 triggers the Hh signalling pathway, and subsequently the Wnt and FGF pathways in order to stimulate regeneration".

Chapter 4. H_2O_2 stimulates regeneration primarily via inflammation-independent mechanisms

4.1 Introduction

4.1.1 Aims

H_2O_2 is a potent pro-inflammatory signal and is known to act as a chemotactant & activator for leukocytes. It is rapidly produced by keratinocytes at the site of injury and is one of the initial wound signals responsible for recruiting leukocytes to the wound, therefore initiating inflammation[43,119,173]. Increasing evidence of links between inflammation and wound healing / regeneration is adding weight to the hypothesis that immune cells are capable of regulating regeneration and therefore inflammation could be a potential candidate for the mediator of the pro-regenerative effects of H_2O_2 described in the previous chapter. Data presented in this chapter aims to address the link between the inflammatory response and regeneration in larval zebrafish. I aimed to determine if the pro-regenerative effects of H_2O_2 are mediated indirectly through the action of the immune cells recruited to the wound, or whether they are mediated via other, inflammation-independent, signalling mechanisms.

4.1.2 Background

Following injury, leukocytes are rapidly recruited to the wound site and are activated in a pro-inflammatory manner to clear invading pathogens and stimulate healing. Activation of leukocytes results in the respiratory burst (the release of ROS from activated neutrophils and macrophages via NADPH family enzymes) in order to sterilise the wound, prolong inflammation and promote healing. However, whilst the high concentration of ROS at wounds was thought to be a direct result of this respiratory burst, it has recently been shown that H_2O_2 is produced at the wound prior to the arrival of the first leukocytes. This production was attributed to resident keratinocytes at the wound and actually attracts the first leukocytes before they begin producing ROS themselves[43,119,173]. Finally, the arrival of neutrophils at the wound actually coincides with a decrease in the local concentration of H_2O_2 and therefore the initial wound-induced H_2O_2 signal should be considered a separate signalling event to the respiratory burst, potentially with separate functions[135].

Considering the promiscuous nature of H_2O_2, it is unsurprising that it interacts with multiple partners and stimulates multiple wound-responses. In addition to its chemotactant roles, it is known to stimulate a number of essential wound responses: it further regulates inflammation by the upregulation of multiple pro- inflammatory and some anti-inflammatory genes in leukocytes[303]; it controls blood coagulation and thrombosis[304]; it regulates cellular proliferation, adhesion and migration[305–307]; and it enhances angiogenesis and wound closure[64].

4.1.2.1 Inflammation in wound healing

Though wound-healing and regeneration are often considered as one continual process in regenerating organisms, the relative priorities of each are clear – the survival of the organism rests on its ability to kill invading pathogens and rapidly restore barrier function therefore this must be carried out before energy is spent on regrowing lost tissue. The inflammatory phase of healing even directly inhibits cellular proliferation and differentiation via the production of IL-1 to ensure this sequential relationship between the two processes[308]. The large number of processes regulated by the wound-induced H_2O_2 signal makes it difficult to pin-point which are simply healing responses and which may be responsible for its pro-regenerative effects. Indeed, all of the H_2O_2 dependent wound-responses contribute to successful wound healing, but non-regenerating organisms share the same responses and do not regrow lost tissue, suggesting that the pro-healing roles of H_2O_2 have been conserved, but the pro-regenerating roles have been inactivated downstream of the H_2O_2 signal.

When trying to identify potential mediators of the pro-regenerative effects of the wound-induced H_2O_2 signal, inflammation stands out as a likely candidate. For starters, the timescale of inflammation fits within the gap between the onset of H_2O_2 signalling and the upregulation of *ihhb*. Wound-induced H_2O_2 is detectable within 5 minutes of wounding and the first neutrophils arrive shortly after at around 17mpa[119]. The H_2O_2 signal continues to intensify (Figure 3.3) and recruit more leukocytes over the next hours with neutrophil numbers peaking at 2hpa and macrophages peaking around 6hpa[309]. Wound-induced *ihhb* expression increases steadily from first being detectable at 1hpa, to showing robust expression at 3hpa, and peaking at 6-12hpa[272]. The early-onset & progressive recruitment of leukocytes generally matches the temporal profile of upregulation of *ihhb* just offset by about an hour, potentially allowing time for leukocytes to stimulate gene expression; it is therefore plausible that H_2O_2 may exert its regulation of *ihhb* & regeneration indirectly, via the initiation of inflammation.

In addition to appropriate timing, a number of human diseases highlight the necessity for a fully-functional immune system to allow a rapid, complete and coordinated healing response. Many conditions associated with impaired healing also present abnormal immune responses: autoimmune diseases such as diabetes, lupus, rheumatoid arthritis and scleroderma present chronically inflamed and poorly healing leg ulcers[310]; chronic granulomatous disease, an immunodeficiency syndrome characterised by a defect in the production of inflammatory ROS by leukocytes, presents unchecked inflammation, delayed healing of wounds & increased scarring[311,312]; ischemic wounds with disrupted blood flow show a decrease in macrophage recruitment concomitant with altered inflammation and delayed re-epithelialisation[313]; finally, aged individuals present altered inflammatory responses with differences in both adaptive and innate immunity[314,315] and even healthy aged individuals heal less rapidly[316].

These responses are often due to misregulated inflammation with fails to resolve in a timely manner, preventing wound closure and the initiation of any subsequent repair. A growing body of evidence is emerging attributing this misregulation to an abnormal balance of pro- and anti- inflammatory macrophages at the wound. Macrophages respond to the wound environment to become activated in different manners to carry out different roles and these can be broadly characterised into two sub-groups – classically-activated (M1) macrophages and alternatively-activated (M2) macrophages. M1 macrophages result from exposure to pathogen associated molecular patterns (PAMPs) and pro-inflammatory cytokines such as TNF-α and INF-γ, whereas M2 macrophages result from exposure to anti-inflammatory cytokines such as IL-4 and IL-10[317]. As one would expect from their respective mechanisms of activation, M1 macrophages act as pro-inflammatory cells whereas M2 macrophages act to resolve inflammation and switch the wound to a pro-healing state.

Studying diabetics has given us insights into the roles of both M1 and M2 macrophages at the wound. Multiple studies point to a simple antagonistic relationship with increased polarisation towards the M1 phenotype associated with impaired healing[318–320] and increased levels of M2 macrophage at the wound can even be used to predict a more rapid & complete healing outcome in human diabetic wounds[319]. Outside of diabetic wounds, artificially induced autophagy also impairs wound closure by polarising macrophages to an M1 phenotype[321], reinforcing the anti-healing role of pro-inflammatory macrophages. However, additional studies have shown precisely the opposite relationship after introducing either M1 or M2 activated macrophages into diabetic wounds. The pro-inflammatory M1 macrophages improved wound healing rates via stimulation of angiogenesis & re-epithelialisation[317], and the anti-inflammatory M2 macrophages delayed wound closure[322].

Although appearing contradictory these results may be reconciled by the assumption of a more complex relationship between inflammation and healing, based on the requirement for an appropriate balance of both pro- and anti- inflammatory cells at the wound to successfully heal after injury[323]. This complex relationship between inflammation and healing is mirrored in an equally, if not more so, complex relationship between inflammation and regeneration.

4.1.2.2 Inflammation in regeneration

Our currently limited understanding of the interplay between inflammation and regeneration is evident in the range of studies across multiple organisms showing both positive and negative roles in regeneration, and some which show no impact at all. One of the major reasons that inflammation has generally been thought to be prohibitive to regenerative healing is because of non-regenerative animals' propensity to finish the healing process with the formation of scar tissue, something which is either resolved or avoided completely in regenerating animals[41,324,325]. Even within individual organisms, there is evidence of inflammation inhibiting regeneration. For example, the loss of regenerative capacity in the refractory period of *Xenopus* tadpole development can be restored in immune compromised individuals[139] and pro-inflammatory stimulation of amputated hind-limbs in *Xenopus* larvae impairs regenerative outgrowh[326]. Furthermore, switching the strongly pro-inflammatory wound response in adult mouse hearts to a minimally inflamed embryonic state reduced fibrotic scarring and enhanced tissue repair[327]. There appears to be a general inverse relationship between scarring and regeneration, and some have even suggested that these processes are mutually exclusive in mammals[167]. This is not however the case in zebrafish where cryoinjury of the heart forms a transient scar which is subsequently degraded to allow regeneration to occur as normal[325], therefore scarring in and of itself does not preclude regeneration.

More recently, inflammation has been observed to have pro-regenerative effects in multiple different regenerative species: inflammation as a whole has been shown to stimulate cardiomyocyte proliferation & is required for regeneration in neonatal mouse heart[71]; zebrafish mutants lacking hematopoietic tissues (i.e. inflammation-deficient) presented a deficiency in fin-fold regeneration with reduced proliferation & increased apoptosis[328]; and artificially induced acute inflammation has been shown by independent studies to improve CNS neural regeneration in zebrafish[329,330].

Studies aimed at delineating the roles of individual immune cells within inflammation have identified that macrophages play vital roles in promoting regrowth suggesting that they may be the primary mediators of the inflammatory regulation. The data support a pro-regenerative effect or even an absolute requirement for macrophages in regeneration: a rapid and sustained macrophage response is observed in *Xenopus* tadpole optic nerve regeneration[331]; following selective macrophage depletion, neonatal mouse heart formed fibrotic scars and failed to regenerate[332], and an independent study also showed that embryonic macrophages convey a pro-regenerative effect when maintained in adult hearts[327]; limb regeneration is completely blocked in macrophage-depleted axolotls[333]; and prevention of macrophage development or macrophage ablation decreased the rate of outgrowth and resulted in abnormal tissue morphology during fin regeneration in larval[309], and adult[59] zebrafish respectively.

In addition to these positive and negative regulatory roles identified, there is evidence that regeneration can be independent of inflammation. For example, the eye is considered an immune privileged organ which precludes inflammation by a combination of physical exclusion of circulating cells via the blood-retinal barrier, an immunosuppressive microenvironment within the eye itself and active regulation of the systemic immune response[334]. Despite this inflammatory-deficient microenvironment, Newts[335] and axolotls[336] are still capable of regenerating their lens and zebrafish can still regenerate retinal glial cells[337]. Outside of the eye, neural regeneration in zebrafish appears unaffected in the inflammation-deficient *cloche* mutant[43] and zebrafish fin regeneration also appears unaffected in *pu.1* morphant larvae which do not develop myeloid lineage cells (macrophages and neutrophils)[113]. These data suggest that there may be cases where inflammation is not necessary in order to regenerate normally. Whether these cases truly represent a completely separate mode of action to regulate regeneration or if they have different cells and signalling mechanisms substituting for immune regulation is, at this stage however, not clear.

Whilst the exact regulatory interactions are likely to be nuanced, the evidence seen certainly demonstrates that immune cells have the capacity to regulate regeneration but they may not be absolutely required in all cases. This confusing array of studies also demonstrates the desperate need for further work to fully characterise and rank the relative importance of the complex interactions between inflammatory cells and regeneration.

4.1.2.3 Methods for immune-modulation

In order to study the impact of inflammation on regeneration, I required a mechanism of modulating the immune response in larvae before wounding. Many different methods have been developed to selectively remove one cell type from a living organism but they all have their merits and limitations.

4.1.2.3.1 Antibody-depletion

In mice, antibody-depletion has been used to remove macrophages by either blocking cell surface receptors required to receive survival signals or by triggering antibody- or complement- dependent cytotoxicity. This method was not used due to concerns of off-target effects[338], combined with a lack of fish-specific antibodies and impracticalities in larval injections.

4.1.2.3.2 Liposome-encapsulated clodronate

The delivery of cytotoxic clodronate to phagocytic cells by encapsulating it in liposomes is a technique that has been used in multiple model organisms to deplete macrophages[333,339,340]. Despite also being engulfed by neutrophils, they do not undergo apoptosis, presumably due to intracellular sequestration or failing to metabolise clodronate it to its cytotoxic form[341], limiting this to a macrophage-only ablation system. The short half-life and limited bioavailability of free clodronate mean that it is generally considered to have low off-target effects[342] although toxicity has been demonstrated in epithelial cells and osteoclasts[343,344].

4.1.2.3.3 Inducible genetic cell ablation systems

Another method for targeted cellular ablation is to introduce a transgene to produce toxins, or enzymes which would synthesise toxins, capable of killing the cell. Having a genetically encoded ablation system raises concerns with both spatial and temporal specificity. Expression of this toxin must obviously be tightly restricted to the desired cell population to avoid widespread damage or even death, but also must be temporally controlled in order to prevent developmental lethality[345]. Although many genetic ablation systems have been developed in different model organisms[346,347] there are few well characterised techniques in the zebrafish.

One that has been validated in zebrafish is the Nitroreductase (Ntr)/ Metronidazole (Mtz) system[184]. This system is based on the expression of the bacterial Ntr enzyme which is required to convert a non-toxic pro-drug (Mtz) into a potent DNA cross-linking agent. This cytotoxic form of Mtz accumulates and resulting in apoptosis of any Ntr-expressing cells. This system has a number of advantages: it is phenotypically silent until the addition of Mtz preventing any developmental defects; it is highly-specific and shows no detectable toxicity to neighbouring non Ntr-expressing cells; and temporal control is achieved easily by the addition and subsequent washing out of Mtz from the media creating an inducible and reversible system. Unfortunately, it does not appear 100% effective with some transgenic cells persisting even after extended Mtz doses.

4.1.2.3.4 Prevent immune development

Instead of finding methods to kill macrophages, it is possible to prevent their development in the first place. Established lines such as *cloche*, *csf1ra* or *pu.1* have mutations in the genes required for leukocyte development and as such do not produce leukocytes and are immune-deficient. Using these, or similar, mutant lines could give insight into the roles of inflammation but the unknown effects of the mutant background must be considered especially considering that the lack of a functional copy of these genes may impact other developmental & regenerative processes completely independently of inflammation. Generating morphants for these genes by injection of morpholino antisense oligonucleotides is another option for studying immune-deficient regeneration but these would similarly alter the developmental background. Additionally, they would require subsequent validation given the propensity of true genetic mutants not to phenocopy any observed morphant phenotype[348].

4.1.2.4 Experimental setup chosen

The Ntr/Mtz inducible cell ablation system was chosen due to its lowest potential for off-target effects. Transgenic lines were sourced from Prof Stephen Renshaw and Dr Tim Chico at the University of Sheffield and these lines used the *GAL4/UAS* system to restrict Ntr expression to the target cells.

The *GAL4*/*UAS* system was initially developed in flies but given its versatility, it has since been optimised for use in zebrafish[349]. It relies on the insertion of two transgenes – one encoding

the yeast transcriptional activator GAL4 driven by a cell-specific promoter and the other encoding a GAL4-responsive (*UAS*) element to drive expression of a gene of interest in a GAL4 dependent fashion[350]. Expression of the gene of interest is therefore restricted to the specific cell populations expressing GAL4. This modular genetic system allows separation of the *GAL4* driver lines and *UAS* lines, thereby allowing maintenance of a number of phenotypically silent transgenic lines which can be easily crossed to produce many different transgenics of interest without the need to design and clone new transgenes nor to establish a new transgenic line from scratch.

The *GAL4*/*UAS* driven Ntr/Mtz ablation system used cell-specific *GAL4* driver lines combined with *UAS:Ntr.mCherry* (*UNM*) lines encoding a nitroreductase-mCherry fusion protein driven by the *UAS* element to allow fluorescent visualisation of transgenic cells. Transgenic larvae were generated by crossing appropriate *GAL4* driver lines with *UNM* lines in order to obtain the desired combination of transgenes for the different ablation experiments. Two different promoters for macrophage *GAL4* lines were used – *csf1ra* & *mpeg1* – and the *mpx* promoter was used for neutrophil specific-expression of GAL4. In addition to these, a triple transgenic containing *UNM*, *mpeg1* and *mpx:GAL4* was created in order to simultaneously ablate neutrophils and macrophages to examine regeneration in an inflammation-independent context.

With Ntr expression restricted to the specific cell populations I wanted to deplete, ablation was achieved by addition of Mtz. The pro-drug was administered for 18hrs before experiments began in order to allow time for the targeted cells to enter apoptosis, as previously validated by both activated caspase 3 and TUNEL staining[184].

4.2 Results

4.2.1 Regeneration is unaffected following macrophage ablation

Although inflammation-deficient zebrafish present equal regenerative ability to wild-type larvae[43,113,122], studies modulating macrophages and neutrophils separately have shown positive and negative impacts on regeneration, respectively[309,332,333]. Taken together, these results suggest that although inflammation as a whole does not appear to affect regeneration, this may be due to the balance of antagonistic regulatory signals from separate cell populations, rather than the lack of any regulatory influence at all.

Macrophages have been the most closely studied leukocytes in relation to regeneration stemming from their well-established inflammation resolving and pro-healing effects[210]. This assumed pro-regenerative role has been supported by studies in multiple species: in mice, muscle regeneration, retinal healing and neonatal heart regeneration are all impaired following depletion of macrophages[332,351,352]; in salamander a complete loss of limb regeneration was observed after liposome-encapsulated clodronate was used to specifically ablate macrophages[333]; in zebrafish, injection of an *irf8* morpholino restricts differentiation of macrophages and although regeneration of the amputated tail was eventually completed, the morphants displayed a decrease in the rate of regeneration and some regenerated tissue contained large vacuoles[309].

In order to investigate cell-specific responses myself, I used the Ntr/Mtz system described above to ablate macrophages to allow us to examine the wound response in a macrophage-depleted environment. In order to target Ntr expression to macrophages, two different *GAL4* driver lines were crossed with the *UNM* lines – *csf1ra:GAL4*, and *mpeg1:GAL4*. I hoped that by using two distinct promoters, I could account for any off-target effects of these individual promoters and increase my confidence that any results I observed were indeed macrophage specific.

4.2.1.1 Macrophage ablation with *csf1ra:GAL4*/*UNM* transgenic lines

Initially, I analysed *csf1ra:GAL4*/*UNM* transgenic larvae for regenerative defects following Mtz-induced cell ablation. The *csf1ra* gene encodes a receptor tyrosine kinase which is expressed in macrophages in larval zebrafish[353]. The gene is, however, also expressed in xanthophores – one of the three classes of pigment cells present in zebrafish. As such, using the *csf1ra* promoter faithfully drives expression of a transgene in macrophages, but also xanthophores[182]. Although expression in this second cell type was not desired, given the limited function of xanthophores they are unlikely to be involved in the regulation of regeneration and therefore ablation of these cells should have little effect on the results. This hypothesis is supported the pigmentation mutant *panther* which contains inactivating mutations of the *csf1ra* gene. These xanthophore-depleted mutants are macrophage replete[354] yet remain capable of regenerating their tail after injury[353], suggesting no requirement for xanthophores in regeneration.

Despite the advantages of using a *GAL4/UAS* system to drive transgene expression, it can be prone to silencing leading to variable expression between transgenic individuals[355]. To combat

this, embryos were screened carefully before use to identify strong expressers. Non-expressing siblings were also selected as controls. The early development of xanthophores allowed the discrimination of transgenic individuals and siblings at 1dpf. Embryos were pre-dosed with Mtz to allow enough time for macrophages to proceed through apoptosis before the wound was inflicted. Larvae were continually dosed in Mtz in order to prevent the development of any new macrophages during the experiment.

In order to validate the ablation system and quantify the extent of cell ablation, the extent of macrophage recruitment to the wound was compared. Images were taken of Mtz- or vehicle-(0.1% DMSO) treated transgenic larvae at 6hpa (a timepoint identified as the time of maximum macrophage recruitment to the wound[309]) and the area of transgenic (mCherry positive) cells within 200µm of the wound margin was quantified. Cell area was chosen as the most representative quantifiable metric from these images as it encompasses total cell number and average cell size, which were both affected following Mtz-treatment (Figure 4.1A). Additionally, in control larvae, the upper range of macrophage recruitment meant that discrimination of individual mCherry positive cells from the whole mCherry positive area to generate accurate cell counts was not possible (Figure 4.1B). Using these metrics, we see that treatment with Mtz reduced the area of transgenic cells at the wound to 8% of the control (Figure 4.1A) confirming a highly significant, though not complete, reduction in the recruitment of macrophages to the wound.

In Chapter 3, two types of injury were inflicted on larvae: fin-fold amputations and pigment-gap amputations. Although these wounds differed in their transcriptional response they were both H_2O_2 dependent, therefore they may both mediate regeneration through the H_2O_2 mediated stimulation of inflammation. Knowing this, I decided to test the regenerative response to both injuries following macrophage ablation.

The extent of regeneration was assessed by measuring the linear distance from the caudal tip of the notochord to the edge of the caudal fin-fold (“regenerate length”). Regenerate length for fin-fold amputations was measured at 48hpa when regrowth had completed, but given the more severe nature of the pigment-gap amputations, they required more time to fully regenerate and were measured at 72hpa.

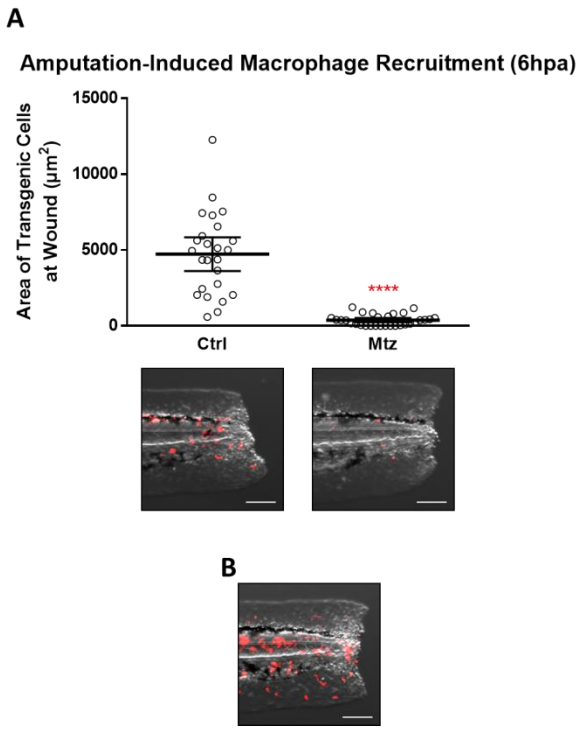

Figure 4.1 – Quantification of macrophage knockdown in *csf1ra:GAL4/UNM* transgenic larvae.
A) Quantification of macrophage knockdown using the *UNM* genetic ablation system in *csf1ra:GAL4/UNM* larvae following 18hr Mtz exposure with inset representative images. **B)** Representative image of a larvae with high levels of macrophage recruitment, showing the difficulty in discriminating individual cells from these images. Scale bars: 100µm.

Macrophage ablation was induced in transgenic larvae with Mtz treatment (Tg Mtz) and compared to two macrophage-replete groups; 1) Mtz-treated non-transgenic siblings (Sib Mtz) in order to control for off-target drug effects; and 2) vehicle-treated transgenic larvae (Tg Ctrl) in order to control for effects of the transgenic background. Neither of these comparisons detected a significant difference on regenerative outgrowth following macrophage ablation following fin-fold resections or pigment-gap level tail amputations (Figure 4.2A, B), suggesting that these cells are dispensable for regeneration to proceed as normal for both injuries.

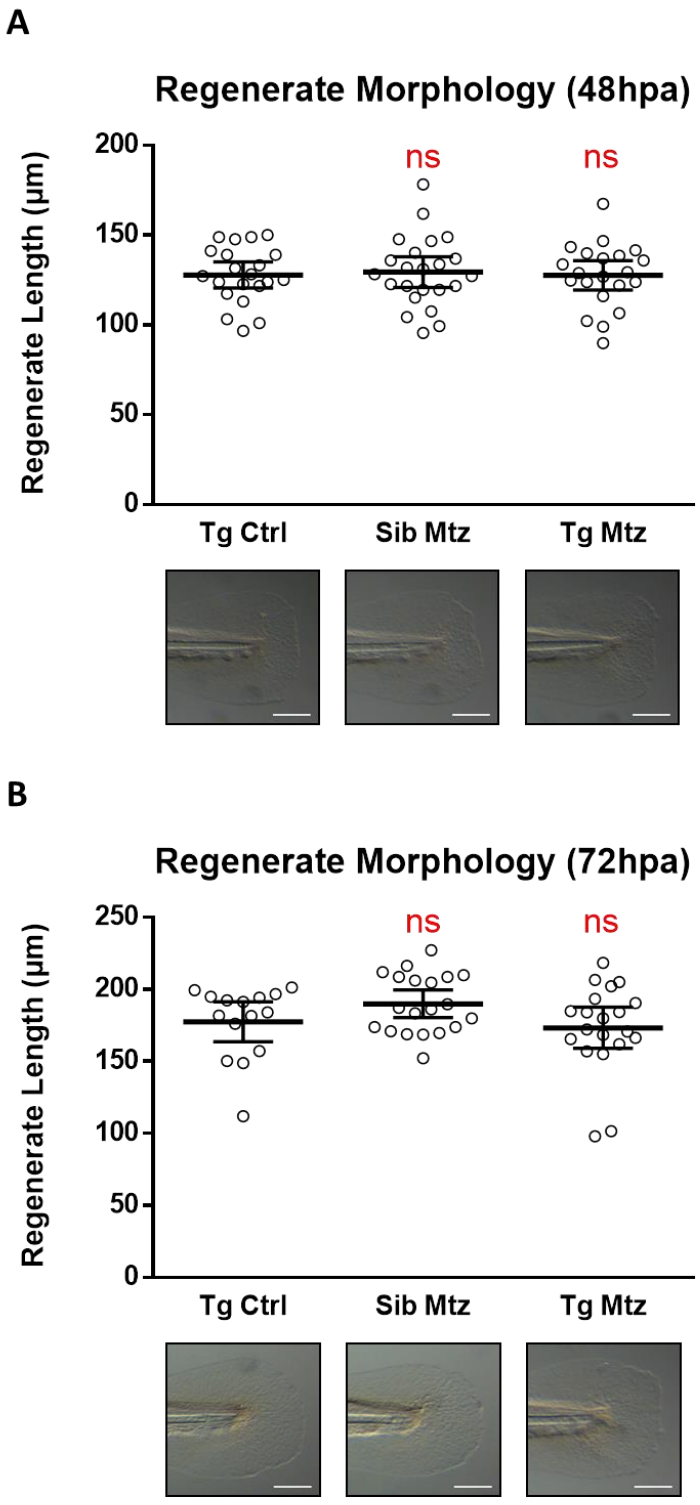

Figure 4.2 – Quantification of regenerate outgrowth following *UNM*-mediated macrophage ablation. Tail amputations were performed at 3dpf in *csf1ra:GAL4/UNM* transgenic larvae (Tg) and their siblings (Sib) and the regenerated tissue was quantified at 48hpa. Quantification of regenerated tissue following fin-fold level amputations (**A**) or pigment-gap level amputations (**B**) with inset images. Scale bars: 100µm.

4.2.1.2 Macrophage ablation with *mpeg1:GAL4/UNM* transgenic lines

The second promoter used to drive expression of Ntr in macrophages was the *mpeg1* promoter. The *mpeg1* gene encodes a bactericidal perforin-like protein[356] and was identified as a macrophage specific gene in two independent studies[179,357]. Use of the *mpeg1* promoter can faithfully drive expression of transgenes in macrophages and no other cell type in zebrafish[179], making the *mpeg1:GAL4* transgenic capable of a more specific targeting of macrophages than the *csf1ra:GAL4*. This transgenic line will also allow more accurate estimation of macrophage ablation due to the absence of mCherry positive xanthophores.

Expression of *mpeg1* is activated later in development than *csf1ra* therefore larvae could not be screened for transgenic individuals or siblings until 2dpf. This delayed the pre-dosing with Mtz until 2dpf and therefore amputations until 3dpf. Amputations were initially performed in the pigment-gap, and assayed for macrophage recruitment to the wounds at 6hpa. Quantification of recruited macrophages showed a large, significant decrease following Mtz-treatment; macrophage area at the wound was reduced to 16% of the vehicle-dosed larvae area (Figure 4.3).

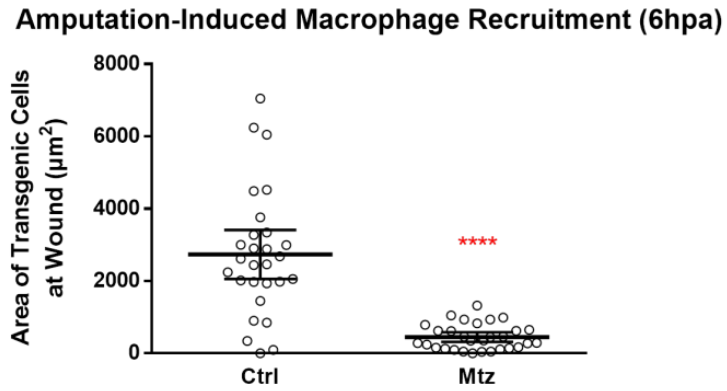

Figure 4.3 – Quantification of macrophage knockdown in *mpeg1:GAL4/UNM* transgenic larvae.
Quantification of macrophage knockdown using the *UNM* genetic ablation system in *mpeg1:GAL4/UNM* larvae following 18hr Mtz exposure.

Regenerate length was measured at 48hpa to compare the extent of regeneration in the samples. When assessing statistical differences between groups, Mtz-specific effects were assessed by comparing Mtz-dosed groups to vehicle-dosed groups for both sibling and

transgenic larvae (Sib Ctrl vs Sib Mtz; Tg Ctrl vs Tg Mtz), and the effect of the transgenic background was assessed by comparing sibling groups to transgenic groups for Mtz-dosed and vehicle-dosed larvae (Sib Ctrl vs Tg Ctrl; Sib Mtz vs Tg Mtz). Neither of these comparisons resulted in a significant effect on regenerative outgrowth (Figure 4.4A). Additionally, to control for the off-target effects of Mtz dosing and any influence of the transgenic background simultaneously, the regenerate length of Mtz-treated transgenic & sibling groups was normalised to their respective vehicle-treated controls (Sib Mtz/Sib Ctrl & Tg Mtz/Tg Ctrl), and directly compared. This additional test did not show any significant difference induced following macrophage ablation (Figure 4.4B). Together, these data support the previous conclusion that macrophages are dispensable for tail regeneration.

In order to test if prolonged Mtz treatment resulted in more complete cell ablation, larvae were treated with Mtz for an additional 24hrs before fin-fold amputations were performed. Following this extended exposure to Mtz, macrophage recruitment reduced to 13% of control levels in Mtz-treated larvae (Figure 4.5). This level of macrophage ablation is similar in scale to that observed from the shorter incubation with Mtz, implying that the extra 24hrs incubation did not notably increase macrophage depletion and the remaining transgenic cells are an unavoidable limitation of the Ntr/Mtz ablation system's incomplete penetrance.

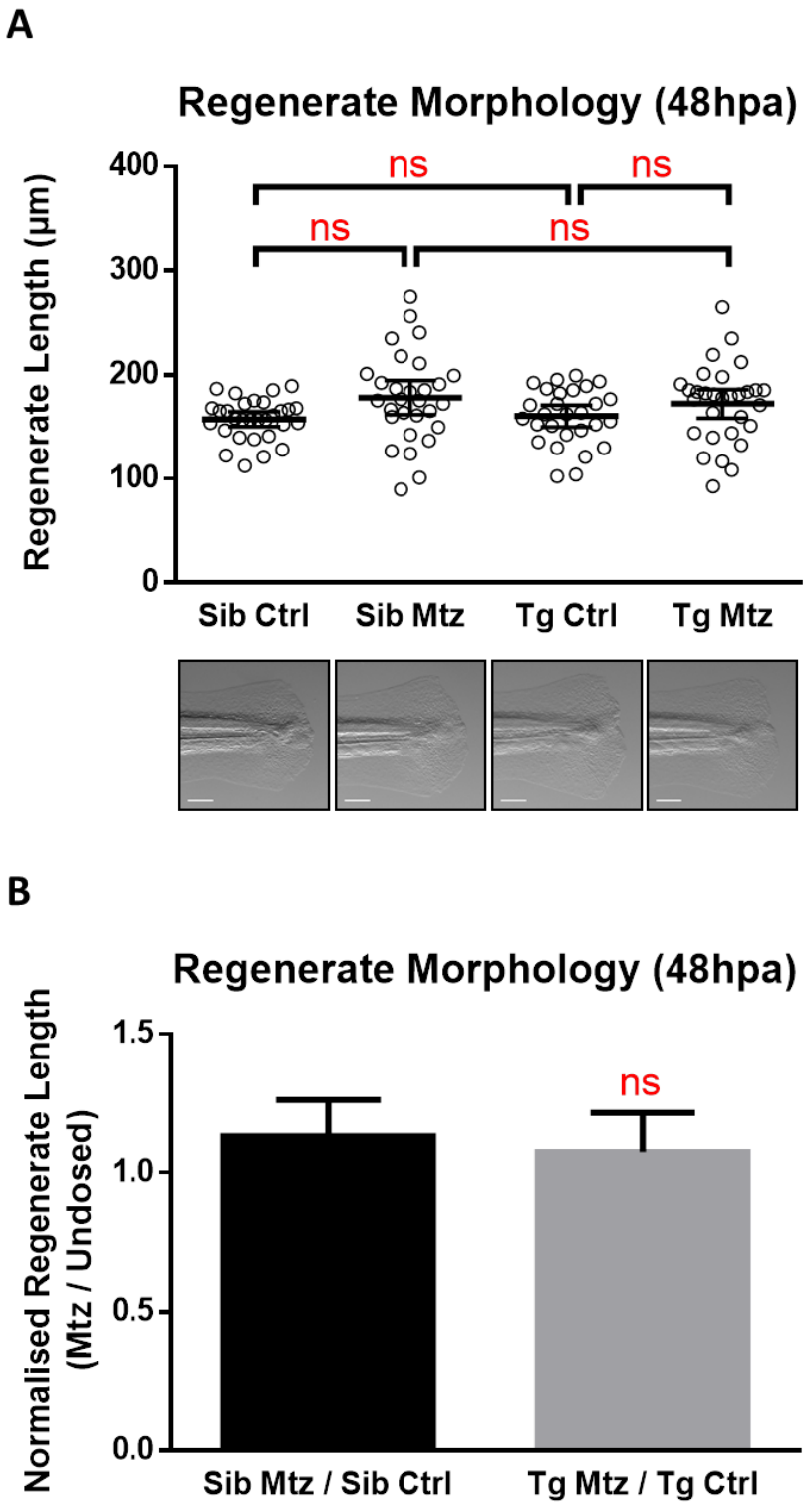

Figure 4.4 – Quantification of regenerate outgrowth following *UNM*-mediated macrophage ablation. Pigment-gap level tail amputations were performed at 3dpf in *mpeg1:GAL4/UNM* transgenic larvae (Tg) and their siblings (Sib) and the regenerated tissue was quantified at 48hpa. **A)** Quantification of regenerated tissue following amputation with inset representative images. Scale bars: 100µm. **B)** Quantification of tissue regenerate comparing Mtz-treated sibling and transgenic groups after normalisation to their respective untreated control group.

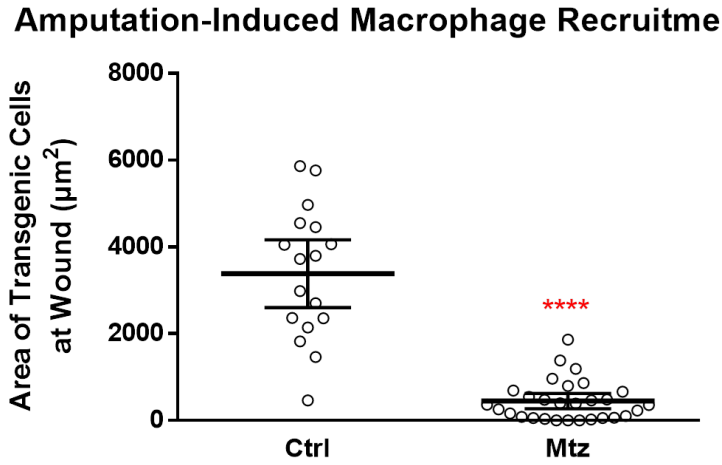

Figure 4.5 – Quantification of macrophage knockdown in *mpeg1:GAL4/UNM* transgenic larvae.
Quantification of macrophage knockdown using the *UNM* genetic ablation system in *mpeg1:GAL4/UNM* larvae following prolonged (42hr) Mtz exposure.

Regeneration was quantified at 48hpa as before, and also at 72hpa to determine if there was any effect on the extent of regrown tissue later in the regenerative process. Analysis of the raw regenerate length did not show any significant difference between the macrophage depleted group (Tg Mtz) compared to the vehicle-dosed transgenic (Tg Ctrl) or the Mtz-dosed sibling (Sib Mtz) groups at either timepoint(Figure 4.6A, B). In addition, no significant difference was detected between sibling and transgenic regenerative outgrowth following normalisation of the data as performed previously (Sib Mtz/Sib Ctrl vs Tg Mtz/Tg Ctrl; Figure 4.6A', B'). Together, these data validate the ablation efficiency of the Ntr/Mtz system and further support the hypothesis that macrophages are not required for regeneration.

Whilst the data presented in Figure 4.5 and Figure 4.6 support that of the previous experiments, it should be noted that they were only conducted once with small sample numbers and therefore should be replicated to increase confidence in the data.

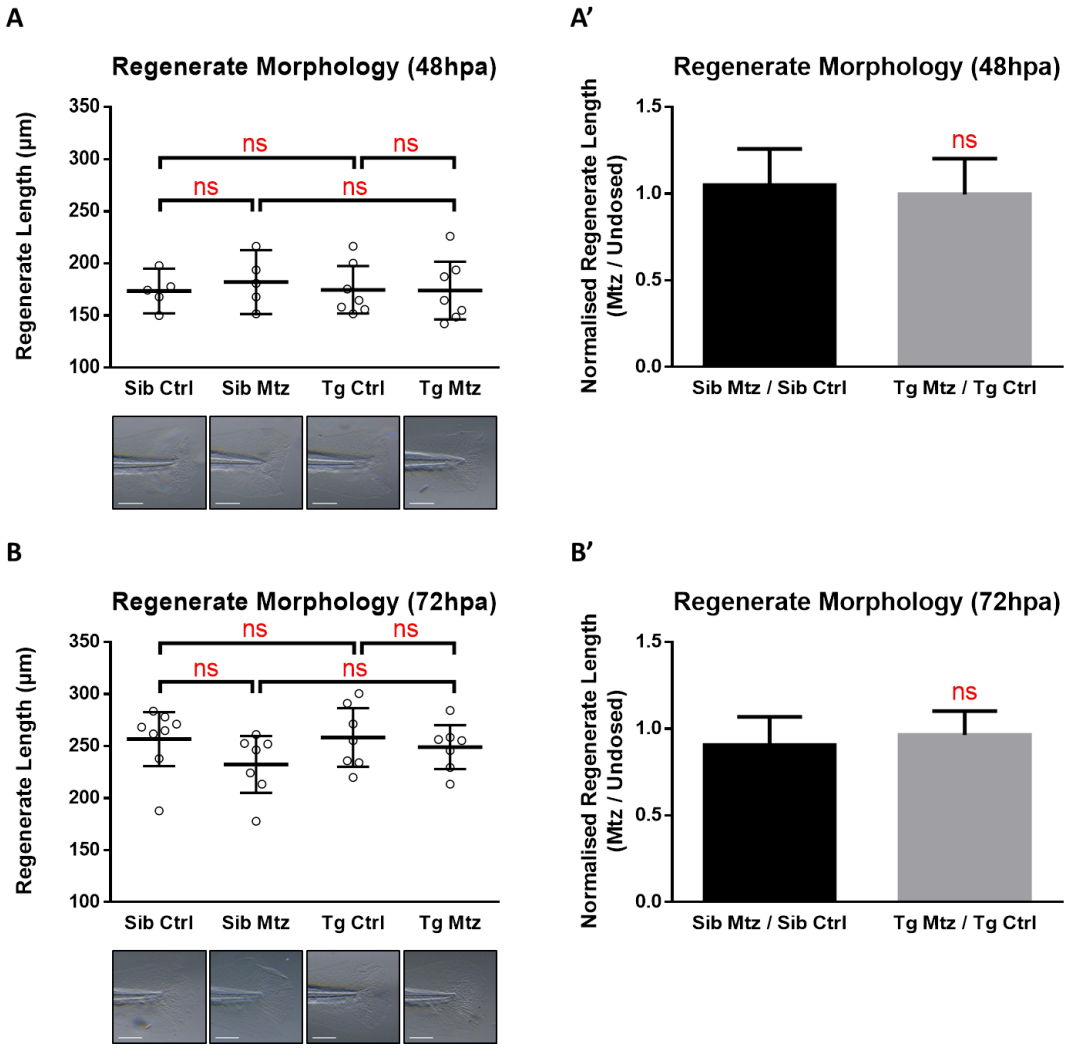

Figure 4.6 – Quantification of regenerate outgrowth following *UNM*-mediated macrophage ablation. Fin-fold level tail amputations were performed at 2dpf in *mpeg1:GAL4/UNM* transgenic larvae (Tg) and their siblings (Sib) and the regenerated tissue was quantified at 48hpa (**A**) and 72hpa (**B**) with inset representative images. Scale bars: 100µm. Quantification of regenerated tissue was repeated by comparing Mtz-treated sibling and transgenic groups after normalisation to their respective untreated control group for 48hpa (**A'**) and 72hpa (**B'**).

4.2.2 Regeneration is unaffected following neutrophil ablation

4.2.2.1 Neutrophil ablation with *mpx:GAL4/UNM* transgenic lines

Having seen no effect of macrophage ablation on regenerative outgrowth, I proceeded to study the role of neutrophils in the regulation of regeneration. Neutrophils are the first responders to the wound, arriving within minutes and well before macrophages[309]. Although growing evidence is highlighting potential anti-inflammatory roles for neutrophils[358], they generally function as pro-inflammatory cells with important roles in pathogen clearance, and

inflammatory cell recruitment & activation[359]. These pro-inflammatory effects would suggest a negative role in healing and regeneration given that chronically inflamed wounds fail to heal[318,319,323], extended inflammation delays healing and regeneration[308]. This hypothesis is supported in mice by a study that shows accelerated wound closure following neutrophil depletion[360] and in zebrafish by work showing more rapid wound-induced cell proliferation & fin regeneration in the neutrophil-depleted *runx1* mutant[309].

It should be noted, however, that one study has shown that neutrophils can play a pro-regenerative role in optic-nerve regeneration in adult mice[361]. Inducing inflammation in the eye following optic nerve injury resulted in an increase in axon-regeneration. This effect was mediated by an upregulation of the atypical growth factor oncomodulin. Induction of inflammation in neutrophil depleted mice however, resulted in a proportional reduction in oncomodulin levels & axon regeneration despite macrophage recruitment remaining unaffected, suggesting that this pro-regenerative role was indeed neutrophil specific. As such, the potential effect of neutrophils on regeneration may be more complex than originally thought.

In order to target Ntr expression to neutrophils, the *mpx* promoter was used. The *mpx* gene encodes myeloperoxidase, the enzyme responsible for converting H_2O_2 into more potent antimicrobials[135], and its promoter has been previously validated as a faithful driver of transgenes in neutrophils[181,362]. Neutrophils do not develop to a mature *mpx*-expressing phenotype until 2dpf, therefore, as for the *mpeg1:UNM* line, screening of embryos was performed at 2dpf. Larvae were continually dosed with Mtz from 18hr before fin-fold amputations were performed on 3dpf larvae, until fixation at 48hpa. Neutrophils are recruited to the wound more rapidly than macrophages and peak at around 2hpa[309], therefore this timepoint was chosen to quantify the extent of cell ablation in the Mtz-treated larvae.

Validation of the ablation efficiency of this line was assayed by both fluorescent quantification (as for macrophages previously) and *mpx in situ* to account for potential silencing of the *UAS:Ntr.mCherry* transgene. Quantification by fluorescent imaging showed a decrease in neutrophil recruitment to 16% (Figure 4.7A), similar to that seen for macrophages previously. Results from the *mpx in situ* showed a more variable reduction in neutrophils to an average of 27%, however some larvae showed a complete absence (Figure 4.7B).

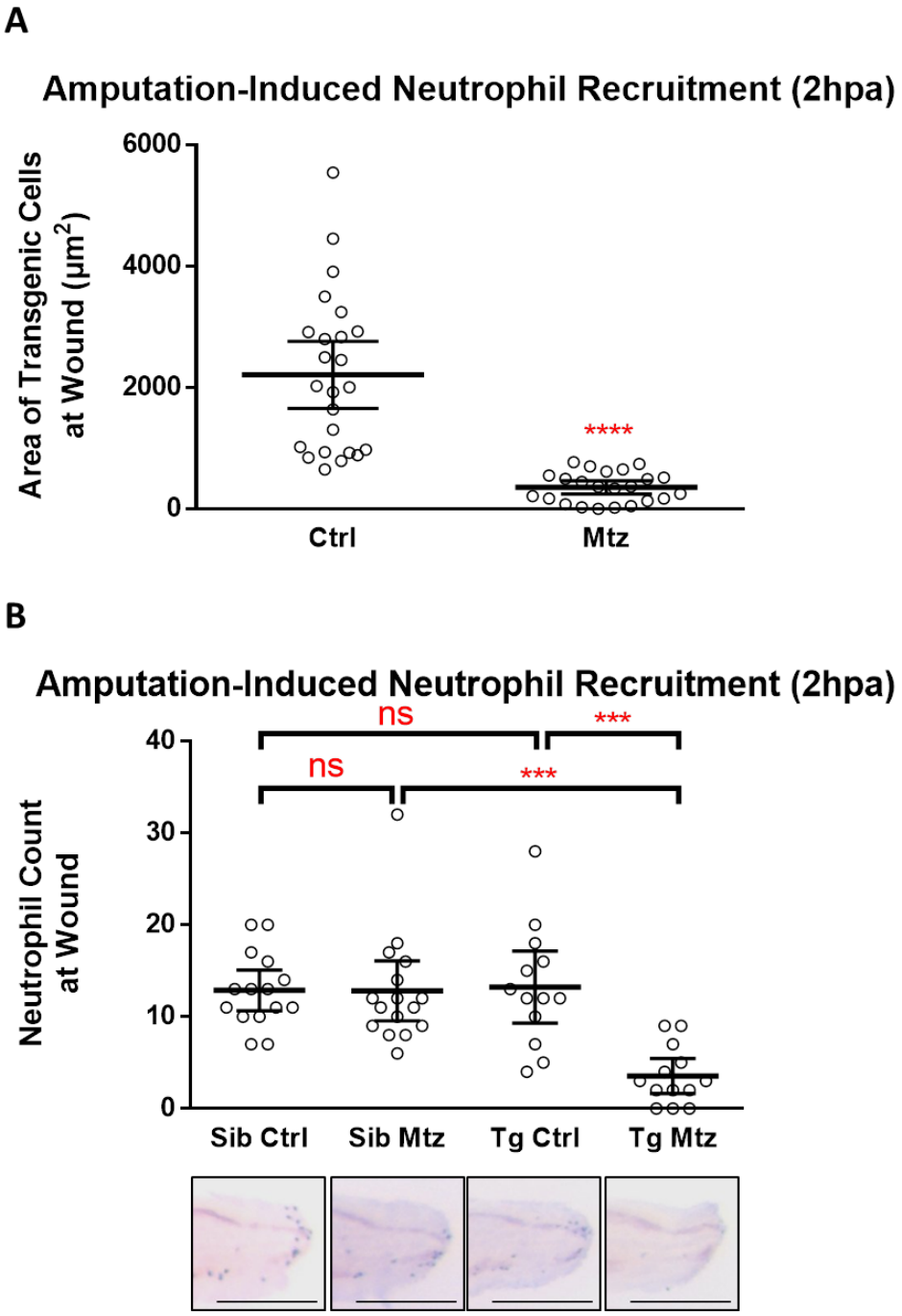

Figure 4.7 – Quantification of neutrophil knockdown in *mpx:GAL4/UNM* transgenic larvae.
Quantification of neutrophil knockdown using the *UNM* genetic ablation system in *mpx:GAL4/UNM* transgenic larvae (Tg) and their siblings (Sib) by visualising transgenic cells by fluorescence (**A**) or WISH for the neutrophil-specific marker *mpx* (**B**) with inset images. Scale bars: 200µm.

Regenerate length was quantified and multiple comparisons between groups were performed as before to identify any statistical differences. Although there was a significant increase in regeneration between the vehicle- and Mtz- dosed transgenic larvae (Figure 4.8A; Tg Mtz vs Tg

Ctrl = 110%), this relationship was also observed in the sibling groups (Figure 4.8A; Sib Mtz vs Sib Ctrl = 112%) suggesting that this was an off-target effect of Mtz, rather than a result of neutrophil depletion. This interpretation is supported by the absence of a significant difference between the Mtz-treated sibling and transgenic groups (Figure 4.8A; Sib Mtz vs Tg Mtz), and by the lack of a statistical difference following normalisation (Sib Mtz/Sib Ctrl vs Tg Mtz/Tg Ctrl; Figure 4.8B). Together, these data show that Ntr-mediated neutrophil depletion had no additional effect on regeneration over Mtz treatment alone, and therefore that neutrophils are not required for regeneration.

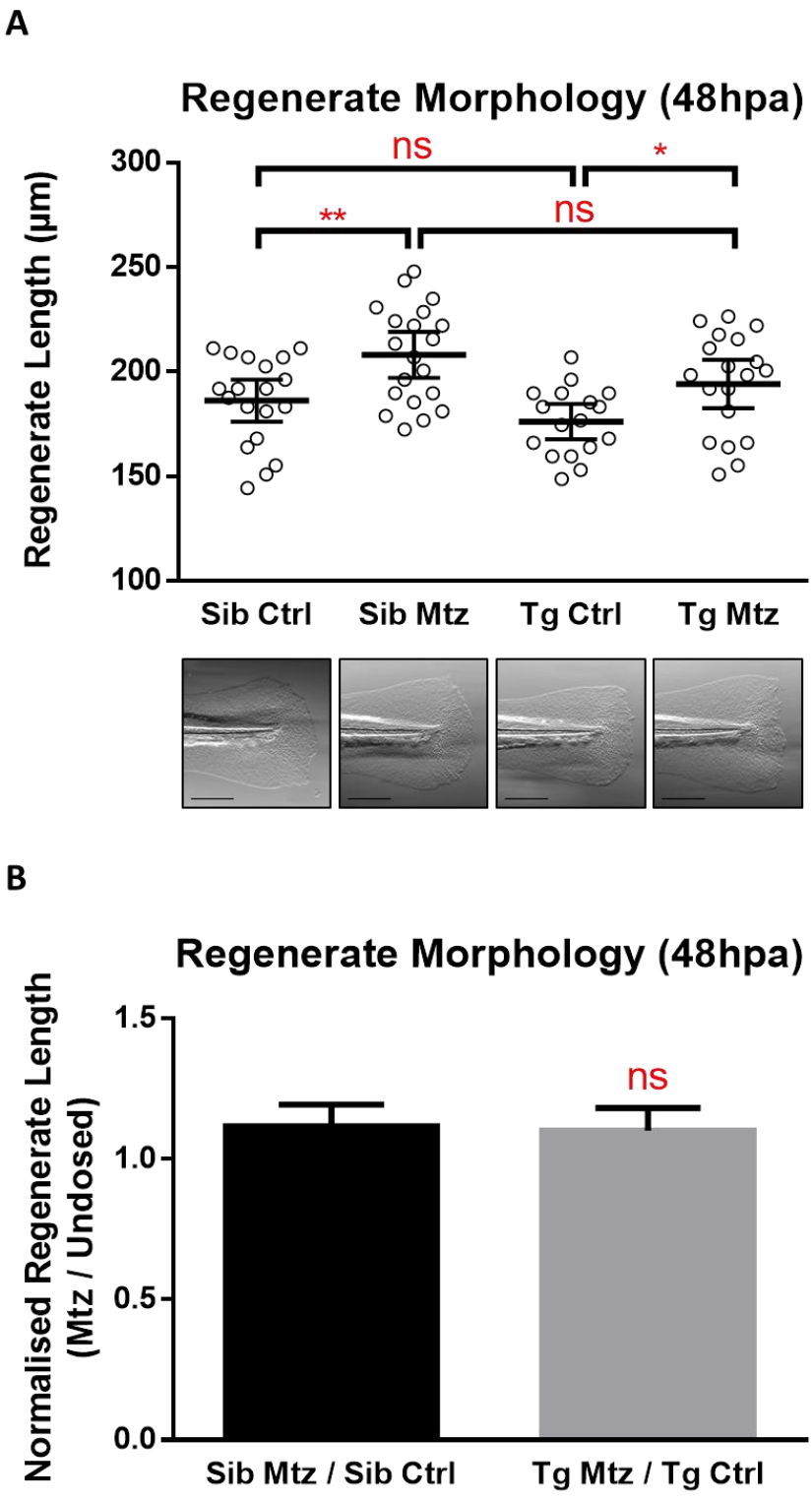

Figure 4.8 – Quantification of regenerate outgrowth following *UNM*-mediated neutrophil ablation. Tail amputations were performed at 3dpf in *mpx:GAL4/UNM* transgenic larvae (Tg) and their siblings (Sib) and the regenerated tissue was quantified at 48hpa. **A)** Quantification of regenerated tissue following amputation with inset representative images. Scale bars: 200µm. **B)** Quantification of tissue regenerate comparing Mtz-treated sibling and transgenic groups after normalisation to their respective untreated control group.

4.2.3 Regeneration is unaffected following leukocyte ablation

4.2.3.1 Leukocyte ablation with *mpeg1:GAL4/mpx:GAL4/UNM* transgenic lines

Having seen no impact on regeneration from ablating either macrophages or neutrophils, I wanted to study regeneration in an inflammation-deficient environment by simultaneously ablating both macrophages and neutrophils. A deficit in neutrophils at the wound may be compensation by the presence of macrophages and vice-versa so depleting both cell types at once may present a different phenotype. For these experiments, the *mpeg1:GAL4* and the *mpx:GAL4* lines were used to target transgene expression to macrophages and neutrophils, respectively. The *mpeg1:GAL4* line was chosen due to its enhanced specificity for macrophages compared to the additional expression seen in xanthophores in the *csf1ra:GAL4* line. Given that both cell types present a peak in recruitment at different times after wounding, ablation was assessed at the point of maximum combined leukocyte recruitment – 6hpa[309].

The double transgenic *mpeg1:GAL4*/*UNM* line was crossed with the *mpx:GAL4* line and larvae screened for strongly expressing triple transgenics after the onset of *mpeg1* and *mpx* expression at 2dpf. Transgenics were identified by the number of labelled cells (Figure 4.9A) in the larvae but also on the distribution & morphology of those cells. Transgenic *mpeg1:UNM* larvae were identified by the high density of cells around the yolk[363,364] and a wide distribution of cells over the entire body (Figure 4.9B). In contrast, *mpx:GAL4* transgenic larvae were characterised by a more sparse distribution across the whole body with higher density in the head and the peripheral blood island just caudal to the yolk extension[185,365](Figure 4.9C). Morphologically, macrophages appeared larger and more irregularly-shaped (Figure 4.9B) than the small & rounded neutrophils (Figure 4.9C).

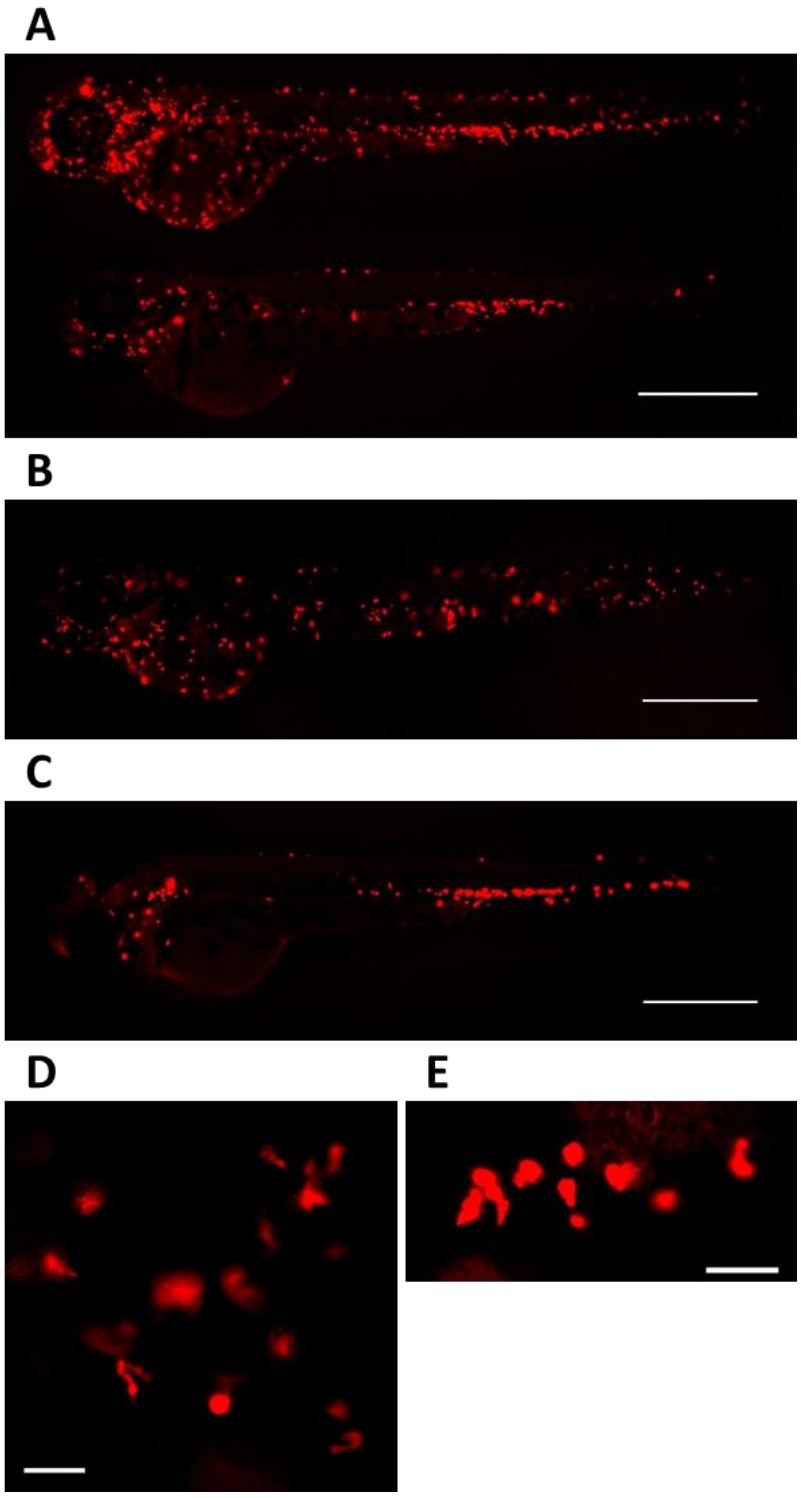

Figure 4.9 – Identification of *mpeg1:GAL4/UNM*, *mpx:GAL4/UNM* and *mpeg1:GAL4/mpx:GAL4/UNM* transgenic larvae.
Representative images showing how to discriminate between larvae different transgenic combinations. Larvae with *UNM* labelled macrophages and neutrophils showed a clear increase in the number of labelled cells visible (**A** top, vs **A** bottom). Larvae were also identified by the distinct location of the labelled macrophages (**B**) and neutrophils (**C**) as well as the differing cell size and shape of macrophages (**D**) and neutrophils (**E**). Scale bars: 500µm (**A**, **B**, **C**) / 50µm (**D**, **E**).

Cellular ablation was quantified as before using area of fluorescence at the wound and showed a decrease in recruited leukocytes to 9% of control levels (Figure 4.10), consistent with the efficiencies of individual ablation lines.

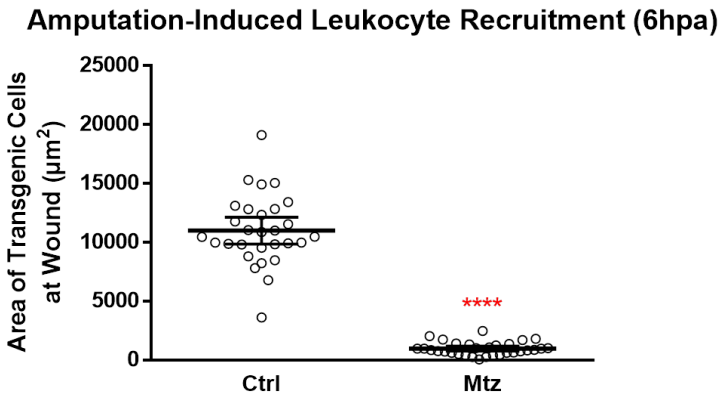

Figure 4.10 – Quantification of leukocyte knockdown in *mpeg1:GAL4/mpx:GAL4/UNM* transgenic larvae.
Quantification of macrophage & neutrophil knockdown using the *UNM* genetic ablation system in *mpeg1:GAL4/mpx:GAL4/UNM* larvae.

Fin-fold only amputations were initially performed and comparisons between groups were performed as above and no significant differences were identified in the regenerate of the fin-fold amputations (Figure 4.11A, C), a result mirrored following normalisation (Sib Mtz/Sib Ctrl vs Tg Mtz/Tg Ctrl; Figure 4.11B).

In addition to fin-fold amputations, pigment-gap level tail amputations were performed and the regenerate quantified at 48hpa. A number of the pigment-gap amputations appeared to regenerate less completely and presented abnormal gross morphology of the caudal fin with a much more irregular shape in all groups (Figure 4.12A). Because of this, the pigment-gap amputations were quantified by both regenerate length and regenerate area (the total area of tissue beyond the caudal tip of the notochord) in order to better represent the data than by a single linear measurement.

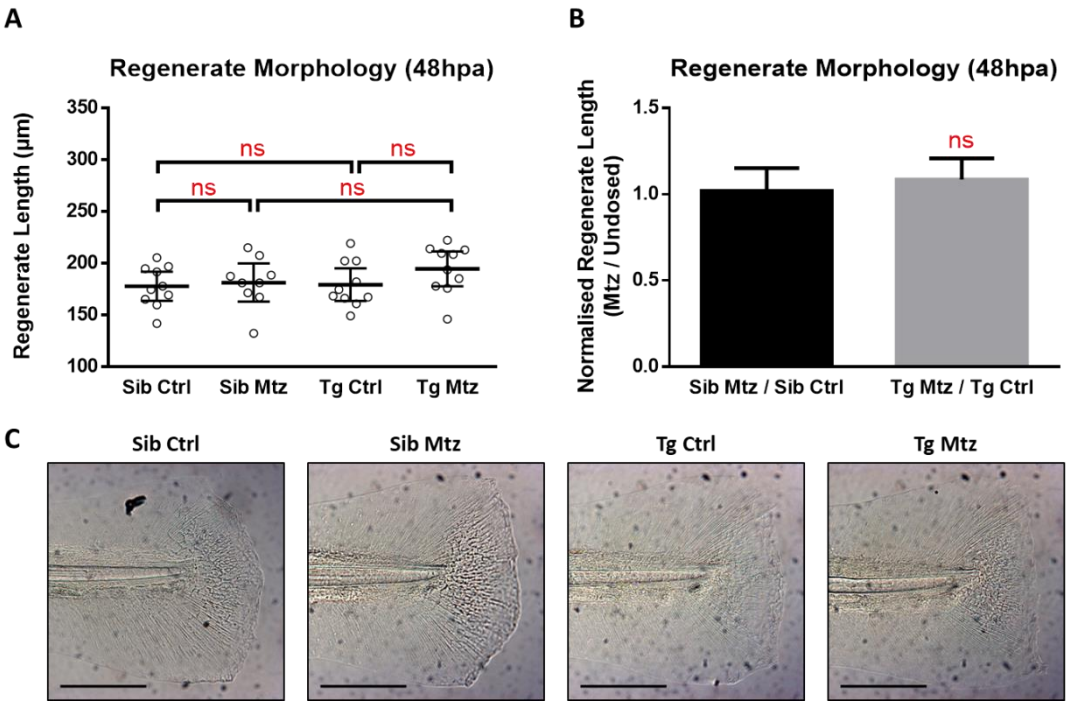

Figure 4.11 – Quantification of regenerate outgrowth following *UNM*-mediated leukocyte ablation. Fin-fold only amputations were performed at 3dpf in *mpeg1:GAL4/mpx:GAL4/UNM* transgenic larvae (Tg) and their siblings (Sib) and the regenerated tissue was quantified at 48hpa. **A)** Quantification of regenerated tissue following amputation. **B)** Quantification of tissue regenerate comparing Mtz-treated sibling and transgenic groups after normalisation to their respective untreated control group. **C)** Representative images used for quantification. Scale bars: 200µm.

Both methods of quantifying regeneration following pigment-gap amputations presented the same conclusion, that the only significant difference between groups was between the Mtz-treated sibling and transgenic larvae (Figure 4.12B, C; Sib Mtz vs Tg Mtz). But in the absence of a matching significant difference between the Mtz- and vehicle-treated transgenic larvae this result is not robust, and no significant difference was detected following normalisation (Sib Mtz/Sib Ctrl vs Tg Mtz/Tg Ctrl; Figure 4.12D, E). Together, these data show that Ntr-mediated leukocyte depletion had no significant additional effect on regeneration over Mtz treatment alone in either wound type, and therefore that leukocytes are not required for regeneration.

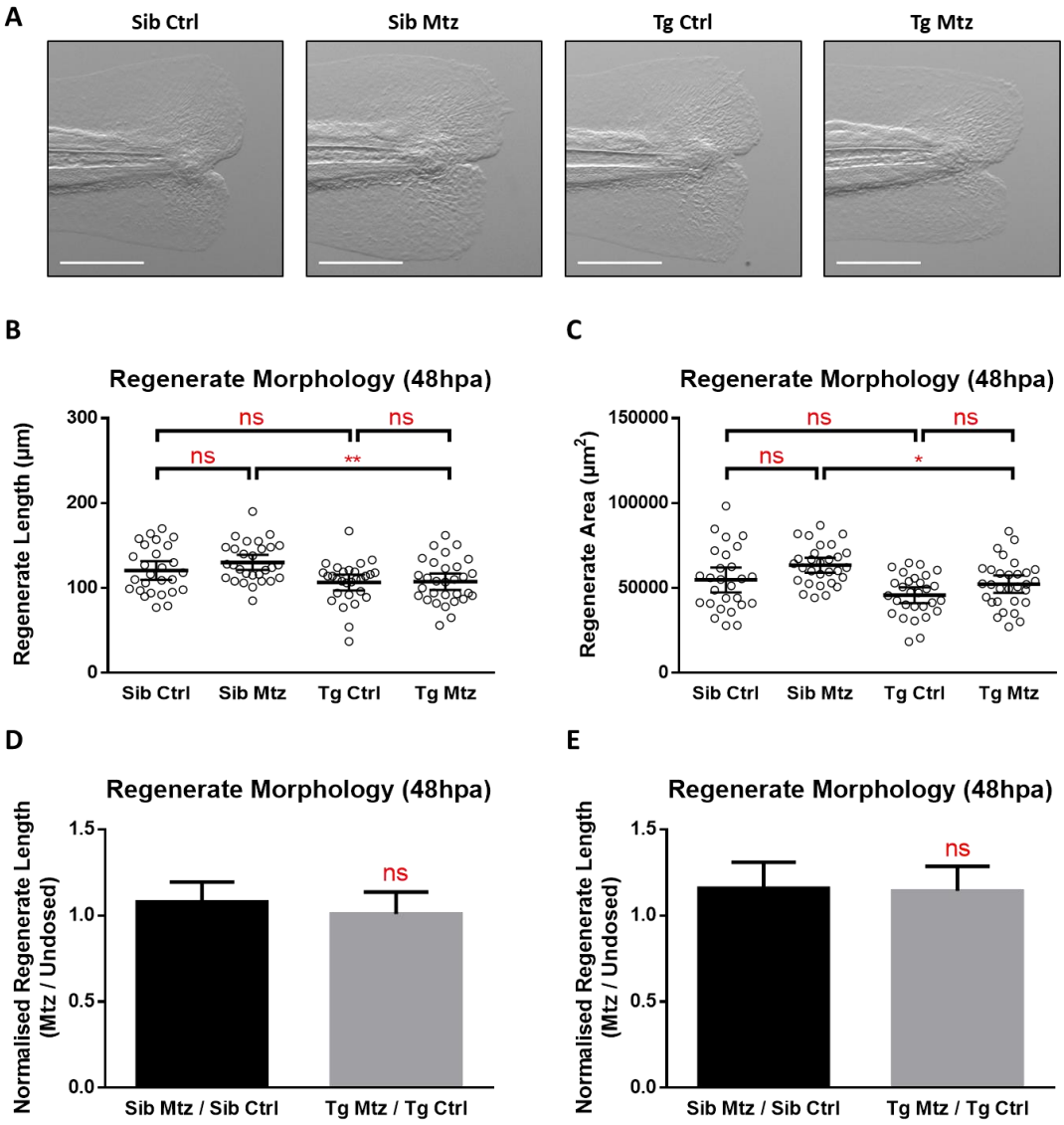

Figure 4.12 – Quantification of regenerate outgrowth following *UNM*-mediated leukocyte ablation. Pigment-gap level tail amputations were performed at 3dpf in *mpeg1:GAL4/mpx:GAL4/UNM* transgenic larvae (Tg) and their siblings (Sib) and the regenerated tissue was quantified at 48hpa. **A)** Representative images used for quantification. Scale bars: 200µm. Quantification of regenerated tissue following amputation by regenerate length (**B**) and by regenerate area (**C**). Quantification of tissue regenerate comparing Mtz-treated sibling and transgenic groups after normalisation to their respective untreated control group for regenerate length (**D**) and regenerate area (**E**).

4.2.4 Leukocyte recruitment and *ihhb* upregulation have similar temporal characteristics

In addition to assessing the effect of inflammation on regenerate morphology, I wanted to investigate if leukocytes affected the activation of H_2O_2 dependent regeneration signalling.

Having identified Hh as the upstream activator of H_2O_2 dependent regeneration signalling, I analysed the relationship between leukocytes and the extent of *ihhb* upregulation. These experiments aimed to address whether leukocytes are required to act as mediators by which H_2O_2 can indirectly trigger regeneration signalling, or if this is an inflammation-independent signal.

I initially examined the timing of both neutrophil recruitment (by Sudan Black staining) and *ihhb* upregulation (by WISH) following amputations, knowing that both were rapidly induced in similar timeframes to see if these were sequential or parallel processes. Neutrophil recruitment appeared to slowly & steadily increase from the time of wounding with little to no lag in response (Figure 4.13A) whereas *ihhb* upregulation was not detectable until 2hpa (Figure 4.13B). These data demonstrates that leukocyte recruitment occurs prior to the induction of *ihhb* and therefore may be responsible for, or contribute to, *ihhb* regulation. However, more detailed analysis suggests that there is no linear relationship between neutrophil recruitment and *ihhb* expression in these samples: when analysed for a correlation between neutrophil number and *ihhb* stain area within each timepoint, no significant correlation between the variables was identified (Table 4.1); linear regression of the data points showed no clear relationship with near-zero coefficient of determination (R^2) in samples where staining was detected suggesting no linear relationship between neutrophil number and *ihhb* staining (Figure 4.13C, Table 4.2); F-test analysis did not detect any significant deviation from zero for the regression lines, again suggesting no linear relationship (Table 4.3); and the presence of multiple outliers showing both high *ihhb* expression with low neutrophil counts and vive-versa (Figure 4.13C).

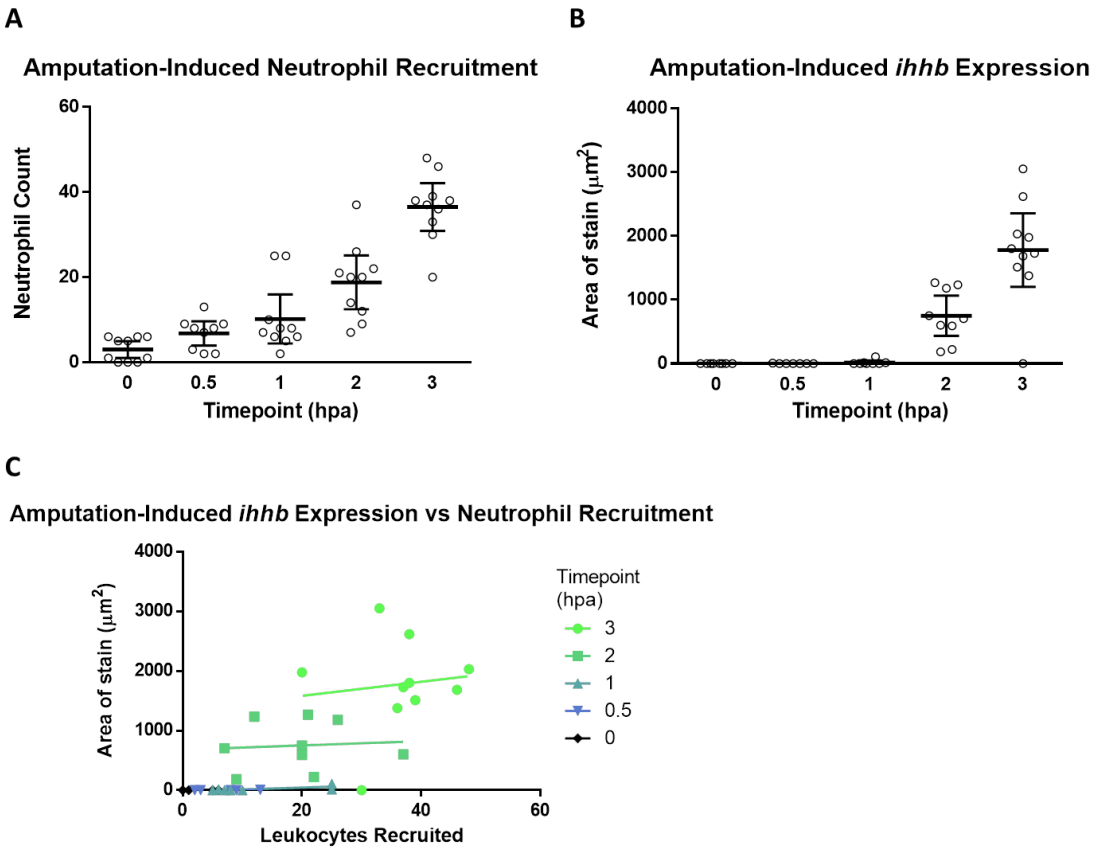

Figure 4.13 – Timecourse of amputation-induced neutrophil recruitment and *ihhb* expression.
A) Quantification of neutrophil recruitment to the wound as measured by sudan black staining. **B)** Quantification of wound-induced *ihhb* expression. **C)** Correlation of neutrophil recruitment and *ihhb* expression over time.

Spearman Correlation Test	0hpa	0.5hpa	1hpa	2hpa	3hpa
Number of XY pairs	8	7	8	9	10
r value	Horizontal line	0.6236	0.2242	0.1088	0.08511
P value (two-tailed)	-	0.2857	0.5875	0.7844	0.8184
Significant? (alpha = 0.05)	-	No	No	No	No

Table 4.1 – Correlation between wound-recruited neutrophils and *ihhb* expression.
Spearman correlation test did not detect a significant correlation between the number of neutrophils recruited to wounds and the extent of *ihhb* expression at any of the timepoints.

Linear Regression	0hpa	0.5hpa	1hpa	2hpa	3hpa
Slope	-	0.4176 ± 0.1957	3.102 ± 1.293	3.666 ± 16.70	11.78 ± 35.82
Y-intercept	-	-1.725 ± 1.470	-17.58 ± 18.06	678.6 ± 354.0	1349 ± 1335
Equation	-	Y = 0.4176X - 1.725	Y = 3.102X - 17.58	Y = 3.666X + 678.6	Y = 11.78X + 1349
R^2	-	0.4766	0.4894	0.006839	0.01334

Table 4.2 – Calculation of regression lines for wound-recruited neutrophils and *ihhb* expression.
Analysis of linear regression between the number of neutrophils recruited to wounds and the extent of *ihhb* expression returned R^2 values of near 0 at timepoints with detectable *ihhb* staining (2 and 3hpa), suggesting no linear relationship between the two variables.

F-Test of Regression Line	0hpa	0.5hpa	1hpa	2hpa	3hpa
Total number of values	-	7	8	9	10
F value	-	4.552	5.752	0.0482	0.1082
DFn, DFd	-	1, 5	1, 6	1, 7	1, 8
P value	-	0.086	0.0534	0.8325	0.7507
Significant deviation from zero?	-	No	No	No	No

Table 4.3 – F-test analysis of the linear regression model of wound-recruited neutrophils and *ihhb* expression.
Analysis of linear regression between the number of neutrophils recruited to wounds and the extent of *ihhb* expression returned very low F values at timepoints with detectable *ihhb* staining (2 and 3hpa), suggesting no linear relationship between the two variables.

Considering that the timing of these processes is so similar, simply assessing the sequence of activation is not the clearest way to identify a causal relationship between the two. Therefore, I used the cell ablation transgenics to once again assess regeneration in the presence and absence of leukocytes to see if there was any detectable impact on the regulation of wound-induced *ihhb*.

Double transgenic *mpeg1:GAL4/UNM* larvae were used to selectively deplete macrophages alone given that the literature suggests that they have the greatest pro-regenerative role of the inflammatory cells[309]. Larvae were screened at 2dpf, pre-dosed with Mtz for 18hrs and tails were amputated at the pigment-gap at 3dpf. Larvae were continually treated with Mtz until fixation at 6hpa.

Quantification of macrophage ablation showed a reduction to 10% of control levels (Figure 4.14). The WISH results highlighted a reduction in *ihhb* expression after Mtz-treatment in

transgenic larvae (Figure 4.15A; Tg Ctrl vs Tg Mtz), but also in siblings (Figure 4.15A; Sib Ctrl vs Sib Mtz). This, combined with the lack of a significant difference between sibling and transgenic larvae when dosed with Mtz (Figure 4.15A; Sib Mtz vs Tg Mtz) suggests that Mtz itself may have off-target effects on *ihhb* expression and this is not a result of macrophage depletion in the transgenic individuals.

As before, in order to control for effects of the genetic background & off-target effects of Mtz dosing and determine ablation-specific effects, expression levels of *ihhb* were normalised (Sib Mtz/Sib Ctrl & Tg Mtz/Tg Ctrl) and compared (Figure 4.15B). No significant difference was observed between the two normalised averages, suggesting that macrophage depletion does not have an additive effect on *ihhb* expression over that of Mtz-treatment alone.

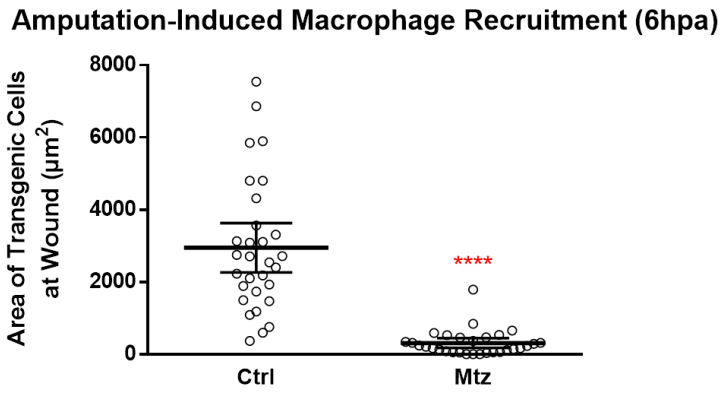

Figure 4.14 – Quantification of macrophage knockdown in *mpeg1:GAL4/UNM* transgenic larvae. Quantification of macrophage knockdown using the *UNM* genetic ablation system in *mpeg1:GAL4/UNM* larvae following 18hr Mtz treatment.

Triple transgenic *mpeg1:GAL4*/*mpx:GAL4*/*UNM* larvae were also used to deplete both macrophages and neutrophils simultaneously. Larvae were screened, dosed and wounded as for the previous experiment. Leukocyte ablation efficiency was quantified using the area of transgenic cells at the wound as before but also by measuring expression of a leukocyte-specific protein. The *lcp1* gene encodes l-plastin, a small protein with actin & Ca^{2+} binding domains important in cytoskeletal arrangements and is specifically expressed in leukocytes in zebrafish[187,366]. An anti-Lcp1 antibody was used to label leukocytes in all 4 sample groups (Sib Ctrl, Sib Mtz, Tg Ctrl, Tg Mtz) and z-stacked confocal images were taken for each larva. These images were used to measure the volume of cells recruited to the wound and also estimate

cell counts as the 3D images enabled individual cells to be discerned using the 3D Objects Counter plugin in ImageJ[190] unlike the overlapping 2D leukocyte signal used previously.

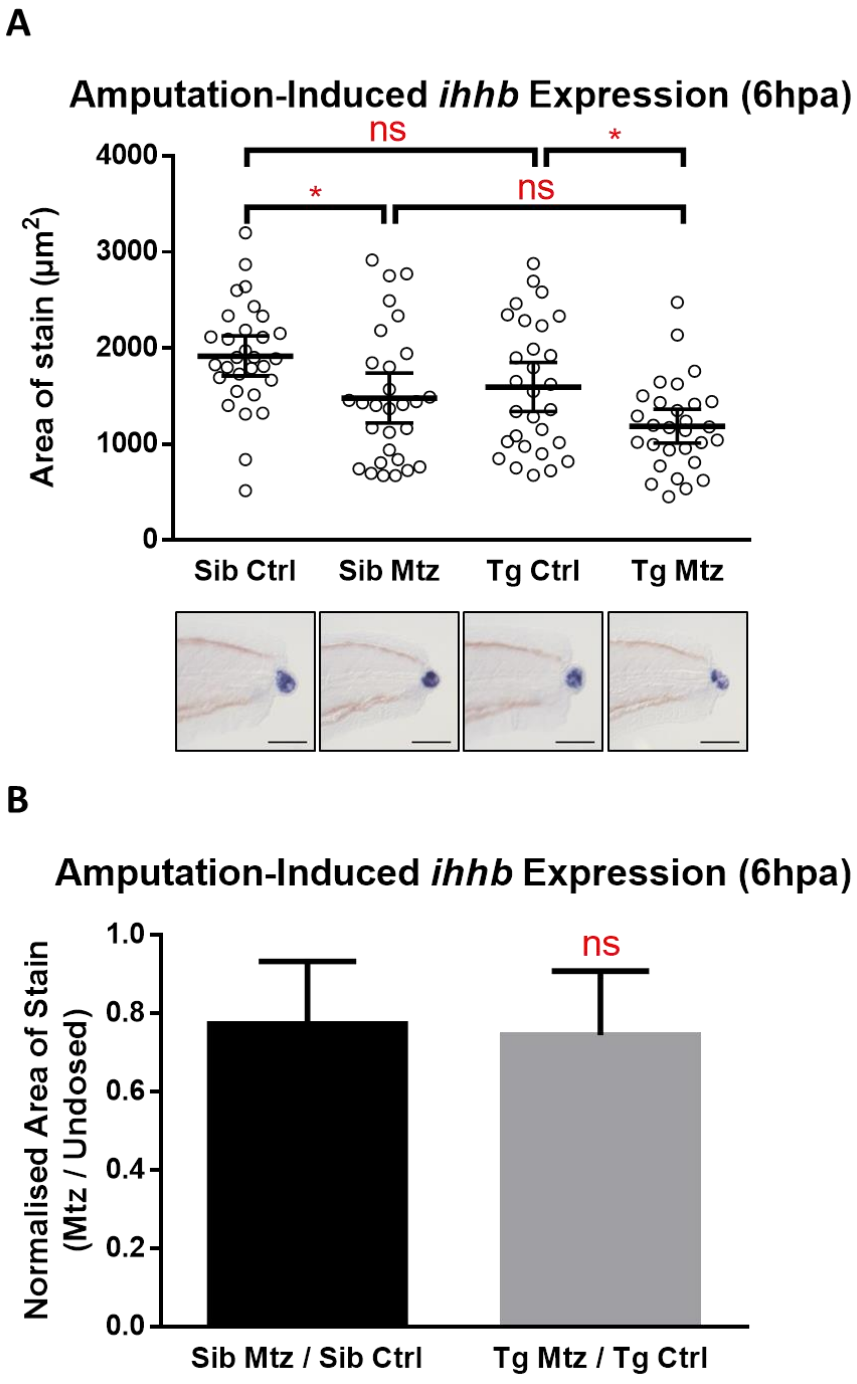

Figure 4.15 – Quantification of *ihhb* expression following *UNM*-mediated macrophage ablation. Tail amputations were performed at 3dpf in *mpeg1:GAL4/UNM* transgenic larvae (Tg) and their siblings (Sib) and the amputation-induced *ihhb* expression was quantified at 6hpa. **A)** Quantification of *ihhb* expression following amputation with inset representative images. Scale bars: 200μm. **B)** Quantification of *ihhb* expression comparing Mtz-treated sibling and transgenic groups after normalisation to their respective untreated control group.

Estimations of ablation efficiency by both transgene expression area and Lcp1 expression volume produced very similar estimates, bolstering the confidence in the accuracy of the quantifications. Transgenic larvae treated with Mtz recruited 6% of the area that vehicle-treated transgenics did (Figure 4.16A) and 7% of the volume (Figure 4.16B; Tg Ctrl vs Tg Mtz). One surprising result was seen when comparing the Mtz-treated siblings to the vehicle-treated sibling controls, the total volume of the Lcp1 expressing cells reduced to 19% of control levels (Figure 4.16B; Sib Ctrl vs Sib Mtz). Given this apparent effect of Mtz alone to downregulate Lcp1 expression, in order to determine if Ntr-driven ablation had an additive effect and decreased Lcp1 expression further, Mtz-treated larvae were normalised to their respective vehicle-dosed controls and compared again. This comparison of normalised leukocyte cell volume showed a significant reduction to 36% of sibling levels in transgenic larvae (Figure 4.16C), showing that although Mtz may directly decrease total leukocyte cell volume itself, that leukocyte ablation exacerbates this reduction even further.

Similar results were obtained when estimating ablation using cell counts. Mtz treatment reduced the number of cells recruited to 16% of vehicle treatment in transgenic larvae (Figure 4.16D; Tg Ctrl vs Tg Mtz). A more modest reduction of 43% was also seen in Mtz treated siblings compared to untreated controls (Figure 4.16D; Sib Ctrl vs Sib Mtz). As with cell volume, Mtz-treated transgenic and sibling cell counts were normalised to their respective untreated controls to examine the additive effect of Ntr-driven ablation. Transgenic larvae showed a reduction to 38% of sibling levels further supporting that leukocyte ablation is more severe in the transgenic larvae than their siblings (Figure 4.16).

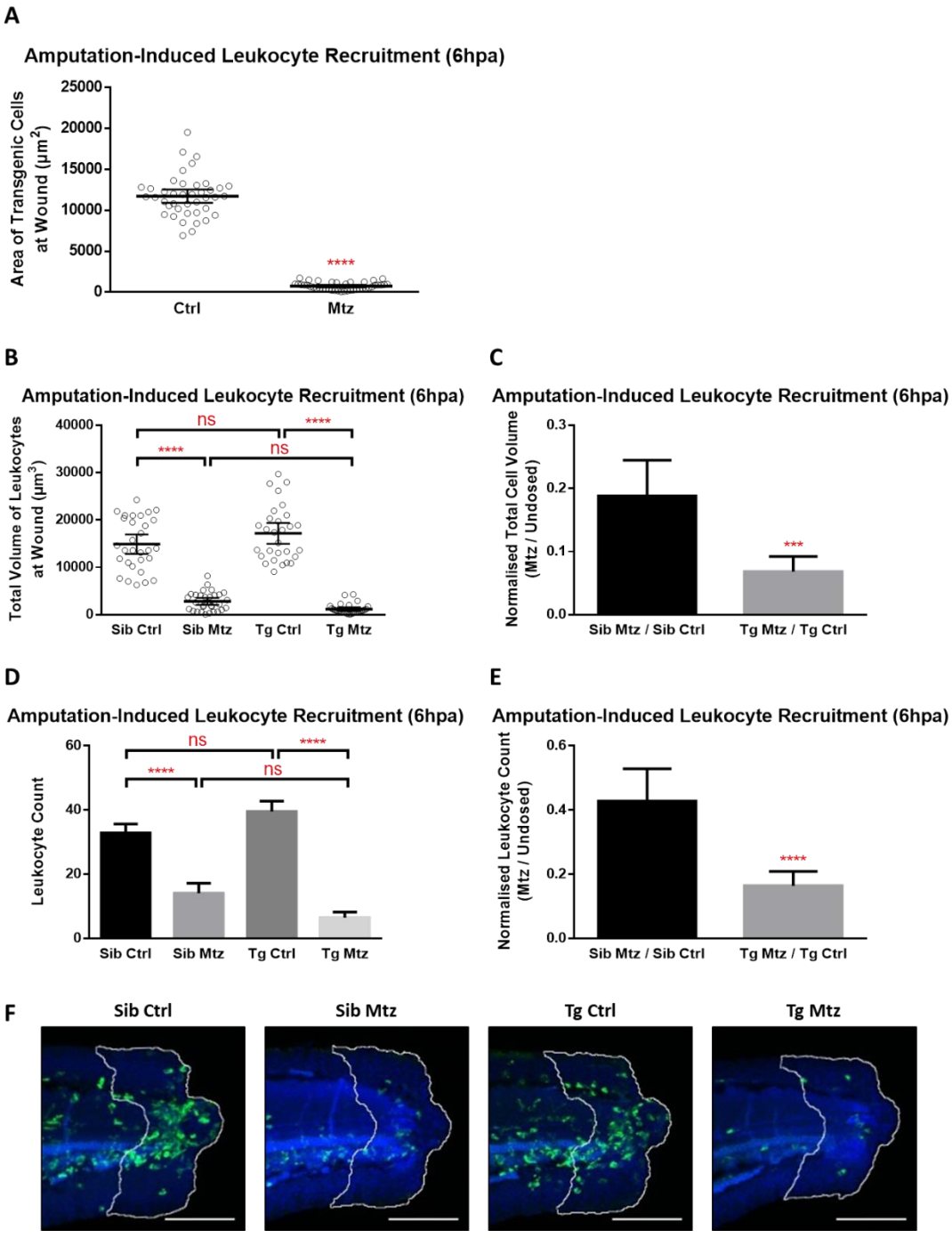

Figure 4.16 – Quantification of leukocyte knockdown in *mpeg1:GAL4/mpx:GAL4/UNM* transgenic larvae using the *UNM* genetic ablation system.
Pigment-gap level tail amputations were performed at 3dpf in *mpeg1:GAL4/mpx:GAL4/UNM* transgenic larvae (Tg) and their siblings (Sib) and the extent of leukocyte recruitment was quantified at 6hpa. Quantification of macrophage & neutrophil knockdown following 18hr Mtz treatment was performed by visualisation of transgenic cells by fluorescence (**A**), by measuring total volume of Lcp1 expression (**B**) or by counting leukocytes (**D**) in confocal z-stacks of the wound area. Quantification of Lcp1 expression and z-stack leukocyte count were further compared between Mtz-treated sibling and transgenic groups after normalisation to their respective untreated control group (**C**, **E**). **F)** Representative images used for quantification – max intensity z-projection of confocal stacks. Blue: DAPI, green: lcp1, white: outline of the wound area. Scale bars: 200µm.

The *ihhb* expression was quantified using a fluorescent WISH protocol to allow simultaneous imaging of Lcp1 and *ihhb* in the larvae. The expression patterns observed following leukocyte ablation match the relationship observed following macrophage ablation alone (Figure 4.15 vs Figure 4.17). Mtz treatment causes a significant decrease in *ihhb* expression in both sibling (Figure 4.17A; Sib Ctrl vs Sib Mtz) and transgenic larvae (Figure 4.17A; Tg Ctrl vs Tg Mtz), but not between Mtz-treated sibling and transgenic larvae (Figure 4.17A; Sib Mtz vs Tg Mtz). This suggests, as for macrophage depletion, that Mtz has a direct inhibitory effect on *ihhb* expression that is not mediated by Ntr-mediated cell ablation. This conclusion is reinforced when analysing normalised *ihhb* expression in the transgenic and sibling groups in order to detect any additive effects of leukocyte depletion compared to the off-target Mtz-effects; by normalising the *ihhb* expression of Mtz-treated transgenic & sibling groups to their respective vehicle-treated controls as before (Sib Mtz/Sib Ctrl & Tg Mtz/Tg Ctrl), no significant difference was detected between *ihhb* expression levels of sibling and transgenic groups (Figure 4.17B). This therefore demonstrates that despite the significant additional decrease in recruited leukocytes to the wound (Figure 4.16C), there is no additional decrease in *ihhb* expression (Figure 4.17B).

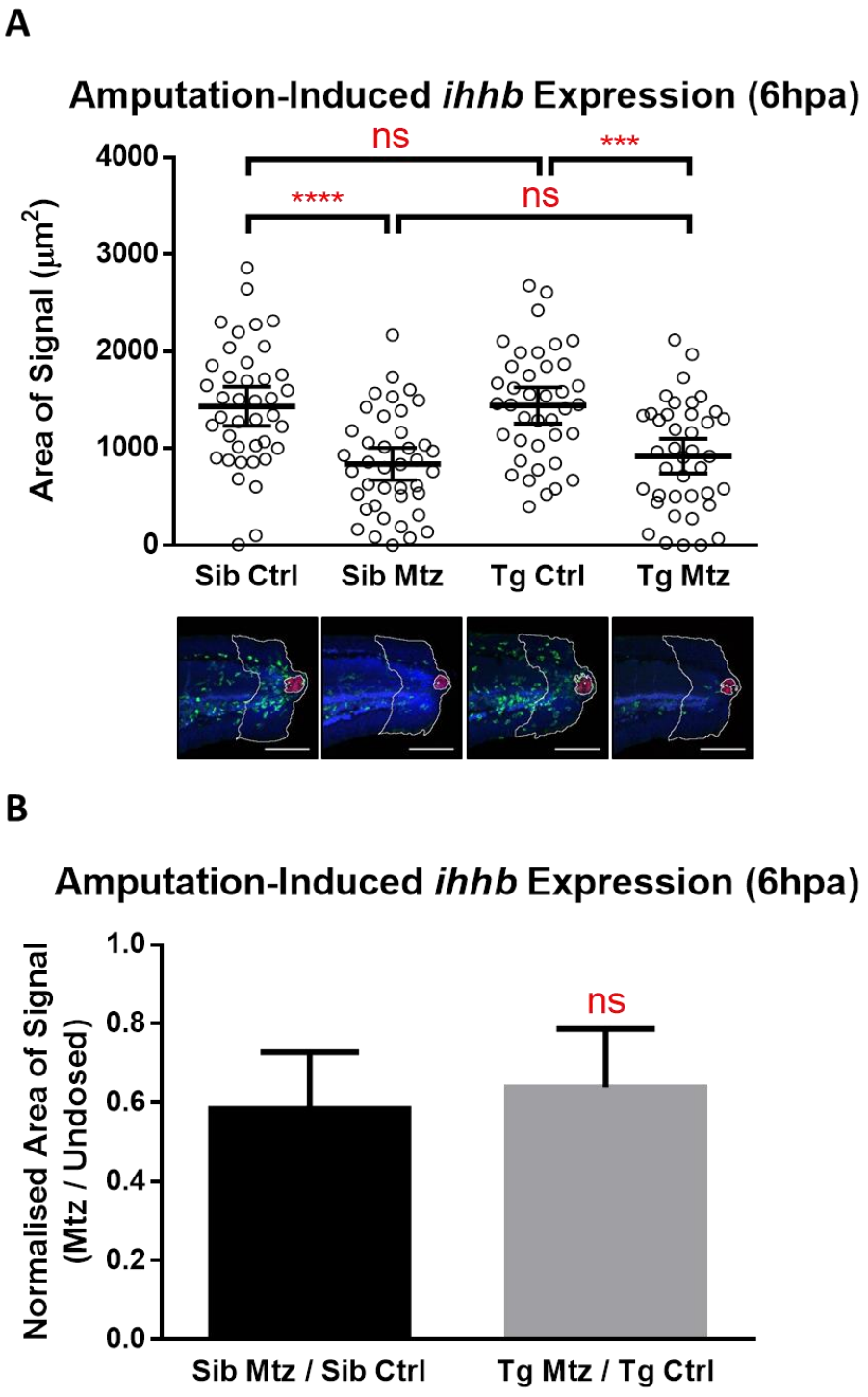

Figure 4.17 – Quantification of *ihhb* expression following *UNM*-mediated macrophage ablation.
Tail amputations were performed at 3dpf in *mpeg1:GAL4/UNM* transgenic larvae (Tg) and their siblings (Sib) and the amputation-induced *ihhb* expression was quantified at 6hpa. **A)** Quantification of *ihhb* expression following amputation with inset representative images (max intensity z-projection of confocal stack). Blue: DAPI, green: Lcp1, red: *ihhb*, white: outline of the whole wound area and the limit of the detected *ihhb* staining within that area. Scale bars: 100µm. **B)** Quantification of *ihhb* expression comparing Mtz-treated sibling and transgenic groups after normalisation to their respective untreated control group.

4.3 Discussion

4.3.1 Conclusions from my data

4.3.1.1 Leukocyte ablation does not affect regenerative outgrowth

Cell depletion was validated by fluorescent detection of Ntr.mCherry in transgenic cells, by *mpx* WISH and immunohistochemistry for L-plastin expression and regenerative outgrowth was compared to leukocyte-replete controls. In multiple experiments, ablation of macrophages, neutrophils or the simultaneous ablation of both, failed to significantly alter the observed regenerative response. In addition to the regenerate outgrowth, tissue morphology appeared unaffected.

Although no significant ablation-induced effects could be identified, even after assessing regeneration at different timepoints or in response to different severity of wounds, some raw data appeared to show significant effects of cell ablations. On closer inspection of the controls it is unlikely that these are cell-depletion specific effects: 1) Neutrophil-depletion by Mtz-treatment of transgenic larvae showed a significant increase in regenerate length (Figure 4.8A; Tg Mtz), but the Mtz-treated sibling controls showed an almost identical increase in regrowth (Figure 4.8A; Sib Mtz) and normalising Mtz-treated larvae to their vehicle-treated controls showed an almost identical upregulation in both groups (Figure 4.8B). This suggests that Mtz itself may be conveying a small pro-regenerative effect, a trend that is mirrored, but does not reach significance, in many of the other experiments (Figure 4.6A, Figure 4.12A, B, D). 2) Additionally, after simultaneous macrophage and neutrophil ablation, when quantified by both length and area, the regenerate appeared significantly smaller in the depleted group than the Mtz-treated sibling control group (Figure 4.12B, D; Tg Mtz vs Sib Mtz). This was not considered a true effect of the cell ablation due to the fact that this difference was not detectable after normalising regenerate to the appropriate vehicle treated control groups (Figure 4.12C, E) and that there was no significant difference seen between the vehicle-treated transgenic controls (Figure 4.12B, D; Tg Mtz vs Tg Ctrl).

4.3.1.2 Leukocyte ablation does not affect regenerative signalling

When assessing if leukocytes can regulate regenerative signalling it is difficult to draw any conclusions from simply assessing the timings of neutrophil recruitment and *ihhb* expression as both processes occur over very similar time-frames (Figure 4.13A, B). Examining the range of

neutrophil recruitment and *ihhb* expression within single timepoints gave clearer insights. Once *ihhb* expression was detectable at 2hpa and 3hpa, there was no significant correlation, nor linear relationship between the number of recruited cells and the extent of expression (Figure 4.13C). This, in addition to multiple outliers showing both high *ihhb* expression with low neutrophil counts (and vive-versa) suggests that neutrophils do not regulate *ihhb* expression, and that these processes are occurring independently in similar time-frames.

Perhaps unsurprisingly, results from the ablation experiments regarding regulation of wound-induced *ihhb* expression were broadly similar to those of regenerate outgrowth; despite the high levels of leukocyte ablation, no clear ablation-induced effects on *ihhb* expression were seen. Analysis of the data is, however, complicated by the apparent effect of Mtz dosing alone on *ihhb* expression. Both macrophage ablation and simultaneous macrophage and neutrophil ablation resulted in a reproducible and significant reduction in the area of *ihhb* expression in Mtz-treated transgenic larvae (Figure 4.15A, Figure 4.17A; Tg Ctrl vs Tg Mtz) but also in Mtz-treated sibling controls (Figure 4.15A, Figure 4.17A; Sib Ctrl vs Sib Mtz). This pointed to an effect of Mtz treatment alone, independent of the Ntr-mediated ablation seen in Mtz-treated transgenic larvae. When comparing the Mtz-treated transgenics to Mtz-treated siblings, there is no significant difference between the groups, suggesting that the attenuation of wound-induced *ihhb* is mediated entirely by the Mtz treatment and that there is no additional effect of Ntr-mediated ablation of macrophages or macrophages & neutrophils. This is further supported by a lack of significant difference when comparing the normalised (Mtz-dosed / Vehicle-dosed) *ihhb* expression for transgenics and siblings (Figure 4.15B, Figure 4.17B).

During the analysis of these data, it became clear that Mtz treatment was having considerable off-target effects, even more pronounced than those noted previously. When quantifying cellular recruitment to the wound by L-plastin immunohistochemistry, both the total cell volume and the recruited cell count show a highly significant reduction from Mtz treatment alone in the sibling group (Figure 4.16B, D). This raises a question about the off-target effects of Mtz treatment; does it induce leukocyte ablation itself even in the absence of Ntr? This potential effect of Mtz could not be identified initially as cell knockdown was estimated by comparing the fluorescent intensity of transgenic Ntr.mCherry expressing larvae and therefore Mtz-treated siblings could not be quantified. Estimations of neutrophil number by *mpx* WISH did not identify any reduction in Mtz-treated siblings, but unfortunately, despite attempts, no reproducible *in situ* probe could be identified for macrophages as a check for macrophage number. The *mpx in situ* suggest that either the Mtz effect is specific to macrophages, or that it may downregulate L-plastin expression but without affecting cell numbers. L-plastin may

therefore be an inappropriate marker for quantification of cell recruitment in this system, and alternative leukocyte markers such as *lysC* could be used instead[367]. Indeed, using alternative leukocyte markers in Mtz-treated wild-type larvae could address whether this observed effect of Mtz is simply an L-plastin specific interaction, or does induce leukocyte ablation. Even if Mtz was shown to only affect L-plastin levels within leukocytes and not affect their viability, this would negatively affect leukocyte motility[368] and likely reduce cell recruitment to the wounds. Considering that a reduction in leukocyte wound recruitment was what I was aiming to achieve in the first place with the Ntr/Mtz ablation system, it could be argued that Mtz treatment alone could be used as an equivalent system to study regeneration in a leukocyte deficient environment. If this was the case, then the observed reduction in *ihhb* expression in Mtz-impaired leukocyte recruitment would indicate a direct link between leukocytes and regenerative signalling, however without knowledge of the mechanism of action by which Mtz reduces leukocyte recruitment and what other off-target interactions may be contributing to this phenotype, I cannot draw meaningful conclusions on this hypothesis.

After normalisation to their appropriate vehicle-dosed controls, it is clear that transgenic larvae have an additional decrease in both total leukocyte volume and leukocyte count (Figure 4.16C, E), showing that Ntr-mediated ablation was responsible for a further reduction in recruited cells. Comparing these normalised data simultaneously controls for different baseline regeneration of transgenic vs sibling groups as well as the Mtz-specific effects and allows comparison of the effects of ablation compared to leukocyte-replete siblings. As such, it is the most appropriate comparison to make and this comparison does not detect any additive impact on *ihhb* expression levels (Figure 4.15B, Figure 4.17B) even after the additional reduction in recruited cells from ablation (Figure 4.16C, E). This analysis, along with the uncertain effect of Mtz mean that these data do not support a strong role for leukocytes in the regulation of regenerative signalling, however additional experiments would be required to completely discount this possibility.

4.3.2 Inconsistencies with published data

As discussed in the introduction to this chapter, when I started this project a regulatory link between inflammation and regeneration was becoming clear in multiple regenerating organisms. Studies in mouse, *Xenopus* and axolotl all showed clear pro-regenerative functions of macrophages and severe impairment of regeneration following ablation[71,327,331–333]. Despite

this, evidence for a regulatory link between inflammation and regeneration in zebrafish was more confusing, with some data suggesting that macrophages are required for complete regeneration caudal fin[309], but other studies in leukocyte-deficient fish suggetsing that inflammation is dispensible for regeneration of both nerves and caudal fin[43,113,122].

My results consistently show that neither macrophages nor neutrohils are required to initiate or regulate regeneration, however this conclusion is in contrast to a study performed concurrently to my work. The Moon lab (University of Washington) used the same Ntr/Mtz genetic ablation system to reduce the number of macrophages recruited to the wound and observed impaired caudal fin regeneration in both adult and larval zebrafish[59]. They observed a decrease in the rate of regenerate growth in Mtz-treated transgenic fish and they also noted a large increase in aberrant regenerate morphology suggesting an additional role for macrophages in patterning the outgrowth. The study was carried out in adult fish, but the authors repeated the work in larval fish and saw the same defects, albeit at a more modest level, suggesting at least partially conserved mechanisms in larval and adult regeneration.

The differences in response observed in my work and the Moon study may stem from the fact that they used a transgenic line where Ntr was driven directly from the *mpeg1* promoter instead of indirectly via the *GAL4*/*UAS* system as I did. Given the propensity of *GAL4*/*UAS* transgenics to silencing and variable transgene expression levels, this may result in less penetrant ablation from Mtz treatment. However, my estimations of ablation efficiency (~85% by cell count using L-plastin immunohistochemistry, and ~70% by *mpx* WISH) were generally comparable to those reported by the Moon lab (80-90% by cell count) and therefore this doesn't appear to have had a substantial effect.

It is possible that there is a necessary minimum number of macrophages required that could functionally compensate for those killed by the Mtz treatment, and that the small difference in ablation efficiencies between the two data sets results in them falling either side of this threshold, thus explaining the differing results. Alternatively, larval strain differences or subtle differences in the mechanism of wounding (quantity of tissue loss, plus the serverity of damage caused to the remaining cells e.g. a precise, clean scalpel cut vs. a more blunt, tearing action inflicting sheer forces on the remaining cells) contributed to the differing results.

Finally, it should be noted that neither my work nor the Moon study quantified systemic ablation efficiencies, and reported only counts of macrophages that were recruited to the wound. Any differences in the number of macrophages remaining in systemic circulation could

conceivably affect the regeneration response as non-recruited leukocytes have been shown to be capable of influencing the wound environment. A recent study showed that zebrafish fin-fold regeneration can be influenced by a myeloid-derived secreted factor capable of acting from a distance[328]. Two inflammation-deficient hematopoietic mutants *cloche* and *tal1* both displayed increased apoptosis of regenerating cells followed by a decrease in regenerative proliferation. These defects were rescued by the addition of extract from wild-type embryos (but not mutant embryos) to wounded tails, even after heat-inactivation suggesting that the pro-regenerative effects are mediated by a heat-stable diffusible signalling molecule derived from either macrophages or neutrophils.

Unfortunately, without further experiments it is difficult to pin-point the exact reasons for the differences between our data, and we must question which conclusion is correct. Due to the incomplete ablation of leukocytes neither study can explicitly exclude any role for these cells in the regulation of regeneration, but when data from the wider field is considered we can decide which is more likely to be correct.

Interestingly, the data from the Moon lab may allign with a previously reported pro-regenerative role for macrophages in zebrafish regeneration. The study observed a decrease in regenerate rate as well as large vacuoles present in the regenerating tissue in macrophage depleted larvae[309]. It is not certain, however, if this phenotype was a consequence of a macrophage deficiency *per se*, as macrophage depletion was induced using an *irf8* morpholino, and this technique prevents macrophage development by skewing the differentiation of myeloid progenitors towards neutrophils instead. This means that the regeneration defects seen could be linked with the increase in neutrophil population rather than the reduced macrophage presence and highlights the difficulties in characterising precise roles for such similar and interconnected cell types.

In addition to the Moon lab's work, two more stuides have been published during the writing of my thesis which also support a direct role for macrophages in regeneration in zebrafish. The first used both chemical (clodronate liposomes) and genetic (*mpeg1:Ntr*) strategies to show that macrophage depletion resulted in impaired larval fin-fold regeneration at both early and late timepoints[369]. The authors noted a concomitant decrease in cellular proliferation and JNK activation, and linked this to the presence of classically-activated (M1-like) *tnfa+* macrophages. The regeneration defects of macrophage-deficient larvae were able to be rescued by parabiosis with wild-type larvae in a TNF-dependent manner. The authors posit that M1-like macrophages are critical for blastema formation and cellular proliferation via the secretion of

TNFα and also provided evidence that M2 macrophages can also play a pro-regenerative role, possibly via late-stage ECM remodelling.

The second study relied on clodronate liposomes to ablate macrophages in larval zebrafish and noted an excessive and prolonged inflammatory response which increased apoptosis at the wound and impaired regeneration. The authors specifically noted that wound levels of the pro-inflammatory cytokine IL1β were elevated in *clo* mutants (myeloid deficient), *pu.1* (leukocyte deficient) and *irf8* (macrophage deficient) morphants, but not *csf3r* (neutrophil deficient) morphants. This resulted in poor regeneration which could be rescued by IL1β knockdown with *il1b* morpholinos or by immune supression with dexamethasone. The authors provide evidence that the IL1β signal is produced by the epidermal cells at the wound and is required to stimulate regeneration pathways including FGF and JNK, but that macrophages are essential to quench the IL1β signal in a timely manner and resolve inflammation to allow regeneration to proceed.

Furthermore, data continues to be published in other regeneration models such as the African spiny mouse demonstrating that macrophages are required to initiate and regulate regeneration[164,165]. When taken together, the data suggest that macrophages are indeed more likely to regulate regeneration and that my work simply failed to detect this relationship following Ntr-mediated ablation.

4.3.3 Follow-on work

The effectiveness of the ablation was consistently observed to be ~90% of target cells when measured by area or volume, but more modest reductions were seen when quantified by cell number. Using an *mpx* WISH to estimate neutrophil count, Mtz treatment resulted in ~70% decrease compared to all other controls (Figure 4.7B), and estimates of leukocyte count from z-stacked confocal images of L-plastin staining were ~85% lower than transgenic controls (Figure 4.16). Resilient cells did, however, present abnormal cell morphology with reduced protrusions and a much smaller and more rounded shape (Figure 4.1A & Figure 4.16F), suggesting that they may be in the process of apoptosing and therefore non-functional. Even if they are not yet undergoing apoptosis, the cells are likely to be functionally impaired, especially in phagocytic ability which is dependent on pseudopodia protrusion. Considering these limitations, the area metric was considered more appropriate for estimation of ablation efficiency. Further tests for apoptosis markers (e.g. annexin V, or acridine orange staining)

combined with functional tests of the treated embryos' phagocytic ability or clearance rate of introduced pathogens could more accurately assess the true state of these cells.

Another issue with the system is the observed impact of Mtz on both regeneration and *ihhb* expression. The Ntr/Mtz ablation system was designed to have an improved off-target profile compared to previously used substrates such as CB1954 which was known to be metabolised to a cell-permeable cytotoxic molecule resulting in significant toxicity to neighbouring cells[370]. Mtz was chosen as a new substrate as it does not suffer this issue once metabolised[184]. Unfortunately, Mtz itself appears to impact the larvae even in the absence of Ntr, suggesting that the molecule is interacting with unknown targets. The relatively high concentration (low mM) and prolonged exposure to Mtz may potentiate the physiological effects of low-affinity interactions or allow bioaccumulation, increasing the chances of these off-target effects. Although ablation-specific effects can be determined in spite of this by the normalisation technique employed above, identification of a more inert substrate may aid subsequent studies using this system.

In order to further investigate the relationship between inflammation and regeneration, I would recommend repeating the experiments with a second, independent leukocyte deficient system. As discussed previously, there are a number of different methods available to achieve this, but considering that the Ntr/Mtz ablation system causes highly specific but incomplete ablation, the best complementary technique would be one with the most complete ablation, even at the risk of off-target ablation. As such, I would look to use clodronate liposomes which have been shown to very effectively systemically deplete macrophages[333,339,340]. Whilst normally administered by injection, immersion protocols have been developed that would allow simple administration in zebrafish larvae[371]. Unfortunately, no highly effective inducible ablation systems to target neutrophils have been characterised in zebrafish, therefore individual neutrophil ablation may not be possible. As an alternative, the *runx1* mutant line could be used which lacks the Runx1 transcription factor required for neutrophil development resulting in a strong (although not complete) neutrophil deficiency[372]. Similarly, the *pu.1* mutant line fails to develop the myeloid progenitor for both macrophages and neutrophils[373,374] and therefore could be used to assess regeneration in the absence of both cell types, possibly in combination with *runx1* morpholino to ensure full leukocyte eradication[372]. It would be interesting to see if these additional experiments would detect a regeneration deficiency in our model and if this was linked to the expression of Hh ligands, bringing our data more in line with the field as a whole.

4.3.4 Summary

The data presented here show a reproducible cell ablation system, capable of reducing the extent of macrophage and/or neutrophil wound-recruitment to ~10% of wild-type levels. None of the transgenic lines used resulted in a detectable defect associated with cellular depletion in regenerative outgrowth or signalling. Whilst I hypothesised that leukocytes do not regulate regeneration in my model, the limits of the Ntr/Mtz ablation system mean that I cannot conclude that leukocytes are absolutely dispensable for regeneration for two reasons: 1) The small number of ablation-resilient cells may be able to functionally compensate for the depleted leukocytes, and 2) There may be systemic signalling from leukocytes not recruited to the wound.

In addition, data from multiple independent labs is repeatedly pointing to a strong pro-regenerative role for macrophages in zebrafish and other regenerating model organisms. In light of this accumulating evidence I conclude that inflammation, and specifically macrophages, are important initiators and regulators of regeneration in zebrafish as well as many other regenerating species. The fact that I failed to detect any regeneration defects following leukocyte depletion is not conclusive evidence that no relationship exists and may be indicative of a high degree of functional redundancy within leukocytes and that only a small number of cells are required to maintain their pro-regenerative effects, or that they can effectively signal from large distances[328].

Therefore, although my data does not provide evidence to support my original hypothesis that "Wound-induced H_2O_2 dependent inflammation is required for regeneration to proceed", I have confidence in the evidence of the field as a whole that this is indeed true. No data has been published as of yet which links inflammation to the wound-induced Hh activation I described in Chapter 3, so I hypothesise that H_2O_2 stimulates regeneration by two independent methods: 1) by driving recruitment of the immune cells to the wound[119,173], and 2) by stimulating developmental signalling. I have therefore updated my working hypothesis to: "H_2O_2 stimulates regeneration via the initiation of inflammation, independently of its roles in regulating developmental pathway signalling".

Chapter 5. H_2O_2 activates Hh signalling via SFK activation and notochord extrusion

5.1 Introduction

5.1.1 Aims

The aim of the experiments described in this chapter was to identify the molecular effectors of the pro-regenerative effects of wound-induced H_2O_2. In Chapter 3, I described the process by which wound-induced H_2O_2 initiates regeneration via the upregulation of Hh ligands in the notochord resulting in an activation of the Hh signalling pathway, and subsequently Wnt, FGF and regenerative outgrowth (Figure 3.33). In Chapter 4, I provide evidence that this signalling is not mediated by the H_2O_2 dependent recruitment of immune cells. Here I use chemical inhibitors to identify H_2O_2 dependent intracellular signalling pathways which are required for the upregulation of Hh ligands, thereby providing a molecular link between redox regulation and regeneration signalling.

5.1.2 Background

5.1.2.1 Physiological roles of ROS

Historically, H_2O_2 and other ROS have been considered to have deleterious roles in physiological settings. Oxidative stress was known to be toxic for cells and induce apoptosis or cell death via non-specific and irreversible oxidation of essential cellular components including proteins, lipids and DNA[375], and ROS were most notorious for their role in the inflammatory respiratory burst where they act to disinfect the wound from invading microorganisms[376]. In addition, elevated ROS are known to present in a number of disease states[377]. These observations helped to cement the reputation of ROS as little more than mediators of cell dysfunction and death, but it has become apparent that cellular and molecular responses to ROS depend hugely on their concentration and duration of exposure[375]. At low concentrations, ROS are responsible for multiple regulatory roles in physiological conditions which are essential for the normal functioning of cells[378–381], can stimulate cell growth[382–386] and ROS have now been accepted as essential to maintain health and combat disease[387]. These findings have led to a new characterisation of ROS as essential regulators and the understanding that

maintenance of cellular ROS levels within physiological limits is what is necessary to avoid damaging effects.

5.1.2.1.1 Sources of ROS

The two main sources of ROS production within the cell are the Nox family enzymes and mitochondria. The Nox family of enzymes consist of the classical Nox enzymes as well as the related Duox enzymes, and contain multiple members that are reasonably well conserved between eukaryotic species as divergent as algae, worms, flies, fish and humans[237,388,389]. In zebrafish the Nox family comprises Nox1, Nox2, Nox4, Nox5 and Duox[237] which appear to have similar distribution of cellular expression patterns during development, although differ in their expression levels and are therefore likely to be subject to divergent regulatory controls[390]. The Nox family enzymes have specifically evolved to produce ROS when required and have therefore been thought to be the main regulator of cellular redox balance as other contributors appeared to produce ROS in a passive fashion as a by-product of their normal metabolism; for example, the primary source of ROS production from mitochondria is superoxide formed by electron leaked to oxygen from complex I and complex III in the electron transport chain[199]. Recently though, new evidence has emerged suggesting that this process can in fact be regulated and therefore mitochondria should also be considered capable of actively influencing redox signalling in both health and disease [391–393].

The classical Nox enzymes synthesise superoxide from molecular oxygen using NADPH as an electron donor[388]. This superoxide either spontaneously dismutes to H_2O_2, or can be actively converted by superoxide dismutase (SOD) which is present in high concentrations in the mitochondria, the cytoplasm and the extracellular space[394]. This abundance of SOD, combined with its high efficiency, means that the majority of superoxide is almost instantly converted into H_2O_2 and therefore the majority of ROS signalling is mediated by the less reactive H_2O_2 which can diffuse over large distances to function as a signalling molecule *in vivo*[119,173,201]. In contrast to the classical Nox enzymes, the Duox enzymes contain an extra peroxidase-like domain, as well as Ca^{2+} binding EF-hand domains (which are also present on Nox5), and can be modulated by the binding of maturation factors, suggesting that they are subject to more complex regulatory controls. These maturation factors are important for proper sub-cellular localisation and catalytic activity[395], but also appear to convey an extra intramolecular dismutation activity, resulting in the spontaneous conversion of superoxide into H_2O_2 before release[396]. Although there are many more enzymes which produce ROS (including xanthine

oxidase, lipoxygenases, cyclooxygenases and cytochrome p450 enzymes), this is normally as a by-product of their normal catalytic activity, rather than their specific function and their contribution to the whole-cell redox state is poorly characterised[198,381].

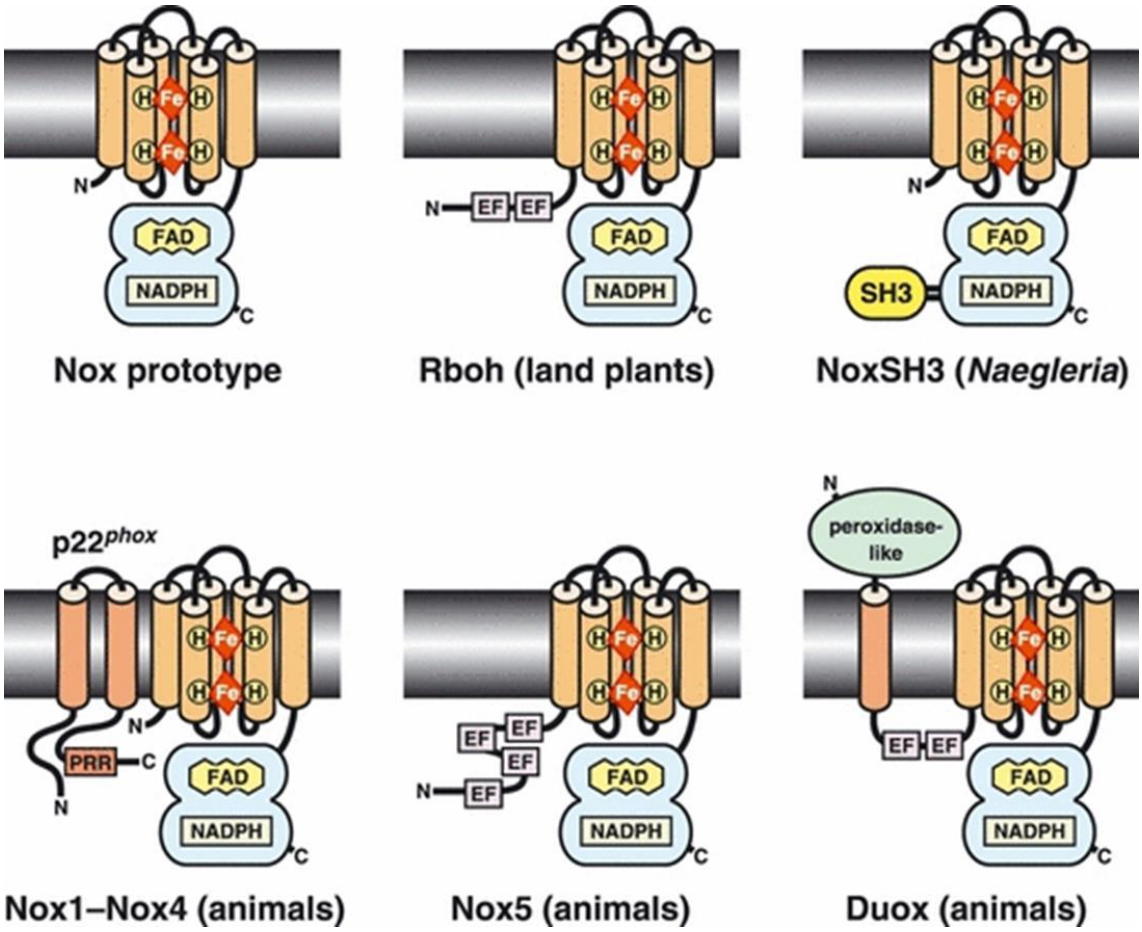

Figure 5.1 – NADPH oxidase family enzymes (reproduced from Sumimoto, 2008[388]).
Scematic structures of the main sub-types of Nox-family enzymes. Cylinders represent six transmembrane α-helices, EF denotes Ca^{2+} binding EF-hand domains.

5.1.2.1.2 ROS sequestration and regulation

The redox balance within cells is controlled via the regulation of ROS production from the above sources but also by ROS removal by antioxidant systems. By the coordinated regulation of both ROS synthesis and conversion, cells can precisely control their redox state and subsequent redox-sensitive signalling pathways whilst preventing ROS levels ever reaching cytotoxic concentrations. The main cellular antioxidant systems are the glutathione peroxidase and peroxiredoxin enzyme families which use the small thiol-containing biomolecules

glutathione and thioredoxin as oxidant acceptors. This process requires cofactors capable of donating electrons, often NADPH or FADH, and therefore cellular availability of the reduced forms of both cofactors are also vital for maintaining redox homeostasis. Under physiological conditions about 99% of the total glutathione is in the reduced state, maintaining a considerable buffer for even sudden and dramatic increases in ROS levels to be eliminated without causing irreversible oxidative damage[394].

5.1.2.1.3 Signalling by ROS

The high concentrations of ROS present in cases of oxidative stress prevent the normal biological functioning of molecules within cells, causing cell dysfunction and death. Oxidative stress is deleterious to the viability of the cell due to the widespread non-discriminatory and, most harmfully, irreversible oxidation of molecules, but at lower concentrations of ROS, these oxidative modifications can be limited, localised and reversible lending them to function as regulatory signals via transient post-translational modifications of biomolecules.

Within the cell, sulphur-containing species act as the predominant mediators of redox sensing, often present as thiols due to their strongly reducing chemistry. For protein modifications, the thiol (R-SH) containing amino acids cysteine and methionine are the primary mediators of redox control[397]; whilst it is possible for non-sulphur containing amino acids to be redox-reactive (e.g. histidine, tryptophan and tyrosine), these interactions are much less frequent and less well characterised[398] and therefore in this section I will focus on sulphur-mediated redox control.

At physiological pH, cysteine thiol groups are deprotonated and therefore more nucleophilic and more likely to become oxidised by ROS. Whilst it is becoming apparent that methionine is also an important transducer of redox control of cellular functions[399–401], this reaction is around four-fold slower and therefore is less useful for rapid regulatory control[401]. Oxidation of thiols can result covalent modifications converting it into a number of different groups, some common examples include: sulfenyl (R-SOH), sulfinyl ($R\text{-}SO_2H$) or sulfonyl ($R\text{-}SO_3H$) groups. These modifications render the sulphur atom unavailable for electron donation, thereby potentially impeding catalytic function if the cysteine residue is required for normal enzymatic metabolism. Alternatively, these new groups can impact protein-protein interactions and therefore sub-cellular localisation, have steric effects and modify protein tertiary structure. In addition to the conversion of a thiol group, oxidation can form di-sulphide bonds (R-S-S-R)

either inter- or intra-molecularly and hence alter protein tertiary structure or covalently join two molecules together[397,398].

The biological impact of thiol oxidation can vary from protein to protein and also the type & position of modification caused. Although initially thought to always function as an inactivating reaction, it is now understood that oxidation can alter protein function both positively and negatively. For example many protein phosphatases require a thiol-containing cysteine residue to be catalytically active and modification of this thiol group by oxidation will inactive the enzyme[124,402,403], but direct oxidative activation of some kinases and peptidases have also been reported[173,289,404].

One interesting method of oxidative regulation relies on a more complex relationship between oxidative modifications and enzyme activity has been demonstrated for the Na,K-ATPase[405]. This enzyme has multiple cysteine residues available for oxidation and whilst oxidation of these residues did not have a significant effect on enzyme activity, it did prevent them from reacting with glutathione which was identified as an inhibitor of catalytic function. Therefore, in this instance, oxidation appears to competitively maintain enzyme activity and this highlights the diversity of regulation that is possible from this system. In this way, ROS are capable of significantly affecting the kinome and cellular signalling, and ROS are also known to be able to directly regulate cellular activity on a transcriptional level via redox-sensitive transcription factors[381].

Redox modifications of sulphur-containing species are easily reversible by the antioxidant systems described above, allowing proteins to revert to their reduced conformation and therefore nullifying the redox-mediated activation or inhibition. Thiol modification therefore creates a dynamic equilibrium between the local ROS levels and the activation state of biomolecules and allows rapidly reversible control of multiple cellular components based on the redox environment. What is less well understood is how specificity is imparted on a system which reacts with any available thiol. It is thought that sub-cellular co-localisation of the ROS sources and targets allows some rudimentary control over specificity, with evidence showing that lipid rafts form clusters of proteins including Nox family enzymes[406–408], within the cellular membrane and that these lipid rafts are required for the transduction of Duox-dependent H_2O_2 signalling[409]. This could aid in the specificity of redox interactions by co-localising ROS sources and targets, but this would not explain how specificity is achieved in cases such as wounding where the H_2O_2 signal floods the local supracellular environment or how it can diffuse across distances of up to 200µm to act as a long-range chemoattractant[119,173,201]. Identifying

mechanisms conferring specificity onto the redox control system will be essential in fully understanding the impact of redox manipulation and is an ongoing investigation in the field. Taken together, these studies demonstrate how ROS levels can be used as a nuanced post-translational regulatory mechanism with varied and potent effects on cellular responses.

5.1.2.2 Hh pathway in regeneration

The Hh pathway is an essential developmental pathway, highly evolutionary conserved between even divergent metazoa[410]. It plays central roles in stimulating cell growth as well as patterning in embryonic development and aberrant pathway regulation has been linked to multiple cancers, highlighting its powerful mitogenic properties[411,412]. The Hh pathway is one of the many developmental pathways which are reactivated during regeneration and whose inhibition results in severe regeneration defects[77,115,209,283,413–415], therefore it is central to our understanding of regenerative outgrowth. In our larval zebrafish regeneration model, Hh has been identified as an important effector of the wound-induced H_2O_2 signal, so below I will give a brief outline of the signalling pathway and suggest mechanisms by which it may be regulated by redox signalling.

5.1.2.2.1 Hh pathway overview

A general schematic of the Hh pathway is presented in Figure 5.2 below. In its simplest form, the pathway is as follows: in the absence of Hh ligand, the cell-surface receptor Patched (Ptch) inhibits the activity of Smoothened (Smo), which results in the proteolytic cleavage of the full-length Gli transcriptional activator (GliFL) to form the a transcriptional repressor (GliR) which lacks the C-terminal transactivating domains of GliFL and therefore represses the expression of Hh target genes. In the presence of Hh ligand, it binds to Ptch and alleviates the inhibition on Smo, allowing GliFL to enter the nucleus without being truncated and bind to, and activate the expression of, Hh target genes.

The details of many of these interactions are still unknown, or incompletely understood as they are complex and multifactorial but this is thought be how Hh is able to trigger a variety of context-dependent cellular responses and function simultaneously as a morphogen, mitogen and stem cell maintenance signal. The pathway does not appear to function as a simple on/off switch for Hh target genes and the effects of exposing cells to Hh ligand depend greatly on

both the concentration and duration of exposure[416,417]. This is thought to be transduced to an appropriate genetic response via the relative ratio of GliFL/GliR and therefore cells can respond dynamically to the graded expression of a single transcription factor as seen in the developing neural tube where a gradient of Shh precisely specifies multiple different neuronal sub-types[416].

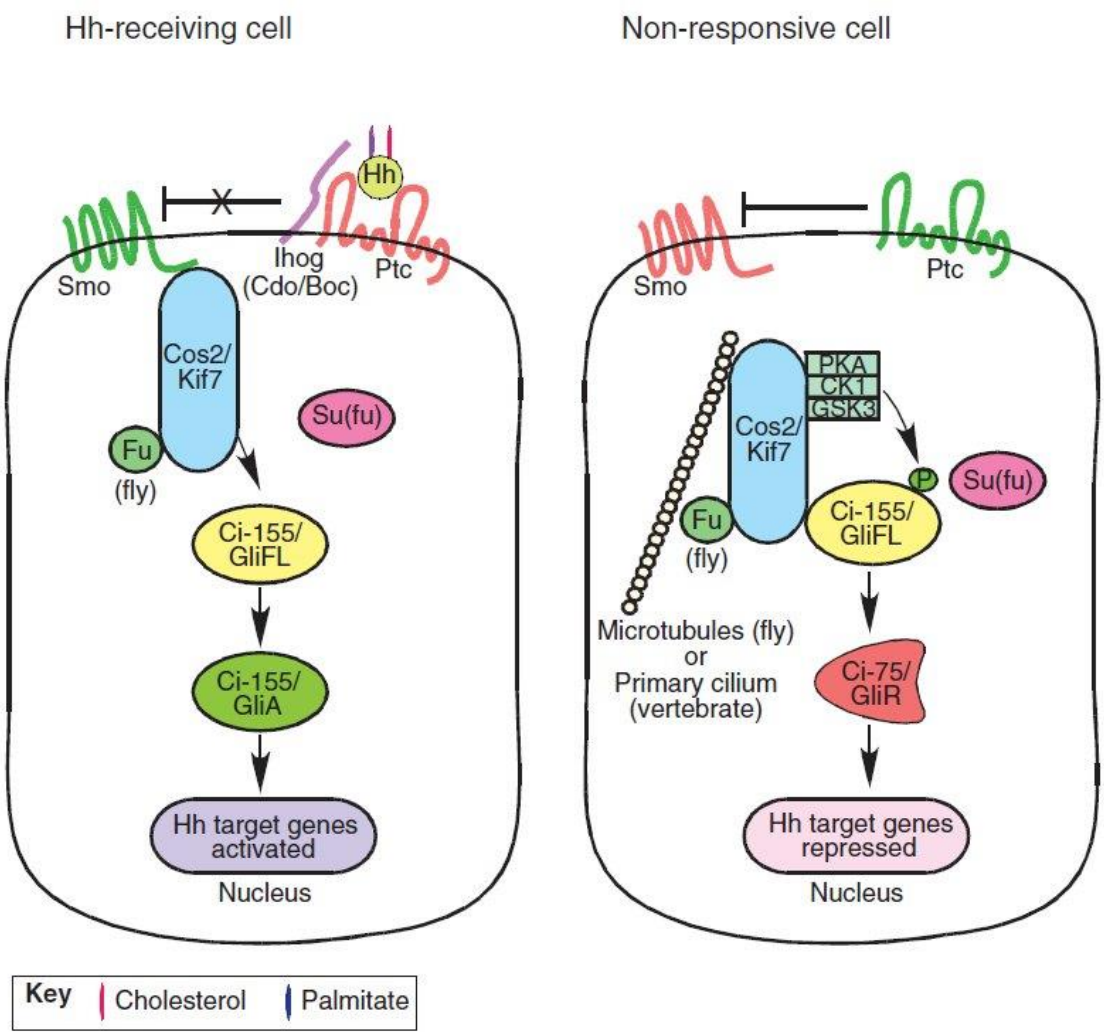

Figure 5.2 – The Hh pathway (reproduced from Wilson & Chuang, 2010[418]).
Simplified schematic of the cellular transduction of the Hh pathway. In the non-responsive cell on the right, Ptc (Ptch) inhibits Smo to release the components of the cytoplasmic Hh components, allowing phosphorylation and subsequent proteasomal cleavage of Gli to the GliR transcriptional repressor which downregulates Hh target genes. In the Hh-receiving cell on the left, Hh ligand binds Ptc lifting its inhibition of Smo. Smo therefore binds components of the cytoplasmic Hh cascade, preventing them from forming a complex with Gli. This prevents its phosphorylation and cleavage and the full-length Gli (GliFL/GliA) transcriptionally activates Hh target genes.

5.1.2.2.2 Potential for redox regulation

Owing to the relative complexity of the Hh pathway, there are a number of molecules within the activation cascade which could be targeted by redox signalling, although to date there has been no evidence that any of these are directly regulated by ROS. The Hh pathway is, however, regulated by cross-talk from a myriad of other intracellular signalling pathways, many of which are known to be redox-sensitive, and therefore I hypothesised that H_2O_2 regulated Hh activation indirectly via one or more of these pathways. For example, there is evidence that glucocorticoid, SFK, JAK, p38 MAP Kinase and MAP2K signalling can all impair regeneration[113,122,419–422], and these pathways have been separately shown to be redox-sensitive[122,173,423–427]. Whether these pathways regulated Hh signalling or are regulated by H_2O_2 in a regenerative context is unknown, but they offer potential control mechanisms and therefore they were targeted in a screen of potential inhibitors of wound-induced *ihhb* upregulation as described below.

5.2 Results

The data presented in this chapter aims to identify the molecular effectors and characterise the process by which wound-induced H_2O_2 leads to the induction of Hh ligands and activation of Hh and subsequent regenerative signalling pathways. This was achieved via pharmacological perturbation of the wound response combined with WISH techniques for gene expression and immunohistochemistry for post-translational protein modifications.

5.2.1 Hh ligands are upregulated as an immediate-early wound response

From the previous experiments using WISH to detect transcription of the Hh ligands *ihhb* and *shha*, I know that they are rapidly upregulated in an H_2O_2 dependent fashion within hours of wounding. Due to the speed of this onset, I thought it likely that this was an immediate-early wound-response, i.e. direct transcriptional regulation that does not require the translation of new proteins to regulate the transcriptional targets. In order to test this hypothesis I used cycloheximide to inhibit protein synthesis[191,428] in the larvae and analysed the response. In order to optimise and validate the dosage of cycloheximide, I used the *hs:dkk1-GFP* transgenic line which expresses GFP-tagged Dkk1 upon heatshock. Dkk1 is a negative regulator of the Wnt pathway, but for the purposes of these experiments, the biological function of Dkk1 was

irrelevant, it was simply picked as a readout for *de novo* protein translation as quantified by GFP fluorescence following heatshock. Whole-body GFP fluorescence was compared between three groups of transgenic larvae: 1) vehicle-treated with heat-shock, 2) cycloheximide-treated with heat-shock, and 3) cycloheximide-treated without heat-shock. Heat-shock significantly increased GFP fluorescence demonstrating successful *de novo* translation of Dkk1-GFP which was inhibited in the presence of cycloheximide (Figure 5.3). Although heat-shock and wounding are two different stressors, the experiments here demonstrate that this cycloheximide treatment is capable of blocking new protein translation, and as such can be expected to block any protein translation following wounding. This cycloheximide treatment was then used to investigate whether protein translation was required for the upregulation of *ihhb* transcripts at the wound. Although the wound morphology appeared more variable, no significant difference in the amount of *ihhb* expression was detected between the cycloheximide-treated and vehicle-treated groups (Figure 5.4), suggesting that this response is not dependent on newly translated proteins and that *ihhb* induction is, indeed, an immediate-early wound response.

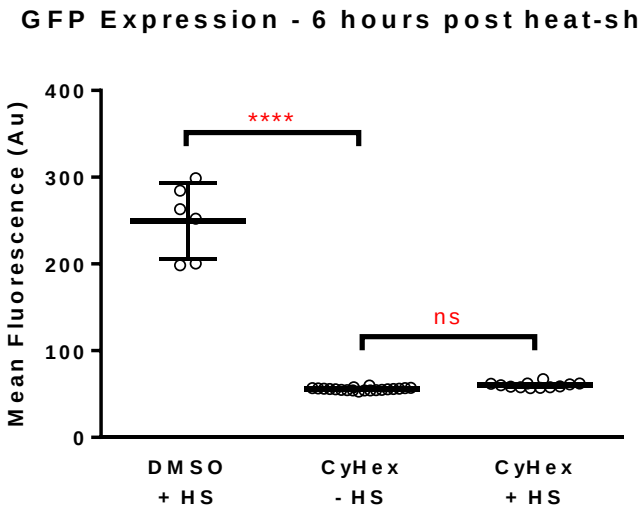

Figure 5.3 – Validation of cycloheximide treatment to prevent *de novo* protein synthesis.
Quantification of heat-shock induced Dkk1-GFP expression in *hs:dkk1-GFP* transgenic larvae. Larvae were treated with vehicle control (DMSO) or cycloheximide (CyHex) from 1hr prior to heat-shock (38.8°C for 2hrs) until being imaged at 6hrs post heat-shock.

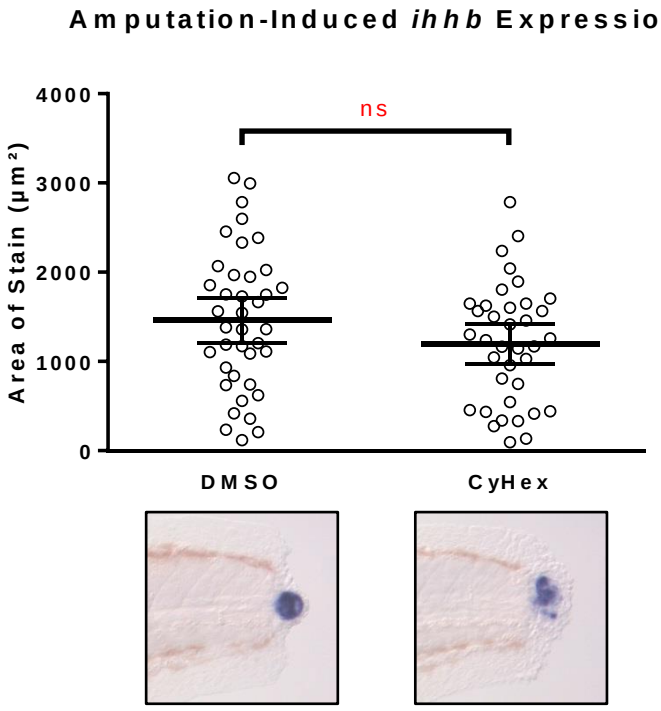

Figure 5.4 – Amputation-induced *ihhb* expression following inhibition of *de novo* protein translation. Quantification of amputation-induced *ihhb* expression as assayed by WISH with inset representative images.

5.2.2 Hh ligands are upregulated by SFK and MAP2K activation

Having seen that Hh is regulated by H_2O_2 in an immediate-early manner, I next sought to identify molecular targets capable of mediating this method of regulation. Candidates needed to be redox sensitive (either directly via oxidative post-translational modification or indirectly through post-translational modification of another redox-sensitive molecule) as well as capable of regulating Hh ligand transcription. A number of candidates were identified from the literature and a screen was carried out using chemical regulators (beclomethasone to stimulate glucocorticoid signalling, PP2 to inhibit SFKs, ruxolitinib to inhibit JAK1/2, SB203580 to inhibit p38 MAP Kinase and U0126 to inhibit MAP2K) with an *ihhb* WISH as the readout. The screen identified two treatments that significantly inhibited *ihhb* expression post-wounding – the SFK inhibitor PP2, and a high concentration (100µM) dose of the MAP2K inhibitor U0126 (Figure 5.5). An additional array of inhibitors (KN-62 to inhibit CaM kinase II, Y-27632 to inhibit ROCK-II, FK506 to inhibit calcineurin, LY294002 to inhibit PI3 Kinase and PD168393 to inhibit EGFR) was also tested by Maria Garcia Romero from our lab but found no significant impact on

ihhb expression (data not shown). These initial results were subsequently validated in follow-up experiments which replicated the findings (Figure 5.6). Inhibition of SFKs with PP2 appeared to have the greatest effect with a near complete inhibition of *ihhb* upregulation and the SFK Fynb had been previously implicated as redox-sensitive and essential for zebrafish larval fin regeneration making it the likely effector[122]. Given the more potent effect and the regeneration link, we focused on SFKs rather than MAP2K signalling in subsequent work, although this should be followed-up as it may act as an important co-regulator of initiation of regenerative signalling. In addition to this inhibition of *ihhb* upregulation, PP2 treatments precluded wound-induced Hh pathway activation as assayed by *ptch1* expression (Figure 5.7). These data further supports the conclusion that SFK activation is required to induce regenerative Hh signalling post-wounding.

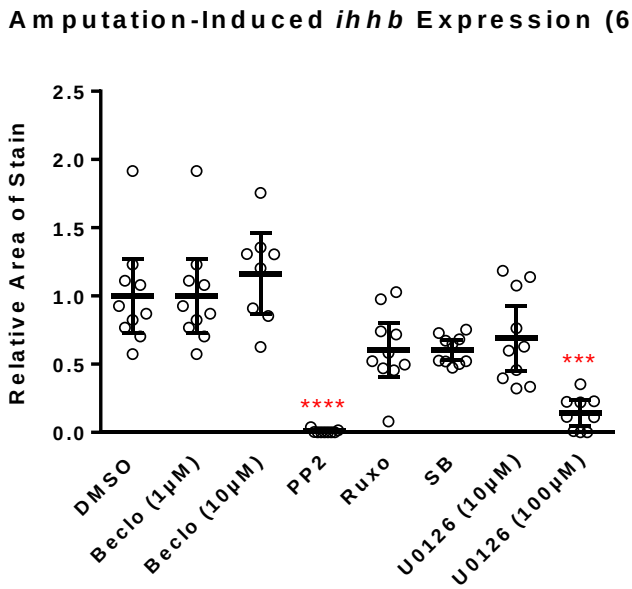

Figure 5.5 – Screening of inhibitor panel for regulators of amputation-induced *ihhb* expression.
A small panel of inhibitors for pre-selected cellular targets were tested for their ability to regulate amputation-induced *ihhb* expression. Relative *ihhb* expression is plotted as assayed by WISH.

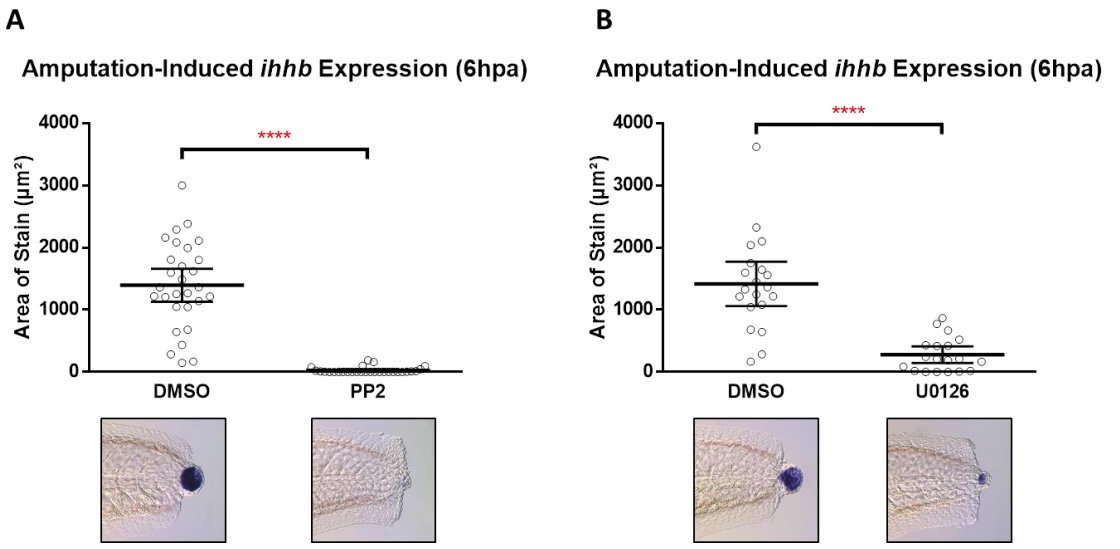

Figure 5.6 – Repeated screening of inhibitor panel hits for regulators of amputation-induced *ihhb* expression.
The two most effective compounds identified from the previous screen were repeated to confirm their inhibition of amputation-induced *ihhb*. Relative *ihhb* expression is plotted as assayed by WISH with inset representative images.

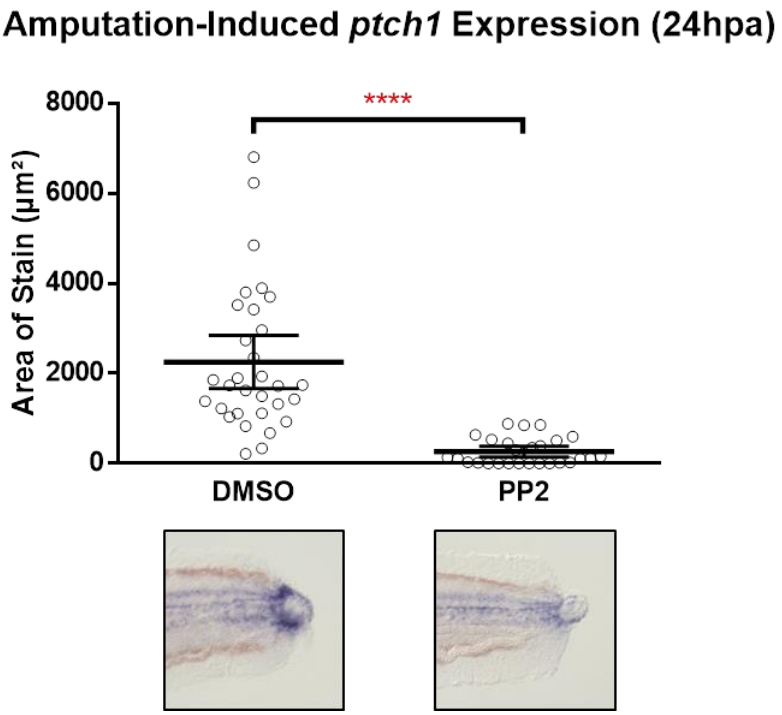

Figure 5.7 – PP2 inhibits the amputation-induced activation of the Hh signalling pathway.
Quantification of the amputation-induced expression of *ptch1*, a marker of Hh pathway activation, with inset representative images.

5.2.3 SFK activation is H_2O_2 dependent and acts in a cell non-autonomous manner

Having observed that inhibition of SFKs can attenuate the wound-induced upregulation of Hh ligands and Hh pathway activation, I next aimed to show that SFKs were also redox-sensitive and therefore capable of mediating the H_2O_2 dependent regulation of Hh ligands. Previous work from the Huttenlocher lab had shown that SFKs are activated at the wound in a H_2O_2 dependent manner rapidly after wounding and SFK activation is required for regeneration in zebrafish larval tails[122]. This supported my hypothesis that SFKs could be responsible for transducing the H_2O_2 signal, but I wanted to corroborate this in our own model. Firstly, I examined SFK activation following wounding using an anti-phospho-Src antibody which binds specifically to phosphorylated, activated, SFKs. Larvae were imaged either in the presence of vehicle control (DMSO) or DPI to inhibit H_2O_2 production. In the vehicle-treated group, a rapid and transient activation can be seen, peaking at around 45mpa, before falling back to basal levels within 3hrs (Figure 5.8, DMSO). Treatment with DPI severely attenuated this activation, with the peak remaining less intense and basal levels of activation returning in just over an hour (Figure 5.8, DPI). These data support the hypothesis that SFKs are activated at the wound in a H_2O_2 dependent manner, and therefore this combined with the ability to regulate *ihhb* levels demonstrated above position SFKs as a direct effector of the H_2O_2 regulation of Hh ligands.

It was interesting to note that although I observed a link between H_2O_2 and *ihhb* transcription via SFKs, SFK activation and *ihhb* upregulation appear to be induced in separate cell populations. One would expect such a spatially-restricted (Figure 3.10), rapid and transcriptionally independent (Figure 5.4) control of transcription to act cell-autonomously, i.e. *ihhb* upregulation in the notochord cells would be driven by SFK activation within those same cells. I examined if this was the case by using confocal microscopy and immunohistochemistry to more accurately image notochord cells (using an anti-keratan sulphate antibody) and SFK activation following wounding. Wound-induced activation of SFKs appears to be restricted to the epithelial cells along the plane of injury and show no co-localisation with the keratan sulphate staining (Figure 5.9). This suggests that notochord cells themselves do not activate SFKs in response to injury and that the SFK signal must be transduced to the notochord cells to induce *ihhb*.

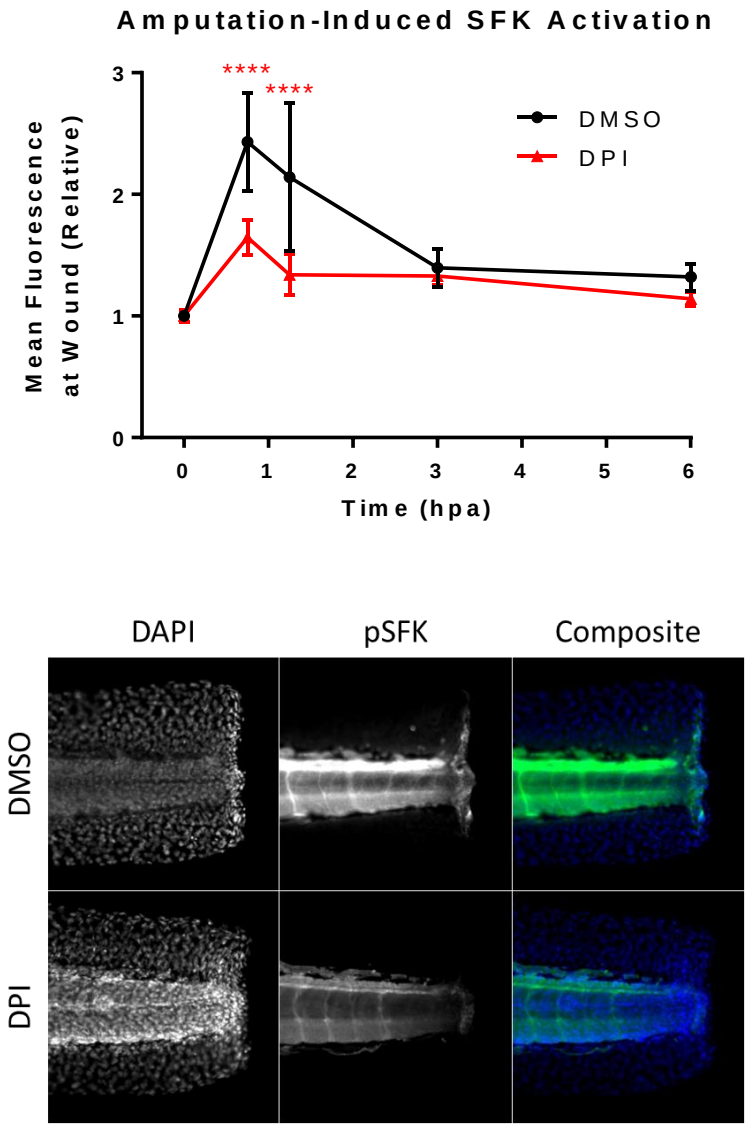

Figure 5.8 – DPI inhibits the amputation-induced activation of SFK at the wound.
Quantification of the amputation-induced activation of SFKs at the wound site over time with inset representative images from 45mpa.

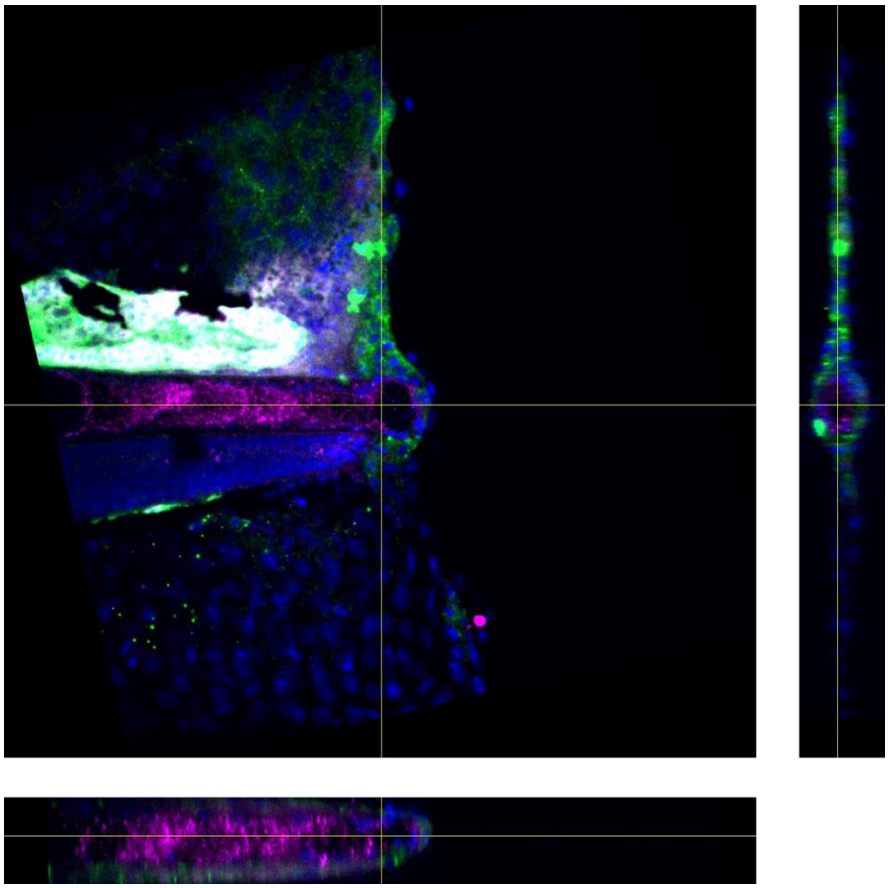

Figure 5.9 – Localisation of SFK activation post-amputation.
Representative image of amputated tail 1hpa. Confocal z-stack was taken to reconstruct the orthogonal view shown. Yellow crosshairs show the positioning of each image within the stacks. Blue: DAPI, green: pSFK, purple: keratan sulphate (notochord marker).

When trying to identify the mechanism by which SFK activation in epithelial cells can almost immediately stimulate *ihhb* upregulation in notochord cells, I re-analysed the previous *ihhb* WISH data for DPI and PP2 treated larvae. Whilst both DPI and PP2 treatment had decreased *ihhb* expression, there were differences in the effect on the wound morphology with each drug. Exposure to DPI did not overtly change the tissue structure at 6hpa and larvae presented a wound with extruded notochord as seen in vehicle-treated larvae (Figure 3.10), exposure to PP2, however, appeared to greatly reduce the volume of cells extruded from the notochord (Figure 5.6A). In addition to this, vehicle-treated larvae show a strong positive correlation between notochord extrusion and *ihhb* upregulation, and treatment with DPI or MCI-186 breaks this correlation. This can be seen by plotting the 95% prediction bands from the control groups, and counting the number of treatment points that fall outside of this range (Figure

5.10). If more than 5% of all values fall outside of this range, then they can reasonably be considered a separate population to the control group. DPI and MCI treated groups diverge from the control group's correlation with 58% and 52% of points, respectively, outside of the 95% prediction bands (Figure 5.10A, B), but PP2 treatment did not diverge significantly from the control group with no points falling outside of the 95% prediction bands (Figure 5.10C). These differences suggest that H_2O_2 and SFKs may regulate *ihhb* in different manners and that there is a more direct relationship between SFK activation, notochord extrusion and *ihhb* upregulation. Interestingly, U0126 appears to act in a similar manner to PP2 rather than DPI or MCI-186 with only 5% of points falling outside the 95% prediction band (Figure 5.10D), suggesting that MAP2K activation stimulates *ihhb* in a mechanism more similar to that of SFKs than H_2O_2. Furthermore, the extent of *ihhb* staining also appeared to be dependent on the length of PP2 treatment (Figure 5.11A, B) and the extent of *ihhb* expression still correlates to the extent of extrusion within these different duration of treatments whether started pre- or post- wounding (Figure 5.11A', B'). Together, this suggests that SFK activation stimulates notochord extrusion in a continual fashion and that *ihhb* upregulation is dependent upon that extrusion.

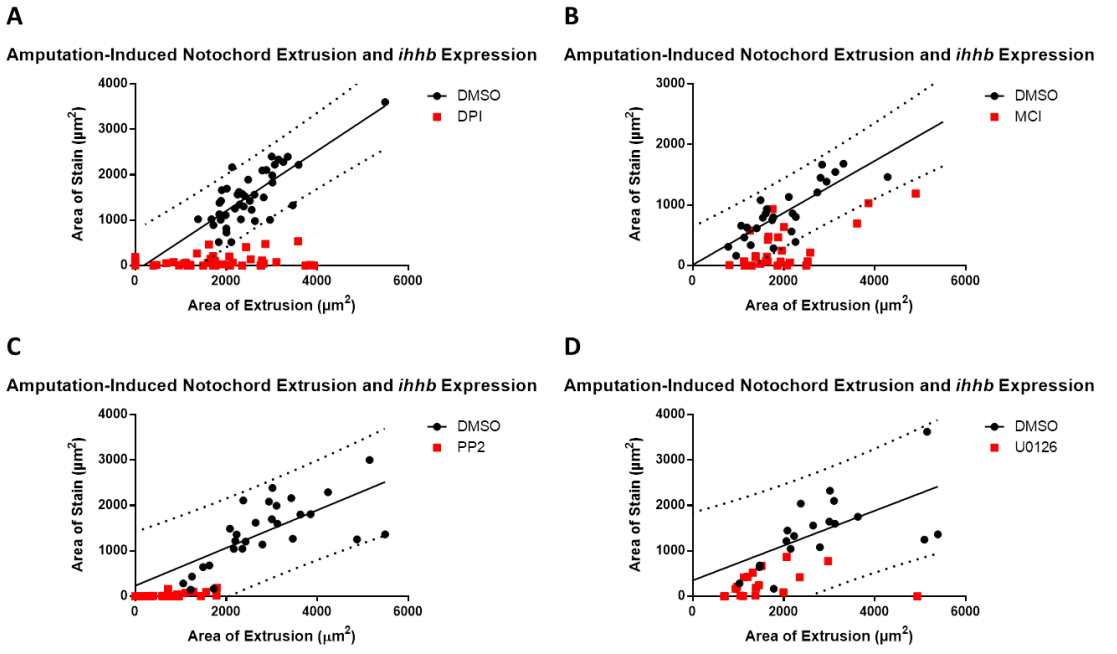

Figure 5.10 – Correlation between amputation-induced notochord extrusion and *ihhb* upregulation.
Scatter-plots showing the relationship between amputation-induced notochord extrusion and *ihhb* upregulation following treatment with DPI (**A**), MCI-186 (**B**), PP2 (**C**) or U0126 (**D**). Solid and dotted lines represent the linear regression line and the 95% prediction band of the DMSO controls for each treatment. If more than 5% of points for any given treatment fall outside the 95% prediction bands of the DMSO controls, they can be considered a separate population.

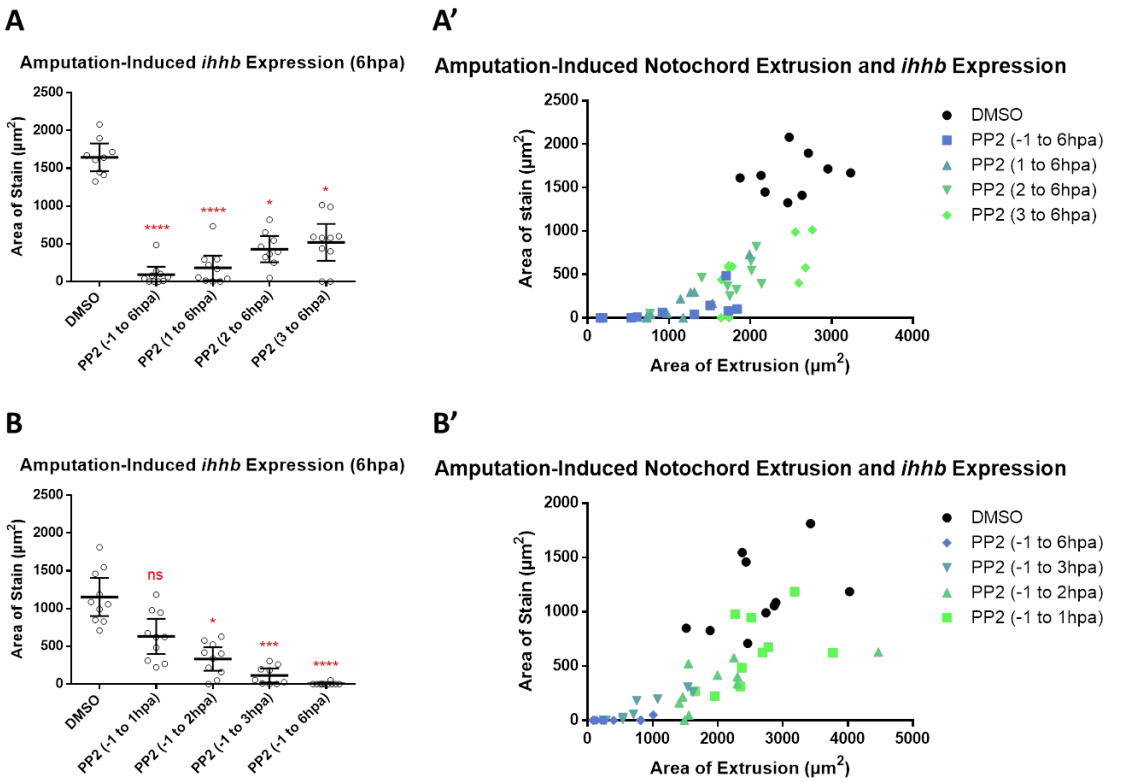

Figure 5.11 – Temporal characteristics of PP2 regulation of amputation-induced notochord extrusion and *ihhb* expression.
A, B) Quantification of amputation induced *ihhb* expression following PP2 treatment at different timepoints and for different durations. **A', B')** Scatter-plots showing the relationship between notochord extrusion and *ihhb* expression in these samples.

5.2.4 Hh ligand upregulation is dependent on notochord extrusion

As explained in Chapter 3, part of the normal wound response is the formation of a contractile acto-myosin cable around open wounds which aids in wound closure. This process is microtubule-dependent and can be disrupted by the microtubule depolymerising agent nocodazole[429]. As such, I aimed to use nocodazole to inhibit wound contraction to see if this alone was capable of inhibiting *ihhb* upregulation even in the presence of normal H_2O_2 and SFK signalling. Treatment with nocodazole significantly impaired notochord extrusion and *ihhb* upregulation at both 3hpa (Figure 5.12A, A', C) and 6hpa (Figure 5.12B, B', C). When extrusion was plotted against *ihhb* expression, a strong positive correlation was observed with only 3% of points falling outside the 95% prediction bands of the control group (Figure 5.12D). This relationship appeared similar to that seen following PP2 and U0126 exposure but was, however, more variable than either treatment and included some larvae where extrusion had

still occurred. To confirm that this attenuation of *ihhb* transcription resulted in a downregulation of Hh signalling, *ptch1* WISH was performed, which corroborated that ligand downregulation also downregulated pathway activation for both doses (Figure 5.13). Together, these data show that simply by preventing notochord extrusion with nocodazole, regenerative signalling can be prevented, suggesting that the H_2O_2 dependent SFK activation could act via exerting physical forces on notochord cells to induce *ihhb* within those cells.

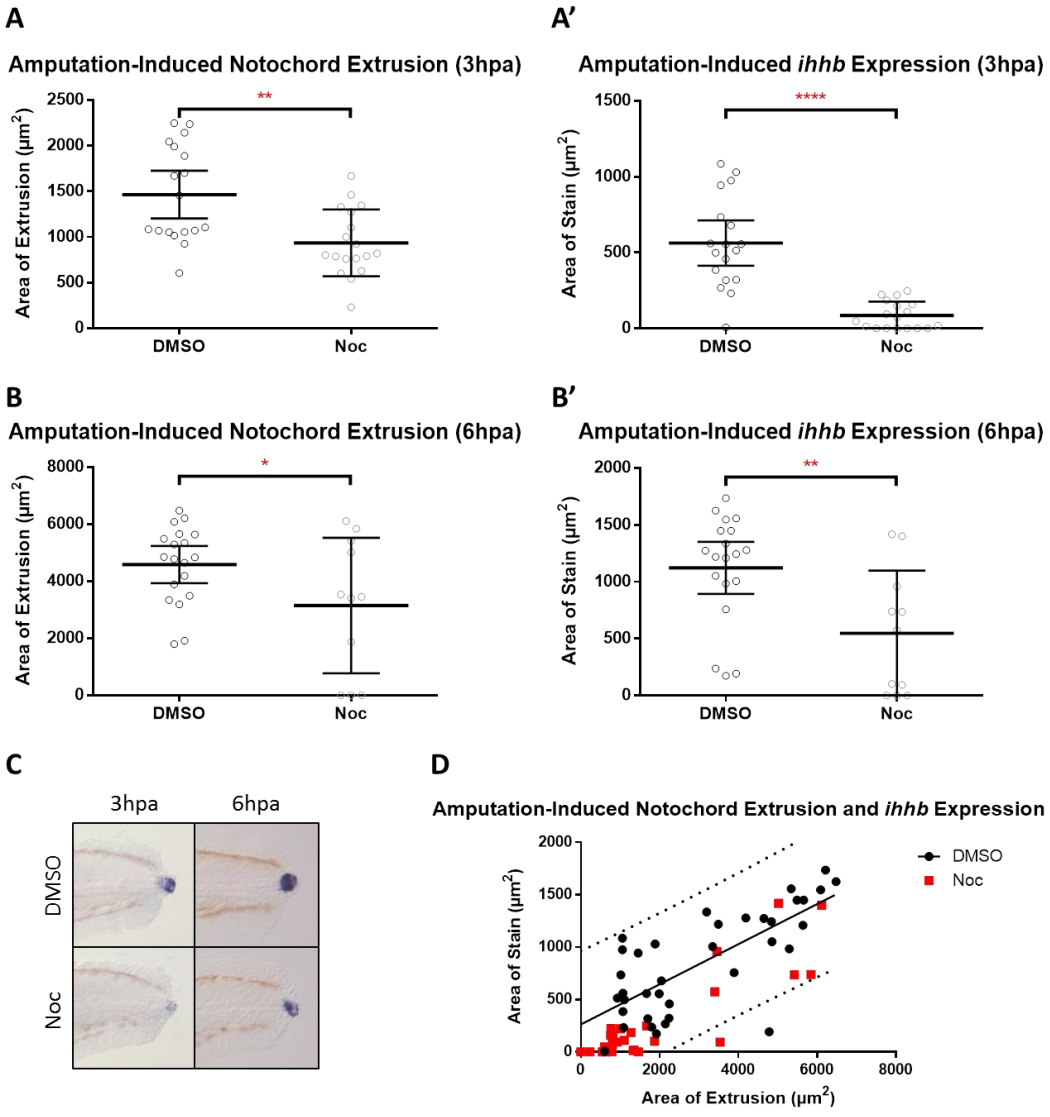

Figure 5.12 – Nocodazole regulation of amputation-induced notochord extrusion and *ihhb* expression. **A, B)** Quantification of amputation induced notochord extrusion (**A**, **B**) and *ihhb* expression (**A'**, **B'**) following 3hr (**A**, **A'**) or 6hr (**B**, **B'**) treatment with nocodazole (Noc). **C)** Representative images of *ihhb* WISH samples quantified in **A** and **B**. **D)** Scatter-plot showing the relationship between amputation-induced notochord extrusion and *ihhb* upregulation of these samples. Solid and dotted lines represent the linear regression line and the 95% prediction band of the DMSO controls for each treatment. If more than 5% of points for any given treatment fall outside the 95% prediction bands of the DMSO controls, they can be considered a separate population.

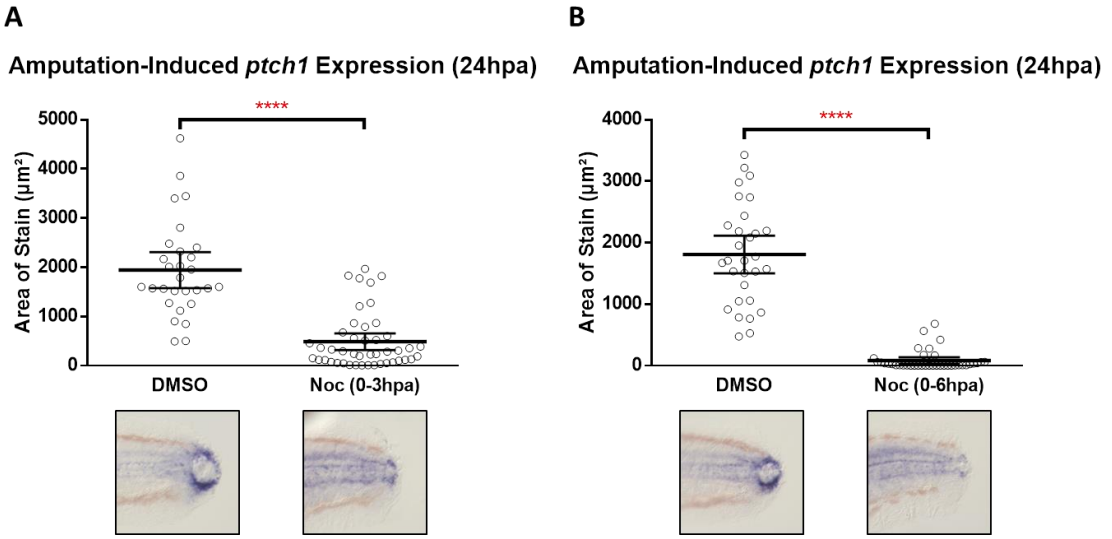

Figure 5.13 – Noc inhibits the amputation-induced activation of the Hh signalling pathway.
Quantification of the amputation-induced expression of *ptch1*, a marker of Hh pathway activation, following either 3hr (**A**) or 6hr (**B**) treatment with Noc with inset representative images.

After discovering a direct correlation between notochord extrusion and *ihhb* expression following PP2 and nocodazole treatments, I wanted to further investigate DPI treatments as these did not appear to show the same relationship. If, as I and others have shown, SFKs are activated by H_2O_2, and this SFK activation induces notochord extrusion, then inhibiting H_2O_2 with DPI should also inhibit notochord extrusion, but this is not observed in my previous experiments. I wanted to test if different DPI doses could impact notochord extrusion in a similar manner, as would be expected if SFKs were the redox-sensitive effector linking H_2O_2 to *ihhb* regulation. Both extended and delayed DPI doses were tested alongside the standard 2hr pulse dose from 1hr prior to wounding till 1hr post amputation. When quantified, the standard pulse DPI treatment did show a small but significant decrease in the notochord extrusion (Figure 5.14A, DPI (-1 to 1hpa) vs DMSO) and this could be increased to a much more severe inhibition by extending the DPI dose (Figure 5.14A, DPI (-1 to 6hpa)). Delaying the dose to between 0 and 2hpa did not make any significant difference in notochord extrusion, but delaying it any later prevented any effect on the wound tissue morphology (Figure 5.14A, DPI (1 to 3hpa) and DPI (2 to 4hpa)). Wound-induced upregulation of *ihhb* was only inhibited by DPI treatments which significantly inhibited notochord extrusion (Figure 5.14B, DPI (-1 to 1hpa), DPI (-1 to 6hpa) and DPI (0 to 2hpa)), but when comparing notochord extrusion verses *ihhb* expression directly, these groups did not show any correlation between extrusion and *ihhb* expression as seen for PP2 and U0126. Taken together, these data suggest that early

production of H_2O_2 is required to promote notochord extrusion, but that H_2O_2 production may be protracted, perhaps only at lower concentrations, and this may continue to regulate notochord extrusion via prolonged SFK activation. It also suggests that H_2O_2 may regulate *ihhb* via additional, SFK-independent, methods, as not all of the variation in *ihhb* expression can be explained by notochord extrusion in DPI-treated samples.

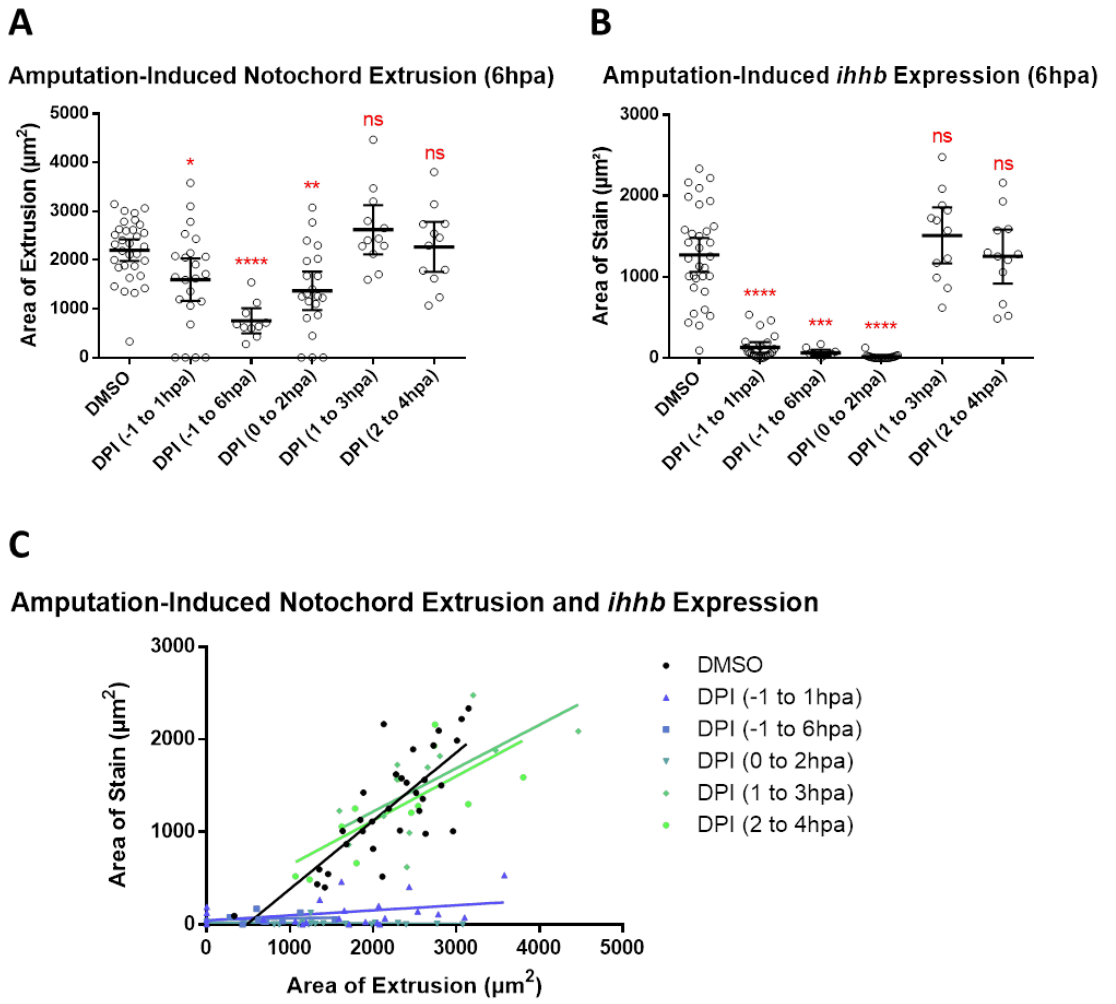

Figure 5.14 – Temporal characteristics of DPI regulation of amputation-induced notochord extrusion and *ihhb* expression.
Quantification of amputation induced notochord extrusion (**A**) and *ihhb* expression (**B**) following DPI treatment at different timepoints. **C)** Scatter-plot showing the relationship between notochord extrusion and *ihhb* expression in these samples.

5.3 Discussion

Data presented in Chapter 3 demonstrates that wound-induced H_2O_2 stimulates regeneration by initiating a regenerative signalling cascade by activating the Hh pathway (and subsequently Wnt and FGF pathways) and data presented in this chapter describes a mechanism by which this wound-induced H_2O_2 achieves the upregulation of Hh ligands.

5.3.1 H_2O_2 mediates upregulation of *ihhb* via SFK dependent notochord extrusion

Firstly, by blocking *de novo* protein translation, I demonstrate that *ihhb* is upregulated as an immediate-early wound response and has no requirements for protein synthesis. This shows that *ihhb* upregulation must be achieved by direct modulation of constituent transcriptional regulators (Figure 5.4). Whilst this seemed likely from the speed at which Hh ligands are upregulated, it helped to narrow the search for redox sensitive transcriptional regulators knowing that the candidates had to be capable of directly stimulating *ihhb* expression with no intermediate transcriptional steps.

Previous studies have identified some molecular effectors of H_2O_2 in regulating regeneration, but, to date, none had linked H_2O_2 to the initiation of regenerative signalling cascade. Redox sensitive SFKs had previously been described by the Huttenlocher lab to be essential for regeneration[122], but that study did not show any link to regenerative signalling. The data presented here supports that work and builds upon it, providing evidence that SFK activation is required to initiate Hh signalling via the upregulation of *ihhb* (Figure 5.6 & Figure 5.7). The unexpected finding that SFKs rapidly induce *ihhb* expression but in a cell non-autonomous fashion (Figure 5.8 & Figure 5.9) combined with the observation that SFK inhibition also inhibits notochord extrusion (Figure 5.6) led us to hypothesise that these processes were linked.

SFKs are promiscuous kinases with multiple targets, and attempting to identify the specific target was not possible in the timeframe, but this may be of interest in the future. If I had had the time to investigate this, I would have proceeded as follows: Firstly, the exact SFK member responsible should be identified by more specific inhibitors, or anti-sense morpholino methods and then these findings should be confirmed with a knockout (or inducible knockout, if the SFK is required in embryonic development) transgenic. ChIP analysis of the *ihhb* regulatory region

could potentially be used to find candidate regulators by comparing those present after wounding in WT controls but missing in the transgenic, then protein-protein interactions between the SFK and candidate transcriptional regulator could be determined by yeast-2-hybrid experiments or coIP, and *in vitro* kinase assays could also show the ability of the SFK to phosphorylate the candidate. Finally, rescue of *ihhb* upregulation in the SFK mutant by directly activating the candidate (either by genetic or pharmacological means) could confirm the *in vivo* link. Once identified, the precise mechanism of activation could be determined for the SFK in question. ROS are generally thought to act via inhibition of phosphatases due to oxidative inactivation of catalytic cysteines[398] therefore SFK activation may be achieved via alleviating the activity of a deactivating phosphatase, but the direct oxidative phosphorylation is also possible[168,289,398,430]. Further *in vitro* kinase assays in the presence or absence of H_2O_2 could be used to show direct redox regulation and if no difference were detected, it would point to an indirect regulatory mechanism, likely requiring a phosphatase.

5.3.2 Upregulation of *ihhb* in the notochord may be mechanosensitive

Although unable to identify the exact SFK responsible for this interaction, we did know that many SFKs are regulators of cytoskeletal rearrangements, important in cell rigidity and motility as well as wound contraction and closure[431,432], therefore I hypothesised that biophysical forces may be a potential method of transducing the SFK signal to the notochord cells. Following tail amputation, contraction at the wound causes tissue shrinkage, however the high-pressure notochord in unable to shrink and is forced out of the end of the wound forming an extruded 'bead'. The wound-induced upregulation of *ihhb* is tightly restricted to these cells and upon re-examining data, there is a strong positive correlation between notochord extrusion and *ihhb* upregulation under control conditions, a correlation which is lost after inhibiting H_2O_2 but not when inhibiting SFKs alone (Figure 5.10A, B vs C). Although extrusion is significantly lower on average, any PP2 treated larvae which still extrude some notochord appear to show weak upregulation of *ihhb*, suggesting that this may be a causal rather than just correlative link. To investigate this, I used the microtubule depolymeriser nocodazole to prevent wound contraction and therefore notochord extrusion (Figure 5.12A). This treatment led to a significant attenuation of wound-induced *ihhb* even in the presence of both H_2O_2 and SFK activation (Figure 5.12B); a finding that supports my hypothesis that notochord extrusion is required for *ihhb* expression. This treatment was also capable of preventing Hh pathway activation (Figure 5.13) but I did not perform experiments to confirm a subsequent defect in

regenerative outcome by either wound epithelium / blastema formation, or regenerative morphology, which I would have liked to have done with more time. Mechanotransduction of *ihh* has been documented in chondrocytes via stretch activated ion channels, but this upregulation occurs over days of consistent mechanical perturbation rather than the mere hours seen here[433,434]. These studies may however inform follow-up studies and stretch activated ion channels should be investigated in the wound response.

One limitation of using nocodazole is that it is very non-specific given the importance of microtubules for many basic cellular processes. Potential targets of the wound contraction mechanism are actin, myosin, microtubules and Rho GTPases, but inhibition of any of these would also have wide-reaching inhibition of other essential cellular functions such as cell migration, intracellular transport & signalling. In an effort to circumvent this limitation, I attempted to rescue PP2 inhibition of *ihhb* by manually extruding the notochord with forceps after wounding but larvae were often damaged by this technique, showing abnormal wound morphology and no sign of *ihhb* upregulation. A second potential method for perturbing the physical forces at the wound may be harnessing osmotic forces. By wounding larvae in a hypotonic environment, exposed cells should swell by the osmotic influx of water from the media; this could counteract the inward forces of the contracting wound and therefore reduce the extent of notochord extrusion. It may be difficult to identify an osmolarity sufficient to counteract the wound contraction but not to cause severe cell swelling and lysis. Additionally, as explained in chapter 3, osmolarity appears to have a regulatory role on both wound closure and cell migration[226,232] therefore these wounds may respond to changes from normal wound regulation rather than the physical forces alone.

5.3.3 H_2O_2 mediates *ihhb* upregulation via multiple mechanisms

Considering that SFKs are activated in a H_2O_2 dependent fashion to drive notochord extrusion and *ihhb* upregulation, it was unexpected that inhibition of H_2O_2 alone had such a clear reduction in *ihhb* expression without preventing notochord extrusion. Whilst extended doses of DPI did show a more significant inhibition on notochord extrusion (Figure 5.14A), validating this as a H_2O_2 dependent process, it appears that H_2O_2 and SFKs may regulate *ihhb* in different ways and not via a simple linear relationship that we may have expected. DPI treated larvae do not show the same strong correlation between notochord extrusion and *ihhb* upregulation as untreated or PP2 treated larvae (Figure 5.10A, C & Figure 5.14C). This leads me to hypothesise

that whilst SFKs may stimulate *ihhb* expression directly via notochord extrusion, and H_2O_2 is required to initiate this mechanism, H_2O_2 may also regulate *ihhb* via separate mechanisms. Although inhibition of MAP2K appears to affect the wound response similarly to PP2, it may be interesting to see if this part of the same regulation mechanism or if it is working in a different manner. We do not know which cells activate MAP2K, or if MAP2K is redox-regulated in this situation, but if they were activated in the notochord in a H_2O_2 dependent manner, this could provide the extra layer of regulatory control that we see H_2O_2 exerting on the notochord. Unfortunately, at this point I can only speculate as to the relationship and further work will be required to shed light on the matter.

5.3.4 Summary

Data presented in this chapter has characterised the molecular effectors of the wound-induced H_2O_2 response and provided evidence of a mechanistic link between this rapid and transient wound signal and the initiation of regenerative signalling. The model I have proposed is summarised in Figure 5.15 below. In response to wound-induced H_2O_2, *ihhb* is upregulated specifically in the notochord cells as an immediate-early response. This upregulation requires SFK and MAP2K activation as well as notochord extrusion. I propose that H_2O_2 activates SFKs at the wound, which drive wound contraction and force the notochord (already under high pressure) to be extruded. This extrusion stimulates *ihhb* expression via an unknown mechanism, and is subject to further regulatory control that requires H_2O_2 to permit the *ihhb* upregulation. As such, H_2O_2 appears to initiate multiple regulatory cascades which integrate to drive proper regenerative signalling. Here I have identified SFKs as molecular effectors but it is likely that this highly reactive wound signal regulates multiple divergent processes required for proper healing and regeneration.

In relation to my original hypothesis that “Redox sensitive cellular regulators transduce the wound-induced H_2O_2 signal to biochemical signalling pathways essential for regeneration” I can now update this to the following: “Wound-induced H_2O_2 activates the Hh pathway via SFK-dependent transcription of hedgehog ligands driven by extrusion of the notochord”.

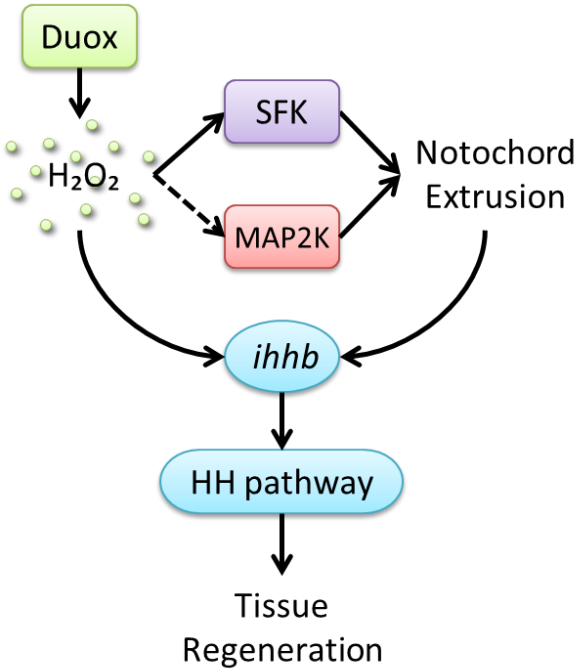

Figure 5.15 – Proposed model for H_2O_2 stimulation of regenerative signalling pathways via Hh activation.
Wound-induced, Duox-derived H_2O_2 activates SFKs and potentially MAP2K which are required for notochord extrusion following amputation. Notochord extrusion and H_2O_2 both positively regulate the up-regulation of Hh ligands *ihhb* and *shha* leading to Hh pathway activation and subsequent regenerative tissue outgrowth to replace the lost tail.

Chapter 6. Larval tail regeneration is not a recapitulation of developmental signalling regimens

6.1 Introduction

6.1.1 Aims

The process of regeneration is sometimes considered as a process of "re-development" given that its end goal is the same as the original developmental process – to grow a new, functional tissue. The processes also share a number of overlapping essential signalling pathways as well as similarities in the supracellular organisation and regulation during development and regeneration, meaning that discoveries in one field have the potential to inform the other.

Considering these similarities and the possibility of translating my results into a developmental setting, this chapter aims to determine if the regeneration mechanisms I have described in Chapters 3 and 5 are also used in development, or if they are an example of a separate set of regulatory interactions. I will address this issue by simply repeating the DPI, MCI-186 and PP2 pharmacological treatments that perturbed regeneration outcome and observe the effects in the developmental process. If inhibiting ROS and SFKs using these methods are capable of inhibiting Hh signalling and subsequent tail development, then I can conclude that this regulatory paradigm is also used in development and may have been co-opted to mediate regeneration at a later stage.

6.1.2 Background

As the field of regeneration research grew, it became apparent that a number of developmental pathways were essential for the successful regeneration of multiple different tissue types in multiple different organisms, leading people to suggest that these organisms may have co-opted their developmental signalling mechanisms to carry out regeneration following injury. This would be unsurprising considering that regeneration can be considered as a form of "re-development" as both processes have a shared endpoint – the formation of new tissue – and require the coordination of the same mechanisms including cellular proliferation, differentiation, migration and remodelling of extracellular matrix. Additionally, given the similarities in the processes used to achieve this endpoint, it would be biologically

efficient to utilise the same signalling pathways with the same regulatory controls rather than attempt to encode a separate mechanism for similar tasks. This hypothesis is clearly an oversimplification and there are pertinent differences between the two processes, not least in the different starting populations of cells (multi-potent & embryonic in development vs lineage committed & mature in regeneration), different starting environments (plastic & proliferative in development vs homeostatic & post-mitotic in regeneration) and different energy requirements (whole-body growth in development vs localised growth in regeneration). Even so, there are multiple examples where developmental and regenerative regimens have been demonstrated to overlap significantly, allowing work from both fields to contribute to the wider understanding of the other.

6.1.2.1 Similarities between tail development and regeneration

6.1.2.1.1 Supracellular structure of the fin bud and the regenerating stump

As mentioned above, it is unsurprising that there is some similarity between developmental and regenerative processes given that they are both designed to achieve the same result of growing new tissue.

This process can be largely simplified to three basic steps: 1) recruiting & stimulating cells to enter a plastic state (initiation), 2) stimulating these cells to proliferate to populate the new tissue (proliferation), and 3) ensuring that cells migrate to the correct position in the new tissue (patterning). In the developing limb and fin buds, these three steps are carried out by three distinct regions of tissue: 1) the apical ectodermal ridge (AER) responsible for initiation, 2) the progress zone responsible for proliferation, and 3) the zone of polarising activity (ZPA) responsible for patterning[435] (Figure 6.1). When compared to the developing tail bud, the regenerating stump spatially divides these three steps in a similar fashion, and whilst it is not an exact copy of the developmental bud, clear similarities can be seen.

In the regenerate, the equivalent structure to the AER is the wound epithelium. These structures are both positioned at the distal-most part of the bud or stump respectively and are both responsible for the secretion of trophic factors to stimulate the formation of their respective underlying regions – the progress zone or the blastema[84,100,435]. Subsequently, they are both responsible for stimulating proliferation in these regions via the secretion of FGFs[82,84,111,436,437]. In the regenerating stump, proliferation is restricted to cells directly underneath the wound epithelium (the blastema)[101], and although proliferation is more

widespread in the developing fin bud, the AER establishes a gradient of proliferation which results in the majority of cell division also being localised to the underlying cells (the progress zone)[438]. Thus, the similarities between the AER and the wound epithelium are clear – both regions are positioned similarly and perform the same biological actions using the same signalling pathways.

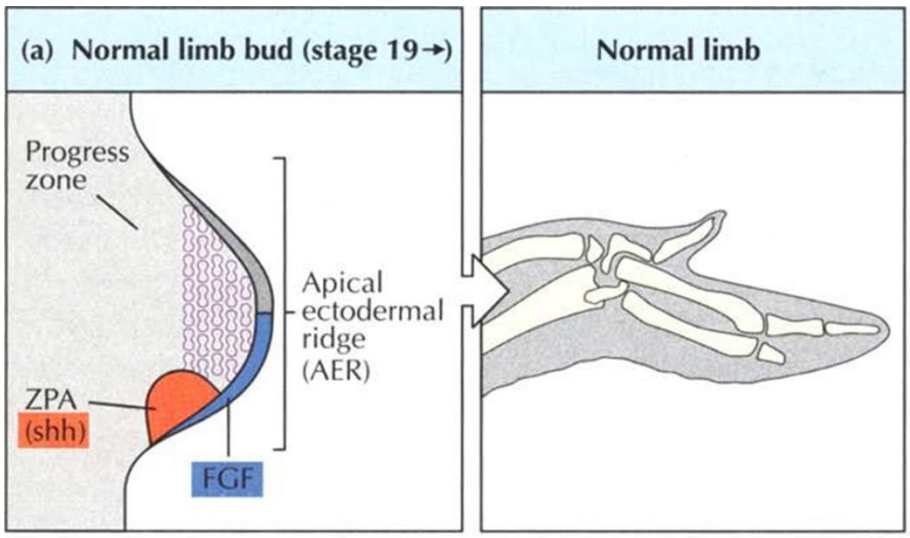

Figure 6.1 – Limb bud development (reproduced from Tanaka & Gann, 1995[439]).
Schematic of the spatial arrangement of the developing chick limb-bud required for normal limb development. Fin development is initiated in a highly conserved fashion to that of limb development with the early fin and limb buds employing the same spatial organisation of the AER, prgoress zone and the ZPA as well as the subsequent morphogen/mitogen gradients.

In the developing fin bud, the area where the majority of cell proliferation takes place is known as the progress zone and it bears some similarities to the blastema which is the region of proliferative cells in the regenerating fin. As described above, they both respond to FGF signalling to drive proliferation, but they also both proliferate in a similar pattern with the distal tip of both the fin bud and the blastema showing a reduction in the rate of cell division. In the regenerating tail, proliferation within the blastema is sharply divided into two regions with the posterior tip proliferating at a 50-fold lower rate than the anterior region[101]. This decrease in proliferation is also seen in the tip of the developing tail, though much more modestly, where the area of the tail-bud posterior to the notochord displays a mitotic index of around 50% of more anterior regions[435]. However, the source of the proliferating cells are different with the progress zone formed from a mass of undifferentiated mesenchymal cells, whilst the blastema is a collection of mature cells that have re-entered the cell cycle to

proliferate in a lineage-restricted manner[57,58,102,103]. In addition to this, the growth of the developing fin bud is also driven by a significant contribution of cell migration from more distant regions of cell proliferation[435], and therefore given these differences in the makeup of the regions, some differences between the regulation of outgrowth in each scenario are to be expected.

The third major region within the developing fin bud, the ZPA, is where the structural similarity ends as there is no defined region in the regenerating stump dedicated to imparting patterning information to the growing tissue. Whilst the ZPA is required in development to establish the anterior-posterior axis to properly pattern the developing tissue[440], in the regenerating fin, the anterior-posterior position of cells appear to be determined by region-specific expression patterns of a number of transcription factors established across the fin during development and hence there is no need for a discrete ZPA[441]. Although less completely understood, intrinsic positional cues also appear to control proximodistal patterning in the regenerating fin via calcineurin regulation of retinoic acid signaling[107], which represents another difference from development where the progress zone appears to define proximodistal identity. The model put forward in the 70's postulates that whilst cells remain within the proliferating progress zone, their potential proximodistal fate is progressive distalising, and as they are forced out of the progress zone by cell division, their fates become fixed. Therefore the cells leaving the progress zone first adopt a more proximal fate than those leaving later and appropriate limb patterning is achieved[442]. Although recent evidence suggests that this model may have limitations and that limb segments are specified at an early stage of limb development and the progress zone acts more to ensure the appropriate proliferation of these committed populations rather than directly determine their differention[443]. Patterning therefore appears to be one process where there is little overlap between development and regeneration and therefore understanding developmental cues may be of limited use in regeneration-specific contexts.

6.1.2.1.2 Regulation of signalling in the developing fin bud and the regenerating stump

The parallels between development and regeneration cover more than just spatial division of labour within the growing tissue. A large number of essential developmental signalling pathways are reactivated during and required for successful regeneration in zebrafish. These include pathways which we have focused on in our lab – Hh, Wnt, FGF and retinoic acid – as well as BMP, Notch, activin, IGF, PDGF and TGF-β[42,99,100]. Although required to be activated, the

regulation of these pathways can vary from development to regeneration and even between different types of regeneration between different organs or age of the fish. More specific examples of similarities between fin development and regeneration include the regulation of multiple homeobox genes.

The *msx* family of homeobox genes are expressed in the developing fins before being downregulated once development has completed, but following injury, all four of the genes are re-established in the regenerate[269]. The upregulation of these genes is required for both development and regeneration of the fins and they are expressed in similar spatial patterns in both scenarios. The most distal cells – the AER in development and the wound epithelium in the regenerate – both express *msxA* and *msxD*, although the AER additionally expresses *msxC*. All four genes are expressed in the mesenchymal cells in the progress zone in development but only *msxB* and *msxC* are expressed in the blastemal cells in the regenerate. Furthermore, these genes appear to be regulated by similar mechanisms with *dlx5a* acting as a positive regulator of *msx* genes in both developmental fin buds and regenerating fins.

In addition to the *msx* genes, expression and function of the homeobox gene *dlx5a* shows similarities in developmental and regenerative conditions. In development, *dlx5a* is expressed in the AER of the fin buds and is required for successful outgrowth of the presumptive fin buds[268]. Morpholino-based knockdown of *dlx5a* (and another closely related family member *dlx6a*) results in a concomitant decrease in the *msxB* and *msxC* genes suggesting that *msx* gene expression is dependent on *dlx*. Similarly, in regeneration *dlx5a* is upregulated within the wound epithelium which, as explained above, can be considered the regenerative equivalent of the developmental AER. Although no studies have explicitly demonstrated a regulatory link between *dlx5a* and *msx* genes, *dlx5a* is expressed within the wound epithelium which co-stimulates the formation of the *msxB* and *msxC* expressing blastema[75,76,116]. Therefore both fin development and regeneration, *dlx5a* is expressed in a similar spatial distribution, and is required for the subsequent expression of *msx* genes and developmental outgrowth.

Despite differences in development and regeneration, advances in one field may still be applicable to the other as so many of the same developmental pathways are used in both. Whilst we may not be able to take whole regulatory schema from one and transpose it directly on the other, molecular level interactions and regulations can still be helpful in increasing our understanding of both processes.

6.1.2.2 Hh signalling in development

The regeneration mechanism I have described in Chapters 3 and 5 places H_2O_2 dependent Hh signalling as the major initiator of regenerative signalling in the larval zebrafish tail. Work by others in our lab have shown that Hh is an upstream regulator of both Wnt and FGF signalling, therefore I will give a brief overview of the current evidence of these three signalling pathways in tail development to assess the feasibility of the regenerative regulatory mechanism also being used in development.

The Hh signalling pathway is known to be required to determine the anterior-posterior patterning of the developing mammalian limb buds[444]. Whilst the requirement for Hh signalling to establish this developmental axis has been confirmed in the developing zebrafish fins (the evolutionary homologous of tetrapod limbs)[445,446], its effects on developmental outgrowth remain less well characterised. Zebrafish mutants for *smoothened* (an essential component of the Hh signalling pathway) as well as *shha*, can show severe defects in pectoral fin cellular proliferation and outgrowth, effects phenocopied by pharmacological inhibition of Hh signalling, but tail development is still maintained[445,446]. This suggests that Hh may play subtly different roles in the regulation of the paired and unpaired fins in zebrafish.

In addition to the direct effects of Hh on developmental signalling, the regenerative mechanism I have described places Wnt and FGF under the control of Hh, and both of these pathways are essential for zebrafish development and specifically larval tail development. Multiple studies using pharmacological treatments, morphants and mutants have shown that *wnt3a* and *wnt8* are specifically required for tail elongation in the developing zebrafish[447–450]. The studies show severely impaired tail extension, with an almost complete lack of tissue forming posterior to the yolk extension. Similarly, a number of studies have also shown that FGF is required for tail elongation and pectoral fin growth and that genetic or pharmacological inhibition of FGF signalling appear to phenocopy Wnt inhibition with severely reduced tail and fin outgrowth[436,437,451–453]. The similarities in the phenotypes of tail development suggested a shared pathway whereby Wnt and FGF were both responsible for the stimulation of tail development. Indeed, it has been shown that Wnt stimulates tail development via FGF activation in a relationship matching the regulatory hierarchy seen by our lab in the regenerating tail. This relationship, however, appears to be more complex in development as FGF is also capable of stimulating Wnt signalling demonstrating significant cross-talk between the two pathways which is absent in regeneration[447,454]. If the regenerative regulatory mechanism was fully replicated during development then, given the severe phenotypes

associated with inhibition of either pathway, Hh dependent activation of Wnt and FGF are strong candidates for effectors of Hh driven tail development.

Whilst no evidence to date has shown that Hh signalling is absolutely required for tail development as it is for tail regeneration, it is known to be an important regulator of patterning in the growing fin bud and outgrowth of pectoral fins therefore is capable of exerting some control over developmental growth. In addition to this, the Wnt and FGF pathways were shown to be stimulated by Hh activation in regenerative signalling and inhibition of either of these pathways results in severe impairment of tail development. Taken together, it is conceivable that Hh signalling could play positive roles in the developmental growth of the tail, a hypothesis that the following results will test.

6.2 Results

Data presented in this chapter aims to address the level of similarity between larval tail regeneration and tail development. I performed some basic experiments to test if the regenerative signalling program of the tail, described in in Chapters 3 and 5, was also utilised in the development of the tail. I aimed to test the importance of H_2O_2 and SFKs in the regulation of developmental signalling and gross tail development. If development and regeneration were similarly regulated, then the same pharmacological inhibitors of these signals that inhibited regeneration should also inhibit development.

6.2.1 Development of the tail bud does not require H_2O_2 or SFK activation

Firstly, I examined the gross morphology of the developing tail bud to investigate if the same pharmacological treatments used to inhibit regenerative outgrowth replicate their effects on developmental outgrowth. Larvae were treated with DPI to inhibit NADPH oxidase-dependent H_2O_2 production, MCI-186 to scavenge ROS from any source, or PP2 to inhibit SFK activation. Dosing was performed from 14-18hpf as the extension of the tail begins at around 14hpf[455], and hence any differences in development could be easily identified over this period. Following dosing, larvae were transferred to fresh E3 media to develop until 24hpf, at which point they were fixed for morphological analysis. Representative images of ~30 larvae are shown below in Figure 6.2.

The concentration of DPI had to be reduced from 150µM (as used in the regeneration experiments performed above) as a 4hr dose of this concentration was poorly tolerated by the larvae with many deaths. The concentration of DPI was reduced to 100µM which has been shown in my MSc work to still inhibit regeneration, though not as strongly as 150µM[136], (Figure 3.3) and therefore should still inhibit developmental outgrowth if similar regulation mechanisms are utilised. Treatment with 100µM DPI did not affect the gross morphology of larval development and the tail bud extended no differently than vehicle treated controls (Figure 6.2; A vs A'), suggesting that Duox and other Nox family enzymes are not required for tail development. To further investigate the role of ROS in development, MCI-186 was also administered to developing larvae at 2mM. Whilst treatment partially reduced development as a whole, including body extension, a tail was still formed (Figure 6.2; B vs B'), suggesting that ROS are not essential for tail formation *per se* but may have positive effects in development in general, a suggestion supported by a growing body of evidence[456,457]. Finally, PP2 (20µM) was administered to analyse the effect of SFK inhibition on tail development. Larvae treated with PP2, like MCI-186, appeared to have impaired overall development, especially in body length, but still produced a tail (Figure 6.2; C vs C'). Upon closer inspection, the notochord in the PP2 treated larvae (shown inset, marked with a white dotted outline) appeared much less extended than in control larvae. This treatment however can give us no information on the mode of action of PP2, and although it may indicate an indirect regulation of development via Hh signalling (as in regeneration), SFKs are known to be required for proper developmental cell movement[458–460] and therefore could conceivably result in impaired cell migration, intercalation and vacuolation, preventing the full extension of the notochord. Further work would be required to identify the mechanism of this SFK-dependent development.

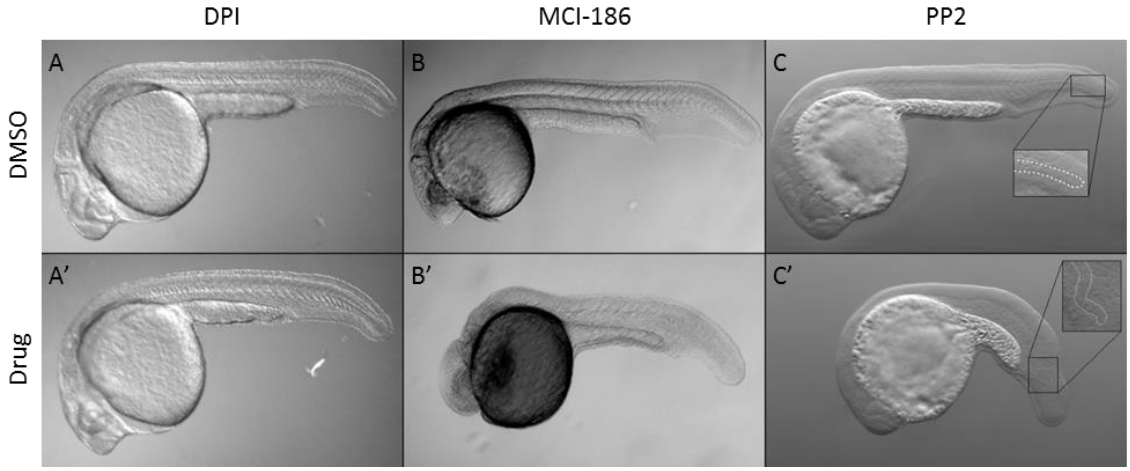

Figure 6.2 – Tail development following DPI, MCI-186 and PP2 treatment.
Larvae were treated with DPI, MCI-186 or PP2 from 14-18hpf and morphology was assessed at 24hpf. Representative images from drug treated larvae (**A**, **B**, **C**) and their respective vehicle-dosed controls (**A'**, **B'**, **C'**) from >20 replicates foe each treatment.

6.2.2 Hh signalling in the developing tail is not regulated by H_2O_2 or SFKs

Having failed to see any dramatic morphological changes in the extension of the tail bud from treating with DPI, MCI-186 or PP2, I wanted to analyse the gene expression patterns to see if I could detect any more subtle perturbations in the developing tail from these treatments.

Focusing on Hh signalling, given its position as the most upstream regulator of regenerative signalling, I carried out WISH in the developing embryo to analyse physiological expression patterns and intensity. Embryos were dosed with DPI, MCI-186 or PP2 from 14-18hpf, as above (identified as the period of maximal tail extension), and were fixed at 18hpf to perform WISH for *ihhb* and *shha*. Representative images of ~30 larvae are shown below in Figure 6.3.

In vehicle-treated controls, both *ihhb* and *shha* are expressed in the notochord, extending into the centre of the tail bud (Figure 6.3; DMSO controls). Expression of *shha* appears more diffuse at the tip of the notochord, suggesting a slightly expanded population of cells expressing *shha* as opposed to *ihhb*, but the patterns are largely identical. No clear difference in the expression patterns or strength of either transcript could be observed following treatment with DPI to inhibit NADPH oxidase-dependent H_2O_2 production (Figure 6.3; A vs A', D vs D'), MCI-186 to scavenge ROS from any source (Figure 6.3; B vs B'), or PP2 to inhibit SFK activation (Figure 6.3; C vs C', E vs E'). The effect of MCI-186 on *shha* expression was not tested; due to the identical

regulation between the two Hh ligands in regeneration, I expect *shha* and *ihhb* to respond identically to MCI-186 treatment in development, but this would have to be explicitly tested in follow-up experiments.

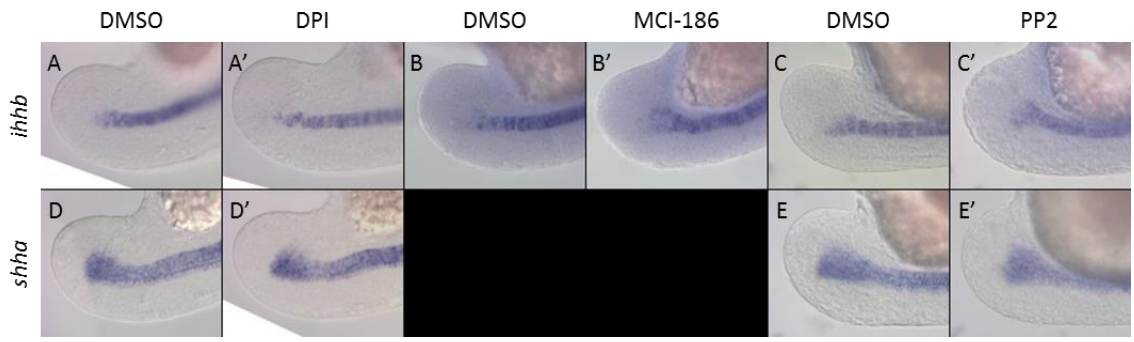

Figure 6.3 – WISH analysis of developmental expression of Hh ligands following DPI, MCI-186 and PP2 treatment.
Larvae were treated with DPI, MCI-186 or PP2 from 14hpf till fixation at 18hpf and WISH was used to assess *ihhb* and *shha* expression at 18hpf. Representative images of drug treated larvae (**A'**, **B'**, **C'**, **D'**, **E'**) and their respective vehicle-dosed controls (**A**, **B**, **C**, **D**, **E**) from >20 replicates for each treatment.

The larval response to DPI, MCI-186 and PP2 treatments during development was subsequently validated using qPCR. As in regeneration, *shha* was presumed to be regulated in an identical fashion to *ihhb* and therefore qPCR was only performed to quantify *ihhb* transcripts. The qPCR method optimised in Chapter 3 was used with 30 larvae pooled per group before extracting RNA. Drug treatments were carried out from 14-18hpf, as above. Data presented is the average of at least 3 separate experiments to account for biological variance. No significant difference was detected between drug and vehicle treatments (Figure 6.4), supporting the WISH data that there is no clear regulation between H_2O_2, ROS or SFKs and *ihhb* expression in developing embryos as we see in the regenerating tail. Whilst the data does appear to show some small variation in expression following treatment with MCI-186 or PP2, these results are quantifying *ihhb* expression from the entire embryo and therefore may be representing a difference in expression in unrelated tissues, especially if these chemical treatments interfere with the progression of overall development as seen above.

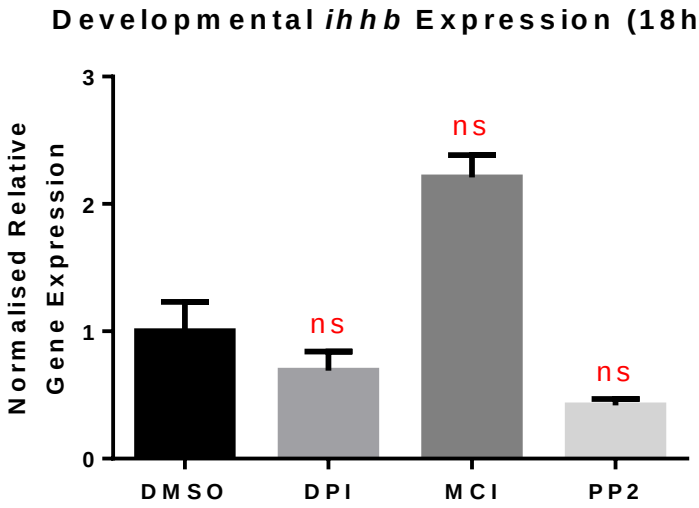

Figure 6.4 – qPCR analysis of developmental expression of *ihhb* following DPI, MCI-186 and PP2 treatment.
Larvae were treated with DPI, MCI-186 or PP2 from 14hpf till fixation at 18hpf and qPCR was used to assess *ihhb* expression at 18hpf. Bars represent the mean relative gene expression (ΔCt) of each treatment from 3 independent experiments, normalised to scale control (DMSO) levels to 1 for easy comparison. Error bars represent SEM.

6.3 Discussion

Data presented in this chapter aimed to address the level of similarity between the molecular processes used in tail development and tail regeneration in the larval zebrafish.

In Chapters 3 and 5, I have shown that in regeneration, the NADPH oxidase family enzyme Duox is activated following wounding to produce H_2O_2, which, in turn, activates SFKs leading to the upregulation of Hh ligands and the initiation of regenerative signalling in the tail. In this chapter, I used the same treatments which inhibited regenerative signalling and outgrowth and analysed the effect on the development of the tail. Analysis of gross morphology (Figure 6.2) or gene expression by WISH (Figure 6.3) and qPCR (Figure 6.4) was unable to detect significant inhibition of tail development to a similar extent as that observed in regeneration. This suggests that the regulatory mechanisms and mitogenic signalling employed during tail regeneration are not a simple recapitulation of developmental processes.

In-depth conclusions of the signalling and regulation mechanisms utilised during tail development cannot be made from these fairly superficial data, and much more work would be required to begin to answer these questions with confidence. However, what we can see

from these results is that the most important regulators that I have identified in larval tail regeneration do not exert the same stringent control over tail development.

6.3.1 Hh and Wnt signalling requirements differ between tail development and tail regeneration

In addition to the experiments I performed, Maria Garcia Romero (another member of our lab) was simultaneously examining the role of regenerative signalling pathways in tail development[91]. She found that exposing embryos to cyclopamine or LDE225 to inhibit the Hh signalling pathway demonstrated that whilst Hh activation is absolutely required for tail regeneration, it does not preclude tail development (Figure 6.5). Furthermore, cyclopamine treatment prevented Wnt activation (as assayed by *tcf7* expression) and *aldh1a2* (labelled here by its old name – *raldh2*) upregulation following tail amputation, but had no effect on the developmental expression of these genes (Figure 6.6). Finally, she showed that inhibition of the Wnt signalling pathway (via exposure to the chemical inhibitor IWR-1 or using the heat-shock inducible *hs:dkk1-GFP* transgenic line) causes a severe inhibition of both regeneration and tail development with little, if any, regenerative outgrowth following tail amputation and a complete lack of development of any structures posterior to the yolk (Figure 6.7).

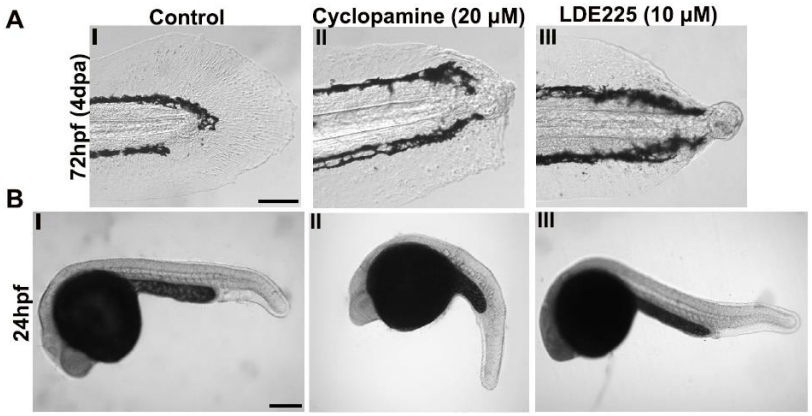

Figure 6.5 – Hh signalling has a different role in tail regeneration than in tail development reproduced from Romero, 2016[91]).
Fish embryos are treated with 20 µM of cyclopamine and 10 µM of LDE and the effects are analysed by morphology. **A** (n=10) and **B I**: Vehicle-treated embryos (n=20), in which normal tail development and regeneration is observed. **A II** (n=10) and **B II**: (n=20) Cyclopamine-treated embryos (continuously), in which tail extension is observed (with some morphological defects) but not regeneration. **A III** (n=10) and **B III**: (n=20) LDE 225-treated embryos (continuously), in which normal tail development is observed but not regeneration. Number of trials N=2. One representative embryo was chosen per picture. Scale bar 100 µm.

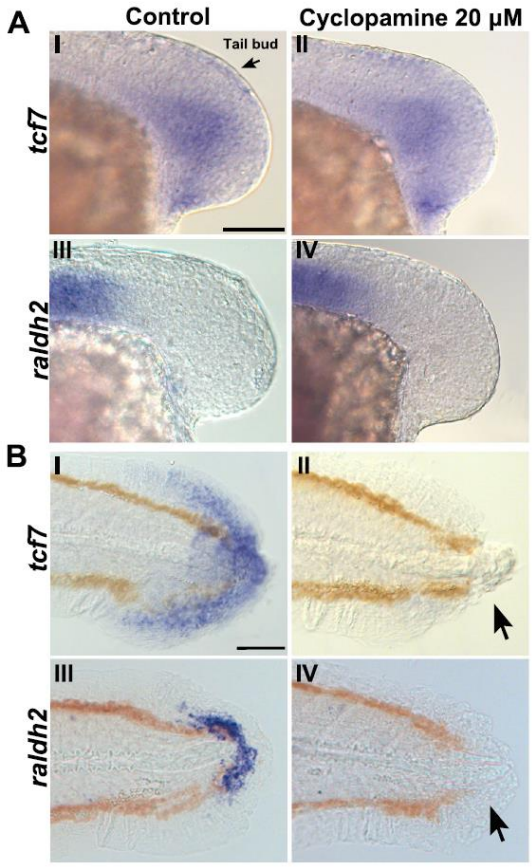

Figure 6.6 – Down-regulation effects the expression of *tcf7* and *raldh2* genes during regeneration but not during tail development reproduced from Romero, 2016[91]).
Fish embryos are treated with 20 µM of cyclopamine. *tcf7* and *raldh2* expression is detected by in ISH. **A I** (n=20), **A III** (N=20),**B I** (n=20) and **B III**: (n=20) Control vehicle-treated fish present normal expression of *tcf7* and *raldh2* during normal tail development and regeneration. **A II** (n=20), **A IV** (n=20) Cyclopamine-treated fish from 75% epiboly to 16 somites present normal expression of *tcf7* and *raldh2*, when compared with controls. **B II** (n=20) and **B IV** (n=20) Fish treated with cyclopamine from 0-48hpa do not show expression of the *tcf7* and *raldh2* genes during regeneration (black arrows) when compared with controls. N=1. One representative embryo was chosen per picture. Scale bar 100 µm.

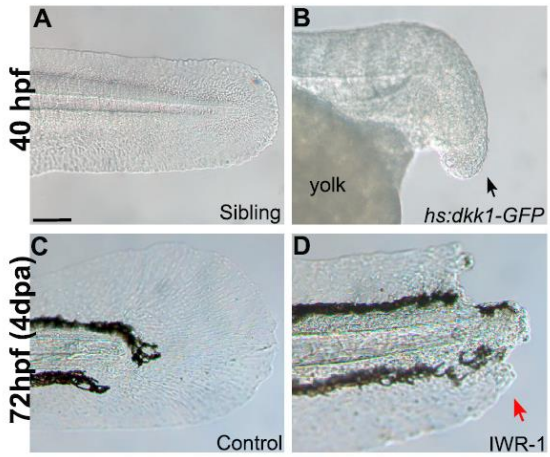

Figure 6.7 – Wnt signalling has a similar role in tail regeneration and tail development (reproduced from Romero, 2016[91]).
Fish embryos are treated with 10 µM of IWR-1 during regeneration for 4 days. *hs:dkk1* embryos are heat shocked for 1 and a half hours at 39°C from 75% epiboly and then allowed to continue with normal development until 40hpa (fish were fixed at this stage). **A** (n=10) and **B**: (n=30) *hs:dkk1* line. Wnt down-regulated embryo did not complete tail formation (black arrow) in contrast to the control. **C** (n=10) and **D**: (n=10) Fish treated continuously with IWR-1 during regeneration did not complete tail outgrowth (red arrow), which was complete in the control. N=1. One representative embryo was chosen per picture. Scale bar 100 µm.

Together, these data support my findings that the regeneration program initiated in the larval tail is not a simple recapitulation of developmental signalling and growth. Hh appears to have a more limited role in tail development and Wnt signalling is clearly much more important.

6.3.2 Similarities and differences in cellular activity in tail development and tail regeneration

When further considering regulation of cellular proliferation in the developing tail bud, more detailed analysis of the cell division patterns described in the introduction to this chapter may actually show another similarity between development and regenerative regulation of outgrowth. I described a reduction in cellular proliferation at the tip of developing tail bud in tissues posterior to the end of the notochord[435], but interestingly, when analysed mediolaterally, the rate of proliferation also varied across the width of the bud. There was a clear mediolateral gradient of mitotic index with the highest in the centre of the bud and the lowest at the lateral edges. Although, no direct link was investigated, this could indicate that

the major determinant of proliferative rate is proximity to the notochord, and that the organ directly stimulates cell division by paracrine signalling. If this hypothesis were to prove true, it would show that in development, as in regeneration, the notochord appears to be an important signalling centre and useful parallels may be able to be drawn on a cell-specific basis.

The differences seen in the regulation of tail development and tail regeneration may stem from the fact that both processes appear to achieve tail outgrowth via slightly different mechanisms. Regenerative proliferation is much more localised, with proliferation restricted to the blastema, whereas developmental growth is achieved by a combination of cellular proliferation in the tail bud and migration of cells from more distal areas[435], and therefore is dependent on non-localised cell proliferation outside of its regulatory influence, as well as the additional regulation of cell migration. In addition, the type of cell dividing in each scenario is different. In development, cells are dividing as part of the pre-determined developmental program and are therefore clearly more responsive to mitogens, whereas the blastema is formed from mature, post-mitotic cells which appear to proliferate in a lineage-restricted manner with little contribution from more plastic progenitor or stem cell populations[57,58,102,103]. These mature cells may not be capable of responding to the same signals as developing cells due to differences in cell surface receptor expression or epigenetic silencing of developmental regulatory genes.

Whilst the regenerative paradigm that I have described in Chapters 3 and 5 is clearly not employed during tail development and therefore I cannot extend my conclusions to cover this process, it may be interesting to see if the paired pectoral fins respond in the same manner as they seem to be more sensitive to Hh signalling during development[445,446], and there could be tissue-specific difference in redox-regulation. It also raises an interesting question of how, and why, the regenerative signalling pathway has evolved to make use of the components of the developmental signalling networks but integrated additional regulatory components and co-opted them to function in a novel mechanism to achieve the same goal.

6.3.3 Summary

In summary, work presented in this chapter aimed to identify if the regenerative signalling regulatory mechanism of the larval tail described in Chapters 3 and 5 is also employed in normal embryonic development. Considering regeneration as a process of “re-development”, I

hypothesised that regulation of regenerative outgrowth may simply be a recapitulation of developmental processes which formed the tail in the first place. Following pharmacological inhibition of either ROS or SFK signalling, larvae successfully developed tails and I could not detect any significant differences in *ihhb* expression by either WISH or qPCR, directly contrasting their effects in regenerating tails. From these data I concluded that the regulatory paradigm I have described in the regenerating tail is not employed in development. Additional data from Maria Garcia Romero showed that Hh does not regulate its regeneration effectors in development and that it is not required for tail formation at all, further suggesting divergent outgrowth strategies. These data allow me to update my original hypothesis that "Wound-induced H_2O_2 has been co-opted as a regulator of regeneration by recapitulating a growth-promoting role also present in tail development" to "H_2O_2 is dispensible for tail development; its growth-promoting roles are specific to tail regeneration and not a recapitulation of developmental signaling regimens".

Chapter 7. Discussion

7.1 General discussion

More detailed analysis and discussion of the results are presented within each chapter but in this chapter I will summarise my findings and consider them as a whole, as well as the wider implications and future work.

7.1.1 Updated model of regeneration

When brought together, the data I have presented in this thesis describes a regulatory mechanism centred around H_2O_2 that is essential for initiating regenerative outgrowth in the larval zebrafish tail (Figure 7.1). This mechanism is capable of transducing the earliest biophysical wound responses into biochemical stimuli which stimulates regenerative outgrowth via activation of highly conserved developmental pathways. As such, it is a good candidate for translation to other species as no 'specialist', regeneration-specific, components are required. In short my proposed mechanism functions as follows:

Wound-induced biophysical stimuli such as mechanical stress, osmotic forces and bioelectricity culminate in the coordinated release of intracellular Ca^{2+} at the site of injury, which propagates away from the wound. This Ca^{2+} wave activates the Nox family enzyme Duox which rapidly establishes a gradient of H_2O_2 highest at the plane of injury, and gradually diminishing as it extends away from the wound. The establishment of this gradient is likely a combination of the stimulatory Ca^{2+} signal decreasing further away from the wound as well as passive diffusion of H_2O_2 in the interstitial fluid.

My data suggests that this transient H_2O_2 signal performs two independent functions: 1) it recruits leukocytes to the wound, and 2) it stimulates the upregulation of the Hh ligands *ihhb* and *shha*. In my experiments, impairment of the recruitment of leukocytes to the wound did not significantly affect regeneration but data from the wider field supports pro-regenerative roles for macrophages, therefore H_2O_2 appears to stimulate multiple pro-regenerative pathways. The upregulation of Hh ligands initiates a cascade of regenerative signalling pathways (Hh → Wnt → FGF) and is required for the formation of the wound epithelium & the blastema and for subsequent regeneration.

Interestingly, this upregulation appears to be precisely restricted to notochord cells, and, more specifically, to notochord cells which have been extruded past the wound margin following amputation. The extrusion of these cells is likely due to the high-pressure notochord resisting SFK stimulated wound contraction, forcing them to move outward. This extrusion stimulates *ihhb* expression via an as-of-yet unknown mechanism, and Hh ligands are subject to further H_2O_2 dependent control to permit this upregulation.

My work shows, for the first time, a molecular link between wound-induced H_2O_2 and the initiation of the essential regenerative signalling pathways and sheds light on the requirements for H_2O_2 in regeneration. Whilst previous redox-sensitive targets have been identified in regeneration, those studies have not shown mechanistic links to the reactivation of the developmental pathways required for regeneration to proceed.

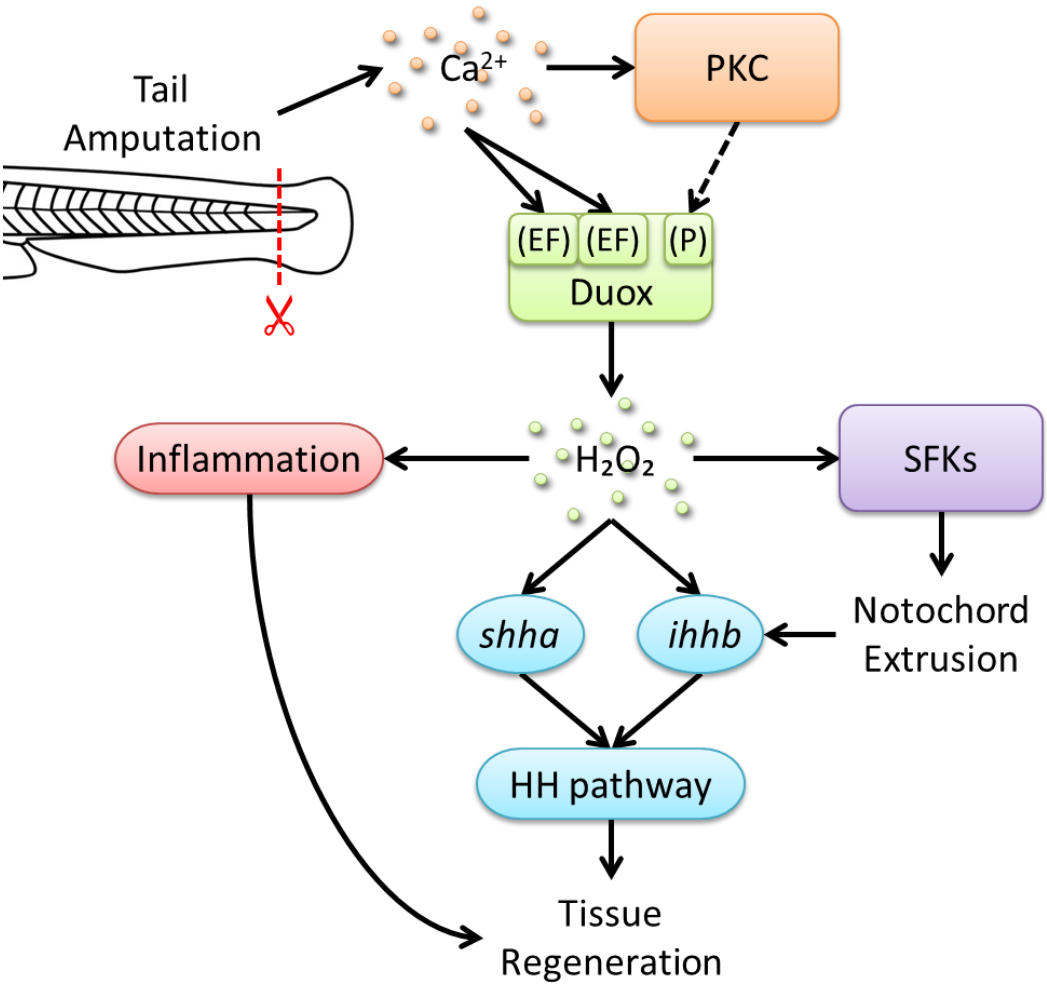

Figure 7.1 – Summary schematic of the regulation and regenerative effectors of wound-induced H_2O_2.

7.1.2 Impact of my results

The regeneration model that I have proposed in larval zebrafish closely matches the recently published data from the Vriz lab on the role of H_2O_2 in adult zebrafish regeneration[415]. They describe a similar regulatory mechanism whereby the adult tail maintains a population of cells that weakly express shh and which upregulate expression in a H_2O_2 dependent manner following wounding to trigger regeneration. In lieu of a notochord in the adult tail, it appears to maintain Shh expression in Schwann cells at the tips of the sensory axons, and injury induces the recruitment of more Shh-positive Schwann cells to the tip of the hemirays to stimulate regeneration. Together, these data suggest that the redox-based regulation of Hh ligands I identified in larval zebrafish is maintained throughout the life of the zebrafish.

Whilst the adult regeneration signalling mechanism described in this study matched the core of the larval mechanism I described above, it did include additional layers of regulation not identified in larvae. For instance, the wound-induced H_2O_2 signal and the expression of Shh in the Schwann cells appear to require the presence of neurons as denervation impaired both, suggesting that paracrine neural signalling is an essential upstream regulator of this mechanism. The study did not however determine if the immediate production H_2O_2 following wounding was affected by denervation, so we cannot conclude if Duox itself is regulated by this neural signalling or if this represents an adult-specific layer of regulation required for the prolonged adult H_2O_2 signal. Additionally, whilst H_2O_2 was required to stimulate Shh expression, Shh expression was also required for the sustained production of H_2O_2 in the wound epithelium, suggesting a positive feedback loop between H_2O_2 and Shh that does not appear to be present in larval regeneration. It will be interesting to see if many other regeneration responses share the same core mechanisms but have evolved additional or divergent regulation mechanisms as this may complicate the translation of this research into therapeutics trying to identify human specific regulatory components.

Tail regeneration in *Xenopus* has also recently been shown to be dependent on the Hh pathway[282]. Using a combination of *in situ* hybridisation and reverse transcription-qPCR, an upregulation of *shh* was observed following tail amputation. Treatment with the Hh pathway inhibitor cyclopamine significantly impaired tail regeneration, an effect that was rescued by the Hh pathway agonist purmorphamine[461] (which competitively displaces cyclopamine[462]). As in the zebrafish, the Hh ligand expression was restricted to the cells of the notochord, and

displayed a low-level endogenous expression that was upregulated in response to injury. One notable difference between the *Xenopus* and zebrafish expression of Hh ligands was the timeframe of expression; in zebrafish *ihhb* and *shha* appear to be upregulated within hours of injury, peak at around 6hpa and return to basal levels at around 30hpa[272], compared to the *Xenopus shh* which is gradually and continually upregulated from 2-7 days post amputation (expression was not measured post 7 days)[282]. Whilst inter-species differences in temporal expression may suggest different mechanisms of regulation, they are similarly related to the temporal characteristics of their respective wound-induced ROS signal; zebrafish exhibit a H_2O_2 wave lasting hours[119] compared to the ROS signal in *Xenopus* which is sustained over days[123]. Taken together, my data and these studies therefore support the idea of conserved redox regulation of Hh ligands between *Xenopus* and zebrafish, but this is yet to be empirically tested. Of further note is that tail regeneration in the axolotl has been shown to rely on *shh* expression in the injured spinal cord, again showing tissues-specific upregulation of Hh ligands following injury driving regeneration[283]. Unfortunately, there is no published data on the wound-induced ROS signal in axolotl, so I cannot conclude that these redox-regulatory mechanisms are also conserved in axolotls, but it is a possibility that should be explored.

Another interesting recent finding in *Xenopus* is that the wound-induced H_2O_2 signal is required for regeneration in order to establish bioelectric signals within the tail stump, suggesting that H_2O_2 may be required to stimulate multiple divergent regenerative mechanisms. Inhibition of ROS production or scavenging ROS resulted in a decrease in cellular depolarisation & altered current densities and subsequently impaired regeneration[141]. Exposure to exogenous H_2O_2 was shown to be able to rescue the bioelectric deficiencies and regeneration following inhibition but also to induce regeneration during the (non-regenerating) refractory period by restoring these pro-regenerative bioelectric properties. Induction of tail regeneration during the *Xenopus* refractory period has been demonstrated before by the genetic or pharmacological immunosuppression of larvae[139]. These two findings seem at odds to one another considering that H_2O_2 is a pro-inflammatory molecule responsible for driving leukocyte recruitment to wounds; therefore H_2O_2 would be anti-regenerative as an immune stimulator, but pro-regenerative as a bioelectric regulator. Patterning and outgrowth of the regenerating zebrafish fin has been shown to be dependent on bioelectric cues[271,463], and bioelectricity is being linked to healing and regeneration in more and more species suggesting that this downstream effector of H_2O_2 could be a promising universal therapeutic approach for the induction of *de novo* regeneration[69,140,250]. It is also interesting to see that two, apparently independent, mechanisms are both capable of restoring the regenerative

capability of *Xenopus* larvae. It is possible that the two processes are capable of co-regulation but if they are distinct pathways then it raises the intriguing possibility of being able to initiate regeneration via completely independent mechanisms, which could lead to multiple potential therapeutic approaches when translating this research into therapies.

Fin regeneration in zebrafish occurs via the same general mechanisms irrespective of age[42,75], however some differences have been documented such as the wound-induced ROS signal being sustained over days in adult fin regeneration[120] compared to hours in the larval process[119]. The work of our lab highlights another difference between adult and larval zebrafish tail regeneration, identifying Hh as the master regulator of signalling instead of Wnt in the adult fin[90]. The difference appears not only in the initiation of signalling, but the subsequent feedback and crosstalk between these pathways as work by Maria Garcia Romero from our lab[91] showed that Wnt and FGF activation do not regulate the Hh pathway as can be seen in adult regenertion[77,90]. Considering these emerging differences, especially in the regulation of regeneration, it will be essential to identify which is most applicable as a model for human regeneration. It has been argued that studying larval regeneration has in-built limitations given that developmental processes are still proceeding and that larval regeneration may therefore be regulated in a separate, developmental-specific manner that is not applicable to adult regeneration where re-growth has to be induced from a much less plastic environment. Even so, it is yet to be seen which model is a closer approximation of the human wound response and, in practice, a more complete understanding both models will likely contribute equally to and translational breakthroughs.

In addition, I present data which calls into question the role of leukocytes in the regulation of regeneration. Recently, many studies have shown links between inflammation and regeneration in the zebrafish, *Xenopus*, axolotl and mammals (as discussed in Chapter 4). Inflammation as a whole is generally considered to impair regeneration whilst macrophages appear to be pro-regenerative. In Chapter 4, I present data that does not detect any significant differences in regenerative outgrowth or the wound-induced regenerative Hh signalling despite a significant ablation of either macrophages, neutrophils or both. Although complete knockdown was not achieved and I cannot rule of long-range systemic signalling[328], my data suggests that neutrophils and macrophages, both alone and together, are dispensable for regeneration to proceed. This adds to a number of studies which have failed to detect a link between inflammation and regeneration and therefore I still consider this area open to debate. The disagreement in the literature may represent significant differences in the regenerative requirements for leukocytes in different species or even different organs within

the same species. Careful work will have to be carried out to define the true roles of these cells in regeneration and it will be interesting to see if a common regulatory role can be proven between species, and it will be most important to fully understand their roles in human healing and regeneration if we are to translate this research into viable therapies.

7.2 Promiscuity of redox signalling

The regeneration mechanism I have outlined in this thesis demonstrates one method by which H_2O_2 can regulate regeneration by activating Hh signalling, but the non-specific nature of H_2O_2 and other ROS mean that they likely react with multiple cellular components and may mediate their pro-regenerative effects via multiple different signalling mechanisms. For example, even using a small-scale screen of only 5 targets identified 2 potential effectors of H_2O_2 signalling. Although I did not confirm MAP2K as a direct target of H_2O_2, it can be activated by H_2O_2 in zebrafish[464] and was implicated as one of the mechanisms by which H_2O_2 stimulates zebrafish heart regeneration[124], so this may be a valid target for wound-induced H_2O_2. It should be noted that one study detected tail amputation-induced MAP2K activation, and whilst they reported impaired regeneration upon inhibition of MAP2K, this appeared to act in a H_2O_2 independent fashion[122]. This is the same study that contradicts my (and other's[216,236]) data that Ca^{2+} is not required for wound-induced H_2O_2 production and may be, in part, due to the wounding model chosen – only a mild and more posterior fin-fold resection instead of the more severe pigment-gap level amputation I used. If this was the case, this may indicate a cell-specific effect for H_2O_2 based on either the different cell populations injured or the different cell populations that are exposed to different concentrations of the H_2O_2 gradient. This is a good example of the potential difficulties in determining the effects of a molecule which has the potential to alter virtually any signalling pathway within cells and this is a difficulty that the redox biology field as a whole needs to address.

7.2.1 Promiscuity of H_2O_2 in regeneration

Whilst I expect H_2O_2 to have multiple signalling roles during regeneration, we are currently only beginning to characterise them. Reductionist data sets such as the one presented here, focusing on a single target of H_2O_2 are required to build up a picture of the many interactions which H_2O_2 is capable of, however, the real challenge will come when we try and integrate all

these individual redox targets into a comprehensive model of regeneration regulation, and infer hierarchies and rank the relative biological importance of each interaction. A systems biology approach using biomathematics will be required to build this overall model[465]. The complexity of redox regulation lies at the post-translational level of proteomics which will introduce challenges to measure these modifications *en masse*, and especially over time, but techniques discussed below are being developed to aid in this task.

Considering the current state of redox research in zebrafish regeneration alone has identified pro-regenerative ROS targets in Hh, Wnt & FGF (from this thesis), SFKs, MAP2K and JNK[120,122,124], as well as cellular responses such as inflammation, reinnervation, differentiation and apoptosis[43,59,120,128]. Expanding this to regeneration in other species, Wnt, FGF, MAP2K, ULK, Rho GTPase and bioelectricity have all been implicated as redox-sensitive regulators[123,129,141,211]. Whilst there does appear to be at least some overlap in the identities of the redox-sensitive regulators between studies, they can often be regulated via different mechanisms complicating the idea of a universally conserved redox-sensitive regeneration paradigm. It may be the case that there is a core set of redox-sensitive, pro-regenerative signalling pathways which are conserved between species but have evolved divergent regulatory controls after speciation. Understanding these core redox-driven regenerative components may lead to better understanding of why some species such as humans cannot regenerate and identify candidates for promoting regeneration. This hypothesis is, however, based on the presumption that the ability to regenerate has been inherited across metazoans from a common ancestor and that regenerative capacity has been progressively inactivated in non-regenerating organisms, something that is still contested[36–39,466]. Indeed, there are even cases of spontaneously evolved regenerative capacity such as in the newt[40], therefore a universal redox-driven regenerative paradigm may not even exist to be characterised in the first place.

7.2.2 Detecting redox regulation

Improvements in detection techniques for oxidative post-translational modifications mean that we now have unbiased proteomics techniques which could be used to identify the full extent of redox targets instead of being limited by pre-selection of candidate molecules[467]. These techniques, which include protein microarrays and mass spectrometry, are however limited to temporal snapshots and therefore careful selection of timepoints within rapidly

reversible redox environments such as wounds will be critical to generate the best data. Candidate-driven approaches such as modified western blots[468,469], can analyse redox dependency of individual targets but they are similarly limited by single-timepoint snapshot readouts.

It is possible that we could create redox-resistant forms of candidate molecules to observe their functions in an altered redox state within a physiologically normal redox environment. For example, fusion of a protein of interest to a H_2O_2 converting enzyme such as catalase could create a local decrease in H_2O_2 concentration and maintain that protein in a reduced state, even when surrounded by high levels of H_2O_2. However, the catalase subunits are ~60kDa and function as a tetrameric structure, therefore creating functional fusion proteins without any steric hindrance of either catalase or the protein of interest would be very difficult. Substituting catalase with a smaller, monomeric enzyme capable of reducing H_2O_2 may make this feasible, such as glutaredoxin which has been successfully fused to a redox sensitive GFP to allow real-time readout of the glutathione redox state[470].

Alternatively, in highly oxidising states (such as the high concentrations of H_2O_2 present at the wound site) a fusion between the protein of interest and glutathione reductase enzyme may aid in desensitising the protein of interest to oxidation. This seemingly counter-intuitive proposition is based on the hypothesis that in the abundance of H_2O_2, the glutathione system will be highly oxidised to counteract the oxidative stress, therefore areas surrounding glutathione reductase enzymes will have a relatively high concentration of reduced glutathione which could act as a localised oxidative buffer and protect the protein of interest from being regulated by H_2O_2. Whether this would work in practice is unknown and would have to be tested and will depend on multiple factors including the availability of electron donors to catalyse the reduction of glutathione, the glutathione equilibrium established within the cell, and the rate of diffusion of reduced glutathione away from the protein of interest.

More simple manipulation of a candidate molecule's redox state may be achieved by introducing point mutations at cysteines to remove redox sensitivity altogether. Although many enzymes have catalytic cysteines, these mutations can be achieved without affecting enzymatic activity, as has been done for the sodium-potassium adenosine triphosphatase[405,471–473]. Although this did not affect the catalytic activity of the enzyme, point mutations of cysteine residues did affect other enzyme characteristics including substrate affinity, stability and sub-cellular localisation[472] therefore any changes to these parameters should be carefully validated when translating this approach to other targets of interest.

Insertion of these fusion constructs as transgenes into zebrafish under inducible promoters (e.g. heat shock) could allow us to investigate the effect of these modified proteins in real time, allowing temporal information to be collected *in vivo* and allow more physiologically relevant interpretation of the data which could provide new insights into molecular redox responses.

7.3 Follow-on work

My data has described a H_2O_2 dependent regulatory mechanism by which larval zebrafish initiate regenerative signalling following tail amputation in the pigment-gap. This has, for the first time, a direct molecular link between H_2O_2 and the initiation of regenerative signalling, but it could be improved and expanded upon. The time constraints of the PhD project mean that I was limited in what I could achieve, but plans for follow-on work would have focused on the following areas.

Firstly, all of my work addressing the signalling interactions of H_2O_2 relied on the use of pharmacological agents to inhibit or activate enzymes and even to visualise H_2O_2. Pharmacological methods were used initially due to the quick and easy nature of dosing to allow rapid identification of targets, but no pharmacological agent has 100% specificity and off-target effects are an accepted limitation of use. Knowing this, an effort was made to validate findings from a single drug treatment with additional treatments that would present a different set of off-target interactions. In this way I hoped to increase confidence that any phenotype observed in all treatments was due to the intended targets only, and not off-target complications. The most reliable data often comes from genetic manipulation of target molecules as this can act with much greater specificity than simple drug treatments. As mentioned in the Introduction, zebrafish are particularly useful for their genetic tractability and therefore validating my pharmacological data with genetic data is the next logical step to increase confidence in the conclusions. During my PhD I did attempt to generate a number of stable transgenic fish lines for this exact purpose, unfortunately, due to a combination of poor expression levels, non-functional transgenes, poor transmission and epigenetic silencing, none of the lines were ever established. The transgenes I synthesised and the details of the failure of the transgenic lines are outlined in Appendix B. Given the time, I would establish the following lines to strengthen my conclusions: 1) inducible dominant negative Duox (transgene provided by Mulero lab[236]) or Duox null mutant to validate all DPI/MCI-186/AA data as Duox-specific; 2)

ubiquitous HyPer3 (H_2O_2 specific fluorescent probe) to visualise H_2O_2 in a more sensitive and quantitative manner, also unlike the PFBSF dye used to visualise H_2O_2, HyPer3 detects H_2O_2 reversibly and can therefore be used to provide real-time readouts over prolonged timecourses; 3) ubiquitous GECO (Ca^{2+} specific fluorescent probe) to visualise Ca^{2+} signalling in a quantitative manner to further investigate the regulatory link between Ca^{2+} and Duox; 4) fluorescent reporter of Hh pathway – either by Hh ligand expression or pathway activation via Hh activated promoters[474] to observe timecourses of Hh pathway dynamics.

Ideally, I would have characterised the calcium regulation of Duox more completely than I had time to do here. It was not the main focus of the project and therefore took a back seat to the other work. Although Ca^{2+} chelation with BAPTA-AM showed severe inhibition of wound-induced H_2O_2, clearly demonstrating that Ca^{2+} is required for the activation of Duox, whether this regulation is direct via the Ca^{2+} binding to its EF hands, or indirectly via PKC-dependent phosphorylation of Duox remains ambiguous from my data. Attempting to reconcile my data with that of the Huttenlocher lab[122] who have previously found Duox not to be regulated by Ca^{2+}, the agent they used to block Ca^{2+} signalling (thapsigargin) works by depleting internal ER Ca^{2+} stores in order to prevent subsequent propagation of a wound-induced Ca^{2+} wave[475]. This treatment would therefore increase cytosolic Ca^{2+}, allowing Ca^{2+} dependent enzymes to bind Ca^{2+} and therefore be pre-activated and not require a second, wound-induced Ca^{2+} flash to achieve full activity. In this case, both direct Duox activation and PKC-mediated Duox activation could still proceed after thapsigargin treatment and the inhibitor would be ineffective, giving false negative results. Conflicting evidence on the effectiveness of thapsigargin in wound-induced H_2O_2 was also presented in a study from the Mulero lab which showed a partial, but significant, reduction in wound-induced H_2O_2 production and neutrophil recruitment. They went on to show that the Ca^{2+} ionophore A23187 could stimulate neutrophil recruitment to wounds via a Duox-mediated mechanism. To sum up, data from my experiments and from the Mulero lab support the hypothesis that Ca^{2+} is required to stimulate Duox-derived H_2O_2 in response to injury in the zebrafish, a finding that is consistent with mammalian studies[238–240] as well as the most detailed work carried out on the Ca^{2+} regulation of Duox in flies[216]. The only evidence against Ca^{2+} regulation of Duox in zebrafish comes from a single drug treatment which works via a mechanism that may produce false negatives and has even been subsequently demonstrated to partially inhibit Duox; therefore I conclude that the activity of Duox is dependent on Ca^{2+}. Unfortunately, even collectively, these data still do not discriminate between a direct or PKC-mediated regulation, and further work will be required to address this issue.

In addition to exploring comparisons between larval and adult fin regeneration as mentioned in the previous section, it would be interesting to investigate the mechanism by which notochord extrusion is transduced into genetic signalling. As mentioned in Chapter 5, similar mechanosensitive mechanisms have been observed in *ihh* regulation in zebrafish chondrocytes, mediated by stretch-activated ion channels[433,434] thereby identifying an immediate candidate to investigate. Initial tests could be performed with the stretch-activated channel blocker gadolinium[476], and then follow-up work with mutants or morpholino-based knockdown could confirm the specific subtype of receptor.

Furthermore, there has been evidence published that inhibition of ErbB signalling through neuregulin and PI3K results in impaired zebrafish tail regeneration with a concomitant inhibition of early notochord extrsuion[477]. It would be interesting to repeat this experiment and see if this mechanism preventing notochord extrusion also impaired Hh activation and would therefore fit into this model, or if this is unrelated to Hh pathways. Additionally, I would like to examine the effect of perturbing H_2O_2 or SFK on the activation of this signalling pathway to see if it is a downstream effector of H_2O_2 or if it represents an independent regulator mechanism for notochord extrusion.

Finally, my zebrafish fin regeneration model shares similarities with the regulatory process of zebrafish heart regeneration. Like the fin, zebrafish heart regeneration is stimulated by Hh pathway activation[478] by Hh ligand secreted from a local organising centre[414] (in this case the bulbous arteriosus – the ventricular outflow tract). In addition to this, heart regeneration also appears to be ROS dependent, mediated via stimulation of Erk1/2 signalling[124]. Although no link between the H_2O_2 and Hh signalling was investigated, it may be interesting to see if these processes are linked as they are in fin. Hh is capable of promoting Erk signalling in a variety of different cellular backgrounds[479–483], and either a direct H_2O_2 driven activation of Erk1/2, or a H_2O_2 augmented co-stimulation of Erk1/2 signalling would be consistent with the data of both studies and is therefore a tempting speculation.

7.4 Closing summary

In this thesis I aimed to address the dearth of knowledge regarding the molecular and cellular effectors of the wound-induced H_2O_2 signal and how it promotes regeneration. I have achieved this using the zebrafish larval tail regeneration as a model system in which to address molecular interactions *in vivo*. The data I have presented in this thesis has shown that wound-

induced H_2O_2 is required to activate SFKs to drive extrusion of the severed notochord following tail amputation. This process of extrusion drives the upregulation of Hh ligands which signal in a paracrine manner to the surrounding cells to activate the Hh signalling pathway, and subsequent regenerative signalling via the Wnt and FGF pathways. In addition, the pro-inflammatory role of H_2O_2 appears important to stimulate regneration indirectly as macrophages are required for sucessful regeneration; therefore H_2O_2 exerts control over multiple parallel regeneration responses.

It is interesting to note that H_2O_2 and Hh pathway activation have been identified as essential for regeneration in every organism in which they have been studied, suggesting a central and conserved role for these signals in regeneration. Furthermore, redox dependent initiation of Hh signalling from a discrete organising centre has been shown in zebrafish larval and adult tail regeneration, *Xenopus* & axolotl tail regeneration, and remains a possibility in zebrafish heart regeneration. The existence of this redox control of Hh signalling across multiple vertebrates may represent a universally conserved regeneration initiation mechanism, and assessing the level of conservation in humans will be important to identify if this would be a good candidate for therapeutic intervention. All the molecular components of regeneration appear to be well conserved in humans, therefore understanding and manipulating our wound response to mimic that of a regenerative organism may be all that is needed to induce regeneration of even complex tissues such as limbs.

Though clinical applications of this research are decades away, they will not be achieved without this groundwork and each interaction and regulatory layer we identify brings us one step closer to designing therapeutics that could transform the quality of life for millions of people worldwide. I am proud to have contributed to the growing body of literature on the subject and hope that future researchers can build upon the discoveries detailed here to achieve tangible benefits to patients' lives.

Chapter 8. Appendix A: ImageJ macros

This appendix consists of the code for each of my ImageJ macros, written in the IJ1 Macro language. They are presented for completeness as the code is written, and whilst there are some annotations within the code, there are no detailed explanation of what the macro is doing at each step and they may therefore be difficult to follow, especially with coding formatting removed.

8.1 Renaming images for blind analysis

```
setBatchMode(true);

function isImage(filename) {
extensions = newArray("tif", "tiff", "jpg", "bmp", "czi", "zvi");
result = false;
for (i=0; i<extensions.length; i++) {
if (endsWith(toLowerCase(filename), "." + extensions[i]))
result = true;
}
return result;
}

path=getDirectory("Choose a Directory");
list=getFileList(path);
outputpath=path+"Blinded\\";
File.makeDirectory(outputpath);
print("Original File,Blinded Name");
names=newArray();

for(i=0;i<list.length;i++){
if (isImage(path+list[i])) {
open(path+list[i]);

//Image analysis
rawpic=getTitle();
temp=floor(random*1000000);
for (j=0;j<names.length;j++) {
if (temp==names[j]) {
temp=temp+random;
}
}
names=Array.concat(names,temp);
rename(temp);
saveAs("Tiff",outputpath+temp+".tif");
```

```
close(temp+".tif");
print(rawpic+","+temp);
//Image analysis
}
}

selectWindow("Log");
save(outputpath+"/Blinding Key.txt");
File.rename(outputpath+"/Blinding Key.txt", outputpath+"/Blinding Key.csv");
selectWindow("Log");
run("Close");

setBatchMode(false);
exit("Macro Completed Sucessfully");
```

8.2 Quantification of wound-induced H_2O_2

```
setBatchMode(true);


function isImage(filename) {
extensions = newArray("tif", "tiff", "jpg", "bmp", "czi", "zvi");
result = false;
for (i=0; i<extensions.length; i++) {
if (endsWith(toLowerCase(filename), "." + extensions[i]))
result = true;
}
return result;
}

IJ.deleteRows(0, nResults);
setForegroundColor(255, 255, 255);
run("Set Measurements...", "area mean standard modal min shape integrated median limit
display redirect=None decimal=3");
path=getDirectory("Choose a Directory");
ROIpath=path+"Fixed Wound ROI\\";
File.makeDirectory(ROIpath);
list=getFileList(path);


for(i=0;i<list.length;i++){
if (isImage(path+list[i])) {
open(path+list[i]);

////Scaling
//for 30X zoomscope:
run("Set Scale...", "distance=701 known=1000 pixel=1 unit=micron");

//////////////////////////////////////////
////Image Analysis
```

```
//for pics with wound left, trunk right
woundlength = 50; //in microns
toUnscaled (woundlength);
rawpic = getTitle();
run("Split Channels");
close("C1-"+rawpic);
selectWindow("C2-"+rawpic);
rename(rawpic);

selectWindow(rawpic);
run("Duplicate...", "title=mask");
run("Auto Threshold", "method=Triangle white");
run("Make Binary");
run("Close-");
run("Open");
run("Fill Holes");
run("Erode");
run("Erode");
run("Erode");
run("Erode");

width = getWidth;
height = getHeight;
getPixelSize(unit, pw, ph);

ParticleMin=(50000);
ParticleMax=(3000000);
run("Analyze Particles...", "size="+ParticleMin+"-"+ParticleMax+" add");
FishCount=roiManager("count");
if (FishCount==0) {
setTool("wand");
setBatchMode("exit & display");
run("Select None");
roiManager("Show None");
waitForUser("Macro Paused", "Select the fish ROI, then click OK");
while (selectionType()==-1) {
setTool("wand");
waitForUser("Macro Paused", "Select the fish ROI, then click OK");
}
roiManager("Add");
setBatchMode(true);
}

else if (FishCount>1) {
setBatchMode("exit & display");
run("Select None");
roiManager("Deselect");
roiManager("Show None");
setTool("wand");
waitForUser("Macro Paused", "Select the fish ROI, then click OK");
while (selectionType()==-1) {
run("Select None");
```

```
roiManager("Deselect");
roiManager("Show None");
setTool("wand");
waitForUser("Macro Paused", "Select the fish ROI, then click OK");
}
roiManager("Add");
setBatchMode(true);
}

roiManager("select", (roiManager("count")-1));
roiManager("rename", "Fish");
fish = roiManager("index");
Roi.getBounds(fx,fy,fw,fh);

roiManager("select", fish);
run("Make Inverse");
Roi.setName("Background");
roiManager("Add");
roiManager("select", (roiManager("count")-1));
BG = roiManager("index");

makeRectangle(fx+1000/pw, 0, 200/ph, height);
Roi.setName("TrunkCol");
roiManager("Add");
roiManager("select", (roiManager("count")-1));
trunkcol = roiManager("index");

roiManager("select", newArray(fish, trunkcol));
roiManager("AND");
roiManager("Add");
roiManager("select", (roiManager("count")-1));
roiManager("rename", "Trunk");
trunk = roiManager("index");

roiManager("select", fish);
roiManager("Add");
roiManager("select", (roiManager("count")-1));
roiManager("rename", "Shifted");
shifted = roiManager("index");
setSelectionLocation(fx+woundlength, fy);
roiManager("Update");

roiManager("select", newArray(fish,shifted));
roiManager("AND");
roiManager("Add");
roiManager("select", (roiManager("count")-1));
roiManager("rename", "Exclude");
exclude = roiManager("index");

roiManager("select", newArray(fish,exclude));
roiManager("XOR");
roiManager("Add");
```

```
roiManager("select", (roiManager("count")-1));
roiManager("rename", "PotentialWound");
potentialwound = roiManager("index");

////////////////////////////For auto setting of wound limit
makeRectangle(fx, fy, 200/pw, fh);
Roi.setName("Gap");
roiManager("Add");
roiManager("select", (roiManager("count")-1));
gap = roiManager("index");
Roi.getBounds(gx,gy,gw,gh);
////////////////////////////For auto setting of wound limit

makeRectangle(gx, 0, gw+woundlength, height);
Roi.setName("WoundCol");
roiManager("Add");
roiManager("select", (roiManager("count")-1));
woundcol = roiManager("index");

roiManager("select", newArray(potentialwound,woundcol));
roiManager("AND");
roiManager("Add");
roiManager("select", (roiManager("count")-1));
roiManager("rename", "Wound");
wound = roiManager("index");
Roi.getBounds(wx,wy,ww,wh);

selectWindow(rawpic);
roiManager("select", wound);
roiManager("measure");
roiManager("select", trunk);
roiManager("measure");
roiManager("select", BG);
roiManager("measure");

roiManager("Deselect");
roiManager("Delete");

close(rawpic);
close("mask");
}
////Image Analysis
//////////////////////////////////////
}

setBatchMode(false);
getDateAndTime(year, month, dayOfWeek, dayOfMonth, hour, minute, second, msec);
saveAs("results", path + "Fixed Wound ROI Results - "+dayOfMonth + "-" + month+1 + "-" +
year +".csv");
selectWindow("Results");
run("Close");
exit("Macro Completed Sucessfully");
```

8.3 Quantification of WISH staining

Macros written for quantifying the area of staining following WISH required two, separate processes. The first macro sets the limits used for the RGB threshold from an input dialog box. The second macro uses these set values to analyse the images.

8.3.1 Setting the RGB threshold limits

```
Dialog.create("Select RGB Filter Parameters");
items = newArray("Pass", "Stop");
Dialog.addRadioButtonGroup("Red:", items, 1, 2, "Pass");
Dialog.addNumber("Min", 0);
Dialog.addNumber("Max", 255);
Dialog.addMessage("\n");
Dialog.addRadioButtonGroup("Green:", items, 1, 2, "Pass");
Dialog.addNumber("Min", 0);
Dialog.addNumber("Max", 255);
Dialog.addMessage("\n");
Dialog.addRadioButtonGroup("Blue:", items, 1, 2, "Pass");
Dialog.addNumber("Min", 0);
Dialog.addNumber("Max", 255);
Dialog.show;
filter=newArray(3);
low=newArray(3);
high=newArray(3);
filter[0]=Dialog.getRadioButton();
filter[1]=Dialog.getRadioButton();
filter[2]=Dialog.getRadioButton();
low[0]=Dialog.getNumber();
high[0]=Dialog.getNumber();
low[1]=Dialog.getNumber();
high[1]=Dialog.getNumber();
low[2]=Dialog.getNumber();
high[2]=Dialog.getNumber();

print("\\Clear");
print(filter[0]);
selectWindow("Log");
saveAs("text",getDirectory("macros")+"/Temp/RGBfilter0.txt");
print("\\Clear");
print(filter[1]);
selectWindow("Log");
saveAs("text",getDirectory("macros")+"/Temp/RGBfilter1.txt");
print("\\Clear");
print(filter[2]);
selectWindow("Log");
saveAs("text",getDirectory("macros")+"/Temp/RGBfilter2.txt");
```

```
print("\\Clear");
print(low[0]);
selectWindow("Log");
saveAs("text",getDirectory("macros")+"/Temp/RGBlow0.txt");
print("\\Clear");
print(low[1]);
selectWindow("Log");
saveAs("text",getDirectory("macros")+"/Temp/RGBlow1.txt");
print("\\Clear");
print(low[2]);
selectWindow("Log");
saveAs("text",getDirectory("macros")+"/Temp/RGBlow2.txt");
print("\\Clear");
print(high[0]);
selectWindow("Log");
saveAs("text",getDirectory("macros")+"/Temp/RGBhigh0.txt");
print("\\Clear");
print(high[1]);
selectWindow("Log");
saveAs("text",getDirectory("macros")+"/Temp/RGBhigh1.txt");
print("\\Clear");
print(high[2]);
selectWindow("Log");
saveAs("text",getDirectory("macros")+"/Temp/RGBhigh2.txt");
print("\\Clear");
selectWindow("Log");
run("Close");
showMessage("in situ macro","RGB filters successfully set");
```

8.3.2 Quantification of images from pre-set RGB threshold limits

```
setBatchMode(true);
function isImage(filename) {
extensions = newArray("tif", "tiff", "jpg", "bmp", "czi", "zvi");
result = false;
for (i=0; i<extensions.length; i++) {
if (endsWith(toLowerCase(filename), "." + extensions[i]))
result = true;
}
return result;
}

path=getDirectory("Choose a Directory");
list=getFileList(path);

//load RGB filter
filter=newArray(3);
low=newArray(3);
high=newArray(3);
f0=File.openAsString(getDirectory("macros")+"/Temp/RGBfilter0.txt");
```

```
f1=File.openAsString(getDirectory("macros")+"/Temp/RGBfilter1.txt");
f2=File.openAsString(getDirectory("macros")+"/Temp/RGBfilter2.txt");
l0=File.openAsString(getDirectory("macros")+"/Temp/RGBlow0.txt");
l0=parseFloat(l0);
l1=File.openAsString(getDirectory("macros")+"/Temp/RGBlow1.txt");
l1=parseFloat(l1);
l2=File.openAsString(getDirectory("macros")+"/Temp/RGBlow2.txt");
l2=parseFloat(l2);
h0=File.openAsString(getDirectory("macros")+"/Temp/RGBhigh0.txt");
h0=parseFloat(h0);
h1=File.openAsString(getDirectory("macros")+"/Temp/RGBhigh1.txt");
h1=parseFloat(h1);
h2=File.openAsString(getDirectory("macros")+"/Temp/RGBhigh2.txt");
h2=parseFloat(h2);
filter[0]=f0;
filter[1]=f1;
filter[2]=f2;
low[0]=l0;
low[1]=l1;
low[2]=l2;
high[0]=h0;
high[1]=h1;
high[2]=h2;
//load RGB filter

print("Channel,Low,High,Filter");
print("Red,"+low[0]+","+high[0]+","+filter[0]);
print("Green,"+low[1]+","+high[1]+","+filter[1]);
print("Blue,"+low[2]+","+high[2]+","+filter[2]);
print("\n");
print("Image,Area (px2),Mean Red,Mean Green,Mean Blue");

for(i=0;i<list.length;i++){
if (isImage(path+list[i])) {
open(path+list[i]);
//Image analysis

run("Set Scale...", "distance=0 known=0 pixel=1 unit=pixel");
rawpic=getTitle();
run("RGB Color");
RGBpic=getTitle();
run("Duplicate...", "title=Original");
close(rawpic);

// RGB Colour Thresholding----------


selectWindow(RGBpic);
run("RGB Stack");
run("Convert Stack to Images");
selectWindow("Red");
rename("0");
```

```
selectWindow("Green");
rename("1");
selectWindow("Blue");
rename("2");

for (j=0;j<3;j++){
selectWindow(""+j);
setThreshold(low[j], high[j]);
setOption("BlackBackground", false);
run("Convert to Mask");
if (filter[j]=="stop")run("Invert");
}
imageCalculator("AND create", "0","1");
imageCalculator("AND create", "Result of 0","2");
for (j=0;j<3;j++){
selectWindow(""+j);
close();
}
selectWindow("Result of 0");
close();
selectWindow("Result of Result of 0");
rename("RGBmask");
run("Despeckle");
// RGB Colour Thresholding----------

run("Images to Stack", "name="+rawpic+" title=[] use");
setSlice(2);
run("Invert", "slice");
setBatchMode(false);
setTool("freehand");
while (selectionType()==-1) {
waitForUser("Macro Paused", "Adjust the mask, select the ROI, then click OK to measure
area");
}
setBatchMode(true);
run("Make Inverse");
run("Fill", "stack");
run("Make Inverse");
setSlice(2);
run("Duplicate...", "title=temp");
selectWindow(rawpic);
setSlice(1);
run("Duplicate...", "title=ColourSample");
close(rawpic);
selectWindow("temp");
rename(rawpic);
run("Make Binary");
run("Set Measurements...", "area display redirect=None decimal=3");
run("Analyze Particles...", "summarize");
selectWindow("Summary");
lines = split(getInfo(), "\n");
values = split(lines[lengthOf(lines)-1], "\t");
```

```
setThreshold(255, 255);
run("Create Selection");

if (selectionType()==-1) {
print(rawpic+",0,N/A,N/A,N/A");
close("ColourSample");
close(rawpic);
}
else {

roiManager("add");
roiManager("select",(roiManager("count")-1));
roiManager("Rename", "Stain");
stain = roiManager("index");
close(rawpic);
selectWindow("ColourSample");
run("RGB Stack");
run("Convert Stack to Images");
selectWindow("Red");
roiManager("select", stain);
getStatistics(area, Rmean, min, max, std, histogram);
close("Red");
selectWindow("Green");
roiManager("select", stain);
getStatistics(area, Gmean, min, max, std, histogram);
close("Green");
selectWindow("Blue");
roiManager("select", stain);
getStatistics(area, Bmean, min, max, std, histogram);
close("Blue");
print(rawpic+","+values[2]+","+round(Rmean)+","+round(Gmean)+","+round(Bmean));
roiManager("Deselect");
roiManager("Delete");
}


//Image analysis
}
}

selectWindow("Log");
save(path+"/RGB-Threshold-Results.txt");
File.rename(path+"/RGB-Threshold-Results.txt", path+"/RGB-Threshold-Results.csv");
selectWindow("Summary");
run("Close");
selectWindow("Log");
run("Close");
setBatchMode(false);
exit("Macro Completed Sucessfully");
```

8.4 Quantification of leukocytes recruited to wounds from brightfield / mCherry 2-channel images

```
setBatchMode(true);

function isImage(filename) {
extensions = newArray("tif", "tiff", "jpg", "bmp", "czi", "zvi");
result = false;
for (i=0; i<extensions.length; i++) {
if (endsWith(toLowerCase(filename), "." + extensions[i]))
result = true;
}
return result;
}

path=getDirectory("Choose a Directory");
list=getFileList(path);
cellThreshold = 350; //min threshold for cell detection
noise1 = 400; //noise tolerance for find maxima 1
noise2 = 500; //noise tolerance for find maxima 2
noise3 = 600; //noise tolerance for find maxima 3

for(i=0;i<list.length;i++){
if (isImage(path+list[i])) {
open(path+list[i]);

//Image analysis

////Scaling
//for 30X zoomscope:
run("Set Scale...", "distance=701 known=1000 pixel=1 unit=micron");
////Scaling

rawpic=getTitle;
run("Split Channels");
c1="C1-"+rawpic;
c2="C2-"+rawpic;
selectWindow(c1);
Xoffset = 200; //value in microns. Positive value extends to the right, negative to the left
Yoffset = 0;
toUnscaled (Xoffset);
toUnscaled (Yoffset);

setBatchMode("exit and display");

makeRectangle(0, 399, 532, 274);
run("To Selection");
run("Select None");
setTool("polyline");

while (selectionType()!=6) {
```

```
waitForUser("Macro Paused", "Draw a polyline along the wound (up to 16 nodes), then click
OK");
}
getSelectionCoordinates(x,y);
z=newArray();
for (j=0; j<x.length; j++) {
z = Array.concat(z, x[j],y[j]);
}

while (z.length>32) {
waitForUser("Macro Paused", "Too many nodes selected. Re-draw the line (up to 16 nodes),
then click OK");
while (selectionType()!=6) {
waitForUser("Macro Paused", "Draw a polyline along the wound (up to 16 nodes), then click
OK");
}
getSelectionCoordinates(x,y);
z=newArray();
for (j=0; j<x.length; j++) {
z = Array.concat(z, x[j],y[j]);
}
}

setBatchMode(true);

if (z.length==4)
makePolygon(z[0],z[1],z[2],z[3],z[2]+Xoffset,z[3]+Yoffset,z[0]+Xoffset,z[1]+Yoffset);
else if (z.length==6)
makePolygon(z[0],z[1],z[2],z[3],z[4],z[5],z[4]+Xoffset,z[5]+Yoffset,z[2]+Xoffset,z[3]+Yoffset,z[0]
+Xoffset,z[1]+Yoffset);
else if (z.length==8)
makePolygon(z[0],z[1],z[2],z[3],z[4],z[5],z[6],z[7],z[6]+Xoffset,z[7]+Yoffset,z[4]+Xoffset,z[5]+Yof
fset,z[2]+Xoffset,z[3]+Yoffset,z[0]+Xoffset,z[1]+Yoffset);
else if (z.length==10)
makePolygon(z[0],z[1],z[2],z[3],z[4],z[5],z[6],z[7],z[8],z[9],z[8]+Xoffset,z[9]+Yoffset,z[6]+Xoffset
,z[7]+Yoffset,z[4]+Xoffset,z[5]+Yoffset,z[2]+Xoffset,z[3]+Yoffset,z[0]+Xoffset,z[1]+Yoffset);
else if (z.length==12)
makePolygon(z[0],z[1],z[2],z[3],z[4],z[5],z[6],z[7],z[8],z[9],z[10],z[11],z[10]+Xoffset,z[11]+Yoffs
et,z[8]+Xoffset,z[9]+Yoffset,z[6]+Xoffset,z[7]+Yoffset,z[4]+Xoffset,z[5]+Yoffset,z[2]+Xoffset,z[3]
+Yoffset,z[0]+Xoffset,z[1]+Yoffset);
else if (z.length==14)
makePolygon(z[0],z[1],z[2],z[3],z[4],z[5],z[6],z[7],z[8],z[9],z[10],z[11],z[12],z[13],z[12]+Xoffset,z
[13]+Yoffset,z[10]+Xoffset,z[11]+Yoffset,z[8]+Xoffset,z[9]+Yoffset,z[6]+Xoffset,z[7]+Yoffset,z[4]
+Xoffset,z[5]+Yoffset,z[2]+Xoffset,z[3]+Yoffset,z[0]+Xoffset,z[1]+Yoffset);
else if (z.length==16)
makePolygon(z[0],z[1],z[2],z[3],z[4],z[5],z[6],z[7],z[8],z[9],z[10],z[11],z[12],z[13],z[14],z[15],z[1
4]+Xoffset,z[15]+Yoffset,z[12]+Xoffset,z[13]+Yoffset,z[10]+Xoffset,z[11]+Yoffset,z[8]+Xoffset,z[
9]+Yoffset,z[6]+Xoffset,z[7]+Yoffset,z[4]+Xoffset,z[5]+Yoffset,z[2]+Xoffset,z[3]+Yoffset,z[0]+Xof
fset,z[1]+Yoffset);
else if (z.length==18)
makePolygon(z[0],z[1],z[2],z[3],z[4],z[5],z[6],z[7],z[8],z[9],z[10],z[11],z[12],z[13],z[14],z[15],z[1
6],z[17],z[16]+Xoffset,z[17]+Yoffset,z[14]+Xoffset,z[15]+Yoffset,z[12]+Xoffset,z[13]+Yoffset,z[1
```

```
0]+Xoffset,z[11]+Yoffset,z[8]+Xoffset,z[9]+Yoffset,z[6]+Xoffset,z[7]+Yoffset,z[4]+Xoffset,z[5]+Y
offset,z[2]+Xoffset,z[3]+Yoffset,z[0]+Xoffset,z[1]+Yoffset);
else if (z.length==20)
makePolygon(z[0],z[1],z[2],z[3],z[4],z[5],z[6],z[7],z[8],z[9],z[10],z[11],z[12],z[13],z[14],z[15],z[1
6],z[17],z[18],z[19],z[18]+Xoffset,z[19]+Yoffset,z[16]+Xoffset,z[17]+Yoffset,z[14]+Xoffset,z[15]+
Yoffset,z[12]+Xoffset,z[13]+Yoffset,z[10]+Xoffset,z[11]+Yoffset,z[8]+Xoffset,z[9]+Yoffset,z[6]+X
offset,z[7]+Yoffset,z[4]+Xoffset,z[5]+Yoffset,z[2]+Xoffset,z[3]+Yoffset,z[0]+Xoffset,z[1]+Yoffset)
;
else if (z.length==22)
makePolygon(z[0],z[1],z[2],z[3],z[4],z[5],z[6],z[7],z[8],z[9],z[10],z[11],z[12],z[13],z[14],z[15],z[1
6],z[17],z[18],z[19],z[20],z[21],z[20]+Xoffset,z[21]+Yoffset,z[18]+Xoffset,z[19]+Yoffset,z[16]+Xo
ffset,z[17]+Yoffset,z[14]+Xoffset,z[15]+Yoffset,z[12]+Xoffset,z[13]+Yoffset,z[10]+Xoffset,z[11]+
Yoffset,z[8]+Xoffset,z[9]+Yoffset,z[6]+Xoffset,z[7]+Yoffset,z[4]+Xoffset,z[5]+Yoffset,z[2]+Xoffse
t,z[3]+Yoffset,z[0]+Xoffset,z[1]+Yoffset);
else if (z.length==24)
makePolygon(z[0],z[1],z[2],z[3],z[4],z[5],z[6],z[7],z[8],z[9],z[10],z[11],z[12],z[13],z[14],z[15],z[1
6],z[17],z[18],z[19],z[20],z[21],z[22],z[23],z[22]+Xoffset,z[23]+Yoffset,z[20]+Xoffset,z[21]+Yoffs
et,z[18]+Xoffset,z[19]+Yoffset,z[16]+Xoffset,z[17]+Yoffset,z[14]+Xoffset,z[15]+Yoffset,z[12]+Xo
ffset,z[13]+Yoffset,z[10]+Xoffset,z[11]+Yoffset,z[8]+Xoffset,z[9]+Yoffset,z[6]+Xoffset,z[7]+Yoffs
et,z[4]+Xoffset,z[5]+Yoffset,z[2]+Xoffset,z[3]+Yoffset,z[0]+Xoffset,z[1]+Yoffset);
else if (z.length==26)
makePolygon(z[0],z[1],z[2],z[3],z[4],z[5],z[6],z[7],z[8],z[9],z[10],z[11],z[12],z[13],z[14],z[15],z[1
6],z[17],z[18],z[19],z[20],z[21],z[22],z[23],z[24],z[25],z[24]+Xoffset,z[25]+Yoffset,z[22]+Xoffset,
z[23]+Yoffset,z[20]+Xoffset,z[21]+Yoffset,z[18]+Xoffset,z[19]+Yoffset,z[16]+Xoffset,z[17]+Yoffs
et,z[14]+Xoffset,z[15]+Yoffset,z[12]+Xoffset,z[13]+Yoffset,z[10]+Xoffset,z[11]+Yoffset,z[8]+Xoff
set,z[9]+Yoffset,z[6]+Xoffset,z[7]+Yoffset,z[4]+Xoffset,z[5]+Yoffset,z[2]+Xoffset,z[3]+Yoffset,z[0
]+Xoffset,z[1]+Yoffset);
else if (z.length==28)
makePolygon(z[0],z[1],z[2],z[3],z[4],z[5],z[6],z[7],z[8],z[9],z[10],z[11],z[12],z[13],z[14],z[15],z[1
6],z[17],z[18],z[19],z[20],z[21],z[22],z[23],z[24],z[25],z[26],z[27],z[26]+Xoffset,z[27]+Yoffset,z[2
4]+Xoffset,z[25]+Yoffset,z[22]+Xoffset,z[23]+Yoffset,z[20]+Xoffset,z[21]+Yoffset,z[18]+Xoffset,z
[19]+Yoffset,z[16]+Xoffset,z[17]+Yoffset,z[14]+Xoffset,z[15]+Yoffset,z[12]+Xoffset,z[13]+Yoffse
t,z[10]+Xoffset,z[11]+Yoffset,z[8]+Xoffset,z[9]+Yoffset,z[6]+Xoffset,z[7]+Yoffset,z[4]+Xoffset,z[
5]+Yoffset,z[2]+Xoffset,z[3]+Yoffset,z[0]+Xoffset,z[1]+Yoffset);
else if (z.length==30)
makePolygon(z[0],z[1],z[2],z[3],z[4],z[5],z[6],z[7],z[8],z[9],z[10],z[11],z[12],z[13],z[14],z[15],z[1
6],z[17],z[18],z[19],z[20],z[21],z[22],z[23],z[24],z[25],z[26],z[27],z[28],z[29],z[28]+Xoffset,z[29]
+Yoffset,z[26]+Xoffset,z[27]+Yoffset,z[24]+Xoffset,z[25]+Yoffset,z[22]+Xoffset,z[23]+Yoffset,z[2
0]+Xoffset,z[21]+Yoffset,z[18]+Xoffset,z[19]+Yoffset,z[16]+Xoffset,z[17]+Yoffset,z[14]+Xoffset,z
[15]+Yoffset,z[12]+Xoffset,z[13]+Yoffset,z[10]+Xoffset,z[11]+Yoffset,z[8]+Xoffset,z[9]+Yoffset,z
[6]+Xoffset,z[7]+Yoffset,z[4]+Xoffset,z[5]+Yoffset,z[2]+Xoffset,z[3]+Yoffset,z[0]+Xoffset,z[1]+Yo
ffset);
else if (z.length==32)
makePolygon(z[0],z[1],z[2],z[3],z[4],z[5],z[6],z[7],z[8],z[9],z[10],z[11],z[12],z[13],z[14],z[15],z[1
6],z[17],z[18],z[19],z[20],z[21],z[22],z[23],z[24],z[25],z[26],z[27],z[28],z[29],z[30],z[31],z[30]+X
offset,z[31]+Yoffset,z[28]+Xoffset,z[29]+Yoffset,z[26]+Xoffset,z[27]+Yoffset,z[24]+Xoffset,z[25]
+Yoffset,z[22]+Xoffset,z[23]+Yoffset,z[20]+Xoffset,z[21]+Yoffset,z[18]+Xoffset,z[19]+Yoffset,z[1
6]+Xoffset,z[17]+Yoffset,z[14]+Xoffset,z[15]+Yoffset,z[12]+Xoffset,z[13]+Yoffset,z[10]+Xoffset,z
[11]+Yoffset,z[8]+Xoffset,z[9]+Yoffset,z[6]+Xoffset,z[7]+Yoffset,z[4]+Xoffset,z[5]+Yoffset,z[2]+X
offset,z[3]+Yoffset,z[0]+Xoffset,z[1]+Yoffset);
else exit("Macro aborted, too many nodes");
```

```
roiManager("Add");
roiManager("select", (roiManager("count")-1));
wound = roiManager("index");
roiManager("Rename", "Wound");
roiManager("Save", getDirectory("macros")+"/Temp/Wound.zip");
close(c1);

//Limit to particle mask for minimum size, then count maxima
selectWindow(c2);
run("Duplicate...", "title="+rawpic+"-Maxima");
run("Duplicate...", "title=Mask");
setThreshold(cellThreshold, 4095);
run("Convert to Mask");
run("Open");
run("Watershed");
roiManager("select", wound);
run("Analyze Particles...", "size=20-5000 include add");
close("Mask");
roiManager("select", wound);
roiManager("Delete");
if (roiManager("count")>=2) {
roiManager("Combine");
roiManager("Add");
}
roiManager("select", (roiManager("count")-1));
cells = roiManager("index");
roiManager("Rename", " noise tollerance "+noise1);
selectWindow(rawpic+"-Maxima");
roiManager("select", cells);
run("Find Maxima...", "noise="+noise1+" output=Count");
roiManager("select", cells);
roiManager("Rename", " noise tollerance "+noise2);
selectWindow(rawpic+"-Maxima");
roiManager("select", cells);
run("Find Maxima...", "noise="+noise2+" output=Count");
roiManager("select", cells);
roiManager("Rename", " noise tollerance "+noise3);
selectWindow(rawpic+"-Maxima");
roiManager("select", cells);
run("Find Maxima...", "noise="+noise3+" output=Count");
close(rawpic+"-Maxima");
roiManager("Deselect");
roiManager("Delete");
//Limit to particle mask for minimum size, then count maxima

//Particle count
selectWindow(c2);
rename("Particles-"+rawpic);
roiManager("Open", getDirectory("macros")+"/Temp/Wound.zip");
setThreshold(cellThreshold, 4095);
run("Convert to Mask");
run("Despeckle");
```

```
run("Open");
run("Watershed");
roiManager("select", wound);
run("Set Measurements...", "area display redirect=None decimal=3");
run("Analyze Particles...", "size=20-Infinity summarize");
close("Particles-"+rawpic);
roiManager("Deselect");
roiManager("Delete");
//Particle count

//Image analysis
}
}

selectWindow("Results");
save(path+"/Maxima Count Results.txt");
File.rename(path+"/Maxima Count Results.txt", path+"/Maxima Count Results.tsv");
run("Close");
selectWindow("Summary");
save(path+"/Particle Results.txt");
File.rename(path+"/Particle Results.txt", path+"/Particle Results.tsv");
run("Close");
selectWindow("Log");
run("Close");
setBatchMode(false);
exit("Macro Completed Sucessfully");
```

8.5 Simultaneous quantification of leukocytes recruited to wounds & *ihhb* fluorescent WISH staining

```
//setBatchMode(true);

function isImage(filename) {
extensions = newArray("tif", "tiff", "jpg", "bmp", "czi", "zvi", "oib", "oif");
result = false;
for (i=0; i<extensions.length; i++) {
if (endsWith(toLowerCase(filename), "." + extensions[i]))
result = true;
}
return result;
}

IJ.deleteRows(0, nResults);
selectWindow("Results");
run("Close");
path=getDirectory("Choose a Directory");
outputPath=path+"Output\\";
File.makeDirectory(outputPath);
multichannelPath=outputPath+"Multi-Channel Tiffs\\";
```

```
File.makeDirectory(multichannelPath);
compositePath=outputPath+"MIP-Composite\\";
File.makeDirectory(compositePath);
woundPath=outputPath+"Wound ROI\\";
File.makeDirectory(woundPath);
ihhbPath=outputPath+"ihhb ROI\\";
File.makeDirectory(ihhbPath);

cellResults=outputPath+"/Cell_Results.tsv"
summaryResults=outputPath+"/Summary_Results.tsv"

list=getFileList(path);

setForegroundColor(255, 255, 255);
setBackgroundColor(0, 0, 0);
run("3D OC Options", "volume surface nb_of_obj._voxels nb_of_surf._voxels
integrated_density mean_gray_value std_dev_gray_value median_gray_value
minimum_gray_value maximum_gray_value centroid mean_distance_to_surface
std_dev_distance_to_surface median_distance_to_surface centre_of_mass bounding_box
dots_size=5 font_size=10 show_numbers white_numbers redirect_to=none");
cellHeadings="SampleVolume (micron^3)Surface (micron^2)Nb of obj. voxelsNb of surf.
voxelsIntDenMeanStdDevMedianMinMaxXYZMean dist. to surf. (micron)SD dist. to surf.
(micron)Median dist. to surf. (micron)XMYMZMBXBYBZB-widthB-heightB-depth\n";
summaryHeadings="SampleCell CountAverage Cell SizeCell Size SDTotal Cell AreaTotal ihhb
AreaMean ihhb IntensityMedian ihhb Intensity\n";
File.saveString(cellHeadings, cellResults);
File.saveString(summaryHeadings, summaryResults);
cellThreshold=2100;
ihhbThreshold=490; //usually between 450 and 600

for(i=0;i<list.length;i++){
if (isImage(path+list[i])) {
  open(path+list[i]);

////////////////////////////////////////
////Image Analysis

/////////////////C1 Define ROI
woundlength = -107; //in microns, +ve for wound left, trunk right, -ve for trunk left, wound
right
toUnscaled (woundlength);
rawpic = getTitle();
run("Split Channels");
selectWindow("C1-"+rawpic);
run("Z Project...", "projection=[Max Intensity]");
c1max = getTitle();
close("C1-"+rawpic);
selectWindow(c1max);
run("Duplicate...", "title=mask");
run("Auto Threshold", "method=Triangle white");
setOption("BlackBackground", true);
run("Convert to Mask");
```

```
run("Invert");
run("Despeckle");
run("Fill Holes");

width = getWidth;
height = getHeight;
getPixelSize(unit, pw, ph);

ParticleMin=(50000);
ParticleMax=(200000);
run("Analyze Particles...", "size="+ParticleMin+"-"+ParticleMax+" add");
FishCount=roiManager("count");
if (FishCount==0) {
setTool("wand");
//setBatchMode(false);
run("Select None");
roiManager("Show None");
waitForUser("Macro Paused", "Select the fish ROI, then click OK");
while (selectionType()==-1) {
setTool("wand");
waitForUser("Macro Paused", "Select the fish ROI, then click OK");
}
roiManager("Add");
//setBatchMode(true);
}

else if (FishCount>1) {
//setBatchMode(false);
run("Select None");
roiManager("Deselect");
roiManager("Show None");
setTool("wand");
waitForUser("Macro Paused", "Select the fish ROI, then click OK");
while (selectionType()==-1) {
run("Select None");
roiManager("Deselect");
roiManager("Show None");
setTool("wand");
waitForUser("Macro Paused", "Select the fish ROI, then click OK");
}
roiManager("Add");
//setBatchMode(true);
}

roiManager("select", (roiManager("count")-1));
roiManager("rename", "Fish");
fish = roiManager("index");
Roi.getBounds(fx,fy,fw,fh);

roiManager("select", fish);
run("Make Inverse");
Roi.setName("Background");
```

```
roiManager("Add");
roiManager("select", (roiManager("count")-1));
BG = roiManager("index");

roiManager("select", fish);
roiManager("Add");
roiManager("select", (roiManager("count")-1));
roiManager("rename", "Shifted");
shifted = roiManager("index");
setSelectionLocation(fx+woundlength, fy);
roiManager("Update");

roiManager("select", newArray(fish,shifted));
roiManager("AND");
roiManager("Add");
roiManager("select", (roiManager("count")-1));
roiManager("rename", "Exclude");
exclude = roiManager("index");

roiManager("select", newArray(fish,exclude));
roiManager("XOR");
roiManager("Add");
roiManager("select", (roiManager("count")-1));
roiManager("rename", "PotentialWound");
potentialwound = roiManager("index");

//setBatchMode(false);
roiManager("Show None");
run("Select None");
roiManager("select", potentialwound);
run("To Selection");
run("Select None");
setTool("line");
waitForUser("Macro Paused", "Draw a line along the rostal edge of the wound, TOP TO
BOTTOM, then click OK");
while (selectionType()!=5) {
roiManager("select", potentialwound);
run("To Selection");
run("Select None");
setTool("line");
waitForUser("Macro Paused", "Draw a line along the rostal edge of the wound, TOP TO
BOTTOM, then click OK");
}
getSelectionCoordinates(x, y);
makePolygon(0,0,x[0]+woundlength,0,x[0]+woundlength,y[0],x[1]+woundlength,y[1],x[1]+wou
ndlength,height,0,height);
Roi.setName("Distal");
roiManager("Add");
roiManager("select", (roiManager("count")-1));
distal = roiManager("index");
run("Make Inverse");
Roi.setName("Woundcol");
```

```
roiManager("Add");
roiManager("select", (roiManager("count")-1));
woundcol = roiManager("index");
//setBatchMode(true);

roiManager("select", newArray(potentialwound,woundcol));
roiManager("AND");
roiManager("Add");
roiManager("select", (roiManager("count")-1));
roiManager("rename", "Wound");
wound = roiManager("index");
Roi.getBounds(wx,wy,ww,wh);
close("mask");
////////////////C1 Define ROI

////////////////C2 Cell count

selectWindow("C2-"+rawpic);
run("Duplicate...", "title=["+rawpic+" mask] duplicate");
mask = getTitle();
run("Auto Threshold", "method=RenyiEntropy white stack use_stack_histogram");
roiManager("select", wound);
run("Clear Outside", "stack");
run("Select None");
run("Despeckle", "stack");
run("Watershed", "stack");
threshold3D = 50;
min3D = 10;
max3D = 1000;
run("3D Objects Counter", "threshold="+threshold3D+" slice=1 min.="+min3D+"
max.="+max3D+" statistics");
String.copyResults;
File.append(rawpic, cellResults);
File.append(String.paste, cellResults);
cellN = nResults;
volArray = newArray(cellN);
for (iii=0; iii<cellN; iii++) {
volArray[iii]=parseFloat(getResult("Volume (micron^3)", iii));
}
Array.getStatistics(volArray, cellMin, cellMax, cellMean, cellSD);
selectWindow("Results");
run("Close");
close(mask);
selectWindow("C2-"+rawpic);
run("Z Project...", "projection=[Max Intensity]");
c2max = getTitle();
run("Duplicate...", "title=copy");
roiManager("select", wound);
run("Clear Outside");
run("Select None");
setThreshold(cellThreshold, 4095);
run("Set Measurements...", "area mean limit display redirect=None decimal=3");
```

```
run("Measure");
close("copy");
cellArea=parseFloat(getResult("Area", nResults-1));
selectWindow("Results");
run("Close");

close("C2-"+rawpic);
//////////////////C2 Cell count

//////////////////C3 intensity
selectWindow("C3-"+rawpic);
run("Z Project...", "projection=[Max Intensity]");
c3max = getTitle();
close("C3-"+rawpic);
mip = rawpic+"_Maximum Intensity Projection";
selectWindow(c3max);
rename(mip);
run("Duplicate...", "title=RGBmax");
selectWindow("RGBmax");
run("Fire");
run("RGB Color");
selectWindow(mip);
run("Duplicate...", "title=mask");
setThreshold(ihhbThreshold, 65535);
run("Convert to Mask");
run("Despeckle");
run("Invert");
run("RGB Color");
run("Concatenate...", "  title=Thresholded image1=RGBmax image2=mask image3=[-- None --
]");
setSlice(2);
//setBatchMode(false);
setTool("freehand");
while (selectionType()==-1) {
waitForUser("Macro Paused", "Adjust the mask, select the ROI, then click OK to measure");
}
//setBatchMode(true);

run("Make Inverse");
run("Fill", "stack");
run("Select None");
setSlice(2);
run("8-bit");
setThreshold(0, 0);
run("Create Selection");
skip=0;
if (selectionType()==-1) {
skip=1;
ihhbArea=0;
ihhbMean="";
ihhbMed="";
close("Thresholded");
```

```
}
else {
roiManager("Add");
roiManager("select", (roiManager("count")-1));
roiManager("rename", "ihhb");
ihhb = roiManager("index");
close("Thresholded");
selectWindow(mip);
roiManager("select", ihhb);
run("Set Measurements...", "area mean median display redirect=None decimal=3");
run("Measure");
ihhbArea=parseFloat(getResult("Area", nResults-1));
ihhbMean=parseFloat(getResult("Mean", nResults-1));
ihhbMed=parseFloat(getResult("Median", nResults-1));
selectWindow("Results");
run("Close");
}

File.append(rawpic+""+cellN+""+cellMean+""+cellSD+""+cellArea+""+ihhbArea+""+ihhbMean+
""+ihhbMed+"", summaryResults);

selectWindow(mip);
rename(c3max);
/////////////////C3 intensity

/////////////////Composite Image Output
run("Concatenate...", "  title=MultiChannelMax keep image1=["+c1max+"]
image2=["+c2max+"] image3=["+c3max+"] image4=[-- None --]");
run("Make Composite", "display=Color");
Stack.setChannel(1);
run("Blue");
Stack.setChannel(2);
run("Green");
Stack.setChannel(3);
run("Red");
run("Add Slice", "add=channel");
wait(50);
Stack.setChannel(4);
run("Grays");
roiManager("select", wound);
Stack.setChannel(4);
run("Draw", "slice");
if (skip==0) {
roiManager("select", ihhb);
Stack.setChannel(4);
run("Draw", "slice");
run("Select None");
}
saveAs("Tiff", multichannelPath+"/"+rawpic+"_MultiChannel - wound ROI & ihhb overlay.tif");
run("Make Composite");
run("Stack to RGB");
run("Select None");
```

```
saveAs("Jpeg", compositePath+"/"+rawpic+"_MIP-Composite - wound ROI & ihhb
overlay.jpg");
close();
close(rawpic+"_MultiChannel - wound ROI & ihhb overlay.tif");
close(c1max);

selectWindow(c2max);
run("Green");
run("RGB Color");
roiManager("select", wound);
run("Draw", "slice");
run("Select None");
saveAs("Jpeg", woundPath+"/"+rawpic+"_Wound ROI - cells.jpg");
close();
close(c2max);

selectWindow(c3max);
run("Red");
run("RGB Color");
roiManager("select", wound);
run("Draw", "slice");
if (skip==0) {
roiManager("select", ihhb);
run("Draw", "slice");
run("Select None");
}
saveAs("Jpeg", ihhbPath+"/"+rawpic+"_Wound ROI - ihhb.jpg");
close();
close(c3max);
/////////////////Composite Image Output

roiManager("Deselect");
roiManager("Delete");

}
}

selectWindow("ROI Manager");
run("Close");

//setBatchMode(false);
exit("Macro Completed Sucessfully");
```

Chapter 9. Appendix B: DNA construct sub-cloning & transgenic zebrafish lines

This appendix consists of details of the transgenic constructs synthesised and the screening of the subsequent transgenic lines to identify stably integrated and expressing founders. It will briefly cover the methods used as well as descriptions of each construct synthesised and details of the attempts made to raise transgenic lines from it.

9.1 Methods

9.1.1 DNA manipulation methods

DNA manipulation was carried out using standard DNA sub-cloning techniques as per manufacturer's instructions using restriction enzyme digests (with various restriction enzymes from NEB), gel extraction (with QIAquick Gel Extraction Kit; Qiagen #28704), ligation (with T4 DNA ligase; NEB #M0202) and transformation (with 10-β competent cells; NEB #C3019 or for ccdB containing constructs One Shot® ccdB Survival™ competent cells; Invitrogen #A10460). Final transgene constructs were synthesised using the Gateway LR Clonase system (Invitrogen #11791) which allows rapid modular construction of constructs using a multi-enzyme recombination system that inserts 3 fragments in a predictable order and orientation into a 4th destination plasmid.

9.1.2 Injection of transgenes

Final constructs were designed with the transgene(s) flanked by tol2 sites to allow transposon-based integration into the embryo's genome. Plasmids were injected directly into the cell of one-cell stage zebrafish embryos at a final concentration of 20ng/µL. Tol2 transposase mRNA was co-injected at a final concentration of 20ng/µL to mediate the transgenesis.

Injected embryos were raised at low density in dishes with regular removal of dead embryos and changing of the E3 media. After screening, transgene-expressing larvae were raised in tanks of ~60 to obtain balanced sex ratios.

9.2 ubi:HyPer

9.2.1 Purpose

To ubiquitously express HyPer – a H_2O_2 specific fluorescent probe – for the visualisation of H_2O_2 in a sensitive manner and in real time.

9.2.2 Construct map

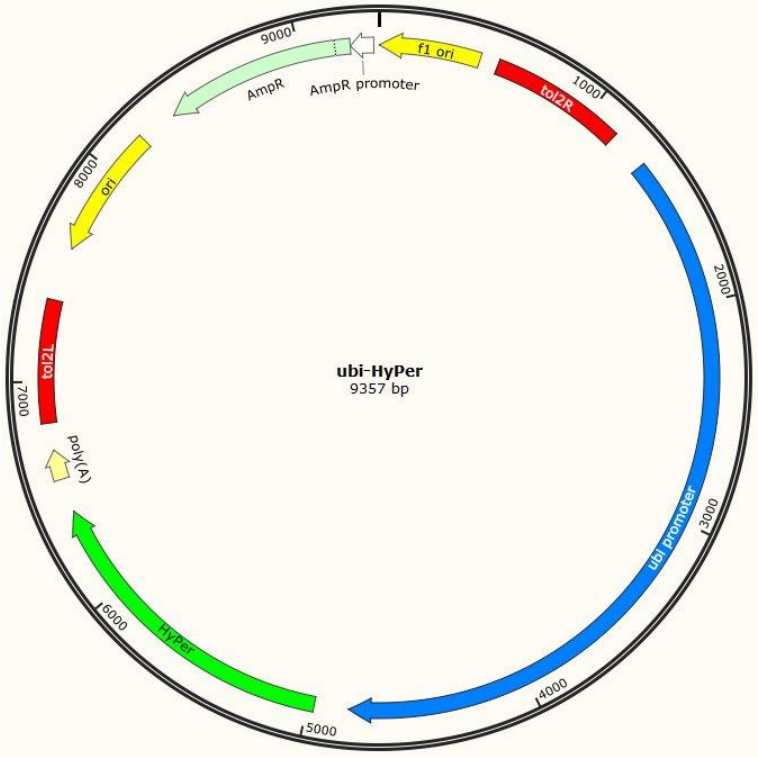

Figure 9.1 – Schematic showing the main features of the *ubi:HyPer* construct.

9.2.3 Screening

Transient expression of HyPer was strong in injected larvae, and they were raised to be screened for stable insertions.

Generation	Screened	Positive Transmission	Positive HyPer Response	Notes
F0	94	16	3 positive 13 not tested	Only larvae from 3 founders were explicitly tested for the appropriate HyPer response as fluorescence was assumed to indicate functional HyPer expression. Functional HyPer response to wound-induced H_2O_2 example timecourse can be seen in Figure 9.2 below.
F1	45	33	9	All 9 individuals transmitted a functional HyPer which responded to H_2O_2 (Figure 9.3) but only to their first brood. Subsequent broods were fluorescent but unresponsive to H_2O_2.
F2	2 tanks of 20 incrossed by marbling	100% of larvae	0% of larvae	Mixed parentage to check whole tanks quickly. All offspring showed fluorescent signal, but were unresponsive to H_2O_2. I confirmed that wound-induced was ROS still present with CellROX Deep Red fluorescent ROS probe (Thermo Fisher #C10422).
F1 (raised from H_2O_2 responsive larvae)	15	0	0	Larvae were only raised if they showed HyPer response to H_2O_2 – when they failed to transmit as adults fin clips were performed to assess HyPer response but transgene expression had ceased and no fluorescence was detectable.

Table 9.1 – Screening of the *ubi:HyPer* line.

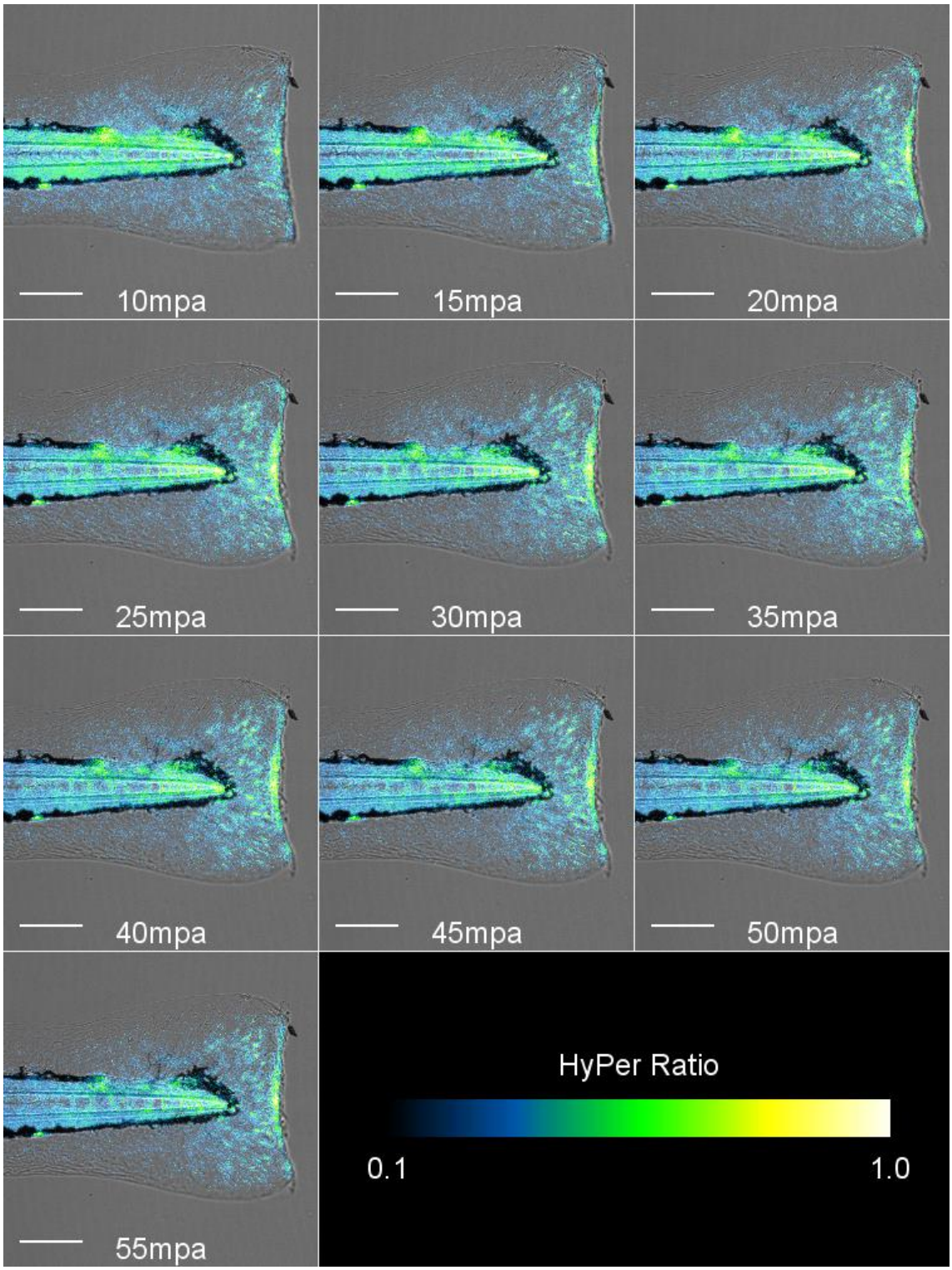

Figure 9.2 – Timecourse of HyPer response to wound-induced H_2O_2 in F0 *ubi:HyPer* larvae.
Following injection of the *ubi:HyPer* construct, mosaic expression of HyPer was seen in multiple larvae. This timecourse shows the wound-induced H_2O_2 response of the HyPer reporter at the wound edge following resection of the caudal fin-fold. Fish were excited using a 488nm laser and images are false coloured based on the ratio of emission at 500nm to that at 420nm – the HyPer ratio – with a higher number corresponding to a higher concentration of H_2O_2.

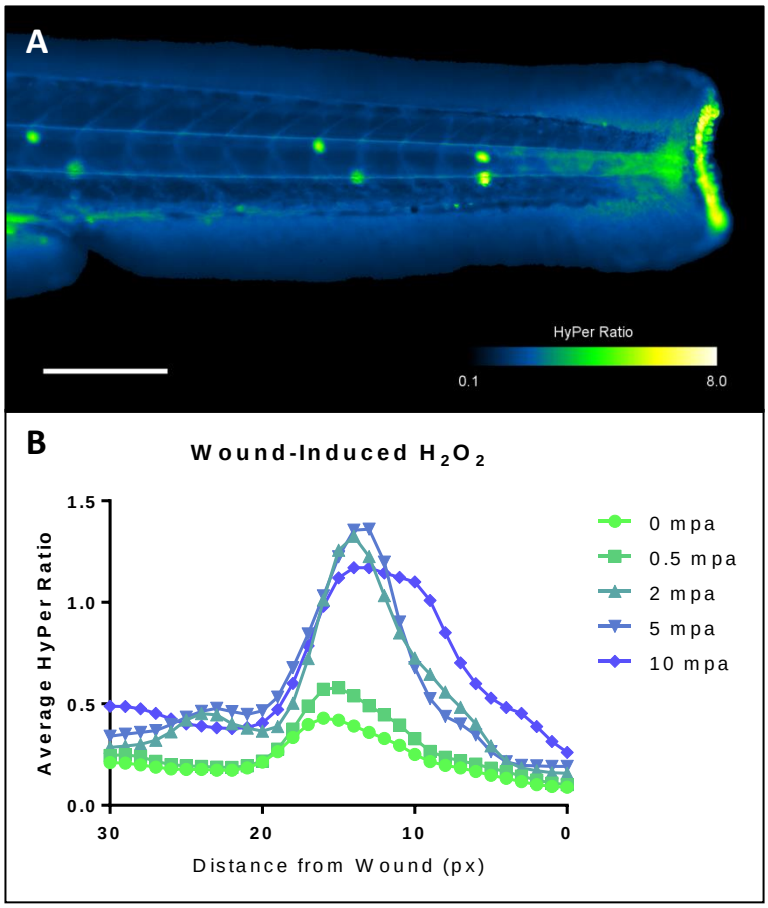

Figure 9.3 – HyPer response to wound-induced H_2O_2 in F1 *ubi:HyPer* larvae.
A) Image of an F1 *ubi:HyPer* larvae showing a robust response to wound-induced H_2O_2 with similar dynamic range as demonstrated in larvae transiently expressing HyPer after injection of HyPer mRNA[119]. **B)** Quantification of wound-induced H_2O_2 signal as HyPer ratio from the caudal tip of the wound into the trunk of the fish. The H_2O_2 signal appears to increase over time and be localised to the wound, suggesting a specific and localised detection of H_2O_2.

9.2.4 Reason for failure

Transgene appears to be silenced within individuals as well as between generations suggesting epigenetic modifications, possibly due to alterations of the redox balance of cells by HyPer reacting with ROS. Some transgenics demonstrated transmission of functional HyPer to their first brood of offspring, but then either transmitted a non-redox sensitive version of HyPer or failed to transmit any fluorescent reporter to subsequent broods. I was not able to decipher why. Some of the characteristics suggest maternal expression of HyPer in the larvae which is not maintained in somatic cells, but males were also able to transiently transmit HyPer to their

offspring so although this may have contributed, it was not the only reason for the observed effects.

9.3 β-actin:BFP/HyPer/GECO MultiLox

9.3.1 Purpose

Using Cre-Lox recombination to allow an inducible, and potentially tissue specific, mosaic expression of BFP (control cells), HyPer (for H_2O_2 visualisation) and GECO (a fluorescent Ca^{2+} reporter[484] for visualisation of intercellular Ca^{2+} levels). The βactin promoter drives BFP constituently until Cre-driven recombination excises the loxN-loxN or loxP-loxP regions to change the constituent expression to HyPer or GECO.

9.3.2 Construct map

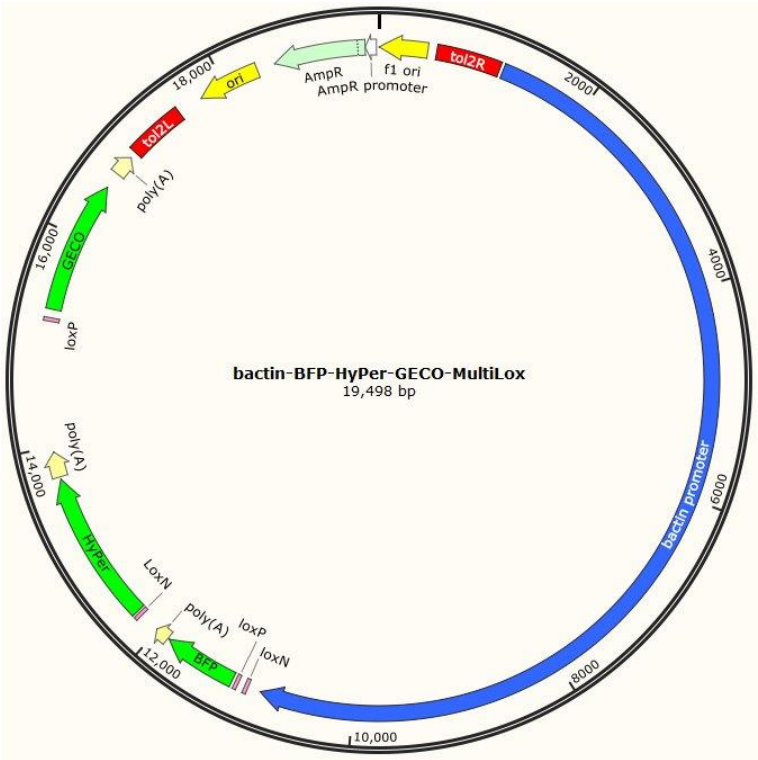

Figure 9.4 – Schematic showing the main features of the β-*actin:BFP/HyPer/GECO MultiLox* construct.

9.3.3 Screening

Transient expression of BFP was strong in injected larvae, and they were raised to be screened for stable insertions.

Generation	Screened	Positive Transmission	Positive Cre-recombination	Notes
F0	28	6 weak	0	Only 6 founders identified with weak BFP expressing offspring. No HyPer or GECO expression detected following cross with HS:Cre lines to induce recombination.

Table 9.2 – Screening of the β-*actin:BFP/HyPer/GECO MultiLox* line.

9.3.4 Reason for failure

Transmission of transgene showed only weak BFP expression and did not show any recombination-mediated expression of HyPer or GECO. Other transgenic lines being generated in the lab simultaneously with the same multi-lox backbone did not show reliable recombination and so this transgenic approach was halted.

9.4 hsp70:DN-Duox-mCherry/cmlc2:EGFP

9.4.1 Purpose

To allow inducible expression of a dominant negative form of Duox to modulate Duox activity in a more specific manner than pharmacologically possible. DN-Duox construct was obtained from the Mulero lab[236] (University of Murcia) and mCherry was sub-cloned into frame at the C-terminus to create a fluorescent fusion protein. A *cmcl2:EGFP* transgenic reporter was included in the construct to allow detection of transgenics by EGFP expression in the heart.

9.4.2 Construct map

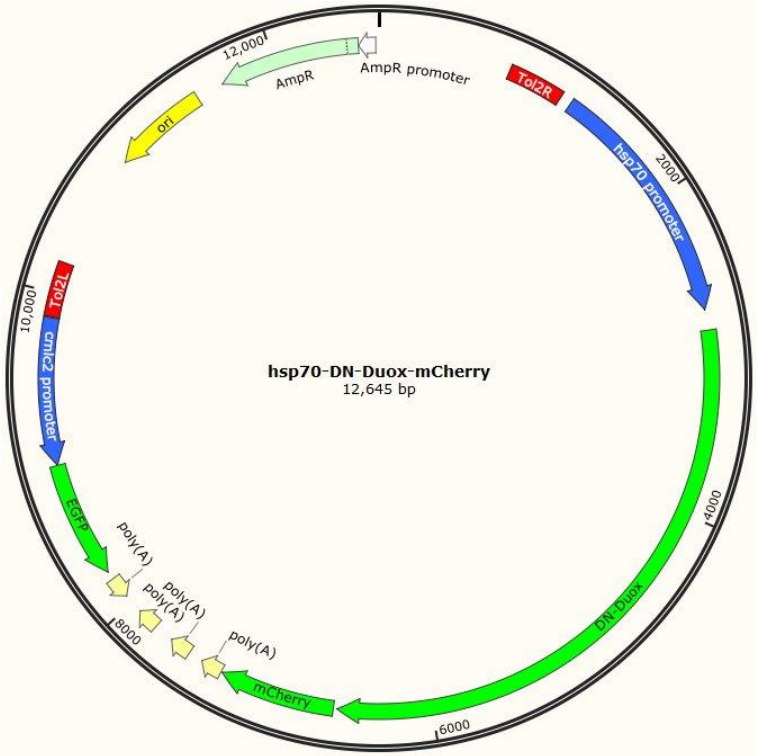

Figure 9.5 – Schematic showing the main features of the *hsp70:DN-Duox-mCherry/cmlc2:EGFP* construct.

9.4.3 Screening

Transient expression of DN-Duox-mCherry was strong after heat-shock in injected larvae. Larvae were raised to be screened for stable insertions.

Generation	Screened	Positive *cmlc2:EGFP* Expression	Positive DN-Duox-mCherry Expression	Notes
F0	72	19	1	Only 3 larvae obtained from the 1 founder, pictures and quantification is shown below. Re-mating of this founder did not yield any further offspring to raise.
F0	3 tanks of 50 incrossed by marbling	0% of larvae	0% of larvae	Mixed parentage to check whole tanks quickly. No offspring showed any transmission.

Table 9.3 – Screening of the *hsp70:DN-Duox-mCherry/cmlc2:EGFP* line.

9.4.4 Reason for failure

Very poor transmission of a functional heat-shock inducible DN-Duox-mCherry, meant only 1 founder identified from over 70 screened. This founder laid 1 brood of 3 larvae with 2 out of 3 carrying transgenic *cmlc2:EGFP* marker and showing heat-shock inducible DN-Duox-mCherry expression (Figure 9.6). This founder did not lay any further broods to raise to establish a stable transgenic line. Analysis of these offspring suggest that the transgene stimulated H_2O_2 production at the wound instead of inhibiting it (Figure 9.7), suggesting that the mCherry fusion may have interfered with the dominant negative effect of this transgene. As such, establishment of this transgenic line was halted.

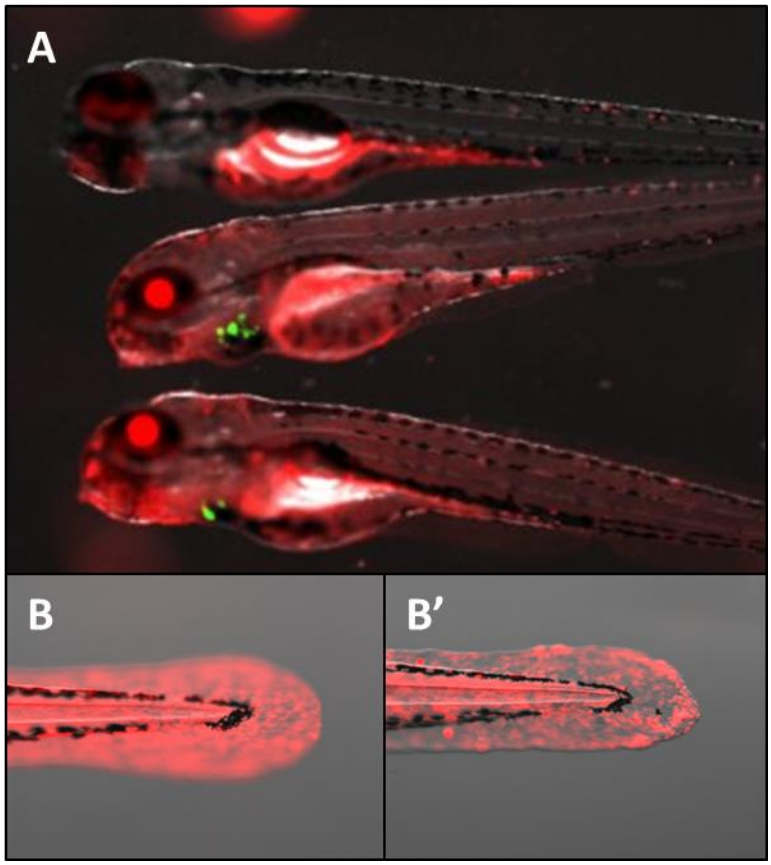

Figure 9.6 – Heat-shock induced DN-Duox-mCherry expression in F1 *hsp70:DN-Duox-mCherry/cmlc2:EGFP* larvae.
A) Image of 3 F1 larvae showing the successful transmission of *hsp70:DN-Duox-mCherry/cmlc2:EGFP* in two larvae (middle and bottom) and one non-transgenic sibling (top). Photo was taken 2hrs post heat-shock. **B)** Images of tails of both transgenic larvae 2hrs post heat-shock showing extent of DN-Duox-mCherry expression.

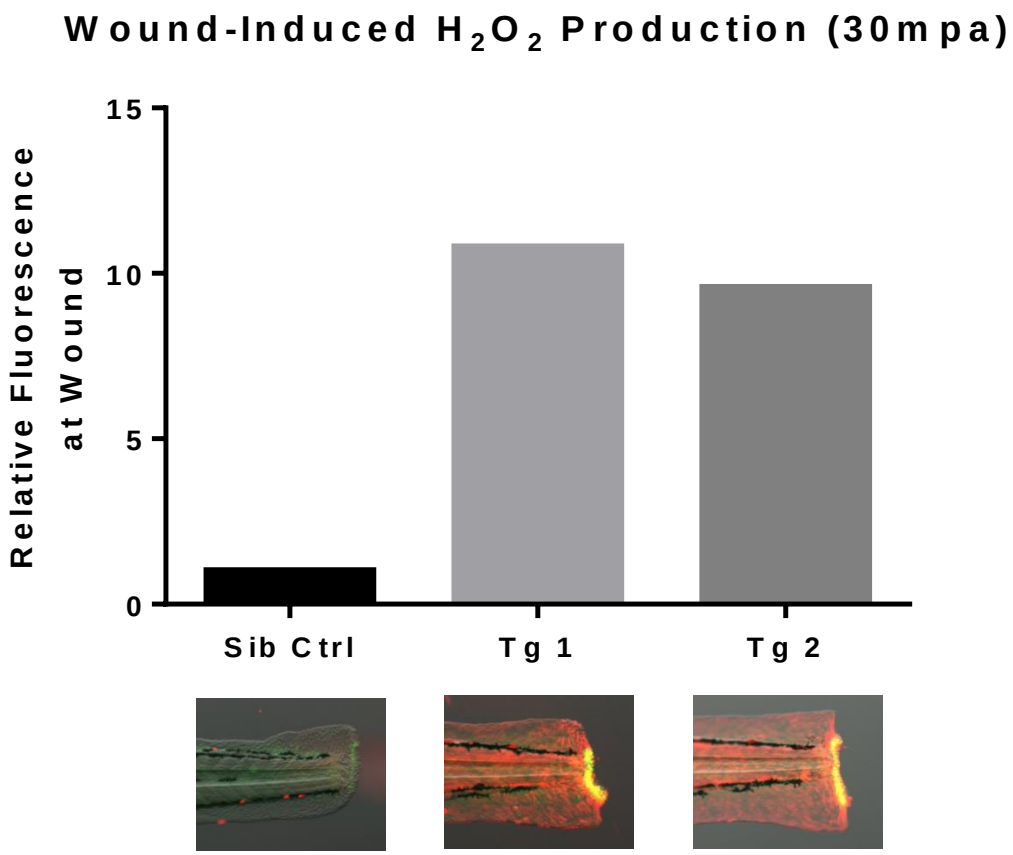

Figure 9.7 – Wound-induced H_2O_2 production in F1 *hsp70:DN-Duox-mCherry/cmlc2:EGFP* larvae.
Wound-induced H_2O_2 was quantified in F1 larvae positive for the *hsp70:DN-Duox-mCherry/cmlc2:EGFP* transgene and a control non-transgenic sibling. Larval tails were amputated 2hrs post heat-shock and the wound-induced H_2O_2 signal was quantified at 30mpa. Strong expression of DN-Duox-mCherry was observed in both transgenic larvae (see inset pictures) and the H_2O_2 signal was greatly increased in both transgenic larvae compared to the sibling control.

9.5 ubi:HyPer3

9.5.1 Purpose

To ubiquitously express HyPer3[485] – an improved version of HyPer with increased dynamic range and sensitivity – for the visualisation of H_2O_2 in a sensitive manner and in real time.

9.5.2 Construct map

Figure 9.8 – Schematic showing the main features of the *ubi:HyPer3* construct.

9.5.3 Screening

Transient expression of HyPer3 was strong in injected larvae and responded to exogenous H_2O_2 (Figure 9.9). Larvae were raised to be screened for stable insertions.

Generation	Screened	Positive Transmission	Positive HyPer3 Response	Notes
F0	34	0	0	No transmission of any fluorescent signal observed in any offspring.
F0	1 tank of 16 incrossed by marbling	0%	0%	Mixed parentage to check whole tanks quickly. No offspring showed any fluorescent signal.

Table 9.4 – Screening of the *ubi:HyPer3* line.

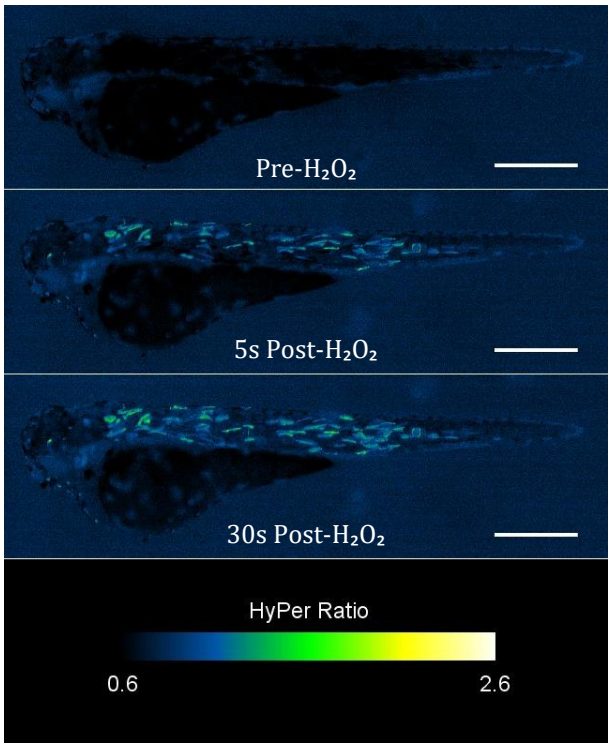

Figure 9.9 – Timecourse of HyPer response to exogenous H_2O_2 in F0 *ubi:HyPer3* larvae.
Following injection of the *ubi:HyPer3* construct, mosaic expression of HyPer3 was seen across larvae and rapidly responded to addition of exogenous H_2O_2.

9.5.4 Reason for failure

No transmission of the transgene, possible lack of tol2 mediated integration and only transient expression seen in injected larvae. Unfortunately I ran out of time to continue developing this line by re-injecting to attempt a more successful integration of the transgene.

9.6 ubi:GECO/cmlc2:EGFP

9.6.1 Purpose

To ubiquitously express GECO for the visualisation of Ca^{2+} signalling in a sensitive manner and in real time. A *cmcl2:EGFP* transgenic reporter was included in the construct to allow detection of transgenics by EGFP expression in the heart.

9.6.2 Construct map

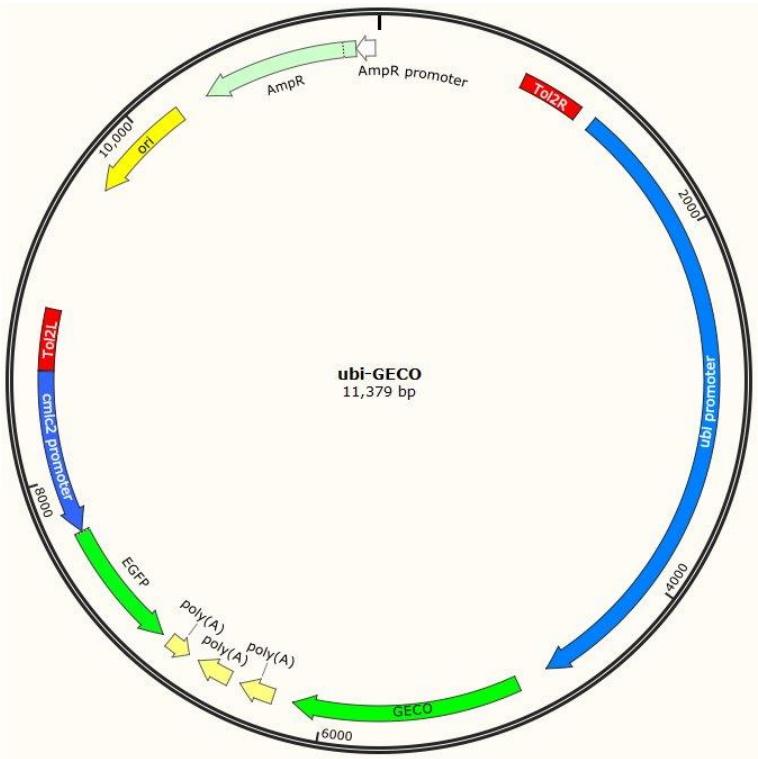

Figure 9.10 – Schematic showing the main features of the *ubi:GECO/cmlc2:EGFP* construct.

9.6.3 Screening

Transient expression of GECO was strong in injected larvae, and they were raised to be screened for stable insertions. Constituent RFP signal was strong, but Ca^{2+} responsiveness of GECO was not tested in injected larvae.

Generation	Screened	Positive *cmlc2:EGFP* Expression	Positive GECO Response	Notes
F0	18	5	0	No RFP signal detectable in any offspring, including those carrying the transgenic marker.
F0	1 tank of 30 incrossed by marbling	30% of larvae	0% of larvae	Mixed parentage to check whole tank quickly. No transgenic offspring showed any RFP signal.

Table 9.5 – Screening of the *ubi:GECO/cmlc2:EGFP* line.

9.6.4 Reason for failure

GECO RFP fluorescence was observed transiently in injected larvae but never in subsequent generations suggesting it was never transmitted. Curiously, the transgenic marker was inherited in some larvae suggesting that either GECO was selectively silenced or that the transgenic marker was inherited independently of GECO, which would be highly unlikely in all of the separate founders. Additionally, no evidence could be seen in transient expressing larvae for the RFP signal to be Ca^{2+} sensitive from observing Ca^{2+} dependent muscle twitches. Ca^{2+} signalling was not a priority of this project and so the development of this transgenic line was abandoned.

9.7 shha:mCherry-lat_arA

9.7.1 Purpose

To visualise the notochord-specific expression of *shha* by driving mCherry expression from a *shha* promoter combined with an transcriptional regulation sequence (*lat_arA*) thought to drive notochord-specific *shha* expression[486,487].

9.7.2 Construct map

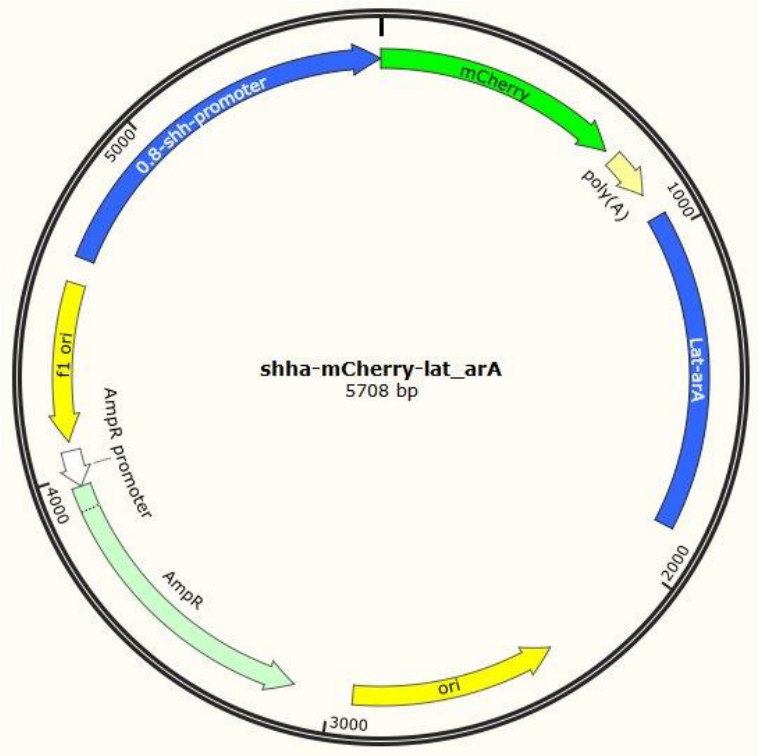

Figure 9.11 – Schematic showing the main features of the *shha:mCherry-lat_arA* construct.

9.7.3 Screening

Transient expression showed sporadic expression throughout the body and somites associated with non-integrating plasmids but also mosaic notochord-specific expression (Figure 9.12), suggesting that the construct would be an appropriate reporter for notochord-specific *shh* expression.

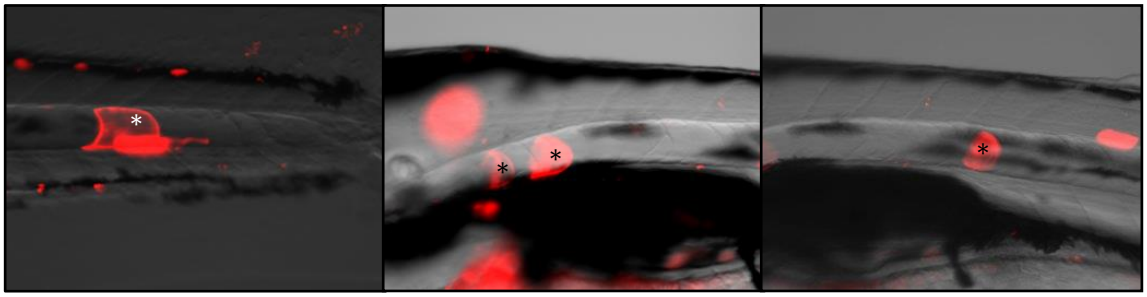

Figure 9.12 – Transient expression of mCherry in larval notochord cells.
Following injection of the *shha:mCherry-lat_arA* construct, mosaic expression of mCherry was seen in multiple cells, including notochord cells marked with asterisks.

9.7.4 Reason for failure

I only tested transient expression. Tol2-flanked construct would have to be sub-cloned and injected.

Bibliography

1. Wagner, D. E., Wang, I. E. & Reddien, P. W. Clonogenic neoblasts are pluripotent adult stem cells that underlie planarian regeneration. *Science* **332,** 811–6 (2011).
2. Singh, A., Tetreault, L., Kalsi-Ryan, S., Nouri, A. & Fehlings, M. G. Global prevalence and incidence of traumatic spinal cord injury. *Clin. Epidemiol.* **6,** 309–31 (2014).
3. Lenehan, B. *et al.* The epidemiology of traumatic spinal cord injury in British Columbia, Canada. *Spine (Phila. Pa. 1976).* **37,** 321–9 (2012).
4. Feigin, V. L. *et al.* Global and regional burden of stroke during 1990-2010: findings from the Global Burden of Disease Study 2010. *Lancet (London, England)* **383,** 245–54 (2014).
5. Savarese, G. & Lund, L. H. Global Public Health Burden of Heart Failure. *Card. Fail. Rev.* **3,** 7–11 (2017).
6. Goodell, M. A., Nguyen, H. & Shroyer, N. Somatic stem cell heterogeneity: diversity in the blood, skin and intestinal stem cell compartments. *Nat. Rev. Mol. Cell Biol.* **16,** 299–309 (2015).
7. Eriksson, P. S. *et al.* Neurogenesis in the adult human hippocampus. *Nat. Med.* **4,** 1313–7 (1998).
8. Kukekov, V. G. *et al.* Multipotent stem/progenitor cells with similar properties arise from two neurogenic regions of adult human brain. *Exp. Neurol.* **156,** 333–44 (1999).
9. Beltrami, A. P. *et al.* Adult cardiac stem cells are multipotent and support myocardial regeneration. *Cell* **114,** 763–76 (2003).
10. Bédard, A. & Parent, A. Evidence of newly generated neurons in the human olfactory bulb. *Brain Res. Dev. Brain Res.* **151,** 159–68 (2004).
11. Garcia-Lavandeira, M. *et al.* A GRFa2/Prop1/stem (GPS) cell niche in the pituitary. *PLoS One* **4,** e4815 (2009).
12. Williams, R. *et al.* Identification and clonal characterisation of a progenitor cell sub-population in normal human articular cartilage. *PLoS One* **5,** e13246 (2010).
13. Tedesco, F. S., Dellavalle, A., Diaz-Manera, J., Messina, G. & Cossu, G. Repairing skeletal muscle: regenerative potential of skeletal muscle stem cells. *J. Clin. Invest.* **120,** 11–9 (2010).
14. Brown, R. S. *et al.* A survey of liver transplantation from living adult donors in the United States. *N. Engl. J. Med.* **348,** 818–25 (2003).
15. Nagasue, N., Yukaya, H., Ogawa, Y., Kohno, H. & Nakamura, T. Human liver regeneration after major hepatic resection. A study of normal liver and livers with chronic hepatitis and cirrhosis. *Ann. Surg.* **206,** 30–9 (1987).
16. Michalopoulos, G. K. Liver Regeneration. *J. Cell Physiol.* **213,** 286–300 (2007).
17. Borowiak, M. *et al.* Met provides essential signals for liver regeneration. *Proc. Natl. Acad. Sci. U. S. A.* **101,** 10608–13 (2004).
18. Huh, C.-G. *et al.* Hepatocyte growth factor/c-met signaling pathway is required for efficient liver regeneration and repair. *Proc. Natl. Acad. Sci. U. S. A.* **101,** 4477–82 (2004).
19. Mitchell, C. *et al.* Heparin-binding epidermal growth factor-like growth factor links hepatocyte priming with cell cycle progression during liver regeneration. *J. Biol. Chem.* **280,** 2562–8 (2005).
20. Berasain, C. *et al.* Amphiregulin: an early trigger of liver regeneration in mice. *Gastroenterology* **128,** 424–32 (2005).
21. Monga, S. P., Pediaditakis, P., Mule, K., Stolz, D. B. & Michalopoulos, G. K. Changes in WNT/beta-catenin pathway during regulated growth in rat liver regeneration. *Hepatology* **33,** 1098–109 (2001).
22. Riehle, K. J., Dan, Y. Y., Campbell, J. S. & Fausto, N. New concepts in liver regeneration. *J. Gastroenterol. Hepatol.* **26,** 203–212 (2011).

23. Best, J. *et al.* Role of liver progenitors in acute liver injury. *Front. Physiol.* **4,** 1–8 (2013).
24. Fujisawa, T. Hydra regeneration and epitheliopeptides. *Dev. Dyn.* **226,** 182–9 (2003).
25. Noda, K. Reconstitution of dissociated cells of hydra. *Zool. Mag* **80,** 99–101 (1971).
26. Gierer, A. *et al.* Regeneration of hydra from reaggregated cells. *Nat. New Biol.* **239,** 98–101 (1972).
27. Tanaka, E. M. & Reddien, P. W. The Cellular Basis for Animal Regeneration. *Dev. Cell* **21,** 172–185 (2011).
28. Agata, K., Saito, Y. & Nakajima, E. Unifying principles of regeneration I: Epimorphosis versus morphallaxis. *Dev. Growth Differ.* **49,** 73–78 (2007).
29. Morgan, T. H. Experimental studies of the regeneration of Planaria maculata. *Arch. für Entwickelungsmechanik der Org.* **7,** 364–397 (1898).
30. Kobayashi, C., Watanabe, K. & Agata, K. The process of pharynx regeneration in planarians. *Dev. Biol.* **211,** 27–38 (1999).
31. Agata, K., Tanaka, T., Kobayashi, C., Kato, K. & Saitoh, Y. Intercalary regeneration in planarians. *Dev. Dyn.* **226,** 308–16 (2003).
32. Sánchez Alvarado, A. & Tsonis, P. A. Bridging the regeneration gap: genetic insights from diverse animal models. *Nat. Rev. Genet.* **7,** 873–84 (2006).
33. Brockes, J. P. & Kumar, A. Comparative aspects of animal regeneration. *Annu. Rev. Cell Dev. Biol.* **24,** 525–49 (2008).
34. Poss, K. D. Advances in understanding tissue regenerative capacity and mechanisms in animals. *Nat. Rev. Genet.* **11,** 710–22 (2010).
35. Bely, A. E. Evolutionary loss of animal regeneration: pattern and process. *Integr. Comp. Biol.* **50,** 515–27 (2010).
36. Tanaka, E. M. & Ferretti, P. Considering the evolution of regeneration in the central nervous system. *Nat. Rev. Neurosci.* **10,** 713–23 (2009).
37. King, R. S. & Newmark, P. A. The cell biology of regeneration. *J. Cell Biol.* **196,** 553–62 (2012).
38. Nachtrab, G. & Poss, K. D. Toward a blueprint for regeneration. *Development* **139,** 2639–42 (2012).
39. Tanaka, E. M. The Molecular and Cellular Choreography of Appendage Regeneration. *Cell* **165,** 1598–1608 (2016).
40. Tanaka, H. V. *et al.* A developmentally regulated switch from stem cells to dedifferentiation for limb muscle regeneration in newts. *Nat. Commun.* **7,** 11069 (2016).
41. Stoick-Cooper, C. L., Moon, R. T. & Weidinger, G. Advances in signaling in vertebrate regeneration as a prelude to regenerative medicine. *Genes Dev.* **21,** 1292–315 (2007).
42. Yoshinari, N. & Kawakami, A. Mature and juvenile tissue models of regeneration in small fish species. *Biol. Bull.* **221,** 62–78 (2011).
43. Rieger, S. & Sagasti, A. Hydrogen Peroxide Promotes Injury-Induced Peripheral Sensory Axon Regeneration in the Zebrafish Skin. *PLoS Biol* **9,** e1000621 (2011).
44. Kizil, C., Kaslin, J., Kroehne, V. & Brand, M. Adult neurogenesis and brain regeneration in zebrafish. *Dev. Neurobiol.* **72,** 429–61 (2012).
45. McCampbell, K. K. & Wingert, R. A. New tides: using zebrafish to study renal regeneration. *Transl. Res.* **163,** 109–22 (2014).
46. Kikuchi, K. Advances in understanding the mechanism of zebrafish heart regeneration. *Stem Cell Res.* (2014). doi:10.1016/j.scr.2014.07.003
47. Howe, K. *et al.* The zebrafish reference genome sequence and its relationship to the human genome. *Nature* **496,** 498–503 (2013).
48. Kalueff, A. V, Stewart, A. M. & Gerlai, R. Zebrafish as an emerging model for studying complex brain disorders. *Trends Pharmacol. Sci.* **35,** 63–75 (2014).
49. Sarmah, S. & Marrs, J. A. Zebrafish as a Vertebrate Model System to Evaluate Effects of Environmental Toxicants on Cardiac Development and Function. *Int. J. Mol. Sci.* **17,**

(2016).
50. Planchart, A. *et al.* Advancing toxicology research using in vivo high throughput toxicology with small fish models. *ALTEX* **33,** 435–452 (2016).
51. Garcia, G. R., Noyes, P. D. & Tanguay, R. L. Advancements in zebrafish applications for 21st century toxicology. *Pharmacol. Ther.* **161,** 11–21 (2016).
52. Jussila, M. & Ciruna, B. Zebrafish models of non-canonical Wnt/planar cell polarity signalling: fishing for valuable insight into vertebrate polarized cell behavior. *Wiley Interdiscip. Rev. Dev. Biol.* **6,** (2017).
53. Jerman, S. & Sun, Z. Using Zebrafish to Study Kidney Development and Disease. *Curr. Top. Dev. Biol.* **124,** 41–79 (2017).
54. Howe, D. G. *et al.* ZFIN, the Zebrafish Model Organism Database: increased support for mutants and transgenics. *Nucleic Acids Res.* **41,** D854-60 (2013).
55. Kardash, E. Current Methods in Zebrafish Research. *Mater. Methods* **2,** (2012).
56. Kelly, A. & Hurlstone, A. F. The use of RNAi technologies for gene knockdown in zebrafish. *Brief. Funct. Genomics* **10,** 189–96 (2011).
57. Knopf, F. *et al.* Bone regenerates via dedifferentiation of osteoblasts in the zebrafish fin. *Dev. Cell* **20,** 713–24 (2011).
58. Tu, S. & Johnson, S. L. Fate restriction in the growing and regenerating zebrafish fin. *Dev. Cell* **20,** 725–32 (2011).
59. Petrie, T. a, Strand, N. S., Tsung-Yang, C., Rabinowitz, J. S. & Moon, R. T. Macrophages modulate adult zebrafish tail fin regeneration. *Development* **141,** 2581–91 (2014).
60. White, R. M. *et al.* Transparent adult zebrafish as a tool for in vivo transplantation analysis. *Cell Stem Cell* **2,** 183–9 (2008).
61. Brockes, J. P. Amphibian limb regeneration: rebuilding a complex structure. *Science* **276,** 81–7 (1997).
62. Mescher, A. L. & Neff, A. W. Regenerative capacity and the developing immune system. *Adv. Biochem. Eng. Biotechnol.* **93,** 39–66 (2005).
63. Bayliss, P. E. *et al.* Chemical modulation of receptor signaling inhibits regenerative angiogenesis in adult zebrafish. *Nat. Chem. Biol.* **2,** 265–73 (2006).
64. Roy, S., Khanna, S., Nallu, K., Hunt, T. K. & Sen, C. K. Dermal wound healing is subject to redox control. *Mol. Ther.* **13,** 211–20 (2006).
65. Fan, Y. & Bergmann, A. Apoptosis-induced compensatory proliferation. The Cell is dead. Long live the Cell! *Trends Cell Biol.* **18,** 467–73 (2008).
66. Tal, T. L., Franzosa, J. a & Tanguay, R. L. Molecular signaling networks that choreograph epimorphic fin regeneration in zebrafish - a mini-review. *Gerontology* **56,** 231–40 (2010).
67. Katsuyama, T. & Paro, R. Epigenetic reprogramming during tissue regeneration. *FEBS Lett.* **585,** 1617–1624 (2011).
68. Parente, V. *et al.* Hypoxia/reoxygenation cardiac injury and regeneration in zebrafish adult heart. *PLoS One* **8,** e53748 (2013).
69. Tseng, A. & Levin, M. Cracking the bioelectric code: Probing endogenous ionic controls of pattern formation. *Commun. Integr. Biol.* **6,** e22595 (2013).
70. Varga, M. *et al.* Autophagy is required for zebrafish caudal fin regeneration. *Cell Death Differ.* **21,** 547–56 (2014).
71. Han, C. *et al.* Acute inflammation stimulates a regenerative response in the neonatal mouse heart. *Cell Res.* **25,** 1137–1151 (2015).
72. Poleo, G., Brown, C. W., Laforest, L. & Akimenko, M. A. Cell proliferation and movement during early fin regeneration in zebrafish. *Dev. Dyn.* **221,** 380–90 (2001).
73. Santos-Ruiz, L., Santamaría, J. A., Ruiz-Sánchez, J. & Becerra, J. Cell proliferation during blastema formation in the regenerating teleost fin. *Dev. Dyn.* **223,** 262–72 (2002).
74. Nakatani, Y., Nishidate, M., Fujita, M., Kawakami, A. & Kudo, A. Migration of mesenchymal cell fated to blastema is necessary for fish fin regeneration. *Dev. Growth*

Differ. **50,** 71–83 (2008).
75. Kawakami, A., Fukazawa, T. & Takeda, H. Early fin primordia of zebrafish larvae regenerate by a similar growth control mechanism with adult regeneration. *Dev. Dyn.* **231,** 693–9 (2004).
76. Schebesta, M., Lien, C.-L., Engel, F. B. & Keating, M. T. Transcriptional profiling of caudal fin regeneration in zebrafish. *ScientificWorldJournal.* **6 Suppl 1,** 38–54 (2006).
77. Lee, Y. *et al.* Maintenance of blastemal proliferation by functionally diverse epidermis in regenerating zebrafish fins. *Dev. Biol.* **331,** 270–280 (2009).
78. Poležajew, L. W. Über die Rolle des Epithels in den anfänglichen Entwicklungsstadien einer Regenerationsanlage der Extremität beim Axolotl. *Wilhelm Roux. Arch. Entwickl. Mech. Org.* **133,** 701–727 (1935).
79. Goss, R. J. Regenerative inhibition following limb amputation and immediate insertion into the body cavity. *Anat. Rec.* **126,** 15–27 (1956).
80. Goss, R. J. The regenerative responses of amputated limbs to delayed insertion into the body cavity. *Anat. Rec.* **126,** 283–97 (1956).
81. THORNTON, C. S. The effect of apical cap removal on limb regeneration in Amblystoma larvae. *J. Exp. Zool.* **134,** 357–81 (1957).
82. Poss, K. D. *et al.* Roles for Fgf signaling during zebrafish fin regeneration. *Dev. Biol.* **222,** 347–58 (2000).
83. Thummel, R. *et al.* Inhibition of zebrafish fin regeneration using in vivo electroporation of morpholinos against fgfr1 and msxb. *Dev. Dyn.* **235,** 336–46 (2006).
84. Whitehead, G. G., Makino, S., Lien, C. L. & Keating, M. T. Fgf20 Is Essential for Initiating Zebrafish Fin Regeneration. *Science (80-.).* **310,** 1957–1960 (2005).
85. Lepilina, A. *et al.* A dynamic epicardial injury response supports progenitor cell activity during zebrafish heart regeneration. *Cell* **127,** 607–19 (2006).
86. Poss, K. D., Shen, J. & Keating, M. T. Induction of lef1 during zebrafish fin regeneration. *Dev. Dyn.* **219,** 282–6 (2000).
87. Kawakami, Y. *et al.* Wnt/beta-catenin signaling regulates vertebrate limb regeneration. *Genes Dev.* **20,** 3232–3237 (2006).
88. Stoick-Cooper, C. L. *et al.* Distinct Wnt signaling pathways have opposing roles in appendage regeneration. *Development* **134,** 479–89 (2007).
89. Chen, B. *et al.* Small molecule-mediated disruption of Wnt-dependent signaling in tissue regeneration and cancer. *Nat. Chem. Biol.* **5,** 100–7 (2009).
90. Wehner, D. *et al.* Wnt/β-catenin signaling defines organizing centers that orchestrate growth and differentiation of the regenerating zebrafish caudal fin. *Cell Rep.* **6,** 467–481 (2014).
91. Garcia Romero, M. M. Molecular and Cellular Dissection of Zebrafish Larvae Tail Regeneration. (The University of Sheffield, 2016).
92. Quint, E. *et al.* Bone patterning is altered in the regenerating zebrafish caudal fin after ectopic expression of sonic hedgehog and bmp2b or exposure to cyclopamine. *Proc. Natl. Acad. Sci. U. S. A.* **99,** 8713–8718 (2002).
93. Pfefferli, C. & Jaźwińska, A. The art of fin regeneration in zebrafish. *Regeneration* **2,** 72–83 (2015).
94. Ferretti, P. & Géraudie, J. Retinoic acid-induced cell death in the wound epidermis of regenerating zebrafish fins. *Dev. Dyn.* **202,** 271–83 (1995).
95. Géraudie, J. & Ferretti, P. Correlation between RA-induced apoptosis and patterning defects in regenerating fins and limbs. *Int. J. Dev. Biol.* **41,** 529–32 (1997).
96. Mathew, L. K. *et al.* Comparative expression profiling reveals an essential role for raldh2 in epimorphic regeneration. *J. Biol. Chem.* **284,** 33642–53 (2009).
97. Blum, N. & Begemann, G. Retinoic acid signaling controls the formation, proliferation and survival of the blastema during adult zebrafish fin regeneration. *Development* **139,** 107–116 (2012).

98. Chablais, F. & Jazwinska, A. IGF signaling between blastema and wound epidermis is required for fin regeneration. *Development* **137,** 871–9 (2010).
99. Gemberling, M., Bailey, T. J., Hyde, D. R. & Poss, K. D. The zebrafish as a model for complex tissue regeneration. *Trends Genet.* **29,** 611–20 (2013).
100. Wehner, D. & Weidinger, G. Signaling networks organizing regenerative growth of the zebrafish fin. *Trends Genet.* **31,** 336–343 (2015).
101. Nechiporuk, A. & Keating, M. T. A proliferation gradient between proximal and msxb-expressing distal blastema directs zebrafish fin regeneration. *Development* **129,** 2607–17 (2002).
102. Singh, S. P., Holdway, J. E. & Poss, K. D. Regeneration of Amputated Zebrafish Fin Rays from De Novo Osteoblasts. *Dev. Cell* **22,** 879–886 (2012).
103. Stewart, S. & Stankunas, K. Limited dedifferentiation provides replacement tissue during zebrafish fin regeneration. *Dev. Biol.* **365,** 339–49 (2012).
104. Laforest, L. *et al.* Involvement of the sonic hedgehog, patched 1 and bmp2 genes in patterning of the zebrafish dermal fin rays. *Development* **125,** 4175–4184 (1998).
105. Smith, a, Avaron, F., Guay, D., Padhi, B. K. & Akimenko, M. a. Inhibition of BMP signaling during zebrafish fin regeneration disrupts fin growth and scleroblasts differentiation and function. *Dev. Biol.* **299,** 438–54 (2006).
106. Stewart, S., Gomez, A. W., Armstrong, B. E., Henner, A. & Stankunas, K. Sequential and opposing activities of Wnt and BMP coordinate zebrafish bone regeneration. *Cell Rep.* **6,** 482–498 (2014).
107. Kujawski, S. *et al.* Calcineurin regulates coordinated outgrowth of zebrafish regenerating fins. *Dev. Cell* **28,** 573–87 (2014).
108. White, J. A., Boffa, M. B., Jones, B. & Petkovich, M. A zebrafish retinoic acid receptor expressed in the regenerating caudal fin. *Development* **120,** 1861–72 (1994).
109. Géraudie, J., Monnot, M. J., Brulfert, A. & Ferretti, P. Caudal fin regeneration in wild type and long-fin mutant zebrafish is affected by retinoic acid. *Int. J. Dev. Biol.* **39,** 373–81 (1995).
110. Kragl, M. *et al.* Novel insights into the flexibility of cell and positional identity during urodele limb regeneration. *Cold Spring Harb. Symp. Quant. Biol.* **73,** 583–92 (2008).
111. Lee, Y., Grill, S., Sanchez, A., Murphy-Ryan, M. & Poss, K. D. Fgf signaling instructs position-dependent growth rate during zebrafish fin regeneration. *Development* **132,** 5173–83 (2005).
112. Bill, B. R., Petzold, A. M., Clark, K. J., Schimmenti, L. A. & Ekker, S. C. A primer for morpholino use in zebrafish. *Zebrafish* **6,** 69–77 (2009).
113. Mathew, L. K. *et al.* Unraveling tissue regeneration pathways using chemical genetics. *J. Biol. Chem.* **282,** 35202–10 (2007).
114. Gavaia, P. J. *et al.* Osteocalcin and matrix Gla protein in zebrafish (Danio rerio) and Senegal sole (Solea senegalensis): comparative gene and protein expression during larval development through adulthood. *Gene Expr. Patterns* **6,** 637–52 (2006).
115. Hadzhiev, Y. *et al.* Hedgehog signaling patterns the outgrowth of unpaired skeletal appendages in zebrafish. *BMC Dev. Biol.* **7,** 75 (2007).
116. Yoshinari, N., Ishida, T., Kudo, A. & Kawakami, A. Gene expression and functional analysis of zebrafish larval fin fold regeneration. *Dev. Biol.* **325,** 71–81 (2009).
117. Zodrow, J. M. & Tanguay, R. L. 2,3,7,8-tetrachlorodibenzo-p-dioxin inhibits zebrafish caudal fin regeneration. *Toxicol. Sci.* **76,** 151–61 (2003).
118. Mathew, L. K., Andreasen, E. A. & Tanguay, R. L. Aryl hydrocarbon receptor activation inhibits regenerative growth. *Mol. Pharmacol.* **69,** 257–65 (2006).
119. Niethammer, P., Grabher, C., Look, a T. & Mitchison, T. J. A tissue-scale gradient of hydrogen peroxide mediates rapid wound detection in zebrafish. *Nature* **459,** 996–9 (2009).
120. Gauron, C. *et al.* Sustained production of ROS triggers compensatory proliferation and is

required for regeneration to proceed. *Sci. Rep.* **3,** 2084 (2013).
121. Buchon, N., Broderick, N. A., Chakrabarti, S. & Lemaitre, B. Invasive and indigenous microbiota impact intestinal stem cell activity through multiple pathways in Drosophila. *Genes Dev.* **23,** 2333–44 (2009).
122. Yoo, S. K., Freisinger, C. M., LeBert, D. C. & Huttenlocher, A. Early redox, Src family kinase, and calcium signaling integrate wound responses and tissue regeneration in zebrafish. *J. Cell Biol.* **199,** 225–34 (2012).
123. Love, N. R. *et al.* Amputation-induced reactive oxygen species are required for successful Xenopus tadpole tail regeneration. *Nat. Cell Biol.* **15,** 222–8 (2013).
124. Han, P. *et al.* Hydrogen peroxide primes heart regeneration with a derepression mechanism. *Cell Res.* **24,** 1091–107 (2014).
125. Wenger, Y., Buzgariu, W., Reiter, S. & Galliot, B. Injury-induced immune responses in Hydra. *Semin. Immunol.* **26,** 277–94 (2014).
126. Santabárbara-Ruiz, P. *et al.* ROS-Induced JNK and p38 Signaling Is Required for Unpaired Cytokine Activation during Drosophila Regeneration. *PLoS Genet.* **11,** e1005595 (2015).
127. Hameed, L. S. *et al.* Environmental changes in oxygen tension reveal ROS-dependent neurogenesis and regeneration in the adult newt brain. *Elife* **4,** e08422 (2015).
128. Pirotte, N. *et al.* Reactive Oxygen Species in Planarian Regeneration: An Upstream Necessity for Correct Patterning and Brain Formation. *Oxid. Med. Cell. Longev.* **2015,** 392476 (2015).
129. Zhang, Q. *et al.* Reactive oxygen species generated from skeletal muscles are required for gecko tail regeneration. *Sci. Rep.* **6,** 20752 (2016).
130. Juarez, M. T., Patterson, R. a, Sandoval-Guillen, E. & McGinnis, W. Duox, Flotillin-2, and Src42A are required to activate or delimit the spread of the transcriptional response to epidermal wounds in Drosophila. *PLoS Genet.* **7,** e1002424 (2011).
131. Gorissen, S. H. *et al.* Dual oxidase-1 is required for airway epithelial cell migration and bronchiolar reepithelialization after injury. *Am. J. Respir. Cell Mol. Biol.* **48,** 337–345 (2013).
132. Fischer, A. J. *et al.* Enhancement of respiratory mucosal antiviral defenses by the oxidation of iodide. *Am. J. Respir. Cell Mol. Biol.* **45,** 874–881 (2011).
133. Klebanoff, S. J. Myeloperoxidase : friend and foe. *J. Leukoc. Biol.* **77,** 598–625 (2005).
134. Flores, M. V. *et al.* Dual oxidase in the intestinal epithelium of zebrafish larvae has anti-bacterial properties. *Biochem. Biophys. Res. Commun.* **400,** 164–168 (2010).
135. Pase, L. *et al.* Neutrophil-delivered myeloperoxidase dampens the hydrogen peroxide burst after tissue wounding in zebrafish. *Curr. Biol.* **22,** 1818–1824 (2012).
136. McCathie, G. Hydrogen Peroxide is an Essential Initiator of Regeneration in the Zebrafish Tail. (The University of Sheffield, 2013).
137. Yakushiji, N., Yokoyama, H. & Tamura, K. Repatterning in amphibian limb regeneration: A model for study of genetic and epigenetic control of organ regeneration. *Semin. Cell Dev. Biol.* **20,** 565–574 (2009).
138. King, B. L. & Yin, V. P. A conserved microRNA regulatory circuit is differentially controlled during limb/appendage regeneration. *PLoS One* **11,** 1–25 (2016).
139. Fukazawa, T., Naora, Y., Kunieda, T. & Kubo, T. Suppression of the immune response potentiates tadpole tail regeneration during the refractory period. *Development* **136,** 2323–2327 (2009).
140. Tseng, A.-S., Beane, W. S., Lemire, J. M., Masi, A. & Levin, M. Induction of vertebrate regeneration by a transient sodium current. *J. Neurosci.* **30,** 13192–200 (2010).
141. Ferreira, F., Luxardi, G., Reid, B. & Zhao, M. Early bioelectric activities mediate redox-modulated regeneration. *Development* **143,** 4582–4594 (2016).
142. Pajcini, K. V., Corbel, S. Y., Sage, J., Pomerantz, J. H. & Blau, H. M. Transient inactivation of Rb and ARF yields regenerative cells from postmitotic mammalian muscle. *Cell Stem Cell* **7,** 198–213 (2010).

143. Hesse, R. G., Kouklis, G. K., Ahituv, N. & Pomerantz, J. H. The human ARF tumor suppressor senses blastema activity and suppresses epimorphic tissue regeneration. *Elife* **4,** 1–23 (2015).
144. Masaki, H. & Ide, H. Regeneration potency of mouse limbs. *Dev. Growth Differ.* **49,** 89–98 (2007).
145. Yu, L. *et al.* BMP signaling induces digit regeneration in neonatal mice. *Development* **137,** 551–9 (2010).
146. Yu, L., Han, M., Yan, M., Lee, J. & Muneoka, K. BMP2 induces segment-specific skeletal regeneration from digit and limb amputations by establishing a new endochondral ossification center. *Dev. Biol.* **372,** 263–73 (2012).
147. Heber-Katz, E., Leferovich, J. M., Bedelbaeva, K. & Gourevitch, D. Spallanzani's mouse: a model of restoration and regeneration. *Curr. Top. Microbiol. Immunol.* **280,** 165–89 (2004).
148. McBrearty, B. A., Clark, L. D., Zhang, X. M., Blankenhorn, E. P. & Heber-Katz, E. Genetic analysis of a mammalian wound-healing trait. *Proc. Natl. Acad. Sci. U. S. A.* **95,** 11792–7 (1998).
149. Clark, L. D., Clark, R. K. & Heber-Katz, E. A new murine model for mammalian wound repair and regeneration. *Clin. Immunol. Immunopathol.* **88,** 35–45 (1998).
150. Leferovich, J. M. *et al.* Heart regeneration in adult MRL mice. *Proc. Natl. Acad. Sci. U. S. A.* **98,** 9830–5 (2001).
151. Gourevitch, D. L., Clark, L., Bedelbaeva, K., Leferovich, J. & Heber-Katz, E. Dynamic changes after murine digit amputation: The MRL mouse digit shows waves of tissue remodeling, growth, and apoptosis. *Wound Repair Regen.* **17,** 447–455 (2009).
152. Gourevitch, D. *et al.* Matrix metalloproteinase activity correlates with blastema formation in the regenerating MRL mouse ear hole model. *Dev. Dyn.* **226,** 377–87 (2003).
153. Gawronska-Kozak, B. Regeneration in the ears of immunodeficient mice: identification and lineage analysis of mesenchymal stem cells. *Tissue Eng.* **10,** 1251–65
154. Gawronska-Kozak, B. Scarless skin wound healing in FOXN1 deficient (nude) mice is associated with distinctive matrix metalloproteinase expression. *Matrix Biol.* **30,** 290–300 (2011).
155. Vinarsky, V., Atkinson, D. L., Stevenson, T. J., Keating, M. T. & Odelberg, S. J. Normal newt limb regeneration requires matrix metalloproteinase function. *Dev. Biol.* **279,** 86–98 (2005).
156. Malloch, E. L. *et al.* Gene expression profiles of lens regeneration and development in Xenopus laevis. *Dev. Dyn.* **238,** 2340–56 (2009).
157. Santosh, N. *et al.* Matrix metalloproteinase expression during blastema formation in regeneration-competent versus regeneration-deficient amphibian limbs. *Dev. Dyn.* **240,** 1127–41 (2011).
158. Bai, S. *et al.* Matrix metalloproteinase expression and function during fin regeneration in zebrafish: analysis of MT1-MMP, MMP2 and TIMP2. *Matrix Biol.* **24,** 247–60 (2005).
159. Lisse, T. S., King, B. L. & Rieger, S. Comparative transcriptomic profiling of hydrogen peroxide signaling networks in zebrafish and human keratinocytes: Implications toward conservation, migration and wound healing. *Sci. Rep.* **6,** 20328 (2016).
160. Fernando, W. A. *et al.* Wound healing and blastema formation in regenerating digit tips of adult mice. *Dev. Biol.* **350,** 301–10 (2011).
161. Matias Santos, D. *et al.* Ear wound regeneration in the African spiny mouse *Acomys cahirinus*. *Regeneration* **3,** 52–61 (2016).
162. Gawriluk, T. R. *et al.* Comparative analysis of ear-hole closure identifies epimorphic regeneration as a discrete trait in mammals. *Nat. Commun.* **7,** 1–16 (2016).
163. Seifert, A. W. *et al.* Skin shedding and tissue regeneration in African spiny mice (Acomys). *Nature* **489,** 561–565 (2012).

164. Simkin, J. *et al.* Macrophages are required to coordinate mouse digit tip regeneration. *Development* dev.150086 (2017). doi:10.1242/dev.150086
165. Simkin, J., Gawriluk, T. R., Gensel, J. C. & Seifert, A. W. Macrophages are necessary for epimorphic regeneration in African spiny mice. *Elife* **6,** 1–26 (2017).
166. Le Provost, G. S. & Pullar, C. E. β2-Adrenoceptor Activation Modulates Skin Wound Healing Processes to Reduce Scarring. *J. Invest. Dermatol.* **135,** 279–288 (2015).
167. Yannas, I. V, Tzeranis, D. S. & So, P. T. C. Regeneration of injured skin and peripheral nerves requires control of wound contraction , not scar formation Relation between Wound Contraction and Scar. 1–29 (2017). doi:10.1111/wrr.12516
168. Sham, D., Wesley, U. V., Hristova, M. & van der Vliet, A. ATP-Mediated Transactivation of the Epidermal Growth Factor Receptor in Airway Epithelial Cells Involves DUOX1-Dependent Oxidation of Src and ADAM17. *PLoS One* **8,** (2013).
169. Ma, Z. *et al.* Self-organizing human cardiac microchambers mediated by geometric confinement. *Nat. Commun.* **6,** 7413 (2015).
170. Yi, H.-G., Lee, H. & Cho, D.-W. 3D Printing of Organs-On-Chips. *Bioengineering* **4,** 10 (2017).
171. Neff, E. P. Printing cures: Organovo advances with 3D-printed liver tissue. *Lab Anim. (NY).* **46,** 57 (2017).
172. Ishida, T., Nakajima, T., Kudo, A. & Kawakami, A. Phosphorylation of Junb family proteins by the Jun N-terminal kinase supports tissue regeneration in zebrafish. *Dev. Biol.* **340,** 468–79 (2010).
173. Yoo, S. K., Starnes, T. W., Deng, Q. & Huttenlocher, A. Lyn is a redox sensor that mediates leukocyte wound attraction in vivo. *Nature* **480,** 109–12 (2011).
174. Schindelin, J. *et al.* Fiji: an open-source platform for biological-image analysis. *Nat. Methods* **9,** 676–82 (2012).
175. Thisse, B. High-resolution in situ hybridization (ISH) to whole-mount zebrafish embryos - 2010 Update. (2010). Available at: https://wiki.zfin.org/display/prot/Thisse+Lab+-+In+Situ+Hybridization+Protocol+-+2010+update. (Accessed: 18th January 2017)
176. Thisse, C. & Thisse, B. High-resolution in situ hybridization to whole-mount zebrafish embryos. *Nat. Protoc.* **3,** 59–69 (2008).
177. Qiagen. *Gene Expression and Function Studies*. *Qiagen Newsletter* (2010). doi:10.1097/INF.0b013e31825d0ebc
178. Schmittgen, T. D. & Livak, K. J. Analyzing real-time PCR data by the comparative CT method. *Nat. Protoc.* **3,** 1101–1108 (2008).
179. Ellett, F., Pase, L., Hayman, J. W., Andrianopoulos, A. & Lieschke, G. J. Mpeg1 Promoter Transgenes Direct Macrophage-Lineage Expression in Zebrafish. *Blood* **117,** (2011).
180. Sadowski, I., Ma, J., Triezenberg, S. & Ptashne, M. GAL4-VP16 is an unusually potent transcriptional activator. *Nature* **335,** 563–4 (1988).
181. Renshaw, S. & Loynes, C. A transgenic zebrafish model of neutrophilic inflammation. *Blood…* **108,** 3976–3978 (2006).
182. Gray, C. *et al.* Simultaneous intravital imaging of macrophage and neutrophil behaviour during inflammation using a novel transgenic zebrafish. *Thromb. Haemost.* **105,** 811–9 (2011).
183. Huang, M., Jia, F.-J., Yan, Y.-C., Guo, L.-H. & Li, Y.-P. Transactivated minimal E1b promoter is capable of driving the expression of short hairpin RNA. *J. Virol. Methods* **134,** 48–54 (2006).
184. Curado, S. *et al.* Conditional targeted cell ablation in zebrafish: a new tool for regeneration studies. *Dev. Dyn.* **236,** 1025–35 (2007).
185. Le Guyader, D. *et al.* Origins and unconventional behavior of neutrophils in developing zebrafish. *Blood* **111,** 132–41 (2008).
186. Colucci-Guyon, E., Tinevez, J.-Y., Renshaw, S. A. & Herbomel, P. Strategies of professional phagocytes in vivo: unlike macrophages, neutrophils engulf only surface-

associated microbes. *J. Cell Sci.* **124,** 3053–9 (2011).
187. Lin, C. S., Aebersold, R. H., Kent, S. B., Varma, M. & Leavitt, J. Molecular cloning and characterization of plastin, a human leukocyte protein expressed in transformed human fibroblasts. *Mol. Cell. Biol.* **8,** 4659–68 (1988).
188. Lin, C. S., Park, T., Zong Ping Chen & Leavitt, J. Human plastin genes. Comparative gene structure, chromosome location, and differential expression in normal and neoplastic cells. *J. Biol. Chem.* **268,** 2781–2792 (1993).
189. Redd, M. J., Kelly, G., Dunn, G., Way, M. & Martin, P. Imaging macrophage chemotaxis in vivo: studies of microtubule function in zebrafish wound inflammation. *Cell Motil. Cytoskeleton* **63,** 415–22 (2006).
190. Bolte, S. & Cordelières, F. P. A guided tour into subcellular colocalization analysis in light microscopy. *J. Microsc.* **224,** 213–32 (2006).
191. Obrig, T. G., Culp, W. J., McKeehan, W. L. & Hardesty, B. The mechanism by which cycloheximide and related glutarimide antibiotics inhibit peptide synthesis on reticulocyte ribosomes. *J. Biol. Chem.* **246,** 174–81 (1971).
192. Ellis, K., Bagwell, J. & Bagnat, M. Notochord vacuoles are lysosome-related organelles that function in axis and spine morphogenesis. *J. Cell Biol.* **200,** 667–679 (2013).
193. Feng, Y., Santoriello, C., Mione, M., Hurlstone, A. & Martin, P. Live imaging of innate immune cell sensing of transformed cells in zebrafish larvae: parallels between tumor initiation and wound inflammation. *PLoS Biol.* **8,** e1000562 (2010).
194. Desp, J. A modern hydrogen peroxide cream for wound healing. *J. Am. Acad. Dermatol.* **64,** AB173 (2011).
195. Loo, A. E. K. *et al.* Effects of Hydrogen Peroxide on Wound Healing in Mice in Relation to Oxidative Damage. *PLoS One* **7,** (2012).
196. Kanta, J. The role of hydrogen peroxide and other reactive oxygen species in wound healing. *Acta Medica (Hradec Kralove)* **54,** 97–101 (2011).
197. Oryan, A., Alemzadeh, E. & Moshiri, A. Biological properties and therapeutic activities of honey in wound healing: A narrative review and meta-analysis. *J. Tissue Viability* **25,** 98–118 (2016).
198. Finkel, T. Signal transduction by reactive oxygen species. *J. Cell Biol.* **194,** 7–15 (2011).
199. Finkel, T. Signal transduction by mitochondrial oxidants. *J. Biol. Chem.* **287,** 4434–40 (2012).
200. Stark, G. Functional consequences of oxidative membrane damage. *J. Membr. Biol.* **205,** 1–16 (2005).
201. Moreira, S., Stramer, B., Evans, I., Wood, W. & Martin, P. Prioritization of Competing Damage and Developmental Signals by Migrating Macrophages in the Drosophila Embryo. *Curr. Biol.* **20,** 464–470 (2010).
202. Wu, Y.-S. *et al.* Studies of macrophage cellular response to the extracellular hydrogen peroxide by tilapia model. *Fish Shellfish Immunol.* **36,** 459–66 (2014).
203. Csató, V. *et al.* Hydrogen peroxide elicits constriction of skeletal muscle arterioles by activating the arachidonic acid pathway. *PLoS One* **9,** e103858 (2014).
204. Sporn, P. H., Peters-Golden, M. & Simon, R. H. Hydrogen-peroxide-induced arachidonic acid metabolism in the rat alveolar macrophage. *Am. Rev. Respir. Dis.* **137,** 49–56 (1988).
205. Sporn, P. H., Marshall, T. M. & Peters-Golden, M. Hydrogen peroxide increases the availability of arachidonic acid for oxidative metabolism by inhibiting acylation into phospholipids in the alveolar macrophage. *Am. J. Respir. Cell Mol. Biol.* **7,** 307–16 (1992).
206. Hornberger, W. & Patscheke, H. Hydrogen peroxide and methyl mercury are primary stimuli of eicosanoid release in human platelets. *J. Clin. Chem. Clin. Biochem.* **27,** 567–75 (1989).
207. Stone, J. R. & Collins, T. The role of hydrogen peroxide in endothelial proliferative

responses. *Endothelium* **9,** 231–8 (2002).
208. Cho, M., Hunt, T. K. & Hussain, M. Z. Hydrogen peroxide stimulates macrophage vascular endothelial growth factor release. *Am. J. Physiol. Heart Circ. Physiol.* **280,** H2357-63 (2001).
209. Sen, C. K. *et al.* Oxidant-induced vascular endothelial growth factor expression in human keratinocytes and cutaneous wound healing. *J. Biol. Chem.* **277,** 33284–33290 (2002).
210. Mirza, R., DiPietro, L. A. & Koh, T. J. Selective and specific macrophage ablation is detrimental to wound healing in mice. *Am. J. Pathol.* **175,** 2454–62 (2009).
211. Xu, S. & Chisholm, A. D. C.elegans epidermal wounding induces a mitochondrial ROS burst that promotes wound repair. *Dev. Cell* **31,** 48–60 (2014).
212. Praetorius, H. A. & Leipziger, J. ATP release from non-excitable cells. *Purinergic Signal.* **5,** 433–46 (2009).
213. Chelliah, V. Two Models of Calcium Spiking. *BioModels Database* (2009). Available at: http://www.ebi.ac.uk/biomodels-main/static-pages.do?page=ModelMonth%2F2009-08. (Accessed: 28th February 2017)
214. Brini, M., Calì, T., Ottolini, D. & Carafoli, E. Intracellular Calcium Homeostasis and Signaling. *Met. Ions Life Sci.* **12,** 119–168 (2013).
215. Hinman, L. E., Beilman, G. J., Groehler, K. E. & Sammak, P. J. Wound-induced calcium waves in alveolar type II cells. *Am. J. Physiol.* **273,** L1242-8 (1997).
216. Razzell, W., Evans, I. R., Martin, P. & Wood, W. Calcium flashes orchestrate the wound inflammatory response through DUOX activation and hydrogen peroxide release. *Curr. Biol.* **23,** 424–9 (2013).
217. Ferris, C. D., Huganir, R. L. & Snyder, S. H. Calcium flux mediated by purified inositol 1,4,5-trisphosphate receptor in reconstituted lipid vesicles is allosterically regulated by adenine nucleotides. *Proc. Natl. Acad. Sci. U. S. A.* **87,** 2147–51 (1990).
218. Frame, M. K. & de Feijter, A. W. Propagation of mechanically induced intercellular calcium waves via gap junctions and ATP receptors in rat liver epithelial cells. *Exp. Cell Res.* **230,** 197–207 (1997).
219. Arcuino, G. *et al.* Intercellular calcium signaling mediated by point-source burst release of ATP. *Proc. Natl. Acad. Sci. U. S. A.* **99,** 9840–5 (2002).
220. Leiper, L. J. *et al.* The roles of calcium signaling and ERK1/2 phosphorylation in a Pax6+/- mouse model of epithelial wound-healing delay. *BMC Biol.* **4,** 27 (2006).
221. Chisholm, A. D. Epidermal Wound Healing in the Nematode Caenorhabditis elegans. *Adv. wound care* **4,** 264–271 (2015).
222. Cordeiro, J. V & Jacinto, A. The role of transcription-independent damage signals in the initiation of epithelial wound healing. *Nat. Rev. Mol. Cell Biol.* **14,** 249–62 (2013).
223. Klepeis, V. E., Weinger, I., Kaczmarek, E. & Trinkaus-Randall, V. P2Y receptors play a critical role in epithelial cell communication and migration. *J. Cell. Biochem.* **93,** 1115–33 (2004).
224. Aihara, E. *et al.* In vivo epithelial wound repair requires mobilization of endogenous intracellular and extracellular calcium. *J. Biol. Chem.* **288,** 33585–97 (2013).
225. Takada, H., Furuya, K. & Sokabe, M. Mechanosensitive ATP release from hemichannels and Ca^{2+} influx through TRPC6 accelerate wound closure in keratinocytes. *J. Cell Sci.* **127,** 4159–71 (2014).
226. Gault, W. J., Enyedi, B. & Niethammer, P. Osmotic surveillance mediates rapid wound closure through nucleotide release. *J. Cell Biol.* **207,** 767–82 (2014).
227. Shabir, S. & Southgate, J. Calcium signalling in wound-responsive normal human urothelial cell monolayers. *Cell Calcium* **44,** 453–64 (2008).
228. Martin, P. & Lewis, J. Actin cables and epidermal movement in embryonic wound healing. *Nature* **360,** 179–83 (1992).
229. Bement, W. M., Mandato, C. A. & Kirsch, M. N. Wound-induced assembly and closure of

an actomyosin purse string in Xenopus oocytes. *Curr. Biol.* **9,** 579–87 (1999).
230. Xu, S. & Chisholm, A. D. A Gαq-Ca^{2+} signaling pathway promotes actin-mediated epidermal wound closure in C. elegans. *Curr. Biol.* **21,** 1960–7 (2011).
231. Antunes, M., Pereira, T., Cordeiro, J. V, Almeida, L. & Jacinto, A. Coordinated waves of actomyosin flow and apical cell constriction immediately after wounding. *J. Cell Biol.* **202,** 365–79 (2013).
232. Enyedi, B., Kala, S., Nikolich-Zugich, T. & Niethammer, P. Tissue damage detection by osmotic surveillance. *Nat. Cell Biol.* **15,** 1123–30 (2013).
233. Fredholm, B. B. Purines and neutrophil leukocytes. *Gen. Pharmacol.* **28,** 345–50 (1997).
234. Chen, Y., Shukla, A., Namiki, S., Insel, P. A. & Junger, W. G. A putative osmoreceptor system that controls neutrophil function through the release of ATP, its conversion to adenosine, and activation of A2 adenosine and P2 receptors. *J. Leukoc. Biol.* **76,** 245–53 (2004).
235. Rampon, C., Gauron, C., Meda, F., Volovitch, M. & Vriz, S. Adenosine enhances progenitor cell recruitment and nerve growth via its A2B receptor during adult fin regeneration. *Purinergic Signal.* **10,** 595–602 (2014).
236. de Oliveira, S. *et al.* ATP modulates acute inflammation in vivo through dual oxidase 1-derived H2O2 production and NF-κB activation. *J. Immunol.* **192,** 5710–9 (2014).
237. Kawahara, T., Quinn, M. T. & Lambeth, J. D. Molecular evolution of the reactive oxygen-generating NADPH oxidase (Nox/Duox) family of enzymes. *BMC Evol. Biol.* **7,** 109 (2007).
238. Nakamura, Y., Ogihara, S. & Ohtaki, S. Activation by ATP of calcium-dependent NADPH-oxidase generating hydrogen peroxide in thyroid plasma membranes. *J. Biochem.* **102,** 1121–32 (1987).
239. Forteza, R. R., Salathe, M., Miot, F., Forteza, R. R. & Conner, G. E. Regulated hydrogen peroxide production by Duox in human airway epithelial cells. *Am. J. Respir. Cell Mol. Biol.* **32,** 462–9 (2005).
240. Ameziane-El-Hassani, R. *et al.* Dual oxidase-2 has an intrinsic Ca2+-dependent H 2O2-generating activity. *J. Biol. Chem.* **280,** 30046–30054 (2005).
241. Nuccitelli, R. Endogenous electric fields in embryos during development, regeneration and wound healing. *Radiat. Prot. Dosimetry* **106,** 375–83 (2003).
242. Wu, L.-J., Sweet, T.-B. & Clapham, D. E. International Union of Basic and Clinical Pharmacology. LXXVI. Current progress in the mammalian TRP ion channel family. *Pharmacol. Rev.* **62,** 381–404 (2010).
243. Berrout, J., Jin, M. & O'Neil, R. G. Critical role of TRPP2 and TRPC1 channels in stretch-induced injury of blood-brain barrier endothelial cells. *Brain Res.* **1436,** 1–12 (2012).
244. Coste, B. *et al.* Piezo1 and Piezo2 are essential components of distinct mechanically activated cation channels. *Science* **330,** 55–60 (2010).
245. Coste, B. *et al.* Piezo proteins are pore-forming subunits of mechanically activated channels. *Nature* **483,** 176–81 (2012).
246. Ge, J. *et al.* Architecture of the mammalian mechanosensitive Piezo1 channel. *Nature* **527,** 64–9 (2015).
247. Lembong, J., Sabass, B., Sun, B., Rogers, M. E. & Stone, H. A. Mechanics regulates ATP-stimulated collective calcium response in fibroblast cells. *J. R. Soc. Interface* **12,** 20150140 (2015).
248. Hoffmann, E. K., Lambert, I. H. & Pedersen, S. F. Physiology of cell volume regulation in vertebrates. *Physiol. Rev.* **89,** 193–277 (2009).
249. Ordway, R. W., Singer, J. J. & Walsh, J. V. Direct regulation of ion channels by fatty acids. *Trends Neurosci.* **14,** 96–100 (1991).
250. Adams, D. S., Masi, A. & Levin, M. H+ pump-dependent changes in membrane voltage are an early mechanism necessary and sufficient to induce Xenopus tail regeneration. *Development* **134,** 1323–35 (2007).

251. Zhao, M., Penninger, J. & Isseroff, R. R. Electrical Activation of Wound-Healing Pathways. *Adv. Skin Wound Care* **1,** 567–573 (2010).
252. Nakanishi, S. & Okazawa, M. Membrane potential-regulated Ca2+ signalling in development and maturation of mammalian cerebellar granule cells. *J. Physiol.* **575,** 389–95 (2006).
253. Nilius, B., Schwarz, G. & Droogmans, G. Control of intracellular calcium by membrane potential in human melanoma cells. *Am. J. Physiol.* **265,** C1501-10 (1993).
254. Chan, J. D. *et al.* 'Death and axes': unexpected Ca^{2+} entry phenologs predict new anti-schistosomal agents. *PLoS Pathog.* **10,** e1003942 (2014).
255. Beane, W. S., Morokuma, J., Adams, D. S. & Levin, M. A chemical genetics approach reveals H,K-ATPase-mediated membrane voltage is required for planarian head regeneration. *Chem. Biol.* **18,** 77–89 (2011).
256. Zhang, D., Chan, J. D., Nogi, T. & Marchant, J. S. Opposing roles of voltage-gated Ca2+ channels in neuronal control of regenerative patterning. *J. Neurosci.* **31,** 15983–95 (2011).
257. Wesley, U. V, Bove, P. F., Hristova, M., McCarthy, S. & van der Vliet, A. Airway epithelial cell migration and wound repair by ATP-mediated activation of dual oxidase 1. *J. Biol. Chem.* **282,** 3213–20 (2007).
258. O'Brien, G. S. *et al.* Developmentally regulated impediments to skin reinnervation by injured peripheral sensory axon terminals. *Curr. Biol.* **19,** 2086–90 (2009).
259. Simões, M. G. *et al.* Denervation impairs regeneration of amputated zebrafish fins. *BMC Dev. Biol.* **14,** 49 (2014).
260. Beck, C. W., Christen, B. & Slack, J. M. W. Molecular pathways needed for regeneration of spinal cord and muscle in a vertebrate. *Dev. Cell* **5,** 429–39 (2003).
261. Mendes, A. F., Caramona, M. M., Carvalho, A. P. & Lopes, M. C. Hydrogen peroxide mediates interleukin-1beta-induced AP-1 activation in articular chondrocytes: implications for the regulation of iNOS expression. *Cell Biol. Toxicol.* **19,** 203–14 (2003).
262. Jaquet, V., Scapozza, L., Clark, R. a, Krause, K. & Lambeth, J. D. Small-molecule NOX inhibitors: ROS-generating NADPH oxidases as therapeutic targets. *Antioxid. Redox Signal.* **11,** 2535–52 (2009).
263. O'Donnell, B. V, Tew, D. G., Jones, O. T. & England, P. J. Studies on the inhibitory mechanism of iodonium compounds with special reference to neutrophil NADPH oxidase. *Biochem. J.* **290 (Pt 1),** 41–9 (1993).
264. Tazzeo, T., Worek, F. & Janssen, L. The NADPH oxidase inhibitor diphenyleneiodonium is also a potent inhibitor of cholinesterases and the internal Ca(2+) pump. *Br. J. Pharmacol.* **158,** 790–6 (2009).
265. Aldieri, E. *et al.* Classical inhibitors of NOX NAD(P)H oxidases are not specific. *Curr. Drug Metab.* **9,** 686–96 (2008).
266. Maeda, H. *et al.* Fluorescent probes for hydrogen peroxide based on a non-oxidative mechanism. *Angew. Chem. Int. Ed. Engl.* **43,** 2389–91 (2004).
267. Mathew, L. K., Sengupta, S. S., Ladu, J., Andreasen, E. a & Tanguay, R. L. Crosstalk between AHR and Wnt signaling through R-Spondin1 impairs tissue regeneration in zebrafish. *FASEB J.* **22,** 3087–3096 (2008).
268. Heude, É., Shaikho, S. & Ekker, M. The dlx5a/dlx6a genes play essential roles in the early development of zebrafish median fin and pectoral structures. *PLoS One* **9,** 1–13 (2014).
269. Akimenko, M. a, Johnson, S. L., Westerfield, M. & Ekker, M. Differential induction of four msx homeobox genes during fin development and regeneration in zebrafish. *Development* **121,** 347–357 (1995).
270. Münch, J., González-Rajal, A. & de la Pompa, J. L. Notch regulates blastema proliferation and prevents differentiation during adult zebrafish fin regeneration. *Development* **140,** 1402–11 (2013).

271. Monteiro, J. *et al.* V-ATPase proton pumping activity is required for adult zebrafish appendage regeneration. *PLoS One* **9,** e92594 (2014).
272. Jankun, P. The Study of Molecular Interactions during Zebrafish Tail Regeneration for use in Glycotherapeutics. (The University of Sheffield, 2017).
273. Fang, M., Adams, J. S., McMahan, B. L., Brown, R. J. & Oxford, J. T. The expression patterns of minor fibrillar collagens during development in zebrafish. *Gene Expr. Patterns* **10,** 315–22
274. McCurley, A. T. & Callard, G. V. Characterization of housekeeping genes in zebrafish: male-female differences and effects of tissue type, developmental stage and chemical treatment. *BMC Mol Biol* **9,** 102 (2008).
275. Wind, S. *et al.* Comparative pharmacology of chemically distinct NADPH oxidase inhibitors. *Br. J. Pharmacol.* **161,** 885–98 (2010).
276. Heumüller, S. *et al.* Apocynin is not an inhibitor of vascular NADPH oxidases but an antioxidant. *Hypertension* **51,** 211–7 (2008).
277. Lange, S. *et al.* Platelet-derived growth factor BB stimulates vasculogenesis of embryonic stem cell-derived endothelial cells by calcium-mediated generation of reactive oxygen species. *Cardiovasc. Res.* **81,** 159–68 (2009).
278. Bayraktutan, U. Coronary microvascular endothelial cell growth regulates expression of the gene encoding p22-phox. *Free Radic. Biol. Med.* **39,** 1342–52 (2005).
279. Diatchuk, V., Lotan, O., Koshkin, V., Wikstroem, P. & Pick, E. Inhibition of NADPH oxidase activation by 4-(2-aminoethyl)-benzenesulfonyl fluoride and related compounds. *J. Biol. Chem.* **272,** 13292–301 (1997).
280. Rigutto, S. *et al.* Activation of dual oxidases Duox1 and Duox2: differential regulation mediated by camp-dependent protein kinase and protein kinase C-dependent phosphorylation. *J. Biol. Chem.* **284,** 6725–34 (2009).
281. Riobo, N. a., Haines, G. M. & Emerson, C. P. Protein kinase C-?? and mitogen-activated protein/extracellular signal-regulated kinase-1 control GLI activation in hedgehog signaling. *Cancer Res.* **66,** 839–845 (2006).
282. Taniguchi, Y., Watanabe, K. & Mochii, M. Notochord-derived hedgehog is essential for tail regeneration in Xenopus tadpole. *BMC Dev. Biol.* **14,** 27 (2014).
283. Schnapp, E., Kragl, M., Rubin, L. & Tanaka, E. M. Hedgehog signaling controls dorsoventral patterning, blastema cell proliferation and cartilage induction during axolotl tail regeneration. *Development* **132,** 3243–3253 (2005).
284. Puente, B. N. *et al.* The oxygen-rich postnatal environment induces cardiomyocyte cell-cycle arrest through DNA damage response. *Cell* **157,** 565–79 (2014).
285. Nakada, Y. *et al.* Hypoxia induces heart regeneration in adult mice. *Nature* **541,** 222–227 (2017).
286. Davalli, P., Mitic, T., Caporali, A., Lauriola, A. & D'Arca, D. ROS, Cell Senescence, and Novel Molecular Mechanisms in Aging and Age-Related Diseases. *Oxid. Med. Cell. Longev.* **2016,** 3565127 (2016).
287. Yun, M. H., Davaapil, H. & Brockes, J. P. Recurrent turnover of senescent cells during regeneration of a complex structure. *Elife* **4,** e05505 (2015).
288. Niethammer, P. Healed by our inner fish? *Oncotarget* **6,** 15732–3 (2015).
289. Hristova, M. *et al.* Identification of DUOX1-dependent redox signaling through protein S-glutathionylation in airway epithelial cells. *Redox Biol.* **2,** 436–446 (2014).
290. Chang, H. Y. *et al.* Gene expression signature of fibroblast serum response predicts human cancer progression: similarities between tumors and wounds. *PLoS Biol.* **2,** E7 (2004).
291. Lennicke, C., Rahn, J., Lichtenfels, R., Wessjohann, L. a & Seliger, B. Hydrogen peroxide - production, fate and role in redox signaling of tumor cells. *Cell Commun. Signal.* **13,** 39 (2015).
292. Li, W., Cao, L., Chen, X., Lei, J. & Ma, Q. Resveratrol inhibits hypoxia-driven ROS-induced

invasive and migratory ability of pancreatic cancer cells via suppression of the Hedgehog signaling pathway. *Oncol. Rep.* **35,** 1718–1726 (2016).
293. Ameziane-El-Hassani, R., Schlumberger, M. & Dupuy, C. NADPH oxidases: new actors in thyroid cancer? *Nat. Rev. Endocrinol.* **12,** 485–494 (2016).
294. Zhang, L. *et al.* Reactive Oxygen Species and Targeted Therapy for Pancreatic Cancer. *Oxid. Med. Cell. Longev.* **2016,** 1616781 (2016).
295. Verrax, J., Taper, H. & Buc Calderon, P. Targeting cancer cells by an oxidant-based therapy. *Curr. Mol. Pharmacol.* **1,** 80–92 (2008).
296. Glorieux, C. & Calderon, P. B. Catalase, a remarkable enzyme: targeting the oldest antioxidant enzyme to find a new cancer treatment approach. *Biol. Chem.* (2017). doi:10.1515/hsz-2017-0131
297. Feng, Y., Renshaw, S. & Martin, P. Live imaging of tumor initiation in zebrafish larvae reveals a trophic role for leukocyte-derived PGE2. *Curr. Biol.* **22,** 1253–1259 (2012).
298. Wu, F., Zhang, Y., Sun, B., McMahon, A. P. & Wang, Y. Hedgehog Signaling: From Basic Biology to Cancer Therapy. *Cell Chem. Biol.* **24,** 252–280 (2017).
299. Koury, J., Zhong, L. & Hao, J. Targeting Signaling Pathways in Cancer Stem Cells for Cancer Treatment. *Stem Cells Int.* **2017,** 2925869 (2017).
300. Gordon, R. E., Zhang, L. & Yang, Z.-J. Restore the brake on tumor progression. *Biochem. Pharmacol.* (2017). doi:10.1016/j.bcp.2017.04.003
301. Zhang, X., Tian, Y., Yang, Y. & Hao, J. Development of anticancer agents targeting the Hedgehog signaling. *Cell. Mol. Life Sci.* (2017). doi:10.1007/s00018-017-2497-x
302. Wang, J. *et al.* Berberine, a natural compound, suppresses Hedgehog signaling pathway activity and cancer growth. *BMC Cancer* **15,** 595 (2015).
303. de Oliveira-Marques, V., Cyrne, L., Marinho, H. S. & Antunes, F. A quantitative study of NF-kappaB activation by H2O2: relevance in inflammation and synergy with TNF-alpha. *J. Immunol.* **178,** 3893–902 (2007).
304. Görlach, A. Redox regulation of the coagulation cascade. *Antioxid. Redox Signal.* **7,** 1398–404
305. Fraticelli, A., Serrano, C. V, Bochner, B. S., Capogrossi, M. C. & Zweier, J. L. Hydrogen peroxide and superoxide modulate leukocyte adhesion molecule expression and leukocyte endothelial adhesion. *Biochim. Biophys. Acta* **1310,** 251–9 (1996).
306. Nishio, E. & Watanabe, Y. The involvement of reactive oxygen species and arachidonic acid in alpha 1-adrenoceptor-induced smooth muscle cell proliferation and migration. *Br. J. Pharmacol.* **121,** 665–70 (1997).
307. Yoon, S.-O., Park, S.-J., Yoon, S. Y., Yun, C.-H. & Chung, A.-S. Sustained production of H(2)O(2) activates pro-matrix metalloproteinase-2 through receptor tyrosine kinases/phosphatidylinositol 3-kinase/NF-kappa B pathway. *J. Biol. Chem.* **277,** 30271–82 (2002).
308. Frangogiannis, N. G. Inflammation in cardiac injury, repair and regeneration. *Curr. Opin. Cardiol.* **30,** 240–5 (2015).
309. Li, L., Yan, B., Shi, Y.-Q. Q., Zhang, W.-Q. Q. & Wen, Z.-L. L. Live imaging reveals differing roles of macrophages and neutrophils during zebrafish tail fin regeneration. *J. Biol. Chem.* **287,** 25353–60 (2012).
310. Shanmugam, V. K. *et al.* Prevalence of immune disease in patients with wounds presenting to a tertiary wound healing centre. *Int. Wound J.* **9,** 403–11 (2012).
311. Godoy, M. C. B. *et al.* Chest radiographic and CT manifestations of chronic granulomatous disease in adults. *AJR. Am. J. Roentgenol.* **191,** 1570–5 (2008).
312. Eckert, J. W., Abramson, S. L., Starke, J. & Brandt, M. L. The surgical implications of chronic granulomatous disease. *Am. J. Surg.* **169,** 320–3 (1995).
313. Roy, S. *et al.* Characterization of a preclinical model of chronic ischemic wound. *Physiol. Genomics* **37,** 211–24 (2009).
314. Swift, M. E., Burns, A. L., Gray, K. L. & DiPietro, L. A. Age-related alterations in the

inflammatory response to dermal injury. *J. Invest. Dermatol.* **117,** 1027–35 (2001).
315. Swift, M. E., Kleinman, H. K. & DiPietro, L. A. Impaired wound repair and delayed angiogenesis in aged mice. *Lab. Invest.* **79,** 1479–87 (1999).
316. Gosain, A. & DiPietro, L. A. Aging and wound healing. *World J. Surg.* **28,** 321–6 (2004).
317. Gu, X. *et al.* Effect of activated autologous monocytes/macrophages on wound healing in a rodent model of experimental diabetes. *Diabetes Res. Clin. Pract.* **102,** 53–9 (2013).
318. Sindrilaru, A. *et al.* An unrestrained proinflammatory M1 macrophage population induced by iron impairs wound healing in humans and mice. *J. Clin. Invest.* **121,** 985–97 (2011).
319. Bannon, P. *et al.* Diabetes induces stable intrinsic changes to myeloid cells that contribute to chronic inflammation during wound healing in mice. *Dis. Model. Mech.* **6,** 1434–1447 (2013).
320. Mirza, R. E., Fang, M. M., Ennis, W. J. & Koh, T. J. Blocking interleukin-1β induces a healing-associated wound macrophage phenotype and improves healing in type 2 diabetes. *Diabetes* **62,** 2579–87 (2013).
321. Guo, Y. *et al.* AGEs Induced Autophagy Impairs Cutaneous Wound Healing via Stimulating Macrophage Polarization to M1 in Diabetes. *Sci. Rep.* **6,** 36416 (2016).
322. Jetten, N. *et al.* Wound administration of M2-polarized macrophages does not improve murine cutaneous healing responses. *PLoS One* **9,** 1–9 (2014).
323. Miao, M. *et al.* Diabetes-impaired wound healing and altered macrophage activation: A possible pathophysiologic correlation. *Wound Repair Regen.* **20,** 203–213 (2012).
324. Gonzalez-Rosa, J. M., Martin, V., Peralta, M., Torres, M. & Mercader, N. Extensive scar formation and regression during heart regeneration after cryoinjury in zebrafish. *Development* **138,** 1663–1674 (2011).
325. Chablais, F., Veit, J., Rainer, G. & Jaźwińska, A. The zebrafish heart regenerates after cryoinjury-induced myocardial infarction. *BMC Dev. Biol.* **11,** 21 (2011).
326. Mescher, A. L., Neff, A. W. & King, M. W. Changes in the inflammatory response to injury and its resolution during the loss of regenerative capacity in developing Xenopus limbs. *PLoS One* **8,** e80477 (2013).
327. Lavine, K. J. *et al.* Distinct macrophage lineages contribute to disparate patterns of cardiac recovery and remodeling in the neonatal and adult heart. *Proc. Natl. Acad. Sci. U. S. A.* **111,** 16029–34 (2014).
328. Hasegawa, T., Nakajima, T., Ishida, T., Kudo, A. & Kawakami, A. A diffusible signal derived from hematopoietic cells supports the survival and proliferation of regenerative cells during zebrafish fin fold regeneration. *Dev. Biol.* **399,** 80–90 (2015).
329. Zou, S., Tian, C., Ge, S. & Hu, B. Neurogenesis of Retinal Ganglion Cells Is Not Essential to Visual Functional Recovery after Optic Nerve Injury in Adult Zebrafish. *PLoS One* **8,** (2013).
330. Kyritsis, N. *et al.* Acute inflammation initiates the regenerative response in the adult zebrafish brain. *Science* **338,** 1353–6 (2012).
331. Wilson, M. A., Gaze, R. M., Goodbrand, I. A. & Taylor, J. S. Regeneration in the Xenopus tadpole optic nerve is preceded by a massive macrophage/microglial response. *Anat. Embryol. (Berl).* **186,** 75–89 (1992).
332. Aurora, A. B. *et al.* Macrophages are required for neonatal heart regeneration. *J. Clin. Invest.* **124,** 1382–92 (2014).
333. Godwin, J. W., Pinto, A. R. & Rosenthal, N. a. Macrophages are required for adult salamander limb regeneration. *Proc. Natl. Acad. Sci. U. S. A.* **110,** 9415–20 (2013).
334. Streilein, J. W. Ocular immune privilege: the eye takes a dim but practical view of immunity and inflammation. *J. Leukoc. Biol.* **74,** 179–85 (2003).
335. Tsonis, P. A., Madhavan, M., Tancous, E. E. & Del Rio-Tsonis, K. A newt's eye view of lens regeneration. *Int. J. Dev. Biol.* **48,** 975–80 (2004).
336. Suetsugu-Maki, R. *et al.* Lens regeneration in axolotl: new evidence of developmental

plasticity. *BMC Biol.* **10,** 103 (2012).
337. Wan, J., Ramachandran, R. & Goldman, D. HB-EGF is necessary and sufficient for Müller glia dedifferentiation and retina regeneration. *Dev. Cell* **22,** 334–47 (2012).
338. Loubaki, L., Tremblay, T. & Bazin, R. In vivo depletion of leukocytes and platelets following injection of T cell-specific antibodies into mice. *J. Immunol. Methods* **393,** 38–44 (2013).
339. de Preux Charles, A.-S., Bise, T., Baier, F., Marro, J. & Jaźwińska, A. Distinct effects of inflammation on preconditioning and regeneration of the adult zebrafish heart. *Open Biol.* **6,** (2016).
340. Miura, S., Takahashi, Y., Satoh, A. & Endo, T. Skeletal callus formation is a nerve-independent regenerative response to limb amputation in mice and Xenopus. *Regeneration* **2,** 202–216 (2015).
341. Van Rooijen, N. & Sanders, A. Liposome mediated depletion of macrophages: mechanism of action, preparation of liposomes and applications. *J. Immunol. Methods* **174,** 83–93 (1994).
342. Yakatan, G. J. *et al.* Clodronate kinetics and bioavailability. *Clin. Pharmacol. Ther.* **31,** 402–410 (1982).
343. Berg, J. T., Lee, S. T., Thepen, T., Lee, C. Y. & Tsan, M. F. Depletion of alveolar macrophages by liposome-encapsulated dichloromethylene diphosphonate. *J. Appl. Physiol.* **74,** 2812–9 (1993).
344. Frith, J. C., Mönkkönen, J., Auriola, S., Mönkkönen, H. & Rogers, M. J. The molecular mechanism of action of the antiresorptive and antiinflammatory drug clodronate: evidence for the formation in vivo of a metabolite that inhibits bone resorption and causes osteoclast and macrophage apoptosis. *Arthritis Rheum.* **44,** 2201–10 (2001).
345. Keller, A., Sweeney, S. T., Zars, T., O'Kane, C. J. & Heisenberg, M. Targeted expression of tetanus neurotoxin interferes with behavioral responses to sensory input in Drosophila. *J. Neurobiol.* **50,** 221–33 (2002).
346. McGuire, S. E., Roman, G. & Davis, R. L. Gene expression systems in Drosophila: a synthesis of time and space. *Trends Genet.* **20,** 384–91 (2004).
347. Lewandoski, M. Conditional control of gene expression in the mouse. *Nat. Rev. Genet.* **2,** 743–55 (2001).
348. Kok, F. O. *et al.* Reverse genetic screening reveals poor correlation between morpholino-induced and mutant phenotypes in zebrafish. *Dev. Cell* **32,** 97–108 (2015).
349. Davison, J. M. *et al.* Transactivation from Gal4-VP16 transgenic insertions for tissue-specific cell labeling and ablation in zebrafish. *Dev. Biol.* **304,** 811–24 (2007).
350. Brand, A. H. & Perrimon, N. Targeted gene expression as a means of altering cell fates and generating dominant phenotypes. *Development* **118,** 401–15 (1993).
351. Tidball, J. G. & Wehling-Henricks, M. Macrophages promote muscle membrane repair and muscle fibre growth and regeneration during modified muscle loading in mice in vivo. *J. Physiol.* **578,** 327–36 (2007).
352. London, A. *et al.* Neuroprotection and progenitor cell renewal in the injured adult murine retina requires healing monocyte-derived macrophages. *J. Exp. Med.* **208,** 23–39 (2011).
353. Parichy, D. M., Ransom, D. G., Paw, B., Zon, L. I. & Johnson, S. L. An orthologue of the kit-related gene fms is required for development of neural crest-derived xanthophores and a subpopulation of adult melanocytes in the zebrafish, Danio rerio. *Development* **127,** 3031–44 (2000).
354. Herbomel, P., Thisse, B. & Thisse, C. Zebrafish early macrophages colonize cephalic mesenchyme and developing brain, retina, and epidermis through a M-CSF receptor-dependent invasive process. *Dev. Biol.* **238,** 274–88 (2001).
355. Akitake, C. M., Macurak, M., Halpern, M. E. & Goll, M. G. Transgenerational analysis of transcriptional silencing in zebrafish. *Dev. Biol.* **352,** 191–201 (2011).

356. McCormack, R., de Armas, L. R., Shiratsuchi, M., Ramos, J. E. & Podack, E. R. Inhibition of intracellular bacterial replication in fibroblasts is dependent on the perforin-like protein (perforin-2) encoded by macrophage-expressed gene 1. *J. Innate Immun.* **5,** 185–94 (2013).
357. Zakrzewska, A. *et al.* Macrophage-specific gene functions in Spi1-directed innate immunity. *Blood* **116,** e1-11 (2010).
358. Kolaczkowska, E. & Kubes, P. Neutrophil recruitment and function in health and inflammation. *Nat. Rev. Immunol.* **13,** 159–75 (2013).
359. Nathan, C. Neutrophils and immunity: challenges and opportunities. *Nat. Rev. Immunol.* **6,** 173–182 (2006).
360. Dovi, J. V, He, L. & Dipietro, L. a. Accelerated wound closure in neutrophil-depleted mice. *J. Leukoc. Biol.* **73,** 448–455 (2003).
361. Kurimoto, T. *et al.* Neutrophils express oncomodulin and promote optic nerve regeneration. *J. Neurosci.* **33,** 14816–24 (2013).
362. Mathias, J. R. *et al.* Resolution of inflammation by retrograde chemotaxis of neutrophils in transgenic zebrafish. *J. Leukoc. Biol.* **80,** 1281–8 (2006).
363. Herbomel, P., Thisse, B. & Thisse, C. Ontogeny and behaviour of early macrophages in the zebrafish embryo. *Development* **126,** 3735–45 (1999).
364. Lavin, Y., Mortha, A., Rahman, A. & Merad, M. Regulation of macrophage development and function in peripheral tissues. *Nat. Rev. Immunol.* **15,** 731–44 (2015).
365. Jin, H. *et al.* Definitive hematopoietic stem/progenitor cells manifest distinct differentiation output in the zebrafish VDA and PBI. *Development* **136,** 647–54 (2009).
366. Eckfeldt, C. E. *et al.* Functional analysis of human hematopoietic stem cell gene expression using zebrafish. *PLoS Biol.* **3,** e254 (2005).
367. Hall, C., Flores, M. V., Storm, T., Crosier, K. & Crosier, P. The zebrafish lysozyme C promoter drives myeloid-specific expression in transgenic fish. *BMC Dev. Biol.* **7,** 42 (2007).
368. Morley, S. C. The actin-bundling protein L-plastin: a critical regulator of immune cell function. *Int. J. Cell Biol.* **2012,** 935173 (2012).
369. Nguyen-Chi, M. *et al.* TNF signaling and macrophages govern fin regeneration in zebrafish larvae. *Cell Death Dis.* **8,** e2979 (2017).
370. Bridgewater, J. A. *et al.* Expression of the bacterial nitroreductase enzyme in mammalian cells renders them selectively sensitive to killing by the prodrug CB1954. *Eur. J. Cancer* **31A,** 2362–70 (1995).
371. Ruyra, A. *et al.* Targeting and stimulation of the zebrafish (Danio rerio) innate immune system with LPS/dsRNA-loaded nanoliposomes. *Vaccine* **32,** 3955–3962 (2014).
372. Jin, H. *et al.* Runx1 regulates embryonic myeloid fate choice in zebrafish through a negative feedback loop inhibiting Pu.1 expression. *Blood* **119,** 5239–49 (2012).
373. Scott, E. W., Simon, M. C., Anastasi, J. & Singh, H. Requirement of transcription factor PU.1 in the development of multiple hematopoietic lineages. *Science* **265,** 1573–7 (1994).
374. Su, F. *et al.* Differential regulation of primitive myelopoiesis in the zebrafish by Spi-1/Pu.1 and C/ebp1. *Zebrafish* **4,** 187–99 (2007).
375. Schieber, M. & Chandel, N. S. ROS function in redox signaling and oxidative stress. *Curr. Biol.* **24,** R453–R462 (2014).
376. Rada, B. & Leto, T. L. Oxidative innate immune defenses by Nox/Duox family NADPH oxidases. *Contrib. Microbiol.* **15,** 164–87 (2008).
377. Alfadda, A. A. & Sallam, R. M. Reactive oxygen species in health and disease. *J. Biomed. Biotechnol.* **2012,** 936486 (2012).
378. Torres, M. & Forman, H. J. Activation of several MAP kinases upon stimulation of rat alveolar macrophages: role of the NADPH oxidase. *Arch. Biochem. Biophys.* **366,** 231–9 (1999).

379. Gabbita, S. P., Robinson, K. a, Stewart, C. a, Floyd, R. a & Hensley, K. Redox regulatory mechanisms of cellular signal transduction. *Arch. Biochem. Biophys.* **376,** 1–13 (2000).
380. Forman, H. J. & Torres, M. Redox signaling in macrophages. *Mol. Aspects Med.* **22,** 189–216 (2001).
381. Holmström, K. M. & Finkel, T. Cellular mechanisms and physiological consequences of redox-dependent signalling. *Nat. Rev. Mol. Cell Biol.* **15,** 411–21 (2014).
382. Burdon, R. H., Gill, V. & Rice-Evans, C. Cell proliferation and oxidative stress. *Free Radic. Res. Commun.* **7,** 149–59 (1989).
383. Burdon, R. H., Gill, V. & Rice-Evans, C. Oxidative stress and tumour cell proliferation. *Free Radic. Res. Commun.* **11,** 65–76 (1990).
384. Sundaresan, M., Yu, Z. X., Ferrans, V. J., Irani, K. & Finkel, T. Requirement for generation of H2O2 for platelet-derived growth factor signal transduction. *Science* **270,** 296–9 (1995).
385. Bae, Y. S. *et al.* Epidermal growth factor (EGF)-induced generation of hydrogen peroxide. Role in EGF receptor-mediated tyrosine phosphorylation. *J. Biol. Chem.* **272,** 217–21 (1997).
386. Gomes, E. C., Silva, A. N. & de Oliveira, M. R. Oxidants, antioxidants, and the beneficial roles of exercise-induced production of reactive species. *Oxid. Med. Cell. Longev.* **2012,** 756132 (2012).
387. Cai, H. NAD(P)H oxidase-dependent self-propagation of hydrogen peroxide and vascular disease. *Circ. Res.* **96,** 818–22 (2005).
388. Sumimoto, H. Structure, regulation and evolution of Nox-family NADPH oxidases that produce reactive oxygen species. *FEBS J.* **275,** 3249–77 (2008).
389. Aguirre, J. & Lambeth, J. D. Nox enzymes from fungus to fly to fish and what they tell us about Nox function in mammals. *Free Radic. Biol. Med.* **49,** 1342–1353 (2010).
390. Weaver, C. J., Leung, Y. F. & Suter, D. M. Expression dynamics of NADPH oxidases during early zebrafish development. *J. Comp. Neurol.* **524,** 2130–2141 (2016).
391. Nemoto, S., Takeda, K., Yu, Z. X., Ferrans, V. J. & Finkel, T. Role for mitochondrial oxidants as regulators of cellular metabolism. *Mol. Cell. Biol.* **20,** 7311–8 (2000).
392. Pérez-Matute, P., Zulet, M. A. & Martínez, J. A. Reactive species and diabetes: counteracting oxidative stress to improve health. *Curr. Opin. Pharmacol.* **9,** 771–9 (2009).
393. Tiganis, T. Reactive oxygen species and insulin resistance: the good, the bad and the ugly. *Trends Pharmacol. Sci.* **32,** 82–9 (2011).
394. Forman, H. J. in *Oxidants in Biology: A Question of Ballance* (eds. Valacchi, G. & Davis, P. A.) 1–18 (Springer Netherlands, 2008). doi:10.1007/978-1-4020-8399-0
395. De Deken, X., Corvilain, B., Dumont, J. E. & Miot, F. Roles of DUOX-Mediated Hydrogen Peroxide in Metabolism, Host Defense, and Signaling. *Antioxid. Redox Signal.* **20,** 2776–93 (2014).
396. Ueyama, T. *et al.* The extracellular A-loop of dual oxidases affects the specificity of reactive oxygen species release. *J. Biol. Chem.* **290,** 6495–6506 (2015).
397. Jacob, C., Doering, M. & Burkholz, T. in *Redox Signaling and Regulation in Biology and Medicine* (eds. Jacob, C. & Winyard, P. G.) 63–122 (Wiley VCH, 2009). doi:10.1002/cbic.201000004
398. Paulsen, C. E. & Carroll, K. S. Cysteine-mediated redox signaling: Chemistry, biology, and tools for discovery. *Chem. Rev.* **113,** 4633–4679 (2013).
399. Hoshi, T. & Heinemann, S. Regulation of cell function by methionine oxidation and reduction. *J. Physiol.* **531,** 1–11 (2001).
400. Kim, G., Weiss, S. J. & Levine, R. L. Methionine oxidation and reduction in proteins. *Biochim. Biophys. Acta* **1840,** 901–5 (2014).
401. Drazic, A. & Winter, J. The physiological role of reversible methionine oxidation. *Biochim. Biophys. Acta* **1844,** 1367–82 (2014).

402. Kwon, J. *et al.* The nonphagocytic NADPH oxidase Duox1 mediates a positive feedback loop during T cell receptor signaling. *Sci. Signal.* **3,** ra59 (2010).
403. Hirakawa, S., Saito, R., Ohara, H., Okuyama, R. & Aiba, S. Dual oxidase 1 induced by Th2 cytokines promotes STAT6 phosphorylation via oxidative inactivation of protein tyrosine phosphatase 1B in human epidermal keratinocytes. *J. Immunol.* **186,** 4762–70 (2011).
404. Son, Y. *et al.* Mitogen-Activated Protein Kinases and Reactive Oxygen Species: How Can ROS Activate MAPK Pathways? *J. Signal Transduct.* **2011,** 792639 (2011).
405. Petrushanko, I. Y. *et al.* S-glutathionylation of the Na,K-ATPase catalytic α subunit is a determinant of the enzyme redox sensitivity. *J. Biol. Chem.* **287,** 32195–205 (2012).
406. Zhang, A. Y., Yi, F., Zhang, G., Gulbins, E. & Li, P.-L. Lipid raft clustering and redox signaling platform formation in coronary arterial endothelial cells. *Hypertens. (Dallas, Tex. 1979)* **47,** 74–80 (2006).
407. Li, P.-L., Zhang, Y. & Yi, F. Lipid raft redox signaling platforms in endothelial dysfunction. *Antioxid. Redox Signal.* **9,** 1457–70 (2007).
408. Zhang, C. & Li, P.-L. Membrane raft redox signalosomes in endothelial cells. *Free Radic. Res.* **44,** 831–42 (2010).
409. Wang, L. *et al.* Lipid raft-dependent activation of dual oxidase 1/H2O2/NF-κB pathway in bronchial epithelial cells. *Am. J. Physiol. Cell Physiol.* **301,** C171-80 (2011).
410. Ingham, P. W., Nakano, Y. & Seger, C. Mechanisms and functions of Hedgehog signalling across the metazoa. *Nat. Rev. Genet.* **12,** 393–406 (2011).
411. Jiang, J. & Hui, C.-C. Hedgehog signaling in development and cancer. *Dev. Cell* **15,** 801–812 (2008).
412. Varjosalo, M. & Taipale, J. Hedgehog: Functions and mechanisms. *Genes Dev.* **22,** 2454–2472 (2008).
413. Satoh, A. *et al.* Characterization of Xenopus digits and regenerated limbs of the froglet. *Dev. Dyn.* **235,** 3316–26 (2006).
414. Wang, J., Cao, J., Dickson, A. L. & Poss, K. D. Epicardial regeneration is guided by cardiac outflow tract and Hedgehog signalling. *Nature* **522,** 226–30 (2015).
415. Meda, F. *et al.* Nerves Control Redox Levels in Mature Tissues Through Schwann Cells and Hedgehog Signaling. *Antioxid. Redox Signal.* **24,** 299–311 (2016).
416. Stamataki, D., Ulloa, F., Tsoni, S. V, Mynett, A. & Briscoe, J. A gradient of Gli activity mediates graded Sonic Hedgehog signaling in the neural tube. *Genes Dev.* **19,** 626–41 (2005).
417. Dessaud, E. *et al.* Interpretation of the sonic hedgehog morphogen gradient by a temporal adaptation mechanism. *Nature* **450,** 717–20 (2007).
418. Wilson, C. W. & Chuang, P.-T. Mechanism and evolution of cytosolic Hedgehog signal transduction. *Development* **137,** 2079–2094 (2010).
419. Fang, Y. *et al.* Translational profiling of cardiomyocytes identifies an early Jak1/Stat3 injury response required for zebrafish heart regeneration. *Proc. Natl. Acad. Sci. U. S. A.* **110,** 13416–21 (2013).
420. Kato, N. *et al.* Critical role of p38 MAPK for regeneration of the sciatic nerve following crush injury in vivo. *J. Neuroinflammation* **10,** 1 (2013).
421. Tasaki, J. *et al.* ERK signaling controls blastema cell differentiation during planarian regeneration. *Development* **138,** 2417–27 (2011).
422. Yun, M. H., Gates, P. B. & Brockes, J. P. Sustained ERK activation underlies reprogramming in regeneration-competent salamander cells and distinguishes them from their mammalian counterparts. *Stem cell reports* **3,** 15–23 (2014).
423. Tanaka, H. *et al.* Redox regulation of the glucocorticoid receptor. *Antioxid. Redox Signal.* **1,** 403–23 (1999).
424. Duhé, R. J. Redox regulation of Janus kinase: The elephant in the room. *JAK-STAT* **2,** e26141 (2013).

425. Eberhardt, W., Huwiler, A., Beck, K. F., Walpen, S. & Pfeilschifter, J. Amplification of IL-1 beta-induced matrix metalloproteinase-9 expression by superoxide in rat glomerular mesangial cells is mediated by increased activities of NF-kappa B and activating protein-1 and involves activation of the mitogen-activated protein ki. *J. Immunol.* **165,** 5788–97 (2000).
426. Gurjar, M. V, Deleon, J., Sharma, R. V & Bhalla, R. C. Role of reactive oxygen species in IL-1 beta-stimulated sustained ERK activation and MMP-9 induction. *Am. J. Physiol. Heart Circ. Physiol.* **281,** H2568-74 (2001).
427. Ray, P. D., Huang, B.-W. & Tsuji, Y. Reactive oxygen species (ROS) homeostasis and redox regulation in cellular signaling. *Cell. Signal.* **24,** 981–90 (2012).
428. Schneider-Poetsch, T. *et al.* Inhibition of eukaryotic translation elongation by cycloheximide and lactimidomycin. *Nat. Chem. Biol.* **6,** 209–217 (2010).
429. Bement, W. M., Mandato, C. A. & Kirsch, M. N. Wound-induced assembly and closure of an actomyosin purse string in Xenopus oocytes. *Curr. Biol.* **9,** 579–87 (1999).
430. Son, Y., Kim, S., Chung, H. T. & Pae, H. O. *Reactive oxygen species in the activation of MAP kinases*. *Methods Enzymol* **528,** (Elsevier Inc., 2013).
431. Parsons, S. J. & Parsons, J. T. Src family kinases, key regulators of signal transduction. *Oncogene* **23,** 7906–9 (2004).
432. Gao, C. Y., Stepp, M. A., Fariss, R. & Zelenka, P. Cdk5 regulates activation and localization of Src during corneal epithelial wound closure. *J. Cell Sci.* **117,** 4089–98 (2004).
433. Wu, Q. Q., Zhang, Y. & Chen, Q. Indian hedgehog Is an Essential Component of Mechanotransduction Complex to Stimulate Chondrocyte Proliferation. *J. Biol. Chem.* **276,** 35290–35296 (2001).
434. Nowlan, N. C., Prendergast, P. J. & Murphy, P. Identification of mechanosensitive genes during embryonic bone formation. *PLoS Comput. Biol.* **4,** (2008).
435. Kanki, J. P. & Ho, R. K. The development of the posterior body in zebrafish. *Development* **124,** 881–93 (1997).
436. Norton, W. H. J., Ledin, J., Grandel, H. & Neumann, C. J. HSPG synthesis by zebrafish Ext2 and Extl3 is required for Fgf10 signalling during limb development. *Development* **132,** 4963–73 (2005).
437. Prykhozhij, S. V & Neumann, C. J. Distinct roles of Shh and Fgf signaling in regulating cell proliferation during zebrafish pectoral fin development. *BMC Dev. Biol.* **8,** 91 (2008).
438. Boehm, B. *et al.* The role of spatially controlled cell proliferation in limb bud morphogenesis. *PLoS Biol.* **8,** e1000420 (2010).
439. Tanaka, E. M. & Gann, A. F. Limb development. The budding role of FGF. *Curr. Biol.* **5,** 594–7 (1995).
440. Chiang, C. *et al.* Manifestation of the limb prepattern: limb development in the absence of sonic hedgehog function. *Dev. Biol.* **236,** 421–35 (2001).
441. Nachtrab, G., Kikuchi, K., Tornini, V. a & Poss, K. D. Transcriptional components of anteroposterior positional information during zebrafish fin regeneration. *Development* **140,** 3754–64 (2013).
442. Summerbell, D., Lewis, J. H. & Wolpert, L. Positional information in chick limb morphogenesis. *Nature* **244,** 492–6 (1973).
443. Dudley, A. T., Ros, M. A. & Tabin, C. J. A re-examination of proximodistal patterning during vertebrate limb development. *Nature* **418,** 539–44 (2002).
444. Singh, B. N. *et al.* Hedgehog signaling during appendage development and regeneration. *Genes (Basel).* **6,** 417–435 (2015).
445. Neumann, C. J., Grandel, H., Gaffield, W., Schulte-Merker, S. & Nüsslein-Volhard, C. Transient establishment of anteroposterior polarity in the zebrafish pectoral fin bud in the absence of sonic hedgehog activity. *Development* **126,** 4817–26 (1999).
446. Barresi, M. J. F., Stickney, H. L. & Devoto, S. H. The zebrafish slow-muscle-omitted gene

product is required for Hedgehog signal transduction and the development of slow muscle identity. **2199,** 2189–2199 (2000).
447. Lekven, A. C., Thorpe, C. J., Waxman, J. S. & Moon, R. T. Zebrafish wnt8 Encodes Two Wnt8 Proteins on a Bicistronic Transcript and Is Required for Mesoderm and Neurectoderm Patterning. *Dev. Cell* **1,** 103–114 (2001).
448. Agathon, a, Thisse, C. & Thisse, B. The molecular nature of the zebrafish tail organizer. *Nature* **424,** 448–452 (2003).
449. Thorpe, C. J., Weidinger, G. & Moon, R. T. Wnt/beta-catenin regulation of the Sp1-related transcription factor sp5l promotes tail development in zebrafish. *Development* **132,** 1763–72 (2005).
450. Martin, B. L. & Kimelman, D. Regulation of Canonical Wnt Signaling by Brachyury Is Essential for Posterior Mesoderm Formation. *Dev. Cell* **15,** 121–133 (2008).
451. Griffin, K., Patient, R. & Holder, N. Analysis of FGF function in normal and no tail zebrafish embryos reveals separate mechanisms for formation of the trunk and the tail. *Development* **121,** 2983–2994 (1995).
452. Griffin, K. J. P. & Kimelman, D. Interplay between FGF, one-eyed pinhead, and T-box transcription factors during zebrafish posterior development. *Dev. Biol.* **264,** 456–466 (2003).
453. Fürthauer, M., Van Celst, J., Thisse, C. & Thisse, B. Fgf signalling controls the dorsoventral patterning of the zebrafish embryo. *Development* **131,** 2853–2864 (2004).
454. Stulberg, M. J., Lin, A., Zhao, H. & Holley, S. a. Crosstalk between Fgf and Wnt signaling in the zebrafish tailbud. *Dev. Biol.* **369,** 298–307 (2012).
455. Kimmel, C. B., Ballard, W. W., Kimmel, S. R., Ullmann, B. & Schilling, T. F. Stages of embryonic development of the zebrafish. *Dev. Dyn.* **203,** 253–310 (1995).
456. Covarrubias, L., Hernández-García, D., Schnabel, D., Salas-Vidal, E. & Castro-Obregón, S. Function of reactive oxygen species during animal development: passive or active? *Dev. Biol.* **320,** 1–11 (2008).
457. Hernández-García, D., Wood, C. D., Castro-Obregón, S. & Covarrubias, L. Reactive oxygen species: A radical role in development? *Free Radic. Biol. Med.* **49,** 130–43 (2010).
458. Tsai, W. Bin, Zhang, X., Sharma, D., Wu, W. & Kinsey, W. H. Role of Yes kinase during early zebrafish development. *Dev. Biol.* **277,** 129–141 (2005).
459. Jopling, C. & den Hertog, J. Fyn/Yes and non-canonical Wnt signalling converge on RhoA in vertebrate gastrulation cell movements. *EMBO Rep* **6,** 426–431 (2005).
460. Murphy, D. A. *et al.* A Src-Tks5 pathway is required for neural crest cell migration during embryonic development. *PLoS One* **6,** (2011).
461. Sinha, S. & Chen, J. K. Purmorphamine activates the Hedgehog pathway by targeting Smoothened. *Nat. Chem. Biol.* **2,** 29–30 (2006).
462. Rominger, C. M. *et al.* Evidence for allosteric interactions of antagonist binding to the smoothened receptor. *J Pharmacol Exp Ther* **329,** 995–1005 (2009).
463. Perathoner, S. *et al.* Bioelectric signaling regulates size in zebrafish fins. *PLoS Genet.* **10,** e1004080 (2014).
464. Osaki, T., Uchida, Y., Hirayama, J. & Nishina, H. Diphenyleneiodonium chloride, an inhibitor of reduced nicotinamide adenine dinucleotide phosphate oxidase, suppresses light-dependent induction of clock and DNA repair genes in zebrafish. *Biol. Pharm. Bull.* **34,** 1343–1347 (2011).
465. Toledano, M. B., Kumar, C., Le Moan, N., Spector, D. & Tacnet, F. The system biology of thiol redox system in Escherichia coli and yeast: differential functions in oxidative stress, iron metabolism and DNA synthesis. *FEBS Lett.* **581,** 3598–607 (2007).
466. Konstantinides, N. & Averof, M. A common cellular basis for muscle regeneration in arthropods and vertebrates. *Science* **343,** 788–91 (2014).
467. Rudyk, O. & Eaton, P. Biochemical methods for monitoring protein thiol redox states in

biological systems. *Redox Biol.* **2,** 803–813 (2014).
468. Denoncin, K., Nicolaes, V., Cho, S.-H., Leverrier, P. & Collet, J.-F. Protein disulfide bond formation in the periplasm: determination of the in vivo redox state of cysteine residues. *Methods Mol. Biol.* **966,** 325–36 (2013).
469. Burgoyne, J. R. & Eaton, P. Detecting disulfide-bound complexes and the oxidative regulation of cyclic nucleotide-dependent protein kinases by H2O2. *Methods Enzymol.* **528,** 111–28 (2013).
470. Aller, I., Rouhier, N. & Meyer, A. J. Development of roGFP2-derived redox probes for measurement of the glutathione redox potential in the cytosol of severely glutathione-deficient rml1 seedlings. *Front. Plant Sci.* **4,** 506 (2013).
471. Shi, H. G., Mikhaylova, L., Zichittella, A. E. & Argüello, J. M. Functional role of cysteine residues in the (Na,K)-ATPase alpha subunit. *Biochim. Biophys. Acta* **1464,** 177–87 (2000).
472. Hu, Y. K., Eisses, J. F. & Kaplan, J. H. Expression of an active Na,K-ATPase with an alpha-subunit lacking all twenty-three native cysteine residues. *J. Biol. Chem.* **275,** 30734–9 (2000).
473. Dergousova, E. A. *et al.* Effect of Reduction of Redox Modifications of Cys-Residues in the Na,K-ATPase α1-Subunit on Its Activity. *Biomolecules* **7,** (2017).
474. Mich, J. K., Payumo, A. Y., Rack, P. G. & Chen, J. K. In vivo imaging of Hedgehog pathway activation with a nuclear fluorescent reporter. *PLoS One* **9,** 1–8 (2014).
475. Thastrup, O., Cullen, P. J., Drøbak, B. K., Hanley, M. R. & Dawson, A. P. Thapsigargin, a tumor promoter, discharges intracellular Ca2+ stores by specific inhibition of the endoplasmic reticulum Ca2(+)-ATPase. *Proc. Natl. Acad. Sci. U. S. A.* **87,** 2466–70 (1990).
476. Ermakov, Y. A., Kamaraju, K., Sengupta, K. & Sukharev, S. Gadolinium ions block mechanosensitive channels by altering the packing and lateral pressure of anionic lipids. *Biophys. J.* **98,** 1018–27 (2010).
477. Rojas-Muñoz, A. *et al.* ErbB2 and ErbB3 regulate amputation-induced proliferation and migration during vertebrate regeneration. *Dev. Biol.* **327,** 177–190 (2009).
478. Choi, W.-Y. *et al.* In vivo monitoring of cardiomyocyte proliferation to identify chemical modifiers of heart regeneration. *Development* **140,** 660–6 (2013).
479. Spence, J. R., Aycinena, J.-C. & Del Rio-Tsonis, K. Fibroblast growth factor-hedgehog interdependence during retina regeneration. *Dev. Dyn.* **236,** 1161–74 (2007).
480. Elia, D., Madhala, D., Ardon, E., Reshef, R. & Halevy, O. Sonic hedgehog promotes proliferation and differentiation of adult muscle cells: Involvement of MAPK/ERK and PI3K/Akt pathways. *Biochim. Biophys. Acta* **1773,** 1438–46 (2007).
481. Dormoy, V. *et al.* The sonic hedgehog signaling pathway is reactivated in human renal cell carcinoma and plays orchestral role in tumor growth. *Mol. Cancer* **8,** 123 (2009).
482. Chang, H., Li, Q., Moraes, R. C., Lewis, M. T. & Hamel, P. A. Activation of Erk by sonic hedgehog independent of canonical hedgehog signalling. *Int. J. Biochem. Cell Biol.* **42,** 1462–71 (2010).
483. Qin, C.-F., Hao, K., Tian, X.-D., Xie, X.-H. & Yang, Y.-M. Combined effects of EGFR and Hedgehog signaling pathway inhibition on the proliferation and apoptosis of pancreatic cancer cells. *Oncol. Rep.* **28,** 519–26 (2012).
484. Zhao, Y. *et al.* An Expanded Palette of Genetically Encoded Ca2+ Indicators. *Science* **333,** 1888–1891 (2011).
485. Bilan, D. S. *et al.* HyPer-3: a genetically encoded H(2)O(2) probe with improved performance for ratiometric and fluorescence lifetime imaging. *ACS Chem. Biol.* **8,** 535–42 (2013).
486. Müller, F. *et al.* Intronic enhancers control expression of zebrafish sonic hedgehog in floor plate and notochord. *Development* **126,** 2103–16 (1999).
487. Hadzhiev, Y. *et al.* Functional diversification of sonic hedgehog paralog enhancers identified by phylogenomic reconstruction. *Genome Biol.* **8,** R106 (2007).